

## Energies of semiconducting surfaces

**Author:**

Taloni, Augusto

**Publication Date:**

1967

**DOI:**

<https://doi.org/10.26190/unsworks/7397>

**License:**

<https://creativecommons.org/licenses/by-nc-nd/3.0/au/>

Link to license to see what you are allowed to do with this resource.

Downloaded from <http://hdl.handle.net/1959.4/61899> in <https://unsworks.unsw.edu.au> on 2024-04-27

CERTIFICATE

School of Physics.

October, 1967.

The Professor of Physics,  
School of Physics,  
University of New South Wales,  
KENSINGTON.

The following thesis is respectfully  
submitted for examination for the award of the Degree of  
Doctor of Philosophy.

I hereby certify that the work embodied  
in this thesis has not been submitted to any other  
University or Institution for the award of a Higher Degree.

*Augusto Taloni*

Augusto Taloni.

ENERGIES  
OF  
SEMICONDUCTING SURFACES

• • •

THESIS  
for the degree of  
DOCTOR OF PHILOSOPHY  
in the  
Faculty of Science,  
University of New South Wales.



Submitted by :

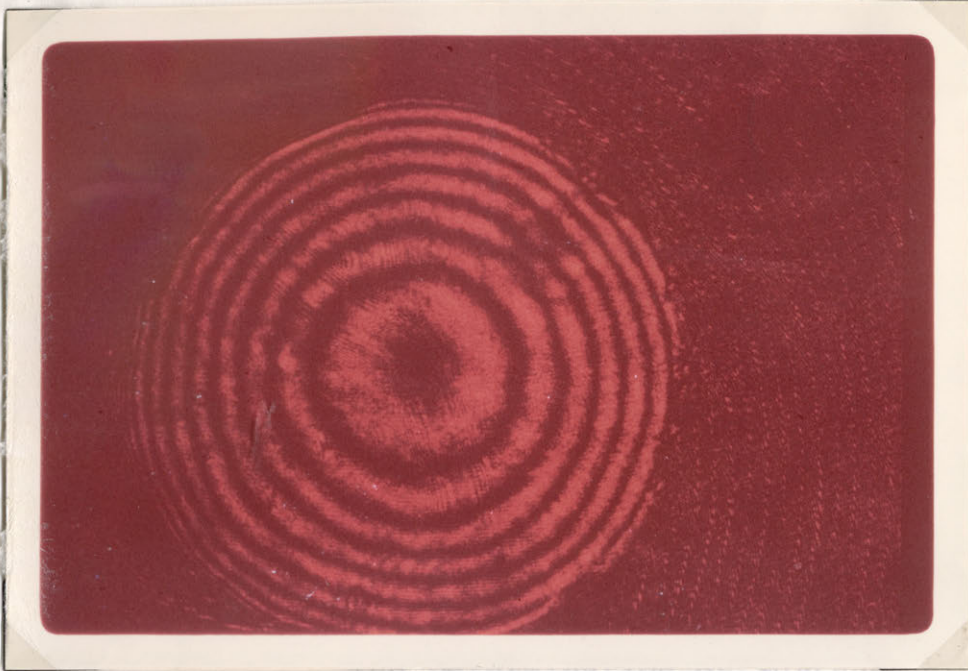
Augusto Taloni

CONTENTS

(i) (11)

page

(xvi)



1

3

8

8

8

9

9

9

9

AN INTERFERENCE PATTERN ACROSS A GERMANIUM  
CRYSTAL TAKEN BY LASER INTERFEROMETRY.  
THE RING SYSTEM SHOWS A RADIUS OF CURVATURE  
OF 200 CMS. (MAGNIFICATION X 15).

16

1.4	Surface Models.	18
1.4.1	Introduction.	18
1.4.2	Clean Surface Models.	19
1.4.2.1	The Hannon Models.	19
1.4.2.1.1	The General (111) Model for 3 - 5 Compounds and Diamond Structure Semiconductors.	19
1.4.2.1.2	The Germanium (111) Surface Model.	20

## CONTENTS

(ii)

page

### SUMMARY

(xvi)

#### CHAPTER 1

#### THE STUDY OF SURFACES.

1.0	General Introduction.	1
1.1	Introduction.	3
1.2	The Energy of Surfaces.	8
1.2.1	Introduction.	8
1.2.1.1	Surface Tension.	8
1.2.1.2	Surface Energy.	9
1.2.1.3	Surface Stress.	9
1.2.1.4	Elastic Strain Energy.	9
1.2.2	The Determination of Surface Tension and Surface Energy for Solids.	9
1.3	The Elastic Strain Energy.	16
1.4	Surface Models.	18
1.4.1	Introduction.	18
1.4.2	Clean Surface Models.	19
1.4.2.1	The Haneman Models.	19
1.4.2.1.1	The General (111) Model for 3 - 5 Compounds and Diamond Structure Semiconductors.	19
1.4.2.1.2	The Germanium (111) Surface Model.	20

1.4.2.2	The Lander and Morrison Germanium (111) Surface Model.	20
1.4.2.3	The Seiwatz Model for the Germanium (111) Surface.	21
1.4.2.4	Palmberg and Peria Modifications to the Haneman and the Lander and Morrison Models.	21
1.4.2.5	The MacRae GaAs and GaSb (111) Surface Models.	22
1.4.3	Cleaved Surface Models.	23
1.4.4	The Gatos Model for the (111) Surfaces of the 3 - 5 Compounds.	25
1.4.4.1	The Cahn and Hanneman Calculation.	26
1.5	Electron Paramagnetic Resonance Studies.	27
<u>CHAPTER 2</u>	<u>PREPARATION OF CRYSTAL SURFACES.</u>	
2.1	Introduction.	30
2.2	Preparation for Polishing.	31
2.3	Polishing of the Crystal Surface.	33
2.4	Formation of Circular Specimens.	34
2.5	Polishing Both Sides of the Crystal.	35

2.6	Identification of the 111 - V Faces.	35
2.7	Final Preparation of Crystal for Experimentation.	36
<u>CHAPTER 3</u>	<u>EXPERIMENTAL ARRANGEMENTS.</u>	
3.0	Introduction.	38
3.1	The Vacuum System.	39
3.2	Formation of the Clean Surface by Ion Bombardment.	39
3.2.1	Introduction.	39
3.2.2	The Crystal Holder.	40
3.2.3	The Dummy Crystals.	40
3.2.4	The Ion Gun and Electrical Connections.	41
3.3	Measurement of the Radius of Curvature - The Laser Interferometer.	42
3.3.1	Introduction.	42
3.3.2	The Laser Interferometer.	43
3.3.2.1	The Light Source.	44
3.3.2.2	Optical Construction of Interferometer.	45
3.3.2.3	Sensitivity.	46
3.3.2.4	The Working Chamber.	47
3.4	Experimental Procedures.	48

3.4.1	Introduction.	48
3.4.2	The Baked and Unbaked System.	48
3.4.2.1	The Baked System.	48
3.4.2.2	The "Unbaked" System.	49
3.4.3	Measurement of Curvature as a Function of Temperature.	49
3.4.3.1	Calibration of Temperature.	49
3.4.3.2	R Versus Temperature.	51
3.4.3.3	Measurement of R as a Function of Ion Bombardment.	52
3.4.3.4	Measurement of R as a Function of Thickness.	52
3.5	Experimental Difficulties.	53
3.5.1	Introduction.	53
3.5.2	Vibration.	53
3.5.3	Ion Focussing.	54
3.5.4	Crystal Stability.	54
<u>CHAPTER 4</u>	<u>EXPERIMENTAL RESULTS.</u>	
4.1	Introduction.	56
4.2	The Effect of Cutting, Abrading and Polishing on Surfaces.	57
4.3	Ion Bombardment Results.	59
4.3.1	Introduction.	59

4.3.2	Germanium Results.	60
4.4	Annealing Results for Germanium.	64
4.4.1	Combined Annealing and Ion Bombardment.	64
4.5	Curvature as a Function of Thickness for Germanium.	69
4.6	Silicon Results.	71
4.7	Indium Antimonide Results.	73
4.7.1	Introduction.	73
4.7.2	Annealing and Ion Bombardment Results.	75
4.7.3	Curvature as a Function of Thickness for Indium Antimonide.	78
4.7.4	Conclusion and Discussion.	79
4.8	Gallium Antimonide Results.	80
4.9	General Conclusion.	82
<u>CHAPTER 5</u>	<u>ELECTRON PARAMAGNETIC RESONANCE EXPERIMENTS AND RESULTS.</u>	
5.1	Introduction.	84
5.2	Electron Paramagnetic Resonance (e.p.r.) Theory.	84
5.2.1	Introduction.	84
5.2.2	Detection of the e.p.r. Signal.	85

5.2.3	The Splitting Factor $g$ , Line Width, Line Shape and Signal Height.	87
5.2.3.1	The $g$ Factor.	87
5.2.3.2	The Line Width.	90
5.2.3.3	The Line Shape.	91
5.2.3.4	Signal Height.	93
5.3	Experimental Arrangement and Results.	94
5.3.1	Experimental Arrangement.	94
5.3.2	Experimental Procedure.	95
5.3.2.1	Testing for Impurities.	95
5.3.3	Experimental Results.	97
5.4	Discussion and Conclusions.	99
<u>CHAPTER 6</u>	<u>COMPUTER CALCULATIONS OF SEMICONDUCTOR SURFACE STRUCTURES.</u>	
6.1	Introduction.	106
6.2	The Interatomic Potential Function.	108
6.3	Calculation of the Minimum Energy of a Ruffled Germanium (111) Surface.	111
6.3.1	Scope of Interactions.	111
6.3.2	Functional Relationship Between Distances.	113
6.3.3	Procedure.	115
6.3.4	Results.	116

6.4	Calculation of the Surface Free Energy of the Germanium (111) Surface.	117
6.4.1	Introduction.	117
6.4.2	Procedure.	118
6.4.3	Results and Conclusion.	119
6.5	Calculation of the Sublimation Energy for Germanium.	119
6.5.1	Introduction.	119
6.5.2	Procedure.	119
6.5.3	Results and Conclusion.	120
6.6	Calculation of the Elastic Constant $C_{11}$ for Germanium.	120
6.6.1	Introduction.	120
6.6.2	Procedure.	121
6.6.3	Results and Conclusion.	122
6.7	General Discussion and Conclusion for Germanium.	122
6.8	Silicon Results.	123
6.9	111 - V Compounds.	124
6.9.1	Introduction.	124
6.9.2	Procedure and Results for the Indium Antimonide Calculations.	128
6.9.3	Conclusion.	129
<u>CHAPTER 7</u>	<u>DISCUSSION AND CONCLUSION.</u>	
7.1	Surface Stresses for Clean A and B Faces of 111 - V Compounds.	131

7.2	Polishing Damage.	131
7.3	Argon Ion Bombardment.	132
7.4	Annealing.	133
7.5	E.P.R. Measurements.	134
7.6	Postulated Model.	134
7.7	Model Tested with Experimental Results.	135
7.8	Computer Calculations.	136
	Acknowledgements.	137
	Appendix 1.	138
	Appendix 2.	144
	Appendix 3.	148
	Appendix 4.	151
	Appendix 5.	154
	References - Chapter 1.	157
	References - Chapter 2.	160
	References - Chapter 3.	161
	References - Chapter 4.	163
	References - Chapter 5.	164
	References - Chapter 6.	166
	Publications.	168

LIST OF ILLUSTRATIONS

		Page
Figure 1.F.1	Showing the Geometry of the Bent Plate.	17
Figure 1.F.2	The Haneman Model for the Germanium (111) Surface.	19
Figure 1.F.3	a) The General Haneman (111) Surface Model. b) The Palmberg and Peria Modification.	19
Figure 1.F.4	a) The Lander and Morrison Germanium (111) Surface Model. b) The Palmberg and Peria Modification.	22
Figure 1.F.5	The MacRae GaAs and GaSb (111) Surface Model.	23
Figure 1.F.6	The Gatos (111) Surface Model.	26
Photo. 2.P.1	This Shows Many Rectangular Crystals Mounted on Stainless Steel with Black Wax, Ready for Polishing. (Magnification X 1).	34
Photo. 2.P.2	An Interference Pattern Across the Polished Faces of a Rectangular and Square Crystal. The Fringes Show the Unwanted Edge Effects. (Magnification X 6).	34
Photo. 2.P.3	This Shows a Slab with Circular Crystals Cut Out of It. The Other Photograph Shows the Interference Pattern Across One of the Circular Crystals.	35
Photo. 2.P.4	The Indium Face of InSb with Characteristic Circular Pit. (Magnification X 500).	36
Photo. 2.P.5	The Gallium Face of GaSb with Characteristic Triangular Pit. (Magnification X 500).	36

Figure 3.F.1	The Vacuum System.	39
Figure 3.F.2	The Crystal Holder Assembly.	40
Figure 3.F.3	The Crystal Holder with Dummies.	40
Figure 3.F.4	The Ion Gun.	42
Figure 3.F.5	Grid Outgas Circuit.	42
Figure 3.F.6	Sputter Shield Outgas Circuit.	42
Figure 3.F.7	Ion Bombardment Circuit.	42
Figure 3.F.8	The Optical System.	45
Figure 3.F.9	$I(r) / I(i)$	46
Figure 3.F.10	The Working Chamber.	48
Figure 3.F.11.	Temperature Calibration Equipment.	50
Figure 3.F.12	Potential Calibration Curve.	50
Figure 3.F.13	Crystal Temperature Calibration.	51
Figure 3.F.14	Temperature of Crystal When Directly Heated as a Function of Time.	51
Figure 3.F.15	Temperature of Crystal Due to Filament Being Switched On.	52
Photo. 3.P.1	Crystals Before and After Ion Bombardment.	54
Photo. 4.P.1 - 4	Effects of Damage on Crystals.	58
Figure 4.F.1	Results of Ion Bombardment on Polished Crystals.	60
Photo. 4.P.5	Results of Ion Bombardment on Crystals Polished on Both Sides.	63
Figure 4.F.2	Results of Annealing on Crystals.	64
Figure 4.F.3	Radius of Curvature Versus Time for Ion Bombardment.	65

Figure 4.F.4	Plot of Log R Versus Log t.	70
Figure 4.F.5	The Effect of Annealing on a Silicon Crystal.	72
Figure 4.F.6	The Effect of Annealing on InSb Crystal, Sb Face Polished.	75
Figure 4.F.7	The Effect of Annealing on InSb Crystal, In Face Polished.	76
Figure 4.F.8	R Versus Time of Ion Bombardment for InSb.	76
Figure 4.F.9	Combined Annealing and Ion Bombardment Effect for InSb.	77
Figure 4.F.10	Plot of Log R Versus Log t for InSb.	78
Figure 4.F.11	Combined Annealing / Ion Bombardment Effect on a Gallium Antimonide Crystal.	81
Figure 4.F.12	Annealing Results for the Four Crystals.	83
Figure 5.F.1	Showing the Precession of the Electronic Moment.	86
Figure 5.F.2	Magnetic Splitting of Energy Levels.	87
Figure 5.F.3	The Standard $Mn^{++}$ Marker with the Signal from Polished Silicon.	89
Figure 5.F.4	Showing Experimental Tube.	95
Figure 5.F.5	Relative Signal Height Versus Temperature for Polished Silicon.	97
Figure 5.F.6	Relative Signal Height Versus Temperature for Polished Silicon - with gases.	97
Figure 5.F.7	Line Width Versus Temperature for Polished Silicon.	97
Figure 5.F.8	Line Width Versus Temperature for Air - Crushed Silicon.	97

Figure 5.F.9	Line Shape for Air Crushed Silicon Versus Temperature.	97
Figure 5.F.10	Line Shape for Polished Silicon Versus Temperature.	97
Figure 5.F.11	Surface Mismatch Model.	104
Figure 6.F.1	Surface Buckling According to the H - Model.	108
Figure 6.F.2	Plotting $M(r)$ as a Function of $r$ for varying values of "a".	109
Figure 6.F.3	Solution of the Morse Potential for the Germanium Lattice.	110
Illustration	The Model of a 111 - V Structure.	113
Figure 6.F.4	View of Second Layer Showing Atom Shifts and Angles.	114
Figure 6.F.5	Minimum Energy of a Rumpled (111) Germanium Surface as a Function of $r^+$ .	116
Figure 6.F.6	Plotting "a" Versus $r^+$ for which the Minimum Energy of the Germanium (111) Surface Occurs.	117
Figure 6.F.7	Solution of (111) Surface Energy Calculations for Germanium.	119
Figure 6.F.8	Solution of Sublimation Energy for Germanium.	120
Figure 6.F.9	The Expression Derived from Keating is Drawn Together with the Solution of the Germanium Elastic Constant $C_{11}$ .	122

Figure 6.F.10	Combination of Surface Free Energy, Sublimation Energy and the Elastic Constant for Germanium.	123
Figure 6.F.11	Minimum Energy of a Ruffled (111) Silicon Surface as a Function of $r^+$ .	124
Figure 6.F.12	Plot of "a" Versus $r^+$ for which the Minimum Energy of the Silicon (111) Surface Occurs.	124
Figure 6.F.13	Solution of Surface Energy Calculation for Silicon.	124
Figure 6.F.14	Solution of Sublimation Energy for Silicon.	124
Figure 6.F.15	The Expression Derived from Keating is Drawn Together with the Solution of the Silicon Elastic Constant $C_{11}$ .	124
Figure 6.F.16	Combination of 6.F.13 and 6.F.15	124
Figure 6.F.17	A Plot of the Ratio of the Two Force Constants Within the Haneman - Russell Restrictions.	128
Figure 6.F.18	$\frac{\alpha_B}{\alpha_A}$ Versus $\frac{D_B}{D_A}$	129
Figure 6.F.19	$\frac{\alpha_B}{\alpha_A}$ Versus $\frac{a_B}{a_A}$	
Illustration	Ion Bombarded InSb Polished on Both Sides.	155

LIST OF TABLES

Table 1.T.1	Measured and Calculated Values of Surface Stress.	14
Table 2.T.1	Crystal Manufacturers.	31
Table 2.T.2	Mechanical Polishing Treatment for the Crystal Surfaces.	34
Table 4.T.1	Results for Polishing Damage on Crystal Surfaces.	57
Table 4.T.2	Depths of Polishing Damage in Ge Detected by Strain.	62
Table 4.T.3	Heat Treatment and Ion Bombardment for Germanium Crystals Polished on Both Sides.	69
Table 4.T.4	Experimental Results for Ge, Si, InSb and GaSb.	82
Table 5.T.1	Showing a Plot of the Derivatives of the Lorentzian and Gaussian Functions.	93
Table 5.T.2	E.P.R. Effects of Annealing on Fine Polished Silicon.	100
Table 5.T.3	Migration Energies for Vacancies Dislocations and Interstitials.	103
Table 6.T.1	Computed Heights of Surface Atoms Above Second Layer.	123
Table 6.T.2	Properties of Clean (111) Surfaces of 111 - V Compounds.	127

SUMMARY

The semiconducting substances indium antimonide and gallium antimonide have opposite (111) surfaces which ideally terminate with different atoms. Principally, it is the aim of this study to measure any surface stress arising out of this asymmetry.

The crystals used were prepared by cutting, abrading and polishing. Since these operations introduce damage to the surface it was essential first to study the nature of this damage and its removal.

As a criterion for the removal of this damage germanium and silicon crystals were also studied. These semiconductors have no (111) surface asymmetry and hence should not exhibit any intrinsic surface stresses of their own.

The stress was measured by noting the radius of curvature (R) or bending of thin (10 - 20 microns) crystals of these substances with a laser interferometer.

Clean surfaces were obtained from the polished crystals by argon ion bombardment.

For the four substances monitoring the radius of curvature as a function of time it was possible, besides forming a clean surface, to determine the depth to which the damage introduced during the polishing

operation extends. This depth was found to be greater than previously reported.

Annealing in vacuum showed a rather interesting result. Application of heat to the polished crystals showed that annealing occurred at relatively low temperatures (50<sup>o</sup> C). This helped in postulating a model for the damaged region.

Supplementary information on the damaged region was obtained by electron paramagnetic resonance studies on polished silicon. It appeared that mechanically polished surfaces had unpaired electrons associated with them.

On the basis of this information a surface mismatch model has been postulated for the damaged region introduced during the preparation of the surface.

Finally computer calculations were conducted on the surface structure of some of these compounds. For the case of germanium a minimum energy calculation using the Morse potential gave a rumpled surface structure which agrees surprisingly well with the H - model for the germanium surface, this being obtained by Low Energy Electron Diffraction studies.

A calculation was also made for silicon.

By varying certain parameters in the Morse potential function, estimates were obtained for the surface stresses of Indium Antimonide. Within the approximations used the results were consistent with the low measured value.

CHAPTER 1. THE STUDY OF SURFACES.

1.0 GENERAL INTRODUCTION.



Any study requires an ultimate aim. The aim here in studying surfaces, and semiconducting surfaces in particular, is to extend the present knowledge of these substances, without necessitating any practical applications.

However, important practical reasons may also be given to justify the study of these surfaces.

Surfaces are formed at the termination of the bulk. In the bulk the crystal may be considered as being made up of a uniform periodic structure. However, because of the discontinuity, the force system acting on the atoms at the surface has lower symmetry. This asymmetry about the surface plane can be expected to give different physical properties at the surface from that of the bulk. For example, the differing potential at the surface, from that in the bulk, allows surface electrons to possess energy states which would be forbidden in the bulk. These are known as Tamm <sup>1)</sup> states. Shockley <sup>2)</sup> has also calculated energy states which would normally be in the forbidden band by terminating the bulk potential at the surface. It is the behaviour of these surface states, which for semiconductors are able to trap electrons, that determines some of the rectifying and photovoltaic properties of these compounds. Transistor action, for example can be greatly influenced

by the interaction of the surface with other surfaces and with ambients. Many electronic properties will also depend on the density, the conductivity and mobility of the electrons in surface states.

Recent developments in high speed computers have also encouraged the research in surface physics. The speed of a computer is limited by the time required for electrical impulses to go from one component to another.

The velocity has a maximum (speed of light) hence shorter paths between components are needed. This is one of the advantages achieved by microminiaturisation<sup>3,4)</sup> of components. This development is based largely on use of thin films and surface layers, and modern active solid state components used in integrated circuitry depend substantially on the properties of semiconductor surface regions.

## 1.1 INTRODUCTION.

The term surface is generally used to describe a boundary region between different media. The surface of concern here is that between solid crystal faces and the surrounding gaseous ambients.

Surfaces may be classified into two main categories, real and clean. Real surfaces are generally prepared by polishing and chemical etching. These surfaces are generally contaminated by chemisorbed materials, and adsorbed gas molecules from the surrounding ambient. Since real surfaces are those most commonly encountered in practice, and because of the ease with which they may be prepared and maintained, they have been the most extensively studied.

Clean surfaces are more difficult to produce and to maintain. They can be prepared by the cleaving of crystals, and by the heating or ion bombardment of real surfaces. Once they are produced they must be kept in ultra - high vacuum ( $10^{-10}$  -  $10^{-9}$  mm Hg) to prevent recontamination. Clean surfaces constitute the closest approximation to the true crystal surface.

Since clean surfaces are the least complicated it is desirable that any study should elucidate these first.

Various aspects of metallic, semiconducting and insulating surfaces have been and are being studied.

These include the electrical and mechanical properties of surfaces, the chemistry of surfaces, and the surface lattice structure.

This present work is mainly concerned with clean semiconductor surfaces. A great deal of interest in semiconductors began after their transistor properties were first discovered by Bardeen and Brattain<sup>5)</sup> in 1948. Continued interest has been maintained with the use of solid state devices in computers and their use in communication systems. A great deal about the surfaces of semiconducting elements and compounds remains to be discovered. Even the surface structures of these are not known and it is partly the aim here to obtain information with regard to this point. Some aspects of the mechanical properties of semiconducting surfaces are also investigated.

Of particular interest in this study are the semiconducting 111 - V compounds. A property of these substances is that opposite (111) surfaces ideally terminate with different atoms. For a compound such as indium antimonide the (111) face is made up entirely of indium or group 3 atoms, sometime denoted as the A surface, while the  $\overline{(111)}$  face is made up entirely of antimony or group 5 atoms, sometime denoted as the B surface. Because of this asymmetry between the two surfaces, it might be expected that some of their properties will be different. Such

differences are in fact known for real, contaminated surfaces.

One property of interest here is the difference in the surface stress between the A and B surfaces. This stress will arise when the surface atoms rearrange themselves to minimise their overall energy. Since the two (111) surfaces contain different atoms it is expected that the stresses set up might also be different.

It is the main purpose of this thesis to determine any surface stress difference that might arise between the clean A and B surfaces of the semiconducting 111 - V compounds, indium antimonide (InSb) and gallium antimonide (GaSb).

To determine this difference measurements have been made of the curvature of thin specimens. This type of measurement has been previously carried out on real, contaminated surfaces. However, any conclusions which were drawn from this regarding clean surfaces would have limited, if any, applicability.

The surfaces used here were prepared by polishing in air. Clearly these are not clean surfaces and some stresses will in fact be produced by the polishing operation itself. However since polishing is a common technique used for preparing crystal surfaces, it was considered desirable to study the strain in these as an aid

in determining when and how the strains were removed. Clean surfaces were then prepared from these by argon ion bombardment. It was, of course, necessary that all the stresses introduced by polishing were removed by the ion bombardment. This allowed the measurement of the amount, and depth, of the stress introduced into the polished surfaces.

To insure that no remanant stresses were left after the ion bombardment, similar polishing / ion bombarding procedures were carried out on the semiconducting substances germanium (Ge) and silicon (Si). These, although having the same diamond structure as InSb and GaSb, do not have any asymmetry in their opposite (111) faces. As such, these surfaces should not exhibit any natural stresses of their own. They were thus used in establishing under what experimental condition all of the stress due to the polishing was removed. This was done by monitoring the stress as a function of time of ion bombardment. These studies were then extended to the III - V compounds so that after ion bombardment of these, any measured stress was due to an intrinsic difference between the two surfaces. In this manner, it was possible to determine the amount and depth of the surface damage introduced during the polishing operation for the four crystal types.

The nature of this damage, and the means of removing the stresses introduced by it were also investigated by other means.

This included annealing the polished crystals for both the clean and real surfaces. This showed that some of the stress was removed by this annealing and, rather surprisingly, that for the four crystal types, relatively low (50 C) temperatures were necessary for this to occur. Elevated temperatures were found sufficient to remove all stresses in all cases.

Further information was obtained by the chemical thinning of polished crystals. In this, the stress introduced by the polishing operation was measured as a function of the crystal thickness.

Real, polished surfaces were also studied by electron paramagnetic resonance (e.p.r.). This was found capable of giving information which could be used in postulating models for the damaged region.

Finally, correlating all of these results with low energy electron diffraction (L.E.E.D.) surface measurements, calculations of surface energy based on some surface models were made for germanium, silicon and indium antimonide.

To conclude we may summarise the scope of this thesis.

- 1) To determine the effect and extent of surface damage on Ge, Si, InSb and GaSb, due to mechanical polishing and ion bombardment, and the effect of annealing on this damage.

- 2) To remove all surface damage from InSb and GaSb to produce clean surfaces, and to measure any stress difference arising out of the asymmetric surface structures.
- 3) To obtain supplementary information about the damage with e.p.r. measurements.
- 4) To correlate these results with L.E.E.D. and to postulate models for the damaged region and for the surface structures.

There are of course many other experimental methods available to give information about surfaces. These include electron microscopy, optical measurements and measurements of contact potential, field effects, photo-electric emission and Auger electron ejection. An excellent summary of these may be found elsewhere <sup>6)</sup> and will not be given in detail here.

## 1.2 THE ENERGY OF SURFACES.

### 1.2.1 INTRODUCTION.

In describing the energies associated with surfaces, many terms have been used often with contradicting or confusing meanings. To avoid this we define here the quantities used in this thesis.

#### 1.2.1.1 SURFACE TENSION.

The "Specific Surface Tension" is the work required to create unit area by a deformation or stretching of the original area.

1.2.1.2            SURFACE ENERGY.

The "Specific Surface Energy" or Surface Free Energy is the reversible work required to create unit area of surface by cleavage or fracture.

1.2.1.3            SURFACE STRESS.

The "Surface Stress" is the force / unit length in the plane of the surface.

1.2.1.4            ELASTIC STRAIN ENERGY.

The "Elastic Strain Energy" or Total Free Energy is the total energy stored in the bulk of the crystal by the application of a force. It can also be thought of as the total work done in changing the position vector  $r_i$  in

the bulk to  $(r_i + \delta r_i)$ .

1.2.2              THE DETERMINATION OF SURFACE STRESS AND SURFACE ENERGY OF SOLIDS.

A distinction should be made here first of all between the experimental determination of surface energy and of surface tension as it could be thought that these two quantities would be obtained in an identical manner.

Although the concept and measurement of surface tension and surface energy for liquids are well known, the case is not so for solids. As was pointed out by Gibbs <sup>7)</sup> these two quantities are identical for liquids but in the case of solids they may have opposite sign as well as differing in magnitude.

It may be easily shown that the relationship between them is given by:

$$E_s = S + A \frac{\partial S}{\partial A} \quad \text{E.1.1}$$

where  $E_s$  is the surface energy  
 $S$  the surface tension  
 and  $A$  the surface area.

In the case of liquids  $E_s$  and  $S$  are identical since the liquid film in the surface layer is maintained at constant density due to the mobility of the molecules, making

$$\left( \frac{\partial S}{\partial A} \right) (\text{Liquids}) = 0 \quad \text{E.1.2}$$

thus giving the equality between the surface energy and surface tension. This is not the case for solids.

A great deal of experimental<sup>8-13)</sup> and theoretical<sup>14-17)</sup> work has been done generally on the surface energy of solids. However, because of the nature of the present problem, this quantity is hard to measure. This is seen when considering some of the methods used in measuring surface energy.

Under usual circumstances the surface energy can be obtained in various ways. Some of these are briefly summarised below:

- 1) Neutral Drop Method. In this, the equilibrium shape of a liquid drop on the surface, is measured. The shape of the drop can then be related to the surface energy.
- 2) Zero Creep Method. In this case the forces acting on a molten crystal filament are balanced against gravitational forces.
- 3) Crystal Cleavage Method. Here a crack is propagated in a crystal by an externally applied force. The bulk dimension of the crystal and this force allows an estimation of the surface energy.
- 4) Dissolving powders Method. This measures the difference in the heat of solution on a powder and a bulk of the same material and the same mass.

A review on these methods and other similar methods may be found in reference 12).

It is seen that these could not be used here. For example, 1) would contaminate the surface

defeating the intended purpose. 2) and 4) would give an average surface energy, but would not enable a distinction between the A and B surfaces. By the definition of surface energy given, it would at first seem that 3) gives a direct measure of this quantity. However, because of the particular atomic structure of the 111 - V compounds, any cleavage of the (111) planes would result in both an A and a B surface being formed. Thus the measured energy would again be an average value.

The surface tension of solids is even more difficult to measure and little work has been done, and this has been mainly confined to inert gas crystals. <sup>18-20)</sup> Until very recently no work had been done to measure the surface tension difference in the 111 - V compounds.

Recently however, Hanneman, Finn and Gatos, <sup>21)</sup> and Finn and Gatos, <sup>22)</sup> have measured the surface tension of some (111) oriented 111 - V compounds by measuring the spontaneous bending of thin (10 microns) rectangular wafers. They reasoned that any difference in surface tension that exists between the A and B surface will cause the thin wafers to bend, with the surface having the greater stress becoming convex. With this reasoning, it becomes a matter of obtaining crystals sufficiently thin enough to be able to detect this difference. Experimentally this difference is then measured from the resulting radius of curvature of the crystal wafers.

For the case where this <sup>radius of</sup> curvature is large (small bending) compared to the thickness of the crystal, it may be shown from standard elasticity theory <sup>21,24,25)</sup> that for perfectly rectangular or for circular specimens

$$\Delta \sigma = \sigma_B - \sigma_A = Y_{(111)} \frac{t^2}{(1 - \nu)} R \quad \text{E.1.3}$$

where the A and B subscripts refer to the opposite faces,  $\sigma$  is the surface stress, R the net radius of curvature, t the thickness,  $\nu$  Poisson's ratio and  $Y_{(111)}$  the Young's modulus for the (111) direction which is given by:

$$Y_{(111)} = 6 (C_{11} + 2C_{12}) C_{44} / (4C_{44} + C_{11} + 2C_{12}) \quad \text{E.1.4}$$

where the C's are the elastic constants. <sup>26)</sup>

Thus this equation allows the determination of the required surface stress difference in terms of known constants and a measurable radius of curvature.

The results obtained by the above authors were then compared with the values calculated from a model of clean semiconducting 3 - 5 surfaces proposed by Cahn and Hanneman <sup>24)</sup> (see section 1.4.3.1). In the development of this model, Cahn and Hanneman <sup>24)</sup> used a qualitative picture of surface atom bonding first suggested by Gatos and Lavine <sup>23)</sup> (see section 1.4.4).

It is of interest to see how the experimental and theoretical values taken from the above agree. These values are compared in Table 1.T.1.

TABLE 1.T.1

<u>111 - V Compound</u>	<u>Thickness (Microns)</u>	<u>Radius of Curvature (cms)</u>	<u>Y (111) (dyne /cm<sup>2</sup>)</u>	<u>Measured <math>\sigma_B - \sigma_A</math> (average) (dyne/cm)</u>	<u>Calculated <math>\sigma_B - \sigma_A</math> (dyne/cm)</u>
InSb	8 - 13	100-200	9.71 X 10 <sup>11</sup>	1.13X10 <sup>3</sup>	0.9X10 <sup>3</sup>
GaSb	6 - 8	25-30	12.82 X 10 <sup>11</sup>	3.5X10 <sup>3</sup>	1.2X10 <sup>3</sup>
GaAs	10 - 25	6-30	17.48 X 10 <sup>11</sup>	5X10 <sup>4</sup>	1.5X10 <sup>3</sup>
InAs	15	5	12.43 X 10 <sup>11</sup>	9X10 <sup>4</sup>	1.0X10 <sup>3</sup>

Although there is some agreement between theory and experiment in the above table, several critical objections may be raised to the Cahn and Hanneman calculations, some of which have already been pointed out by these authors themselves (ref. 24, page 398). In constructing their model, they assume a clean surface, with an atomic surface arrangement as proposed by Gatos and Lavine.<sup>23)</sup> However their experimental surfaces were ones whose final treatment was a mechanical polishing operation. As has already been said, these would have little applications to clean surfaces. Hanneman<sup>27)</sup> has pointed out that the

resulting bending is probably due to a difference in the degree of damage between the two surfaces. Such differences might arise because of an intrinsic difference in the surface properties with regard to polishing. Such differences were reported by Gatos, Lavine and Warekois,<sup>28,29)</sup> who claim that the depth of damage extends more into the B rather than the A surface. Contradicting this, Pugh and Samuels<sup>30)</sup> claim that such an intrinsic difference is not observed. In this case the bending could simply result because of the impossibility of treating the two surfaces in an identical manner. A further objection to Cahn and Hanneman's work is their assumption of the Gatos model for the 3 - 5 compounds. As explained in section 1.4 this model is unable to account for the observed low energy electron diffraction results.

To date no experimental measurements of surface stresses for clean semiconductor surfaces have been reported.

In principle, the method used here for measuring the surface stress difference is the same as that above in as much as the bending of crystals is measured. It would be difficult in fact, to measure this quantity in such a direct manner by any other means. There are however several important differences.

To facilitate the fitting of experimental data to theory, circular rather than rectangular crystals were used. Further, an interferometric rather than a microscopic system was used to measure the radius of curvature, thus insuring greater accuracy. Most important of all however was that the circular specimens were placed in an ultra high vacuum system after polishing. They were then ion bombarded for sufficiently long time to remove any damage that could result by the polishing. Keeping the crystal in ultra high vacuum and annealing then insured a clean, <sup>ordered</sup> surface.

1.3

THE ELASTIC STRAIN ENERGY.

We have seen, E.1.3, that if the bending of the crystal is due to a stress difference between the two surfaces the quantities  $\Delta\sigma$ ,  $t$ , and  $R$  are related by:

$$\Delta\sigma \propto t^2 / R$$

i.e. for constant  $\Delta\sigma$ ,  $R$  varies as  $t^2$ .

On the other hand, it is of interest to determine the functional relationship between  $R$  and  $t$  if the elastic strain energy, rather than the surface stress is a constant for a given polishing operation.

Landau and Lifshitz <sup>31)</sup> show that for a deformed plate whose thickness is small compared with the dimensions in the other two directions, the E.S.E. is given by:

$$E.S.E = \frac{Yt^3}{24(1-\nu^2)} \iint \left[ \left( \frac{\partial^2 \xi}{\partial x^2} + \frac{\partial^2 \xi}{\partial y^2} \right)^2 + 2(1-\nu) \left[ \left( \frac{\partial^2 \xi}{\partial x^2} \right)^2 + \left( \frac{\partial^2 \xi}{\partial y^2} \right)^2 \right] \right] dx dy \quad E.1.5$$

where  $Y$ ,  $t$  and  $\nu$  have the same meaning as above and where  $\xi$  is the vertical displacement of the neutral or non stressed plane from the original undeformed surface.  $x$ ,  $y$  and  $z$  are the usual co-ordinates.

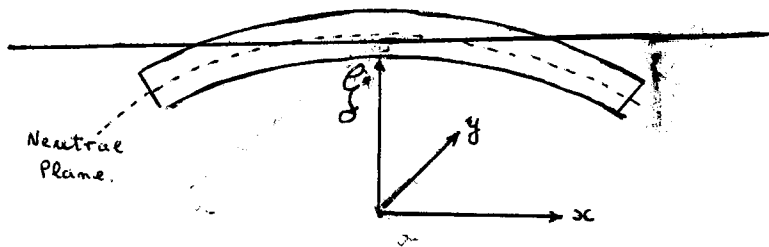


Figure 1.F.1. Showing the geometry of the bent plate.

If we now assume:

- a) The bending is spherical, i.e. defined by
- $$\frac{x^2}{R^2} + \frac{y^2}{R^2} + \frac{z^2}{R^2} = R^2$$
- b)  $\left| \frac{\partial \xi}{\partial z} \right|$  is small, i.e.  $R$  the radius of curvature large,

it is easy to show that the total E.S.E./unit area  $U$ , is given by:

$$U = \frac{Yt^3}{24R^2(1-\nu)} \quad E.1.6$$

Thus if the E.S.E./unit area is a constant for a particular polishing operation  $R$  will vary as  $t^{3/2}$ , differing from the above.

Chemical thinning of polished crystals will be used later on to determine which of these two relationships are applicable.

## 1.4

SURFACE MODELS.

## 1.4.1

INTRODUCTION.

The L.E.E.D. study of surfaces is by now an established technique and details may be found elsewhere. In particular several excellent articles<sup>32-36</sup> are available for a complete coverage in this field.

Briefly, electrons having the de Broglie wave length

$$\lambda = \frac{h}{p} = \sqrt{150.4 / V} \quad \overset{\circ}{\text{A}} \quad \text{E.1.7}$$

where  $h$  = Planck's constant

$p$  = electron momentum

$V$  = accelerating voltage

interact with the ordered structure of the surface giving rise to diffraction patterns. The structure of the surface may then be inferred from the "structure" of the diffraction pattern.

With most of the compounds of interest here, the diffraction patterns exhibit fractional order beams. These imply that the surface atoms have rearranged themselves, forming structures with larger unit cells than would be expected from the bulk. On the basis of these, various authors have suggested different models to account for the fractional order beams. Since surface structures are relevant to this thesis, a summary of the surface models for

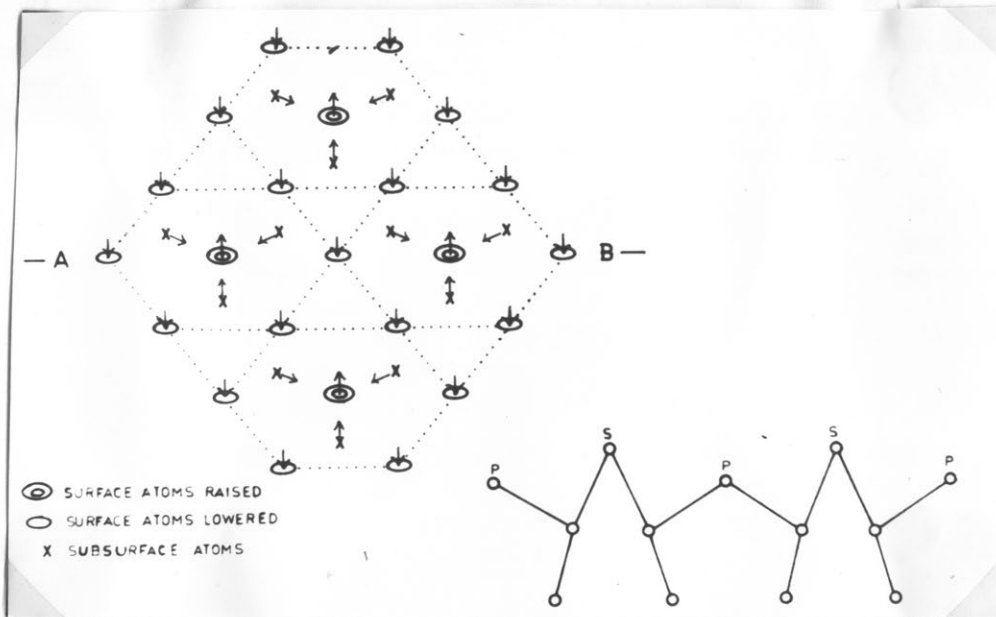


Figure 1.F.2

THE HANEMAN MODEL FOR THE GERMANIUM (111) SURFACE.

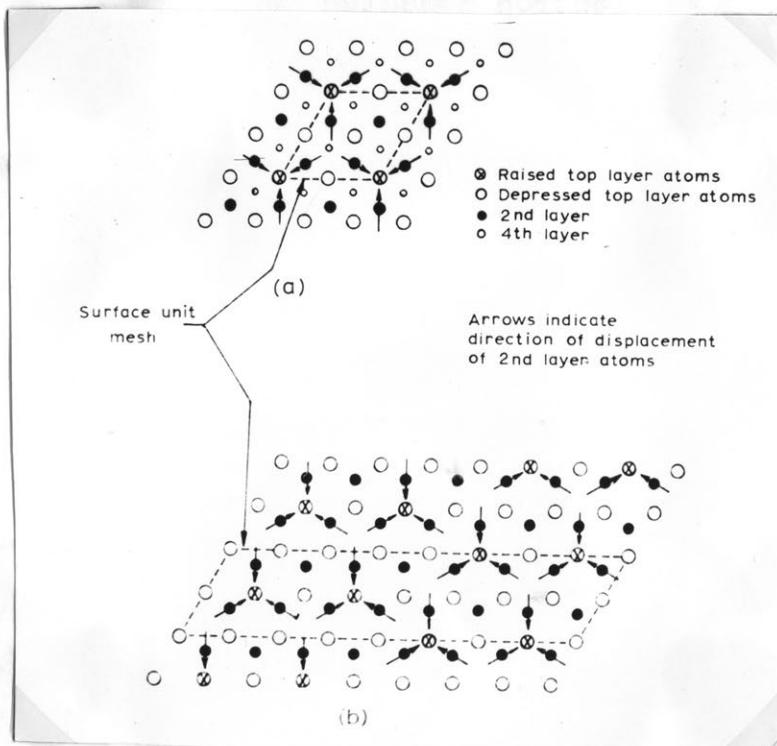


Figure 1.F.3

- a) THE GENERAL HANEMAN (111) SURFACE MODEL.  
 b) THE PALMBERG AND PERIA MODIFICATION.

the studied compounds will be given. References will be given to the experimental results and only a brief summary of the actual model will be given here. The models will be for "clean" or prepared surfaces (see Chapter 3,4) and for ideal or cleaved surfaces. The Gatos model for surfaces and its use by Cahn and Hanneman are also included.

#### 1.4.2 CLEAN SURFACE MODELS.

##### 1.4.2.1 THE HANEMAN MODELS.

##### 1.4.2.1.1 THE GENERAL (111) MODEL FOR III - V COMPOUNDS AND DIAMOND STRUCTURE SEMICONDUCTORS.

To account for the observed half integral order L.E.E.D. beams from clean (111) surfaces from certain diamond structure semiconductors, Haneman<sup>37,38)</sup> has proposed that in general, there is a "rumpling" of the surface which forces some atoms to be displaced upwards and some downwards from the normal surface position. The observed half integral beams can easily be obtained from this model if alternate atoms in alternate rows are raised and if the remaining surface atoms are lowered. See fig. 1.F.2,3.

Haneman concludes this, by considering the unpaired electron that results on the ideal formation of a surface. In the bulk, the four valency electrons for these materials have  $sp^3$  wave functions. On the surface however, only three are bonded, the fourth being a free or "dangling" surface electron. Assuming that this electron, because of the changed environment, becomes p type, then the surface

atoms would be pulled down since their bonds with the second layer would have more  $sp^2$  content, which have planer orbitals. The strain introduced by this "pulling down" can be relieved if certain surface atoms are forced upwards, which follows naturally if their dangling electrons become  $s$  type, so that the three bonds to second layer atoms, being now more  $p$  type, assume a smaller angle ( $90^\circ$ ) than before ( $109^\circ$ ).

#### 1.4.2.1.2 THE GERMANIUM (111) SURFACE MODEL.

This model is a particular case of that already mentioned in 1.4.2.1.1. Using the experimental intensity values obtained by Lander and Morrison,<sup>40)</sup> Hansen and Haneman<sup>39)</sup> have given values for the heights of the raised and lowered atoms of the rumpled surface. The "normal" spacing between the first and second layer is  $0.81 \text{ \AA}$ . In the rumpled surface, the raised and lowered atoms have a spacing of  $0.98 \text{ \AA}$  and  $0.68 \text{ \AA}$  respectively from the second layer, (fig. 1.F.2).

#### 1.4.2.2 THE LANDER AND MORRISON GERMANIUM (111) SURFACE MODEL.

Lander and Morrison<sup>40)</sup> explained their measured fractional order diffraction beams by suggesting a somewhat different model. In this, alternate atoms in alternate rows are completely removed. This conclusion was based on their experimental intensity values which indicated

to them, strong interference between atoms separated by  $4.06 \overset{\circ}{\text{A}}$  and weak interference for those separated by  $7.34 \overset{\circ}{\text{A}}$  at normal electron beam incidence. Their model is seen to explain this, in that the removal of the surface atoms "uncovers", for normal incidence, three out of four atoms at the  $4.05 \overset{\circ}{\text{A}}$  level and one at the  $7.34 \overset{\circ}{\text{A}}$  level. See fig. 1.F.4.

1.4.2.3

THE SEIWATZ MODEL FOR THE GERMANIUM (111) SURFACE.

41)

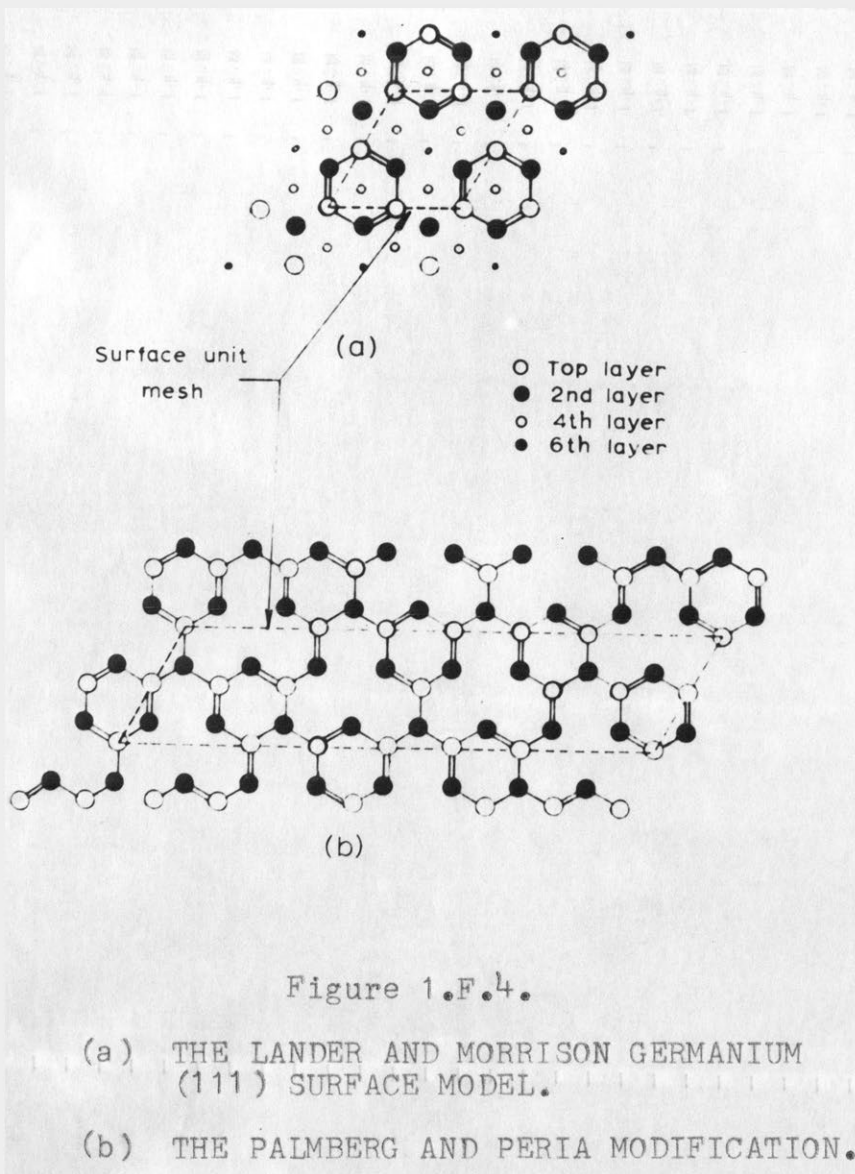
Seiwatz rearranges the surface by first placing on top of the original surface atom in the ideal state, another atom. Paired rows of these "new surface" atoms are then squeezed together until every surface atom has three nearest neighbours, two within the same top layer and the third with the second layer. The remaining fourth valency electron that results from this is now free to go into molecular orbit with the entire length of the "chain". This conclusion was based on empirical evidence involving the stability of this type of overlapping and the binding energies of homopolar diatomic molecules. It has also been possible to fit some of the fractional order beams using this model.

1.4.2.4

PALMBERG AND PERIA MODIFICATIONS TO THE HANEMAN AND THE LANDER AND MORRISON MODELS.

Inadequate ability to interpret L.E.E.D.

patterns makes unambiguous definite statements about



determinations of surface structures not possible at this stage. Further research will have to be carried out before this is possible.

36)

In a recent paper, Palmberg and Peria give L.E.E.D. results for germanium (111) surfaces, in which  $\frac{1}{2}$  order beams are observed. On the basis of this, they have modified both the Haneman and Lander and Morrison models, to give a possible account for this

This is shown in figures 1.F.3 and 1.F.4. They have been unable to rearrange the Seiwatz model to give this larger surface mesh. They conclude that of all the three surface structures proposed for the germanium (111) clean surface, "only that of Haneman is compatible" with their experimental results.

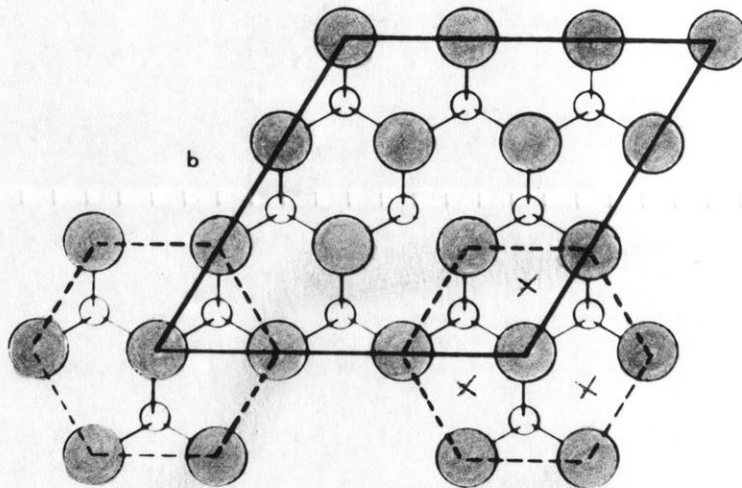
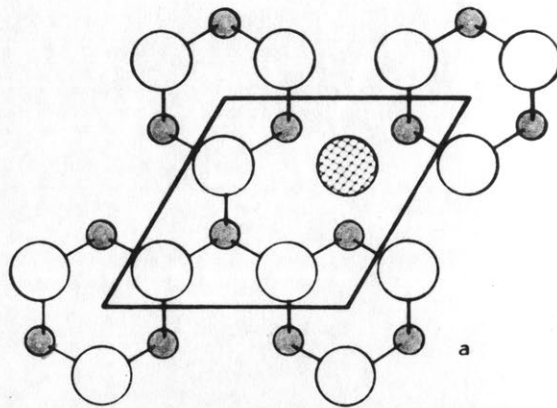
1.4.2.5

THE MACRAE GaAs and GaSb (111) SURFACE MODELS.  
42)

MacRae has obtained L.E.E.D. patterns from both the (111) and (111) surfaces of GaAs and GaSb. These gave  $\frac{1}{2}$  order beams from the A face and  $\frac{1}{3}$  order beams from the B face. An empirical model was then proposed for these two surfaces to account for the fractional order beams. MacRae suggests that the A surface of these compounds either has alternate atoms in alternate rows missing, or else that these have been replaced by the corresponding group V atoms. Thus referring to the figure 1.F.5 a) the atoms in the cross hatched position may be

Figure 1.F.5

THE MACRAE GaAs and GaSb (111) SURFACE MODEL.



OPEN CIRCLES - GROUP 3 ATOMS  
SHADED CIRCLES - GROUP 5 ATOMS  
LARGE CIRCLES - FIRST LAYER  
SMALL CIRCLES - SECOND LAYER

entirely missing or be made up of either arsenic or antimony atoms. This isomorphic replacement would then give a similar diffraction pattern as free group V atoms in this position. It is seen that in this case they would display  $\frac{1}{2}$  order beams.

The model for the B surface is even more speculative than that above. It is suggested that extra group V atoms could be located in symmetrical positions about the hexagons. Referring to figure 1.F.5 b) shows that if these atoms were placed in the positions marked by crosses they could yield  $\frac{1}{3}$  order spots. A detailed fit to diffracted beam intensities was not made with these models.

Similar work has not been carried out on InSb, but presumably, (because of the similarity), a similar model could be proposed.

#### 1.4.3

#### CLEAVED SURFACE MODELS.

An ideal (h k l) surface is defined as that which result if a crystal could be cut, or cleaved, through the (h k l) plane of the crystal without any distortion of the surface being caused during its formation. Because we are primarily concerned with clean surfaces the work done on cleaved surfaces is included here for completeness.

L.E.E.D. studies of cleaved (111) surfaces for silicon and germanium have been carried out by Lander,

Gobeli and Morrison.<sup>43</sup> On the basis of their diffraction results they suggest a model in which surface atoms are displaced in "paired rows". This displacement uncovers substrate atoms which were originally shadowed by the surface ones. These new atoms may then be used to account for some of the details in the diffraction results.

Miller<sup>44)</sup> in this laboratory has adapted the ruffled surface model to fit L.E.E.D. results for the cleaved (111) surface. This model assumes that (12) rows of surface layer atoms (indexed with respect to the rhombic unit cell of an undistorted (111) plane) are alternately raised and lowered with respect to their "normal" heights. Work is being carried out to check the validity of this model. Recent results in this laboratory suggest that a simple form of the ruffled surface model would account for cleaved Ge surface L.E.E.D. patterns.

Finally MacRae and Gobeli<sup>45)</sup> have given a model for the cleaved (110) surfaces of InSb, InAs, GaAs and GaSb based on L.E.E.D. measurements. As may be expected by now, their proposed surface structure is different from that which might be expected from the bulk. A detailed fit to diffracted beam intensities has not been achieved for any of the cleaved surface models.

1.4.4

THE GATOS MODEL FOR THE (111) SURFACES  
OF THE 111 - V COMPOUNDS.

This model was proposed by Gatos and Lavine<sup>23)</sup> on the basis of work carried out by them on the preferential etching characteristics between the two opposite (111) surfaces of some of the 111 - V compounds. They found that at lower temperatures the B surfaces etch at a much faster rate than the A surfaces, (at  $40^{\circ}\text{C}$  Rate B / Rate A = 10), showing that in the case of InSb, for example, the surface terminating with Sb atoms reacts much more than that with In atoms. It is then proposed that this arises because, on the surface, the B atoms are only triply bonded to the lattice, while they would normally have a valency of 5. The surface A atoms on the other hand would be less chemically reactive, since they would form a triple bond with the lattice, and, since they are normally trivalent, would not leave any unpaired electrons.

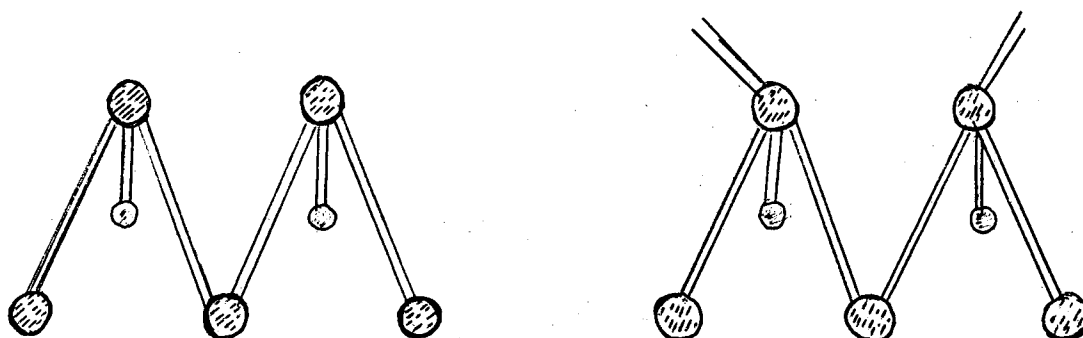
This is illustrated in figure 1.F.6.

It is seen that while this model may satisfactorily explain etching rates, which might, in any case, be entirely dependent on electronic rather than atomic configuration, it cannot account for any of the observed fractional order beams obtained with L.E.E.D. It is true that for the A surfaces the 3 valency electrons might form  $sp^2$  planer orbitals, which could then be "pulled down"

towards the bulk of the crystal. However since this would happen to all the surface atoms, it would result in the same structure, only closer to the second layer.

Figure 1.F.6

THE GATOS (111) SURFACE MODEL.



THE A SURFACE.

THE B SURFACE.

1.4.4.1

THE CAHN AND HANNEMAN CALCULATION.

Using, as a basis, the Gatos surface model, Cahn and Hanneman have calculated the surface stress difference between A and B surfaces.

They do this by first calculating, in terms of a first nearest neighbour stretching and bending force constant, the energy increase per unit volume of a deformed crystal. In this way they can relate these two force constants to the known bulk elastic constants. They

then calculate the energy required to stress the A and B surfaces in the (111) direction using these force constants. This requires the introduction of a quantity  $\Delta \xi$  which is given as the difference in radians between the normal angle for bonding of a surface atom, when trivalently bonded in a separate molecule, and the tetrahedral angle. This results in

$$\sigma_B - \sigma_A = C (\Delta \xi_A - \Delta \xi_B) \quad \text{E.1.8}$$

where C is a constant which depends on bulk constant of the crystal. It is from this equation that the calculated values for  $\sigma_B - \sigma_A$  table 1.T.1 are obtained.

1.5

#### ELECTRON PARAMAGNETIC RESONANCE STUDIES.

As stated above, L.E.E.D. studies are insufficient for determining unambiguously, the structures of certain semiconductor surfaces. This is primarily due to our incomplete knowledge of the mechanisms involved in the scattering of low energy electrons from surfaces. The proposed models for the surface structures have been fitted on a more or less trial basis, with the aim of fitting experimental results. That this is inadequate is clearly demonstrated, when we see how such entirely different models as the Lander and Morrison, and Haneman can be made to fit the same experimental data.

Electron paramagnetic resonance studies were carried out to give supplementary information, which could be related to the stress measurements. This may then be used to obtain a better understanding of the surface configuration.

We note that the various models suggested above for the surfaces, can be considered as belonging to two different categories. On the one hand there are those which incorporate dangling or free surface electrons, which would make them observable in paramagnetic resonance studies, such as the Haneman model, and on the other hand there are those which would have no free electrons. In the Lander and Morrison model, those atoms which according to Haneman would be raised, are removed altogether, allowing the remaining surface atoms to form double bonds with the atom in the second layer. Electron paramagnetic resonance is the ideal way of studying this difference, since it measures precisely any unpaired electrons. Measurements have been reported for clean silicon surfaces, where dangling bond densities of order of 20% and 2% of the surface atom density for cleaved and annealed surfaces respectively, were found.<sup>46)</sup>

Electron paramagnetic studies in the bulk of silicon have also been carried out.<sup>47,48)</sup> It is possible

using modern equipment to measure approximately  $10^{11}$   
unpaired electron spins per gauss of line width. This  
corresponds to a surface area of order  $10^{-3} \text{ cm}^2$  if we assume  
optimum conditions and that every surface atom has an  
unpaired electron giving 1 gauss line width. Using this  
technique information regarding correlation between the E.P.R.  
signal and stress measurements for silicon were obtained  
and the experimental results for this are given in Chapter 5.

CHAPTER 2.            PREPARATION OF CRYSTAL SURFACES.

2.1                    INTRODUCTION.

Experimentally, the preparation of the crystal surfaces required that real surfaces be produced by polishing, from which clean surfaces could be obtained by ion bombardment, continued until the mechanically damaged region was entirely sputtered away.

For the case of indium antimonide and gallium antimonide, it is further required that the A and B surfaces be identified.

Both of these requirements were achieved by adopting standard methods.

In the case of polishing, this involved the mounting of the crystals on flat stainless steel plates, and then grinding and polishing with powders of varying particle sizes. The methods outlined below resulted in a standardised polishing procedure which ensured reproducibility. The surface preparation was the same for all the four crystal types.

Distinguishing the A and B faces has been done by x-ray measurements.

Since the  $111 - V$  compounds crystallise in the zinc blende structure, they characteristically lack a centre of inversion symmetry. Consequently, the magnitudes of the two structure factors  $F(hkl)$  and  $F(\overline{hkl})$  are different. They may be measured by taking X-ray rocking

TABLE 2.T.1

<u>Crystal Type.</u>	<u>Manufacturer.</u>	<u>Crystal Purity.</u>
Ge (n type)	Sylvania Electric Inc. Pennsylvania.	1 to 3 ohm cm at room temperature.
Si (n type)	Merck Inc., U.S.A.	200 - 300 ohm cm at room temperature.
InSb (n type)	Mining & Chemical Products Ltd. England.	Donor concentration less than $5 \times 10^{14}$ /cc.
GaSb (p type)	Mining & Chemical Products Ltd. England.	Donor concentration less than $10^{16}$ /cc.

---

curves. In general, this method is time consuming and in some cases inconclusive. This is because the effect is small and because precise X-ray wavelengths have to be used. In the particular case of the III - V compounds however, the effect is enhanced because of their different surface composition making their observation possible. Having determined the face polarity in this way, it is then possible to correlate this with visible and unique surface features which are developed by chemical etching.

Warekois and Metzger<sup>1)</sup> have given the general theory for InSb, InAs, GaAs and GaSb, and have experimentally differentiated between the two (111) faces of InAs. The same has been done by White and Roth<sup>2)</sup> for GaAs.

Further correlation between chemical etching and X-ray data have been made by Faust and Sagar<sup>3)</sup> for InSb, InAs, GaSb and GaAs. Gatos and Lavine<sup>4,5)</sup> and Venables and Broudy<sup>6)</sup> have also correlated this with dislocation formation. In an excellent article Faust<sup>7)</sup> has given a complete list of etchants that may be used for the identification of many crystallographic faces of semi-conductors.

## 2.2 PREPARATION FOR POLISHING.

The crystals were all obtained commercially (see Table 2.T.1), and were all grown in the (111) direction. Their size was about 2 cms. long and 2 cms. in diameter.

A thin slab,  $1 - 1\frac{1}{2}$  mm. was cut from the main block using a wire saw. The crystals were then given a quick etch to remove the very coarse damage introduced during the cutting operation. The (111) orientation was maintained by taking Laue photographs and applying selective grinding. For reasons of identification of the surfaces, that will be seen later, the InSb was etched in CP<sup>4</sup> and CP<sup>4B</sup> reagents. These are standard reagents. CP<sup>4</sup> consists of Conc. HNO<sub>3</sub>, Conc. HF, and Glacial CH<sub>3</sub>COOH in the volume ratio 5 : 3 : 3. CP<sup>4B</sup> has an added volume ratio of 0.06 of Bromine. The GaSb crystals were always etched in Conc. HNO<sub>3</sub>, Conc. HCl, and H<sub>2</sub>O in the ratio 1 : 1 : 2. The main reason for etching at this and subsequent stages was to remove any surface damage or to chemically thin the crystals. Because it proved satisfactory, Ge and Si were also chemically etched with CP<sup>4</sup> and CP<sup>4B</sup> reagents.

One of the sides of the crystal was next ground on a glass flat using  $12\frac{1}{2}$  micron (white Al<sub>2</sub>O<sub>3</sub>) particles. This was done to ensure flatness of the crystal. This surface was then abraded with  $12\frac{1}{2}$  micron particles using a 40 - 7008 Buehler pad glued on an optical glass flat. It was now very heavily etched to make sure that no remanant abrasion damage remained. At this stage the crystal was about 0.25 m.m.thick. The treated surface was then mounted on a flat (to 2 microns) stainless steel plate with canada

balsam. Care was taken that a uniform, thin (2 - 8 microns) layer of canada balsam lay under the crystal so that control could be kept on the thickness of the crystal at all further stages. It is noted that great difficulties were experienced in etching the crystal uniformly. This was finally achieved by using the same principle for obtaining flatness as is used in the actual polishing operation.

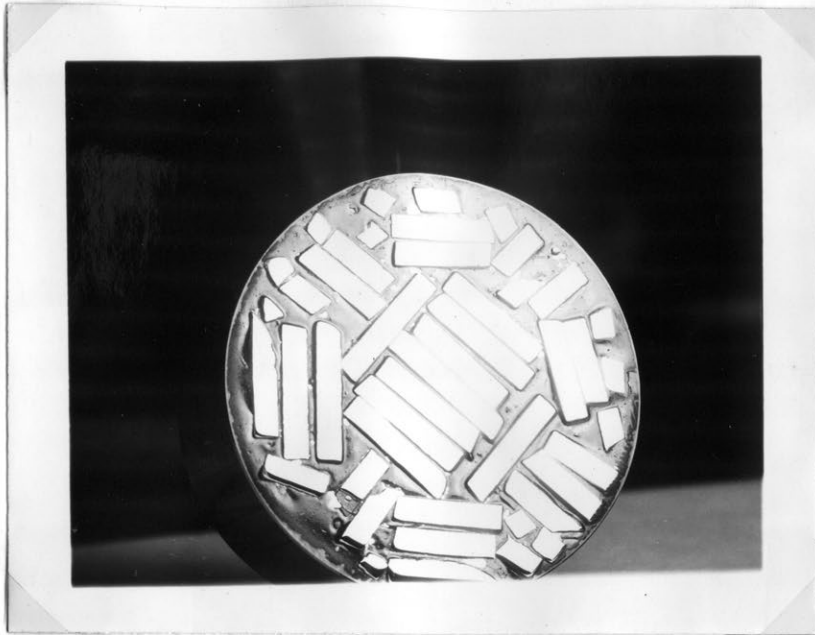
Drops of the etchant are placed on top of polythene etching pads. The etchant is then allowed to wet the crystal by placing the pad several m.m. from the crystal surface without actually touching the surface. The surface tension of the liquid acts so that an area of the surface is covered by the liquid which is approximately equal to the area of the pad. By moving the pad in the same manner as if polishing was being carried out, and thus the liquid moving across the surface in the same way, it has been possible, if time consuming, to obtain uniform etching over areas of 100 square m.m.

### 2.3

#### POLISHING OF THE CRYSTAL SURFACE.

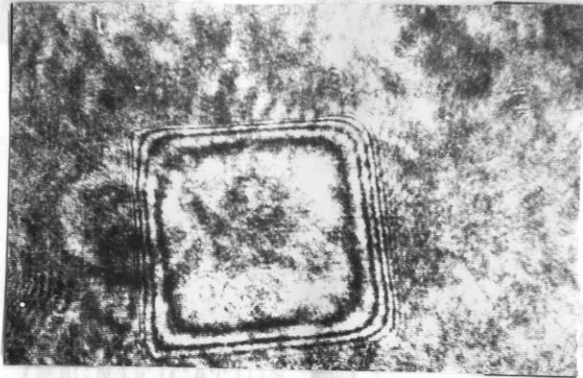
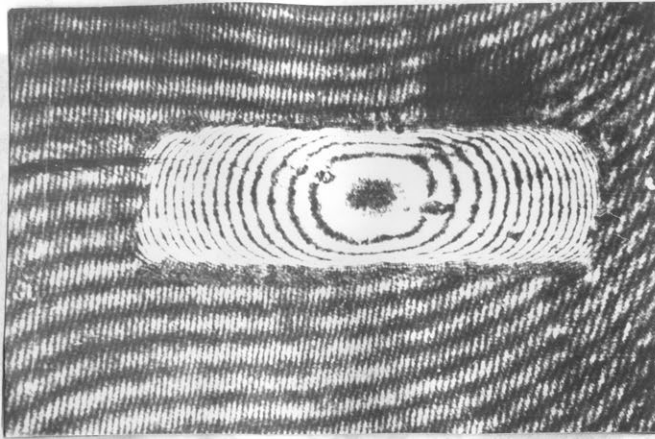
The type of polishing treatment was classified as type 1, (light) and type 2, (heavier). A crystal belongs to either of these classifications, depending on subsequent abrading before polishing.

In type 1 surfaces, the crystal, after having been mounted on the stainless steel block (crystal thickness 0.25 m.m.) is etched until it is about 70 - 130



PHOTOGRAPH 2.P.1.

THIS SHOWS MANY RECTANGULAR CRYSTALS MOUNTED ON STAINLESS STEEL WITH BLACK WAX, READY FOR POLISHING. (MAGNIFICATION X 1).



THIS SHOWS  
STAINLESS  
POLISHING.

ATED ON

PHOTOGRAPH 2.P.2.

AN INTERFERENCE PATTERN ACROSS THE POLISHED FACES OF  
A RECTANGULAR AND SQUARE CRYSTAL. THE FRINGES SHOW  
THE UNWANTED EDGE EFFECTS. (MAGNIFICATION X 6).

TABLE 2.T.2

MECHANICAL POLISHING TREATMENT FOR THE CRYSTAL SURFACES.

Type	1st.treatment after diamond saw.	2nd.treatment	3rd.treatment
1	CP4 (heavy)	$\frac{3}{4}$ micron diamond	
2A	25 micron (B O ) 2 3	$12\frac{1}{2}$ micron particles to remove 5 - 15 micron	$\frac{3}{4}$ micron particles to remove 15-25 micron
2B	" "	" "	" " " to remove 5 - 15 micron
2C	" "	" "	" " " to remove 5 micron

microns thick, and then polished with 0.25 micron diamond paste on a 40 - 7058 felt pad.

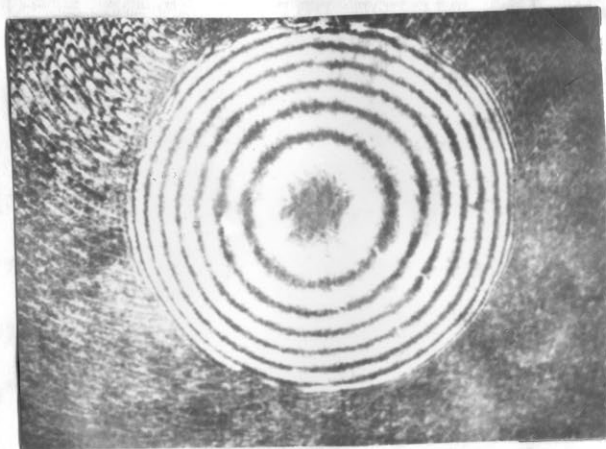
In type 2, a less safe, but more typical treatment was used. The 0.25 m.m. slab was thinned to 10 - 100 microns using 25 micron size grinding particles (B O ) on a Buehler pad. From 5 - 15 microns were then<sup>2 3</sup> removed with 12 $\frac{1}{2}$  micron particles on a 40 - 7008 pad. The final treatments determine the following sub-classification as in Table 2.T.2.

The amount removed in type 2C was just enough to be able to observe interference fringes on the polished surface. Clearly remanant damage from prior treatments would be absent in type 1 surfaces, and present in type 2 surfaces, least in 2A and most in 2C.

2.4

#### FORMATION OF CIRCULAR SPECIMENS.

At the onset of this study, the specimens were cut to the required form before the abrading / polishing operations described above were carried out. These generally were either rectangular or square in shape. Many of these were mounted together in the canada balsam as described above and were treated simultaneously. This procedure however, resulted in edge damage, which affected the fitting of results to theory. (See photographs 2.P.1,2). Better uniformity could be obtained by using circular crystals



PHOTOGRAPH 2.P.3.

THIS SHOWS A SLAB WITH CIRCULAR CRYSTALS CUT OUT OF IT. THE OTHER PHOTOGRAPH SHOWS THE INTERFERENCE PATTERN ACROSS ONE OF THE CIRCULAR CRYSTALS.

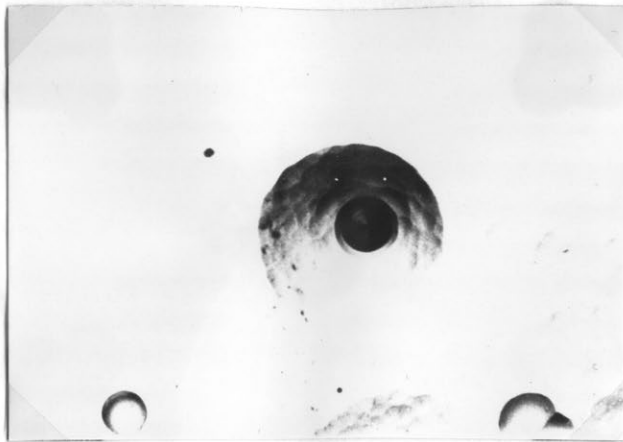
These crystals were obtained from the slabs in section 2.2 by first coating the now polished surface of the crystal with a cold solution of black wax dissolved in p-xylene ( $C_6H_4(CH_3)_2$ ). This was allowed to dry hard at room temperature. After hardening, a circle of the required diameter was impressed on the wax using a sharp edged tube. This impression went through the wax and exposed a narrow ring of the crystal. CP4B etch was continually run over the face of the coated crystal. In a matter of minutes, the underlying canada balsam was exposed. Both the balsam and wax were then removed with p-xylene and the circular crystals freed from the main slab. (See photographs 2.P.3).

#### 2.5 POLISHING BOTH SIDES OF THE CRYSTAL SURFACES.

In some of the early stages, and particularly with germanium and indium antimonide, both sides of the crystals were polished. In this case, type 2A operation was carried out until the crystal was about 200 - 250 microns thick. The canada balsam was then dissolved and the crystal remounted with the polished face downwards. A type 2A operation was then carried out until the crystal reached a thickness of 10 - 30 microns.

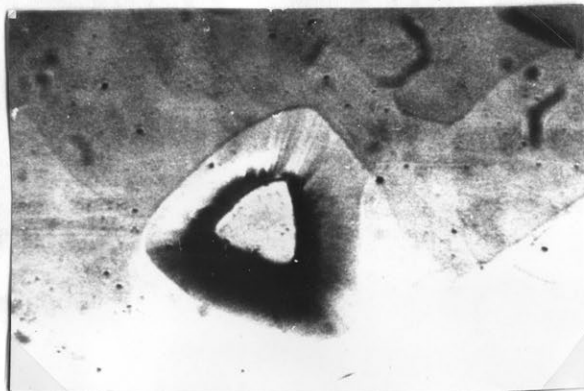
#### 2.6 IDENTIFICATION OF THE 111 - V FACES.

Resulting from the correlation of X-ray measurements with surface features developed during chemical etching, it has been found that, in general, etch pits form only on the surface containing group 111 atoms.



PHOTOGRAPH 2.P.4.

THE INDIUM FACE OF InSb WITH CHARACTERISTIC  
CIRCULAR PIT. (MAGNIFICATION X 500).



PHOTOGRAPH 2.P.5.

THE GALLIUM FACE OF GaSb WITH CHARACTERISTIC  
TRIANGULAR PIT. (MAGNIFICATION X 500).

In particular, the indium face of indium antimonide develops characteristic pits, photograph 2.P.4 when etched with CP<sup>4</sup>B reagent, and the gallium face in gallium antimonide develops characteristic triangles, photograph 2.P.5 when etched with the reagent specified above. This was the method adopted for distinguishing these surfaces.

2.7

FINAL PREPARATION OF CRYSTAL FOR  
EXPERIMENTATION.

The final polishing operation with either type 1 or type 2 crystals is carried out on specimens of thickness 70 - 100 microns. All of the experiments performed (Chapter 4) requires that the final crystal thickness be 10 - 20 microns. The final step in the crystal preparation is therefore to reduce the circular polished crystal to this thickness.

A film of soft black wax dissolved at room temperature in p-xylene is painted on a glass slide. The circular crystal is then gently placed on the wax with the polished face touching the wax. Care is taken so that no wax covers the unpolished surface. When the wax has dried, the unpolished face is etched in the same manner as described above. This thinning is continued until the crystal reaches the required thickness.

The black wax is then dissolved in p-xylene. The crystal is removed, washed with clean p-xylene, and then

with acetone. At this stage it is ready for experimentation.

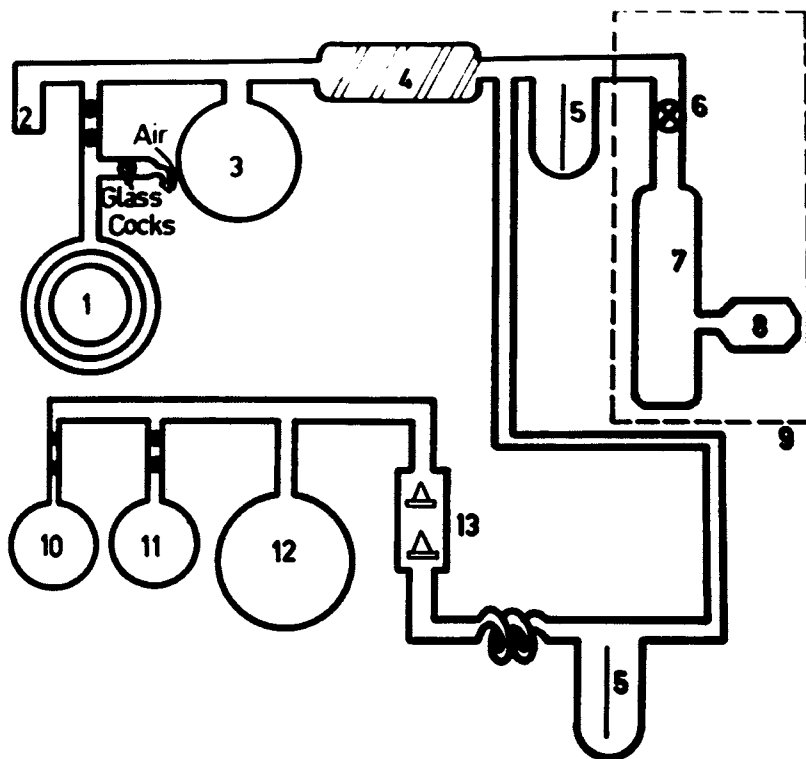
## CHAPTER 3. EXPERIMENTAL ARRANGEMENT.

### 3.0 INTRODUCTION.

Having obtained real surfaces by polishing, it is now necessary to obtain clean surfaces from these. This requires setting up an ultra high vacuum system, so that ion bombardment can be carried out and to maintain the clean surface once it is formed.

It is also necessary that any curvature of the crystal resulting from the surface stress difference be measured, while the crystal is inside the vacuum system. Hence there is a three fold experimental requirement.

- 1) An ultra high vacuum ( $<10^{-9}$  torr) is required to be able to form and maintain a clean surface.
- 2) A method is necessary to form an atomically clean surface.
- 3) Means are required to measure the curvature of the crystal surface.



**LEGEND**

- 1. Backing Pump
- 2.  $P_2O_5$  Water Trap
- 3. Backing Pump volume - 5litres
- 4. Three stage Diffusion Pump
- 5. Liquid Nitrogen Cold Traps
- 6. Bakeable Granville Phillips Valve
- 7. Operating Chamber
- 8. 8 L/S Vacuum Pump
- 9. Oven
- 10. } Spectroscopically pure argon
- 11. } Spectroscopically pure oxygen
- 12. Expansion volume - 5litres
- 13. Double magnetically operated glass valve

Figure 3.F.1.

THE VACUUM SYSTEM.

### 3.1. THE VACUUM SYSTEM.

This consisted of a backing pump, a three stage glass diffusion pump and an 8 litres / sec. getter ion, ("Vacion" brand). The working chamber was separated from the backing and diffusion pump by a liquid nitrogen cold trap. Facilities were available to introduce various gases into the main chamber via a Granville Phillips bakeable valve. The whole system was baked using 3000 watts of power, figure 3.F.1. This was sufficient for the glass to reach 400 C and giving an ultimate pressure of  $< 10^{-9}$  torr. A comprehensive study in vacuum techniques may be found in Dushman.<sup>1)</sup>

### 3.2 FORMATION OF THE CLEAN SURFACE BY ION BOMBARDMENT.

#### 3.2.1 INTRODUCTION.

Formation of atomically clean surfaces by ion bombardment is by now a well known and tried procedure, and one of the most widely used for producing clean surfaces.<sup>2-6)</sup> In the present case the crystal to be ion bombarded was placed on a molybdenum block, which was made negative with respect to earth. Spectroscopically pure argon was leaked into the working chamber to a pressure of  $10^{-4} - 10^{-3}$  torr. The gas was ionised using an electron gun with the filament as the source of the electrons. These were accelerated to the grid held at + 25 volts. This

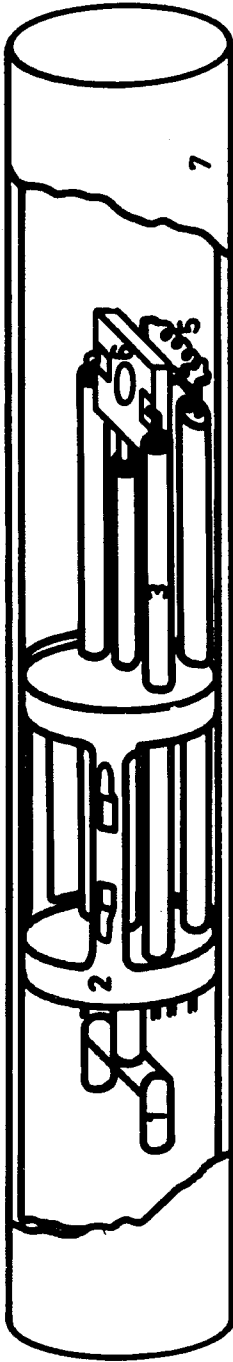


Figure 3.F.2.

THE CRYSTAL HOLDER ASSEMBLY.

LEGEND

1. Molybdenum rod
2. Spring loaded cage
3. Shielded wires
4. Thermocouple
5. Heating filament
6. Molybdenum support block with dummy and circular crystals
7. Glass tubing

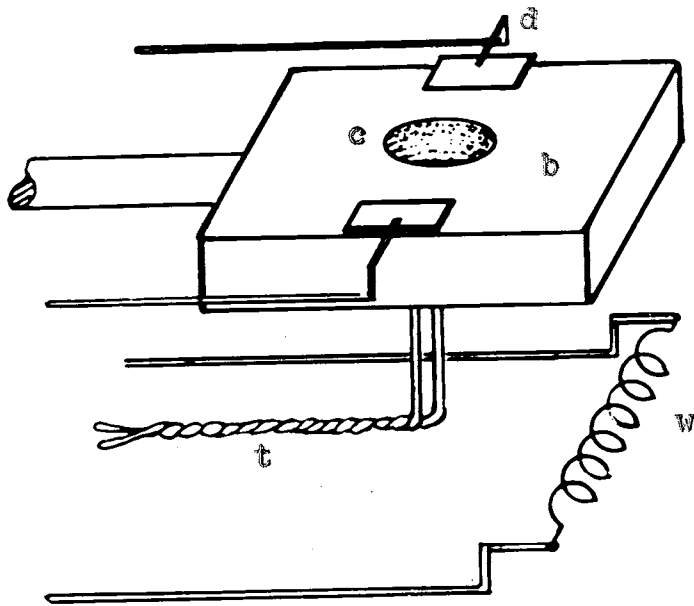


Figure 3.F.3

THE CRYSTAL HOLDER WITH DUMMIES  
SHOWING:

- b) molybdenum block.
- c) circular crystal.
- d) rectangular dummy.
- t) thermocouple.
- w) heating filament.

voltage is such that only 1% doubly ionised argon ions are formed.<sup>7,8)</sup> The operating current of the grid was 15 - 20 ma. The holder was kept at -500 volts with the total current to holder plus crystal being  $100 \mu\text{A} / \text{cm}^2$ .

### 3.2.2 THE CRYSTAL HOLDER.

This consisted of a stable molybdenum block 5 x 20 x 4 mm. supported by a molybdenum rod and held tight inside the glass tube by a spring loaded molybdenum cage. Shielded wires running from the block carried filament current, thermocouple current, as well as dummy crystal current (see below). The shielding was necessary to prevent any sputter deposits from building up and resputtering onto the crystal. A diagram of the crystal holder assembly is given in figure 3.F.2.

### 3.2.3 THE DUMMY CRYSTALS.

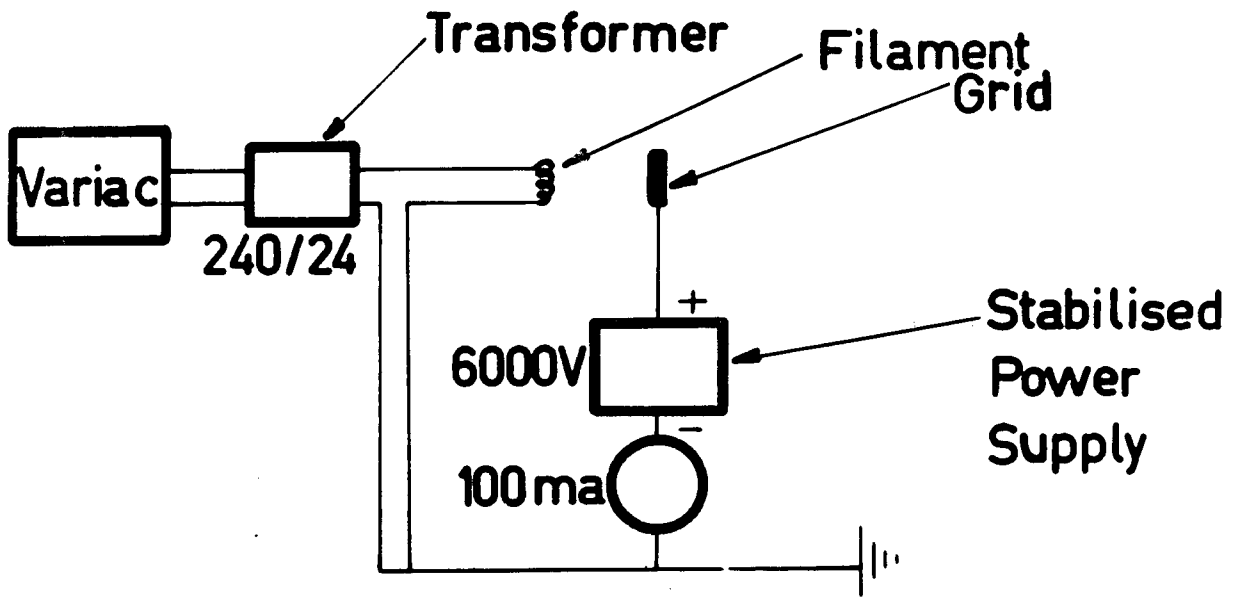
Direct measurement of the current to the circular specimens proved to be impracticable since any leads which were attached to the crystal resulted in distorting the thin (10 - 20 microns) crystal. Current was finally measured by flanking the crystal with two dummies of the same cross sectional area as that of the crystal. The dummies were supported by insulated nickel wires about 0.5 mm. from the crystal holder. See diagram 3.F.3. In this way the current to the dummies indicated the ion current

reaching those areas of the block during ion bombardment and hence its distribution (uniform) from which the current to the crystal was obtained without attempting to provide it with a separate connection.

### 3.2.4 THE ION GUN AND ELECTRICAL CONNECTIONS.

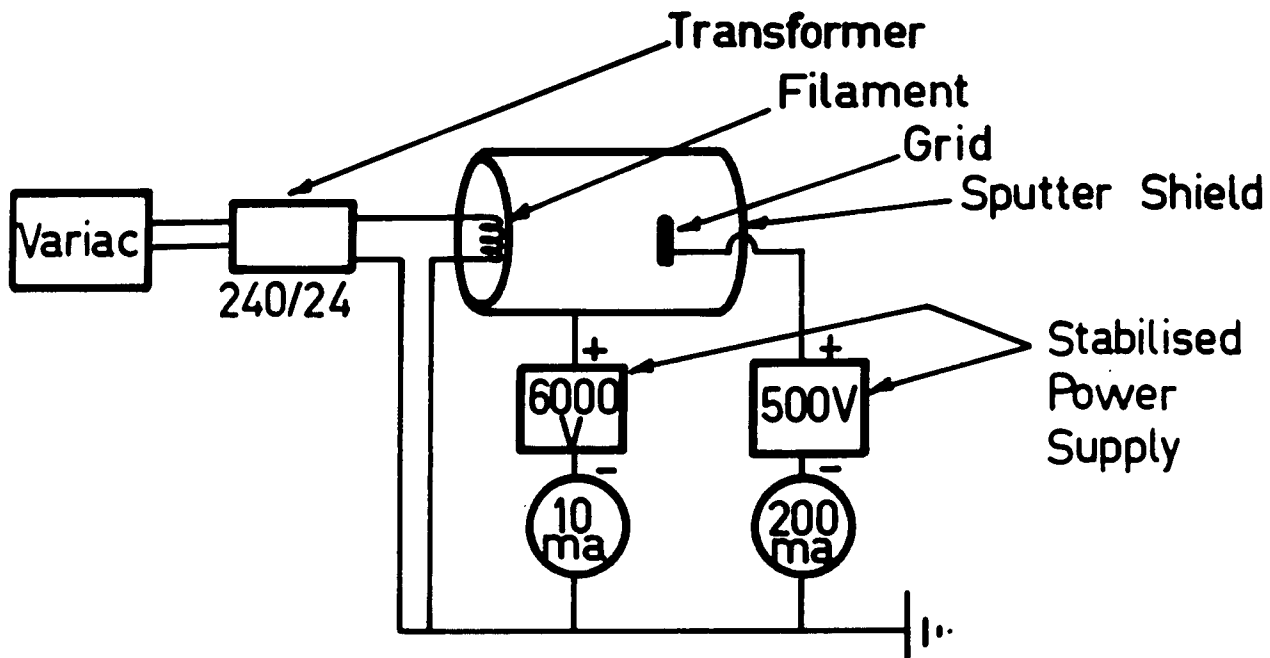
The ion gun is of a standard design for this laboratory and is shown in figure 3.F.4. It consists of a tungsten filament (f), a grid of molybdenum sheet (g) and molybdenum mesh (m). This is surrounded by molybdenum cyclinder (C). The assembly is supported by nickel wires (n).

This construction has been adopted to prevent resputtering onto the crystal. It has been found <sup>9)</sup> that material sputtered from the crystal face by ion bombardment, deposits on the glass tube in the vicinity of the crystal. This material becomes negatively charged from the electrons coming from the filament and can then be sputtered back onto the crystal. The molybdenum cyclinder (C) prevents this resputtering by collecting stray electrons during the ion bombardment.



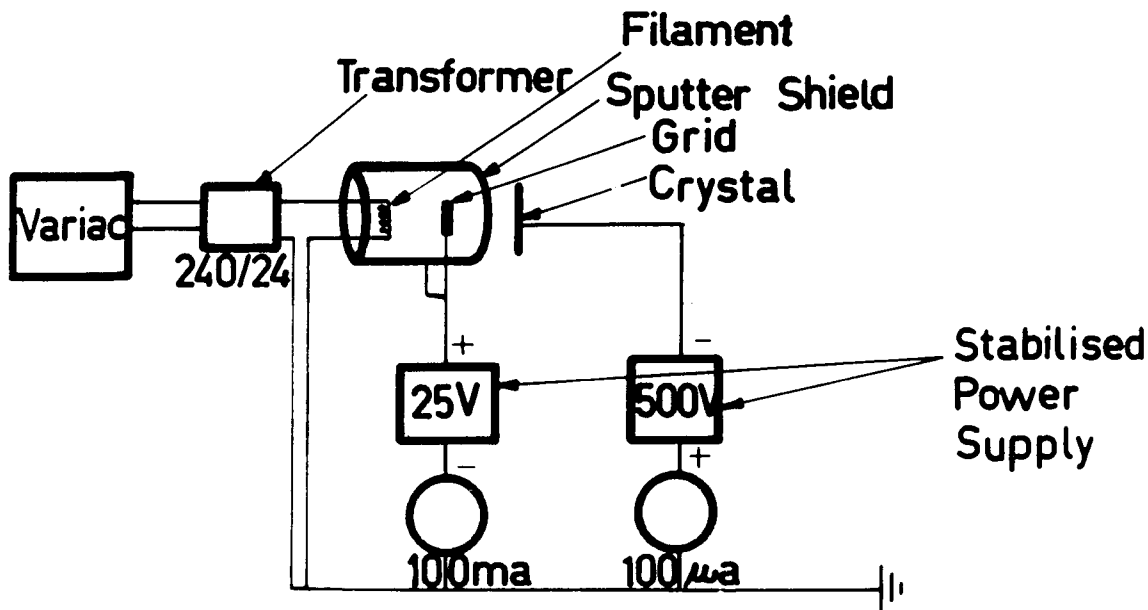
**GRID OUTGAS CIRCUIT**

Figure 3.F.5.



## SPUTTER SHIELD OUTGAS CIRCUIT

Figure 3.F.6.



### ION BOMBARDMENT CIRCUIT

Figure 3.F.7.

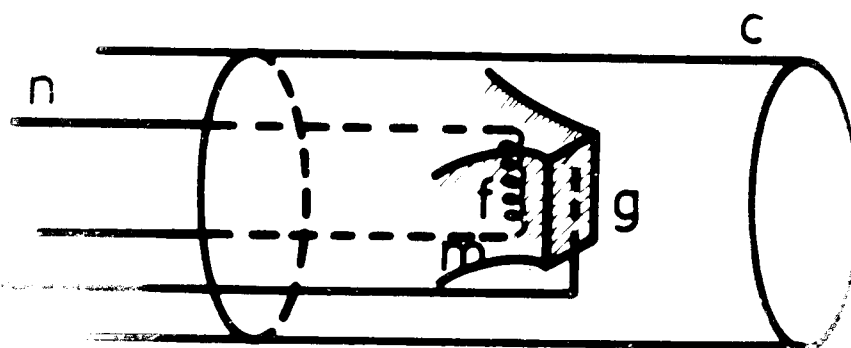


Figure 3.F.4. THE ION GUN.

The electrical connections for outgassing the grid and the sputter shield and for ion bombardment are given in figures 3.F.5, 6, 7.

### 3.3 MEASUREMENT OF RADIUS OF CURVATURE - THE LASER INTERFEROMETER.

#### 3.3.1 INTRODUCTION.

The radius of curvature was measured by obtaining an interference pattern of the polished crystal surface with a standard reference flat placed outside the vacuum system. The relative large spacing (10 cms.) between the crystal and reference flat necessitated the use of a highly monochromatic and coherent light source. In the present case, a helium - neon gas laser was used ( $\lambda = 6328\overset{\circ}{\text{A}}$ ). The use of an interferometric method over ordinary microscopic techniques has the advantages of being able to

continually monitor the radius of curvature as well as providing increased sensitivity.

### 3.3.2 THE LASER INTERFEROMETER.

It was necessary in carrying out the present work that an atomically clean surface be produced and maintained under ultra - high - vacuum conditions. It is also essential that the radius of curvature (R) be measured under these conditions. Hanneman, Finn and Gatos<sup>10)</sup> and Haneman<sup>11)</sup> have in the past measured the sagitta by focusing a microscope through an optical window onto the crystal and refocusing while moving the microscope along the length of the crystal. This was not adopted here for two main reasons.

a) Under high magnification, it was found impossible to focus on the edge of the crystal to an accuracy better than 1 micron. (As determined by multi - readings). This is compared with the maximum obtainable accuracy with a light microscope of 0.2 microns.<sup>12)</sup>

b) Since the objective length of a high power microscope (X1000) is very small, the crystal and holder would necessarily need to be very close to the glass tubing enclosing them. Because part of the present study deals with ion bombarding the crystal surface, it was felt that difficulties would be encountered in successfully ion bombarding the crystal without introducing stray fields due to the surroundings charging up.

In setting up the interferometer, great use was made of some of the work of Tolansky<sup>13)</sup> and of Heavens.<sup>14)</sup>

### 3.3.2.1 THE LIGHT SOURCE.

When obtaining fringes between two surfaces, the maximum distance by which the two surfaces can be separated and interference patterns still observed, is known as the coherence length of the light source used. (In the case of a split beam interferometer, such as the Michelson Morley type, the fringes will be distinct if the optical paths of the two interfering beams are equal within the coherence length).

The coherence length  $L_c$  is shown by Born and Woolf<sup>18)</sup> to be equal to

$$L_c = (\bar{\lambda}_0)^2 / \Delta\lambda_0 \quad \text{E.3.1}$$

where  $L_c$  = Coherence length

$\bar{\lambda}_0$  = Mean wavelength of source

$\Delta\lambda_0$  = Total wavelength range about the mean

and may be described as the average length of a single wave train.

The early work was carried out using Sodium ( $\lambda = 5894 \overset{\circ}{\text{A}}$ ) and Thallium ( $\lambda = 5350 \overset{\circ}{\text{A}}$ ) discharge tubes as light sources. Owing to the measured small coherence length of these sources ( $< \frac{1}{4}$  mm), the reference flat would

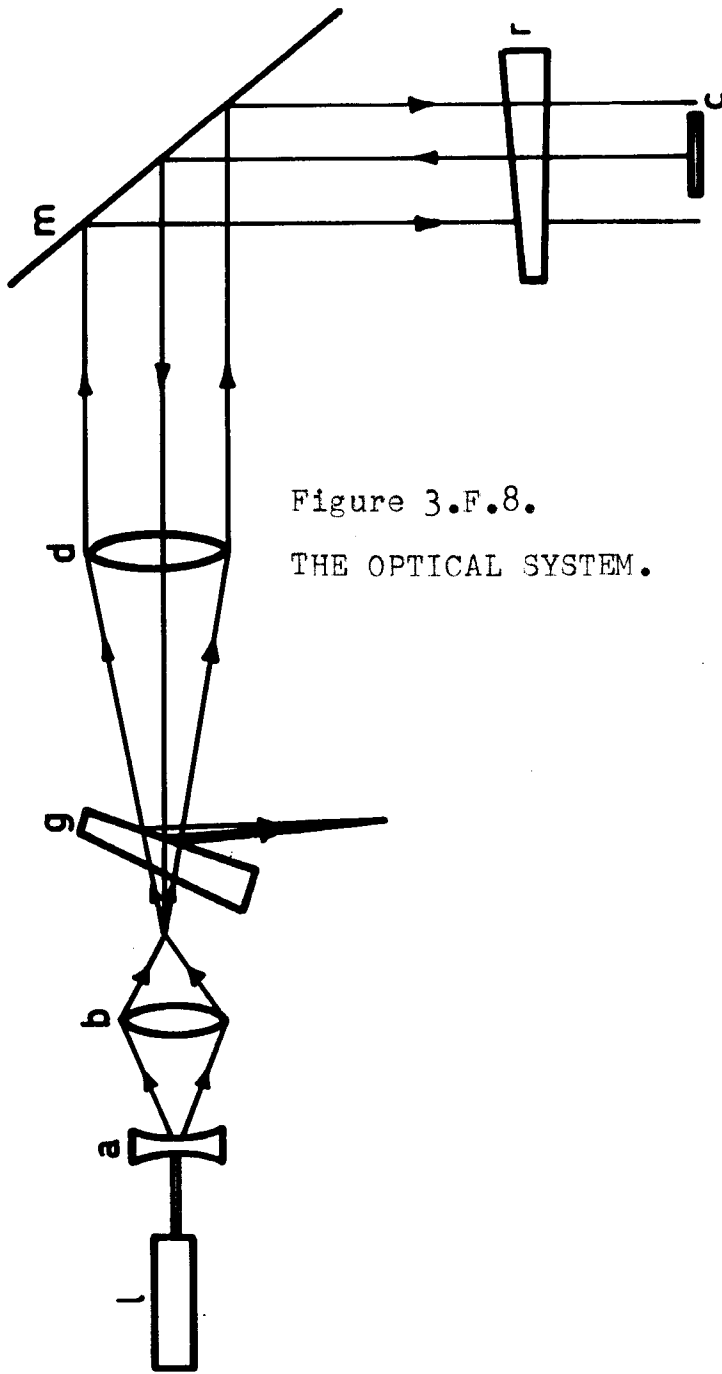


Figure 3.F.8.  
THE OPTICAL SYSTEM.

necessarily have to be this close to the crystal. Apart from the technical difficulties of lining up such a system while inside the vacuum system, the same problems would be encountered as mentioned in 3.3.2b. Added to this, the reference plate would be subjected to many of the same perturbations as the crystal, for example bakeout, and could consequently not remain constant.

A high pressure mercury vapour lamp with  $L_c = 8$  cms. was tried but was not intense enough for the purpose.

In the final arrangement, a helium - neon gas laser supplied by S.O.L.A. Adelaide,  $\lambda = 6328 \overset{\circ}{\text{A}}$  was used. The coherence length of this has not been measured but is certainly greater than several metres and most likely of the order of kilometres.

### 3.3.2.2 OPTICAL CONSTRUCTION OF INTERFEROMETER.

The optical system adopted for the interferometer is shown in figure 3.F.8 where:

- l is the He-Ne laser
- a a diverging lens
- b an objective lens
- d a collimating lens
- g a 50% reflecting titanium coated plate
- m multilayered 99.9% reflecting mirror at  $6328 \overset{\circ}{\text{A}}$
- r reference flat with bottom surface 50% reflecting
- c crystal

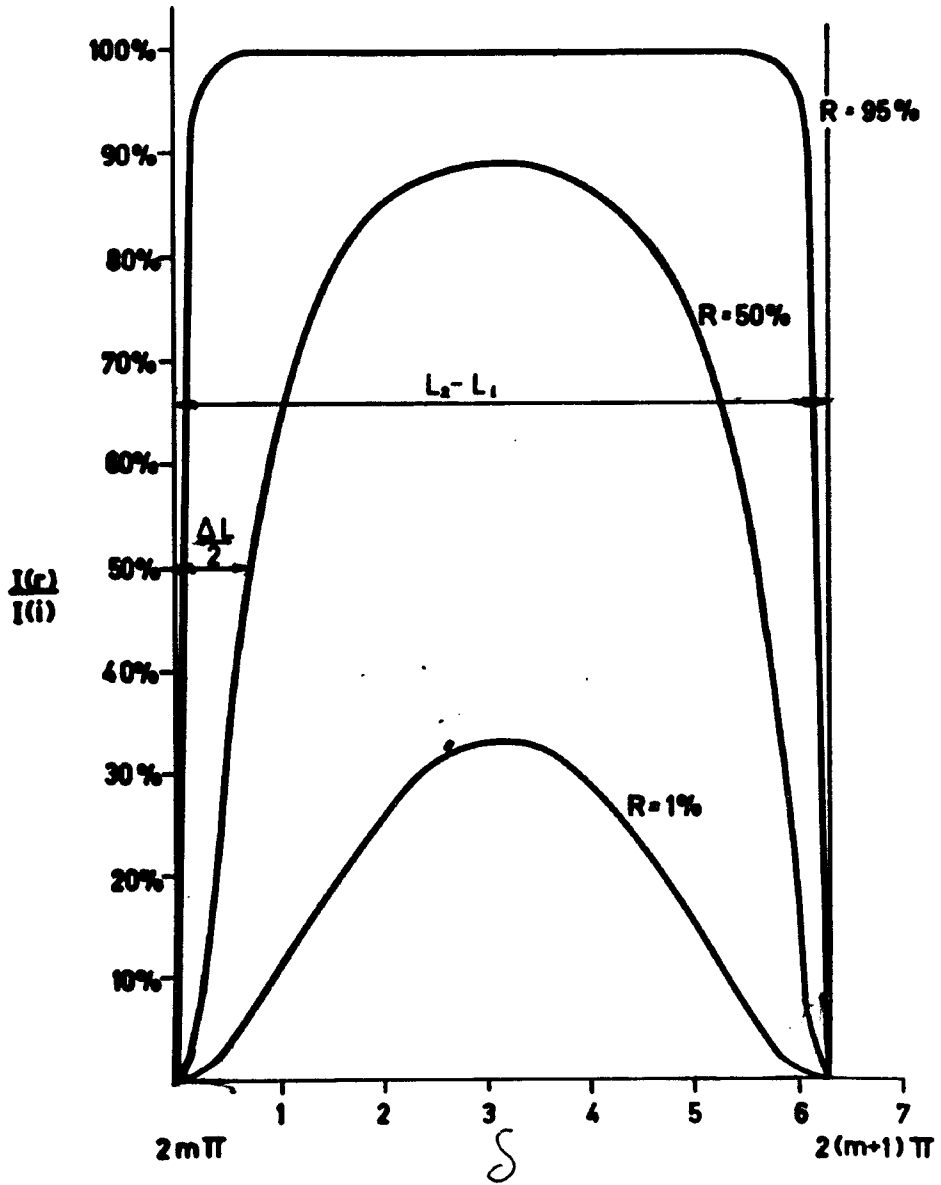


Figure 3.F.9.

(See page opposite).

In this figure we note that both the 50% reflecting mirrors and the reference flat have been tapered. This has been done to eliminate unwanted fringes formed between these surfaces, and with any other part of the optical system, as a consequence of the long coherence length. It was found impracticable to use a conventional pinhole as this resulted in diffraction rings being formed. Instead a strong objective lens b was used.

### 3.3.2.3 SENSITIVITY.

The factor determining the accuracy of measurement in such an interferometer is governed by the absolute and relative reflectivities of the two surfaces concerned. If the two surfaces have the same reflectivity  $R$  then the ratio of the reflected intensity  $I(r)$  to the incident intensity  $I(i)$  is given by <sup>15,16,17)</sup>

$$\frac{I(r)}{I(i)} = \frac{F \sin^2 (\delta/2)}{1 + F \sin^2 (\delta/2)} \quad \text{E.3.2}$$

where  $F = 4R / (1-R)^2$  and  $\delta$  is the phase difference.

This function is drawn in figure 3.F.9 for three different ratios of  $R$ , 1%, 50% and 99%.

Under experimental conditions the reflectivities of the titanium coating and the crystal surface were approximately equal to 50%. This gives, according to the graph, for 50% reflectivity the ratio:

$$\frac{\Delta L}{L_2 - L_1} = \frac{1}{5} \quad \text{E.3.3}$$

where  $L_2 - L_1$  is the measured distance between two fringes.

The expression for the radius of curvature for a crystal with spherical symmetry is given by:

$$R = k (L_2^2 - L_1^2) \quad \text{E.3.4}$$

where  $k$  is a scaling constant.

The measuring uncertainty is at most  $\Delta L$  for both  $L_2$  and  $L_1$ . Therefore the maximum error in  $R$  is given by:

$$\frac{\Delta R}{R} = 40 \times \frac{L_2 - L_1}{L_2 + L_1} \% \quad \text{E.3.5}$$

Experimentally  $\Delta L / (L_2 - L_1) > L_2 - L_1 / (L_2 + L_1)$   
Therefore the percentage error in  $R$  is at most 10% for all measured radii of curvature in this work.

### 3.3.2.4 THE WORKING CHAMBER.

This consists of a pyrex glass tube 3 cms. in internal diameter and 0.5 metres long. At the centre of tube two side arms are attached, one for the ion gun and the other for an optical flat viewing window. Resting on the glass is an aluminium stand which is used to hold the adjustable reference flat. The complete arrangement may be

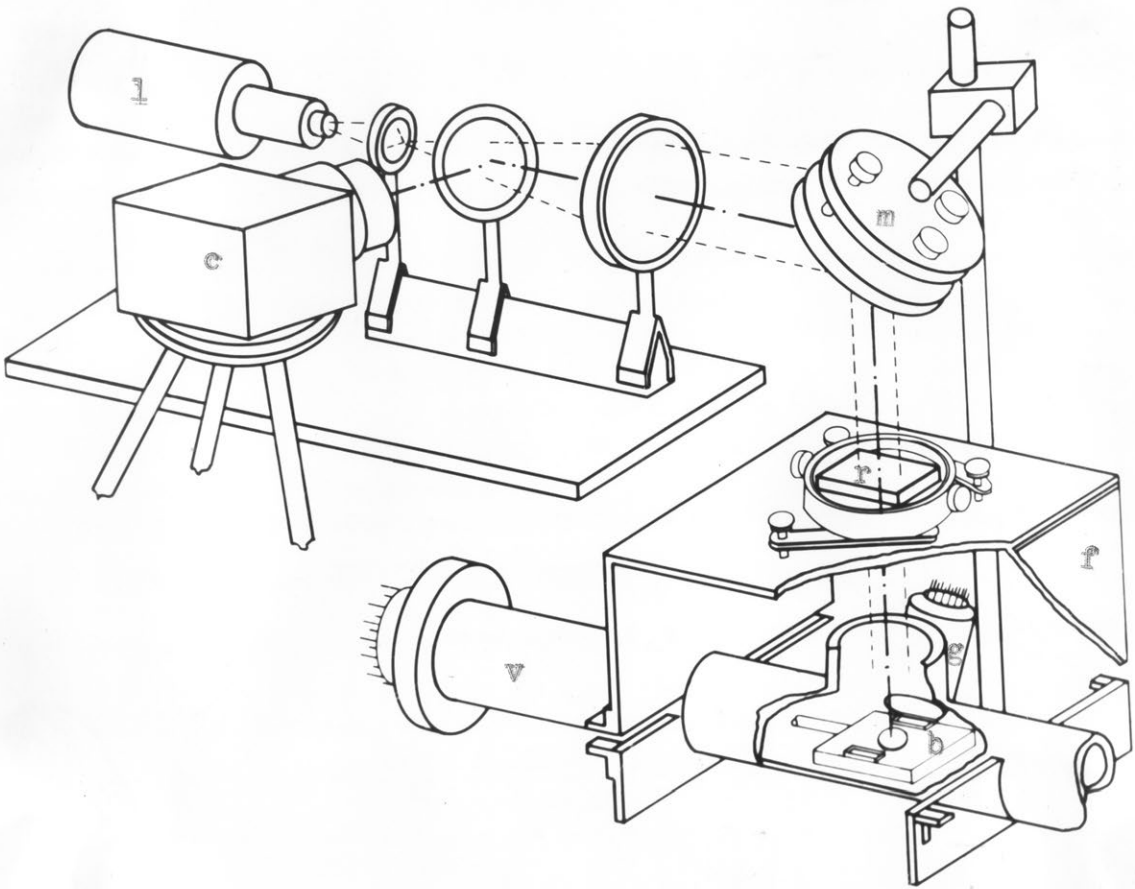


Figure 3.F.10 THE WORKING CHAMBER.

- 1) He-Ne laser.
- m) adjustable mirror.
- r) adjustable reference surface.
- b) molybdenum block with circular crystal and rectangular dummies.
- f) supporting frame.
- g) ion gun.
- v) vacuum tube.
- c) camera.

seen in figure 3.F.10. Although it is not clear from this figure, the geometry of the ion gun (g) is such that the ion beam is at near normal incidence to the crystal surface.

### 3.4 EXPERIMENTAL PROCEDURE.

#### 3.4.1 INTRODUCTION.

After the crystal was placed on the molybdenum support block and gently pushed under the viewing window, adjustments of the reflecting mirror m in figure 3.F.10 were made so that the crystal could be viewed through the camera C. In some cases the whole system including the crystal was baked out while in others the crystal was always kept at room temperature. After the ion gun was outgassed thermal and ion bombardment experiments were carried out.

#### 3.4.2 THE BAKED AND UNBAKED SYSTEMS.

##### 3.4.2.1 THE BAKED SYSTEM.

Bakeout of the system followed standard procedures. After removing the Vacion pump and opening the bakeable valve, the backing pump was switched on. When the system reached  $10^{-3}$  -  $10^{-4}$  torr, the diffusion pump was switched on and after a further half hour, the liquid nitrogen refrigerant applied to the trap. Heaters were switched on for overnight bakeout with the final temperature of the glass reaching  $200 - 230^{\circ}\text{C}$ . With the heaters still on, the liquid nitrogen refrigerant was lowered from the trap, and then, after 20 minutes, replaced.

The heaters were then switched off and while the glass was still hot, the oven raised and Vacion pump switched on. After another 24 hours pumping, the pressure reached  $10^{-9}$  torr.

### 3.4.2.2 THE "UNBAKED" SYSTEM.

In the case where the system was not baked, the procedure followed was identical to that above, up to the point before the oven heaters were switched on. At this point, however, heating tape was wound on all parts of the working chamber with the exception of the immediate vicinity of the crystal. Tape current was controlled to give a glass temperature of  $200^{\circ}\text{C}$  as measured by thermocouples. This was generally continued for four hours. Heating tape was also placed around the Vacion pump. A further 24 hours pumping after this was sufficient to reduce the pressure to below  $10^{-8}$  torr.

### 3.4.3 MEASUREMENT OF CURVATURE AS A FUNCTION OF TEMPERATURE.

#### 3.4.3.1 CALIBRATION OF TEMPERATURE.

The temperature of the crystal was measured by a thermocouple inserted in a small hole drilled in the bottom of the molybdenum block.

To insure that this was in fact the true reading of the crystal, calibration tests were carried out.

Two gold wires were contacted to a thin circular crystal surface of n type germanium, resistivity

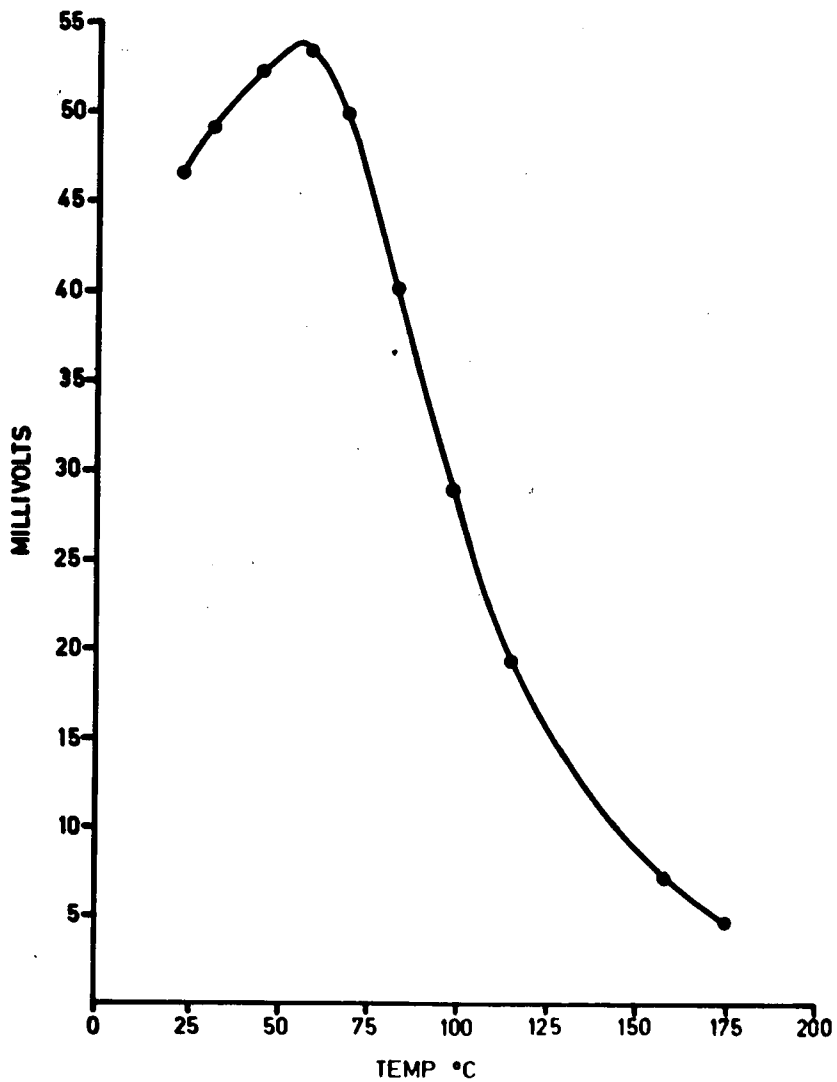


Figure 3.F.12

POTENTIAL CALIBRATION CURVE.

THE ORDINATE MEASURED IN MILLIVOLTS IS PROPORTIONAL TO THE RESISTANCE OF THE CRYSTAL.

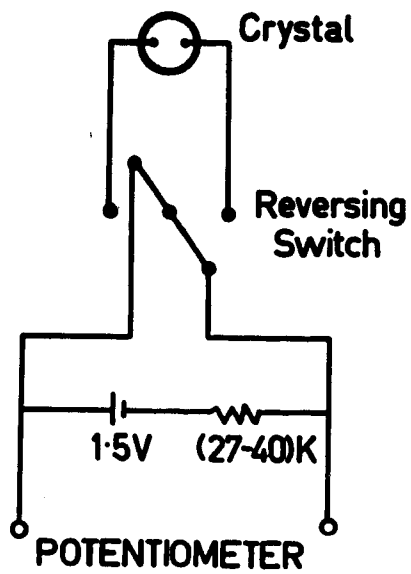
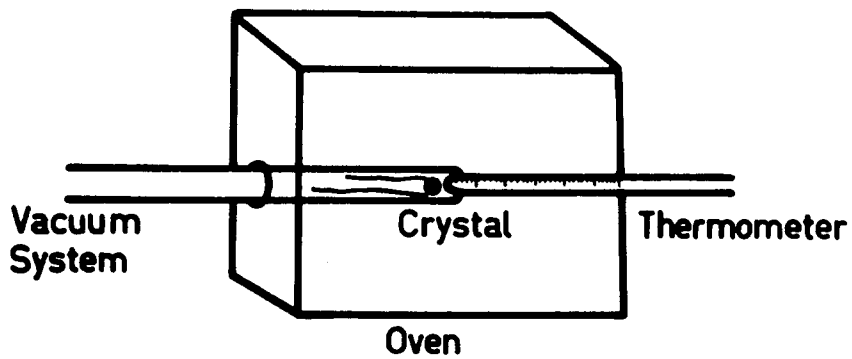


Figure 3.F.11.

TEMPERATURE CALIBRATION EQUIPMENT.

3- $\Omega$ cm., by first alloying the germanium with a gold - antimony alloy ( 0.6 % Sb.). The gold contacts were then alloyed to this at a temperature of 300 - 400 C.

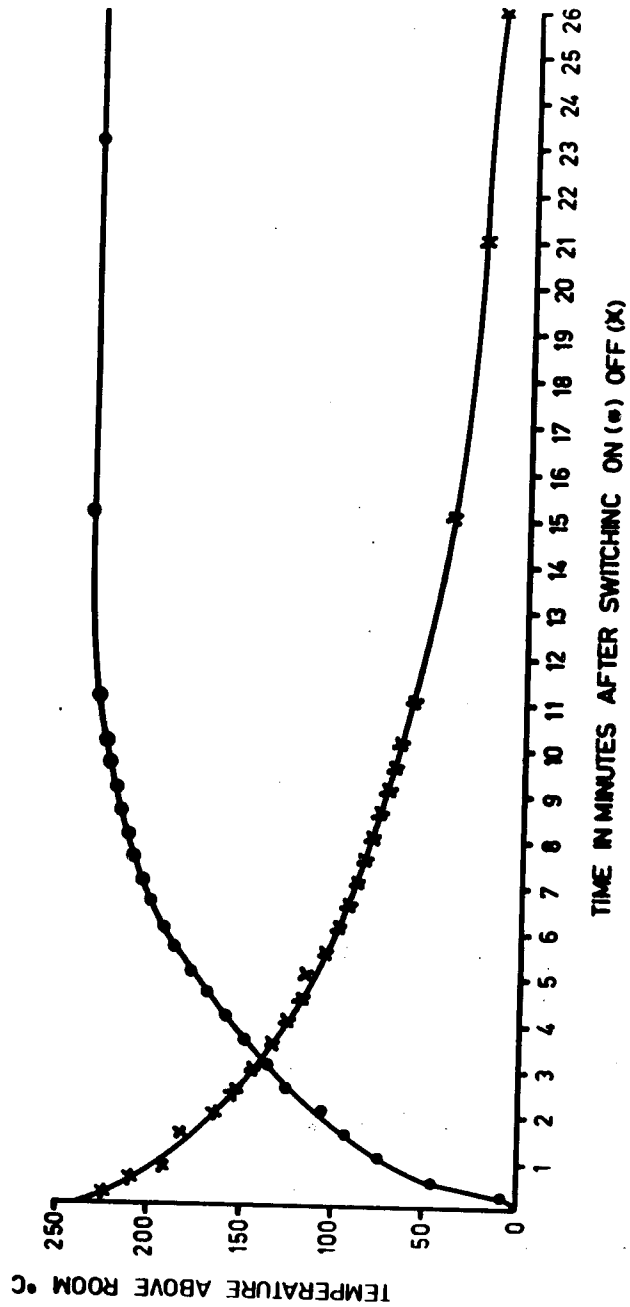
This crystal was then inserted in a vacuum system which was enclosed by an accurately controlled oven. The temperature of the oven was governed with a variac. Approximately one hour was given after a new variac setting to allow the oven to reach thermal equilibrium. The temperature of the crystal was measured by placing a thermometer very close to it, into the reentrant end of the tube outside the vacuum system, figure 3.F.11. The crystal was supplied with a small constant current. By measuring the potential, which is proportional to the resistance of the crystal, a graph could be obtained showing the resistance across the crystal as a function of temperature. Subsequent temperatures of this crystal could then be established by measuring its resistance. The curves obtained, followed that generally expected for these types of crystals <sup>19)</sup> and one particular curve is shown in 3.F.12.

The same crystal was then taken out of this system and placed in the working chamber in the same configuration as when taking actual readings.

Heating of the crystal was achieved by a 500 watt. variac controlled, focused projection lamp placed either on the side of the vacuum tube (direct heating) or

Figure 3.F.14.

TEMPERATURE OF CRYSTAL WHEN DIRECTLY HEATED AS A FUNCTION OF TIME.



- A=Equal gradient line
- B= Direct heating of block and crystal
- C= Direct heating - crystal not touching
- D= Heating bottom of block - crystal touching
- E= Heating of bottom of block - crystal not touching

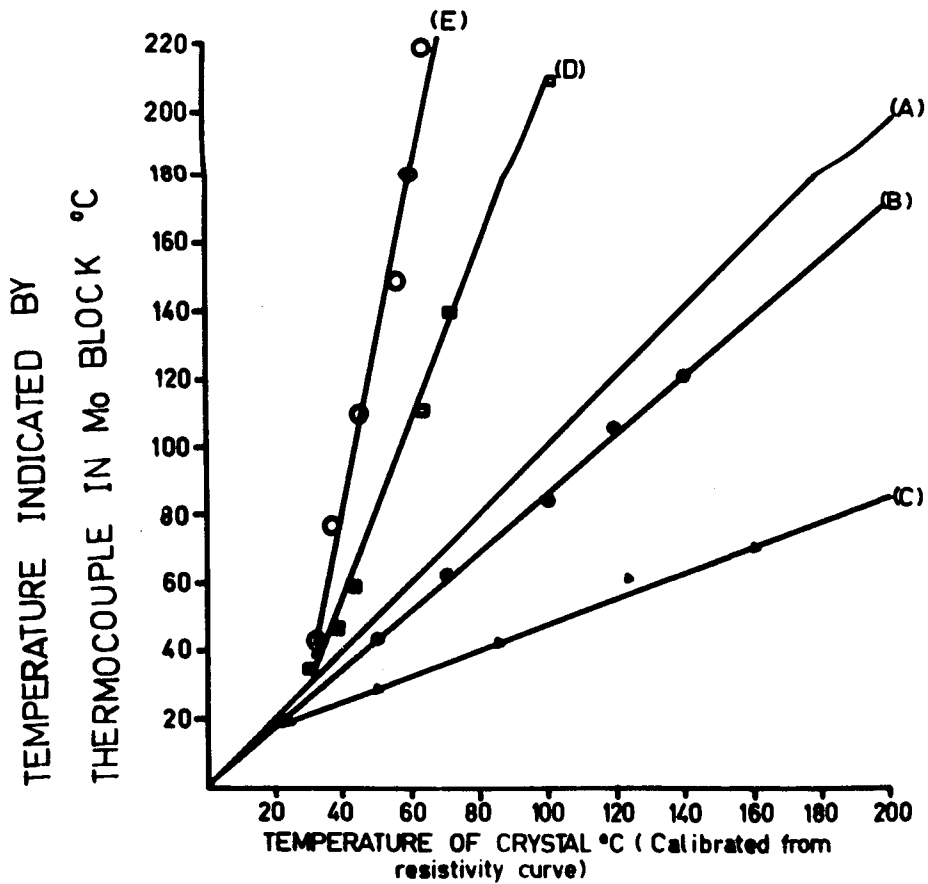


Figure 3.F.13.

CRYSTAL TEMPERATURE CALIBRATION.

underneath the tube (indirect heating). Two positions of the crystal were tried for comparison, in one case the crystal firmly resting on the supporting block (as would be the case under normal conditions), and the second with the crystal not touching the block, this being achieved by the natural springiness of the gold wires. The temperature of the block was measured with the thermocouple and that of the crystal by comparing the voltage with the calibration curve 3.F.12. By varying the power of the lamp, a series of curves were obtained showing the temperature of the molybdenum block as a function of the temperature of the crystal. A typical result is shown in 3.F.13.

It is seen that direct heating gives the closest fit to the equal gradient line. All further annealing was carried out in this way and any subsequent temperatures quoted for the crystals have been corrected.

Equilibrium temperature by direct heating was obtained after approximately 10 minutes, seen in figure 3.F.14, although in general 15 to 20 minutes was given.

#### 3.4.3.2 R VERSUS TEMPERATURE.

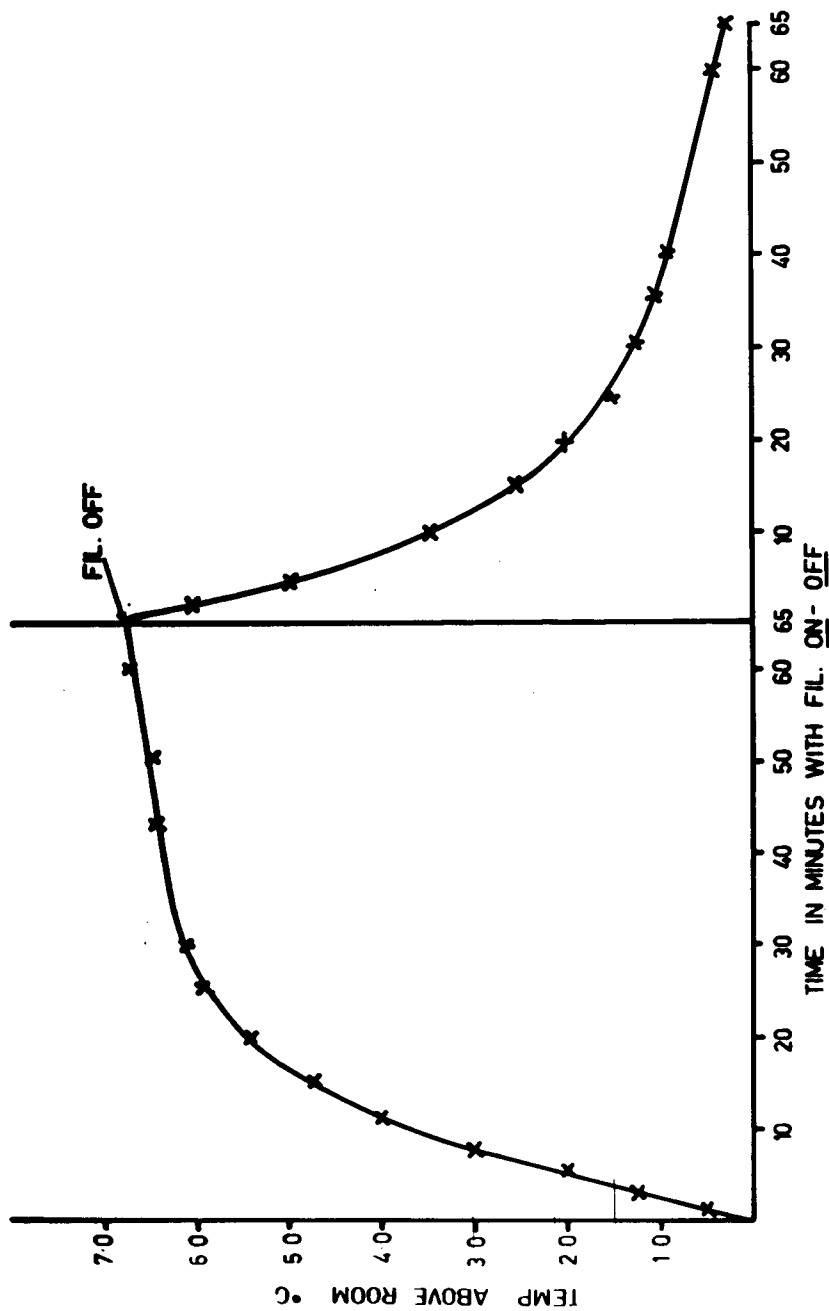
Some measurements concerned the effect of annealing on the radius of curvature.

With the crystal in view and pressures  $< 10$  torr the variac was set at a given voltage.

In the initial stages of heating the fringes

Figure 3.F.15.

TEMPERATURE OF CRYSTAL DUE TO  
FILAMENT BEING SWITCHED ON.



were observed to vibrate quite rapidly making dynamic measurement difficult. This however stopped when equilibrium temperature was reached. The crystal was then allowed to cool down and when ambient temperature was reached, a photograph taken. This cycle is repeated to give an R versus temperature curve.

#### 3.4.3.3 MEASUREMENT OF R AS A FUNCTION OF ION BOMBARDMENT.

Again with the crystal in view, argon was leaked into the system. Filament current was varied to give the required crystal current. During ion bombardment the crystal tended to vibrate slightly but this did not impede observing any changes that occurred. After the specified time of ion bombardment (as measured by a stop watch), and allowing about 15 minutes for stabilisation, (the hot filament was sufficient to raise the temperature of the crystal  $6^{\circ}\text{C}$ , as shown in 3.F.15), photographs were taken. This process was repeated up to the required time of ion bombardment. If the effect of gases on the clean, ion bombarded surface was required, these could be introduced in any of the above stages.

#### 3.4.3.4 MEASUREMENT OF R AS A FUNCTION OF THICKNESS.

These measurements were made in air, and were obtained in the manner described in section 2.7. The flat crystals (70 - 100 microns) were mounted on the wax with the

polished face downwards. After drying, the required amount was removed by etching. The wax was then dissolved with p-xylene, the crystal washed, and the radius of curvature measured. This was repeated as necessary.

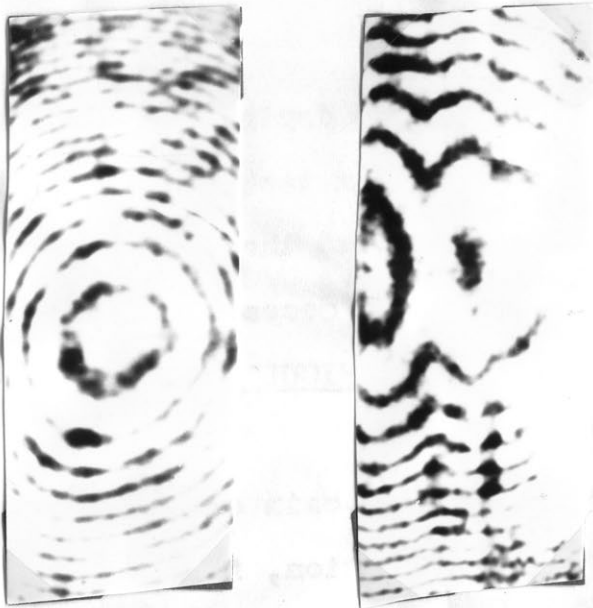
### 3.5 EXPERIMENTAL DIFFICULTIES.

#### 3.5.1 INTRODUCTION.

There were three main experimental difficulties encountered; vibration, ion focussing and crystal stability. These were either eliminated or diminished to a degree sufficient for experimentation.

#### 3.5.2 VIBRATION.

Since the interference fringes are obtained over a relatively large distance, any vibration caused either by a general building movement, or localised disturbances such as rotary pumps, caused the fringes to become blurry and made measurements impossible. Several methods were attempted to overcome this. These included supporting the whole vacuum system and interferometer assembly from fine wires to remove low frequency vibrations, to resting the whole system in a powder base to remove the high frequency vibrations. Finally a simple and yet effective method that was adopted, was to lay a metal sheet underneath the entire assembly. Underneath this sheet were placed eight rubber inner tubes each 25 cms. in diameter.



PHOTOGRAPH 3.P.1.

THE PHOTOGRAPH ON THE LEFT SHOWS A  
RECTANGULAR CRYSTAL BEFORE ANY ION  
BOMBARDMENT. THAT ON THE RIGHT  
AFTER  $\frac{1}{2}$  HOUR ION BOMBARDMENT OF  
50  $\mu$ A, 450 VOLTS, WHEN USING A MICA  
SHEET (3.5.3). (MAGNIFICATION X 7).

These were then partly inflated from a gas cylinder. This proved satisfactory and had the added advantage of being able to be let down if and when required.

### 3.5.3 ION FOCUSING.

The early work on ion bombardment was carried out using a molybdenum holder, which was entirely covered with mica, with the exception of a small area for the crystal. This was done to ensure that the measured current was in fact the crystal current. Several other arrangements involving current shields were also tried. Although these were effective for their purpose, they introduced other difficulties. It was found that during the early ion bombardment the shields charged up causing focusing fields for the subsequent ions. These resulted in preferential removal of the crystal surface. As an illustration, photo. 3.P.1 shows the effect after half hour ion bombardment. This problem was eliminated by adopting the dummy crystal technique as described in section 3.2.3

### 3.5.4 CRYSTAL STABILITY.

In general, the very thin crystals, because of their position in the vacuum system, tended to be susceptible to falling off the holder if subjected to external disturbances such as a slight bump on the system. In particular it was found that when ion bombardment was attempted with accelerating voltages greater than 1000 volts,

the crystal had a tendency, at times, to vibrate initially for half a second or so and then to fall off the holder.

This was attributed to one or a combination of the following:

- a)                    Resonance vibration between filament and supporting block.
- b)                    A quick charge build - up in the inside of the glass vacuum system.
- c)                    The energetic argon ions knocking the crystal off.

                    This was eliminated by carrying out the argon ion bombardment with accelerating voltages less than 1000 volts.

CHAPTER 4.                    EXPERIMENTAL RESULTS.

4.1                            INTRODUCTION.

This chapter gives the results of treatment involving the annealing, ion bombardment and chemical thinning of polished germanium, silicon, gallium antimonide and indium antimonide crystals.

The stress on the surface, as measured by the curvature, has been found, in all cases, to depend on the surface treatment history, and for the case of indium antimonide and gallium antimonide not to be dependent on the particular (111) face, i.e. 111 or V.

Ion bombardment experiments can be expected to determine the amount to which the damage extends into the crystal surface. Monitoring the curvature while stripping surface layers has shown this damage to be greater than previously thought for all four crystal types.

Chemically thinning the surface has given the functional relationship between the surface stress  $\sigma$ , the radius of curvature  $R$ , and the thickness of the crystals. This has been found to be consistent with  $\Delta \sigma \propto t^2 / R$ .

The radius of curvature as a function of annealing temperature has been of particular interest in all four cases. Here it has been found that the annealing, and corresponding increase in  $R$ , commence at surprisingly low temperature ( $\sim 50^\circ \text{C}$ ). This gives some information as to the

possible cause of the surface stress.

4.2

THE EFFECT OF CUTTING, ABRADING AND  
POLISHING ON SURFACES.

It was considered important first of all to establish, in general terms, the effect of the various cutting, abrading and polishing operations on the crystal surfaces. This was done by observing the sign of the resulting radius of curvature, positive when convex, negative when concave, at various stages during the surface preparation.

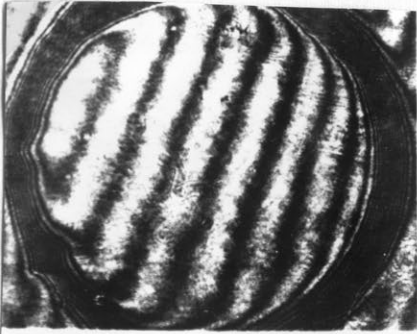
This did not involve placing the crystals inside the vacuum system and the measurements were all made at air pressure.

The results for this are summarised in table 4.T.1.

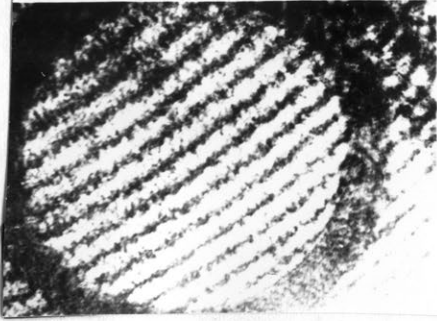
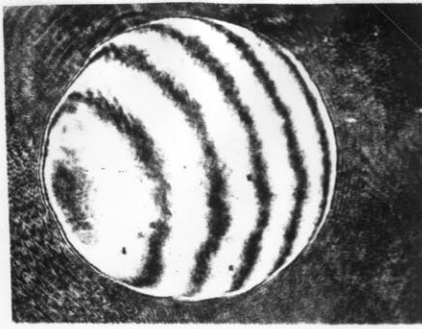
TABLE 4.T.1

<u>Nature of Treatment.</u>	<u>Resultant Curvature.</u>
1) Both sides having been polished in identical manner.	Last side polished (+)
2) Both sides etched then one side polished.	Polished side (+)
3) One side polished with 1 or 2 type treatment the other as cut with wire saw.	Polished side (-)
4) As in 3) with cut side chemically etched.	Polished side (+)

1)



2)



3)

4)

Photographs 4.P.1,2,3,4.

4.P.1 SHOWS A TYPE 2A CRYSTAL ON POLISHING MOUNT.  
 NOTE OUTER DARK RING CAUSED BY ETCH. CRYSTAL  
 BECOMES CONVEX ON REMOVAL FROM MOUNT (photograph 4.P.2).  
 4.P.3,4 SHOWS A SIMILAR RESULT FOR A TYPE 2C CRYSTAL.  
 ( MAGNIFICATION X 8 ).

These results apply to germanium and silicon as well as to both the A and B surfaces of indium antimonide and gallium antimonide.

The table shows that the resulting sign of the curvature depends entirely on the surface damage. This is clearly seen in 2).

When one side is polished but the other more heavily damaged by the cutting operation then the polished side is concave. If the heavy cutting damage is removed by etching without any change in the polished surface, then the polished side becomes concave 3), 4).

An illustration of the effect of the different surface preparations, that is type 1, and type 2, described in chapter 2, on the curvature may be seen from photographs 4.P.1 - 4. These refer to two different germanium crystals. Photograph 4.P.1 is of a type 2A crystal while still mounted on the polishing mount. The large ring around the crystal has been caused by the etch during preparation. Part of the main body of the crystal can also be seen. In 4.P.2 the crystal has been removed from the polishing mount. We note that it is now slightly convex. The next two photographs show the same thing for a type 2C crystal. The effect of the heavier damage and consequently the much higher convexity are seen.

The results of 1) in the above table are

of particular interest. It would be expected that since the surfaces were identically treated the resultant curvature should be zero. This however will depend on the meaning given to "identical".

In the method of preparation one surface of the crystal is polished while the crystal thickness is approximately  $(\frac{1}{4} - \frac{1}{2})$ mm. The other side is necessarily polished with the crystal thickness being smaller. Thus the surfaces cannot be prepared identically but can only be given the same polishing treatments.

These preliminary tests were also of interest in that they failed to show any difference between the A and B surfaces of the 3 - 5 compounds. Treated "identically" both sides gave similar results. This is in agreement with the results of Pugh and Samuels.<sup>1)</sup>

Although these general results were useful in giving a qualitative description of the surface damage, more details can be obtained by the annealing and ion bombardment of these surfaces.

#### 4.3 ION BOMBARDMENT RESULTS.

##### 4.3.1 INTRODUCTION.

Uon bombardment is used here for two purposes. Firstly, by monitoring the radius of curvature as a function of bombarding time an estimate may be given, knowing the amount of surface stripping, of the depth of

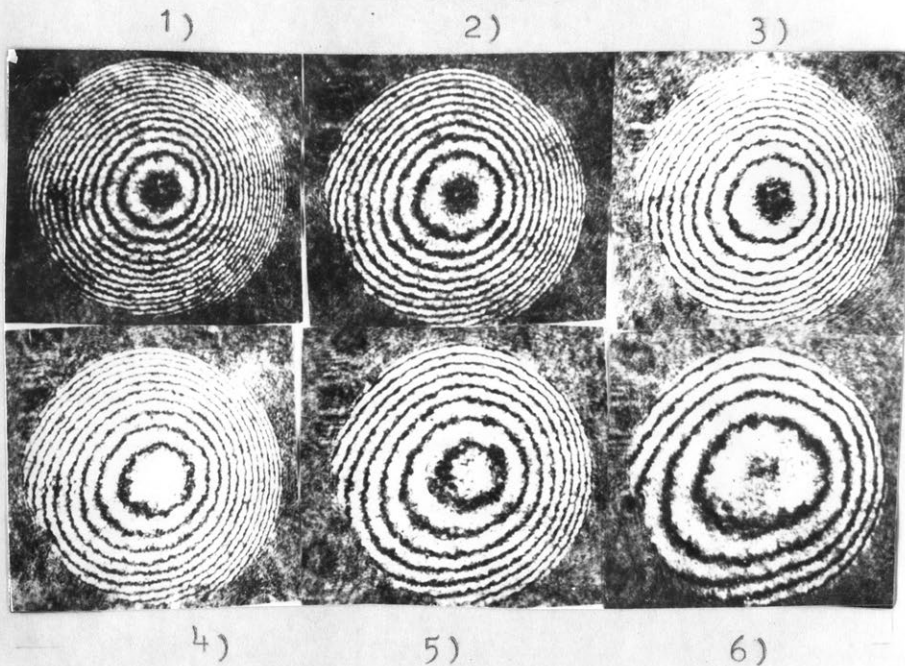
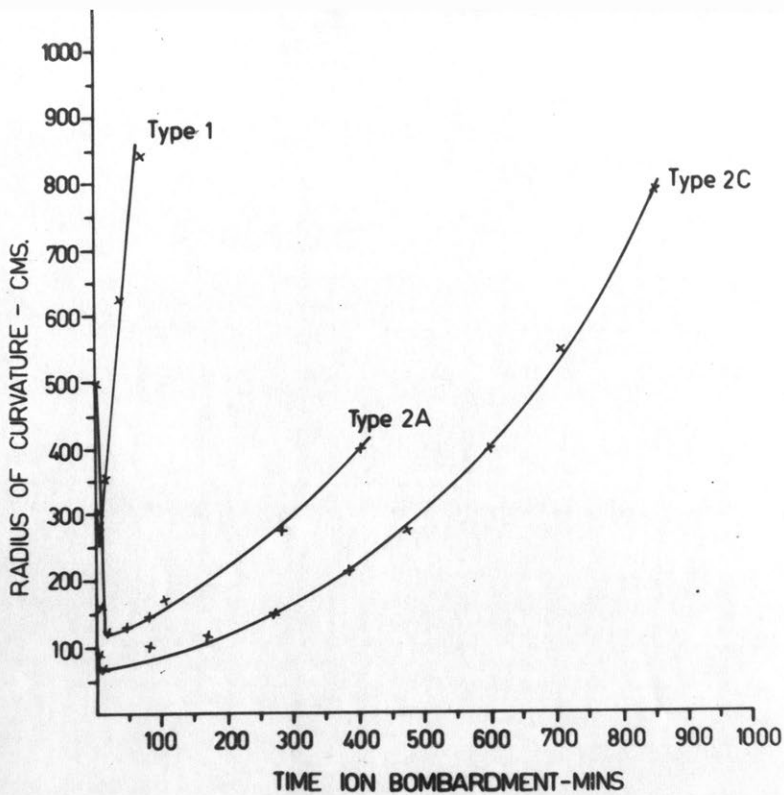


Figure 4.F.1.

THIS SHOWS THE RESULTS OF ION BOMBARDMENT. PHOTOGRAPHS 1 - 6 GIVE THE APPEARANCE OF THE FRINGE SYSTEM FOR A TYPE 2C CRYSTAL. 1 AND 2 SHOWS THE CRYSTAL BEFORE AND AFTER HEATING ( $350^{\circ}\text{C}$ ). THE REST SHOW THE EFFECT OF CONTINUED ION BOMBARDMENT; FROM 3, (20 SEC) TO 6 ( $\sim 10$  HRS). NOTE THE RELATIVELY SLOW RECOVERY AS SHOWN IN GRAPH. (MAGNIFICATION X 7).

damage introduced by polishing. Some work to measure these depths has already been done by others. Measurements by optical inspection of taper sections and by checking chemical and electrical properties,<sup>1,2)</sup> have established that the damage depth for germanium is roughly of the same order as the size of the polishing particles used. Results have also been reported for GaAs and InSb.<sup>3,4)</sup>

In the present case it has been found that the damage extends further into the crystals than given above and that in fact it extends to more than twice the diameter of the particle sizes used for polishing.

A further important result is that continued ion bombardment of crystals polished on one side only, eventually results in their becoming flat ( $R = \infty$ ). This shows that any stress arising out of the ion bombardment itself must be at least below the detection limit.

Ion bombardment was also used to form a clean surface. This is essential if stress measurements of the A and B surfaces of InSb and GaSb are to be made.

#### 4.3.2

#### GERMANIUM RESULTS.

Results for germanium crystals which have been annealed by direct heating without prior system bakeout are given in figure 4.F.1. The results are for crystals chemically etched on one side and polished on the other, and

corresponding to a type 1, 2A and 2C polishing operation. It is seen that for continued bombardment, the radius of curvature increases. Values of R greater than 1000 cms. correspond to about one interference fringe on a crystal, which represents about the detection threshold. In this case equation E.1.3 gives a possible surface tension difference for an ion bombarded / chemically etched surface of less than  $400 \text{ dyne cm}^{-1}$ . As expected, the thickness of crystal that had to be removed from the polished face, before the remanent strains were as small as those from the etched face, were least for type 1 surfaces and most for type 2C surfaces. It is also seen that the rate of recovery is faster for type 1 than type 2C surfaces. This criterion was used to estimate the depth of damage for the different operations. By measuring the crystal ion bombardment current and calculating from the known sputtering yield the amount of crystal surface removed until the surface tension difference was below detection limit, the depth of surface damage was estimated as given in table 4.T.2. 5)

TABLE 4.T.2.

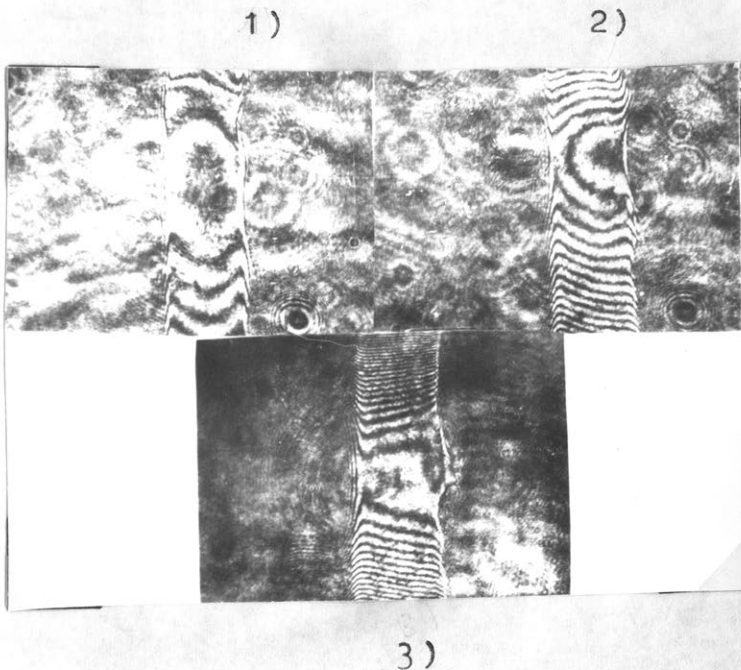
DEPTHS OF POLISHING DAMAGE IN Ge DETECTED BY STRAIN.

<u>1.</u> Surface	<u>2.</u> Max abras- ive pcle. size used.	<u>3.</u> Av.Depth removed with $12\frac{1}{2}$ micron pcles. (microns)	<u>4.</u> Average depth removed with $\frac{1}{4}$ micron pcles. (microns)	<u>5.</u> Remanent damage depth from figure 4.F.1.	<u>6.</u> Deduced orig- inal damage depth due to pcles. in col. 2(add col 3 to 5 (microns)	<u>7.</u> Max. Original damage depth from taper section tech- niques (microns) (ref.2)
Type 1	$\frac{1}{4}$	0	Not relevant	1	1	-
Type 2A	25	10	20	>7	>37	12
Type 2C	25	10	5	>15	>30	12

It is seen that the depth of damage due to polishing with  $\frac{1}{4}$  micron diamond paste is at least 1 micron and the depth due to 25 micron particles is about 40 microns. These depths are appreciably greater than those found by electrical and chemical techniques.<sup>1),2)</sup> This illustrates that the lattice distortions introduced by abrasion and polishing extend below the bottoms of the deepest fissures. As such they would be undetectable by sectioning methods.

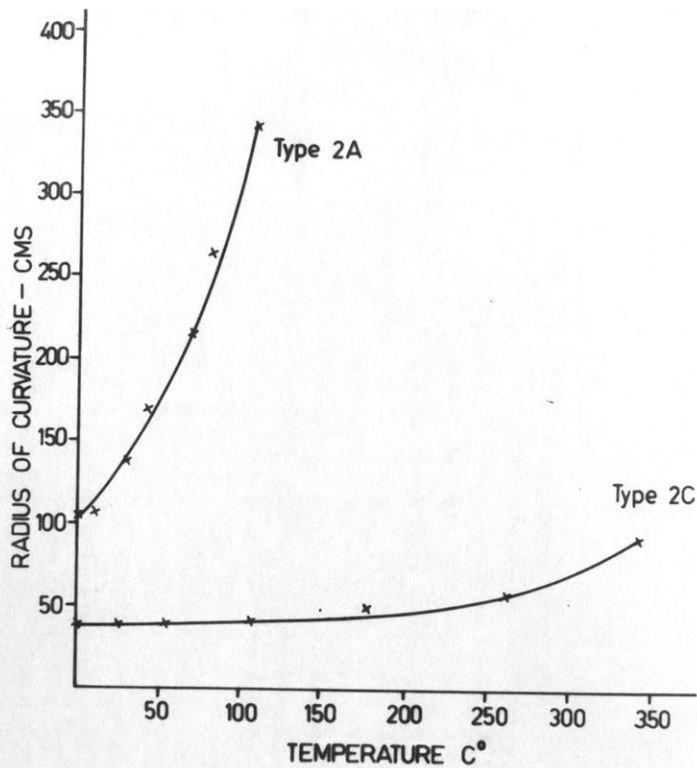
Ion bombardment was also carried out on

crystals having both sides polished. In this case only one side, that facing the electron gun, was able to be bombarded while the other rested on the molybdenum block. Ion bombardment stripping of the top surface always caused it to become more concave, independently of its original sign. This is to be expected since reduction of the top stress allows the bottom (damaged) surface to become convex and hence the top surface concave. This is seen in the case of a rectangular crystal in photograph 4.P.5. These show the crystal inside the vacuum system before and after ion bombardment.



Photograph 4.P.5.

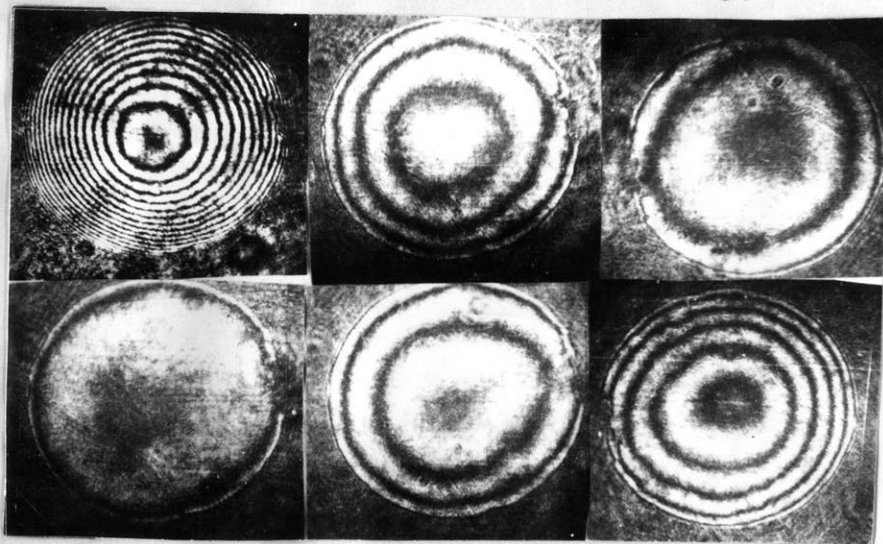
IN THIS CRYSTAL BOTH SIDES HAVE BEEN POLISHED. THE DAMAGE IS APPROXIMATELY THE SAME, SO THAT THE VIEWED SURFACE IS ONLY SLIGHTLY CONCAVE, 1. REMOVING THE DAMAGE FROM THIS SURFACE RESULTS IN THE CRYSTAL BECOMING MORE AND MORE CONCAVE, 2,3. (MAGNIFICATION X 4).



1)

2)

3)



4)

5)

6)

Figure 4.F.2

THE FIGURE SHOWS THE EFFECT OF ANNEALING. THIS IS ILLUSTRATED IN THE PHOTOGRAPHS TOGETHER WITH THE INITIAL RECOVERY DURING ION BOMBARDMENT. 1 SHOWS THE CRYSTAL IN VACUUM. 2 AFTER HEATING TO 105° C AND 3 AND 4 AFTER HEATING TO 270° C AND 330° C RESPECTIVELY. 5 AND 6 SHOW THE CRYSTAL AFTER 3 AND 20 SECOND ION BOMBARDMENT RESPECTIVELY. (MAGNIFICATION X 6).

## 4.4

ANNEALING RESULTS FOR GERMANIUM.

The crystals were annealed at temperatures varying from  $100^{\circ}$  to  $500^{\circ}$  above room temperature. Here again high vacuum ( $10^{-7}$  -  $10^{-8}$  torr) was obtained by placing heating tape around the glassware without a general bakeout. Heat from a focussed projection lamp was then applied directly. All measurements were taken at room temperature and after the crystal had sufficient time to reach equilibrium with its surroundings. In general, annealing always results in an increase in the radius of curvature, that is, the crystals tend to flatten.

Results for a type 2A and 2C specimen are given in figure 4.F.2. The result is of a general nature. This graph serves to illustrate two main points. One of these is that the more damaged crystal, (2C), is affected less than the one with the relatively little damage. Secondly, and quite surprisingly, type 2A crystals show a marked increase in the radius of curvature even at low annealing temperatures.

## 4.4.1

COMBINED ANNEALING AND ION BOMBARDMENT.

It was necessary to establish whether the above effect was genuine or due to surface contamination which might arise because of a background pressure increase during the heating. Fortunately, because of the particular nature of the ion bombardment results this may be easily resolved. Referring to figure 4.F.1 and taking particular

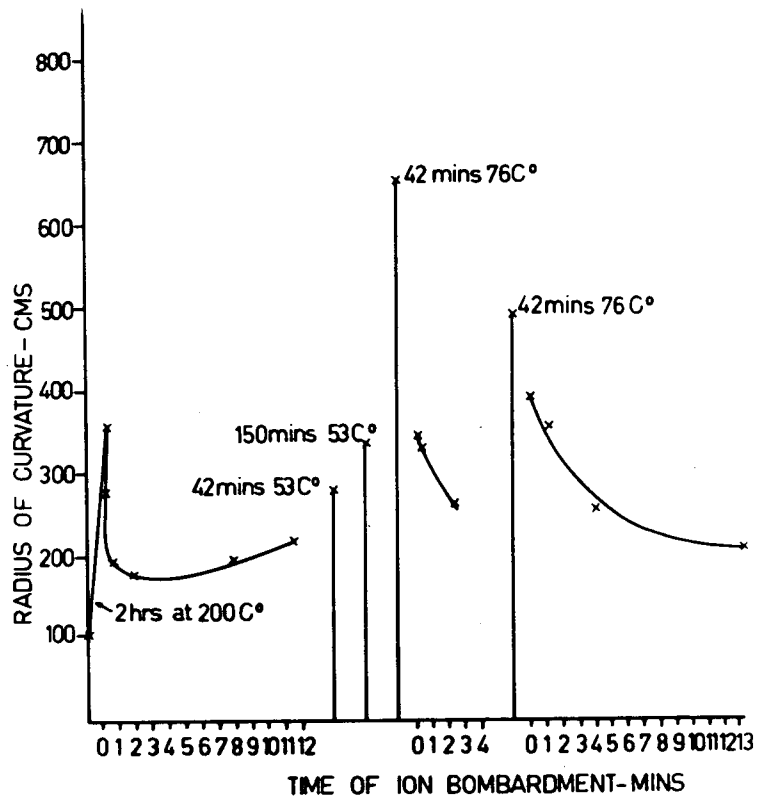


Figure 4.F.3.

RADIUS OF CURVATURE VERSUS TIME OF ION BOMBARDMENT SHOWING VARIOUS HEATING CYCLES. RATE OF SURFACE REMOVAL 1 MICRON / 60 MINUTES.

note of the shape of the curves during the first few minutes of ion bombardment, we see that during this time there is a decrease in R followed by a continuous increase. Again this effect is quite general and varies from crystal to crystal only in degree depending on such things as the extent of the damage and the crystal thickness and the temperature.

We have already seen that annealing (figure 4.F.2) always results in a convex surface becoming less convex (and a concave surface becoming less concave). However it is seen from 4.F.1 that the first few minutes of ion bombardment are sufficient to cause the crystal to become convex again and then to gradually flatten out completely as the ion bombardment is continued.

This recovery effect is shown in photographs accompanying figure 4.F.2 and is further illustrated in figure 4.F.3. In the photographs the first one, 1, shows a convex crystal surface inside the vacuum system, but at air pressure. 4 shows the crystal after it has been heated for 30 minutes at 330 C above room temperature. Finally we see the effect after the removal of several A of the surface by ion bombardment. We note that the crystal is more convex than after heating. It is to be noted however that in no cases have the crystals ever attained the same convexity as that prior to annealing.

An interesting sequence of heating and ion bombardment treatments on a type 2A crystal is shown in figure 4.F.3. The effects of bakeout (200 C at  $10^{-4}$  torr) are mostly removed by a few seconds ion bombardment. With further stripping of the surface the crystal starts to flatten again, a process accentuated by periods of mild heating (42 mins. at 53 C, 150 mins. 53 C and 42 mins. at 76 C). The effects of this heating are partially removed (R reduced from 650 to 350 cm.) by a few seconds ion bombardment, after which three minutes (500 Å stripped) bombardment are required to nearly restore the pre-heating curvature. Annealing at 76 C for 42 minutes again causes flattening (R = 500 cm.), some of which is removed by a few seconds ion bombardment after which a slower recovery of the curvature over about 12 minutes bombardment (0.2 micron stripped) takes place.

This resulting recovery allows us to distinguish between a genuine annealing effect and one caused by surface contamination. In the experiments the rate of surface removal was approximately 1 micron / 60 minutes which corresponds to about 170 Å / minute. The first few seconds, and even longer, of ion bombardment, are then clearly sufficient to remove any surface film, which may be neutralising the strain introduced during polishing, but would remove negligible interior surface damage. Since the original radius of curvature was never

obtained, it is valid to say that genuine annealing has taken place.

The role of the bottom surface, i.e. the one resting on the molybdenum blocks, seems to be negligible. Clearly it cannot be responsible for the observed change in strain either during the annealing or ion bombardment. For, if during annealing, a reaction took place between these two surfaces, then it would be of a permanent nature and could not explain the recovery region which has been seen to be a function of the top surface only. Further such reaction would be causing the crystal to become concave ( in the case of convex crystals), and hence when all surface damage was removed the crystal should become very concave rather than flatten out completely. Finally it may be expected that the evidence for such a reaction might be observable under a microscope when the crystal was removed from the vacuum system. No changes were observable. Thus the above behaviour shows in fact that there are two kinds of effect, one a genuine annealing of the damage introduced during polishing and the other due to some change in surface films. In type 2C crystals the relatively heavy damage is unaffected by the annealing at lower temperatures, and any surface contamination may be expected to play a minor role unless prolonged heating takes place in poor vacuum. Type 1 crystals on the other hand are very

sensitive to temperature changes and even at low temperatures are able to anneal to a great extent. The removal of a surface film by ion bombardment would have little influence on the curvature. A type 2A crystal would lie in the range between. It would be expected to be sensitive to both temperature and initial ion bombardment conditions. This may be seen in figures 4.F.1, 2.

It is thus evident that prolonged ion bombardment in all cases caused the crystals to become flat, indicating that cleaned surfaces had surface stresses below detection threshold ( $400 \text{ dyne cm}^{-1}$ ). Annealing of these surfaces up to  $500^\circ \text{C}$  caused no bending, i.e. any crystals heated to these temperatures remained flat independent of subsequent treatment. Such bombarded and annealed surfaces correspond to those from which good L.E.E.D. patterns are obtained, which thus have surface stresses less than  $400 \text{ dyne cm}^{-1}$ .

We note that in the above we have mainly reported the results of germanium crystals which have been chemically etched on one side and polished on the other, the polished side being convex. Interpretation of results for such specimens is more straightforward than for those damaged on both sides. However results were obtained for the latter kind of specimen too, and are summarised in table 4.T.3.

TABLE 4.T.3.

HEAT TREATMENT AND ION BOMBARDMENT FOR GERMANIUM CRYSTALS  
POLISHED ON BOTH SIDES.

- |    |                           |    |   |
|----|---------------------------|----|---|
| a) | Viewed Surface<br>Convex  | 1) | Annealing results in the surface becoming less convex.  |
|    |                           | 2) | Initial ion bombardment causes partial recovery of convexity.   |
|    |                           | 3) | Continued ion bombardment results in the surface first flattening, and then becoming increasingly concave with continued ion bombardment. |
| b) | Viewed Surface<br>Concave | 1) | Annealing results in the surface becoming less concave.   |
|    |                           | 2) | Initial ion bombardment causes partial recovery of concavity.   |
|    |                           | 3) | Continued ion bombardment increases concavity.  |

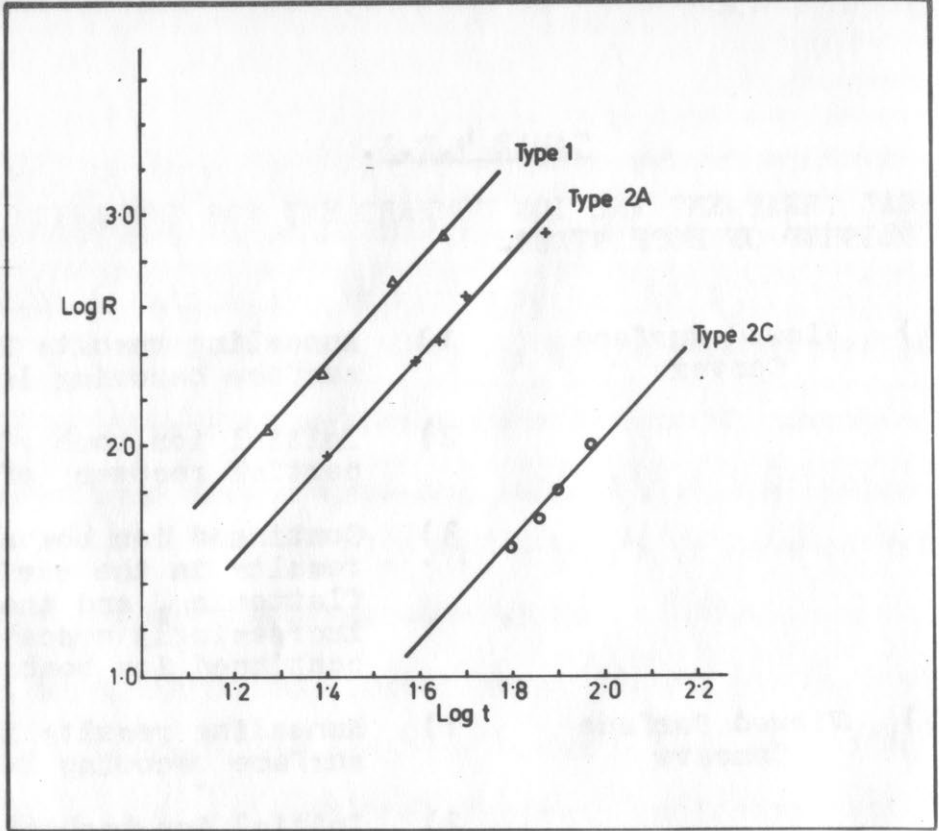
4.5

CURVATURE AS A FUNCTION OF THICKNESS  
FOR GERMANIUM.

The variation of the radius of curvature as a function of thickness depends on whether the surface stress difference, or the bulk energy, are constant for a given surface treatment. We see from equation E.1.3,

$$\Delta \mathcal{C} = \mathcal{C}_B - \mathcal{C}_A = \frac{Y}{(1-\nu)} \frac{t^2}{R}, \text{ that for a given} \quad (111)$$

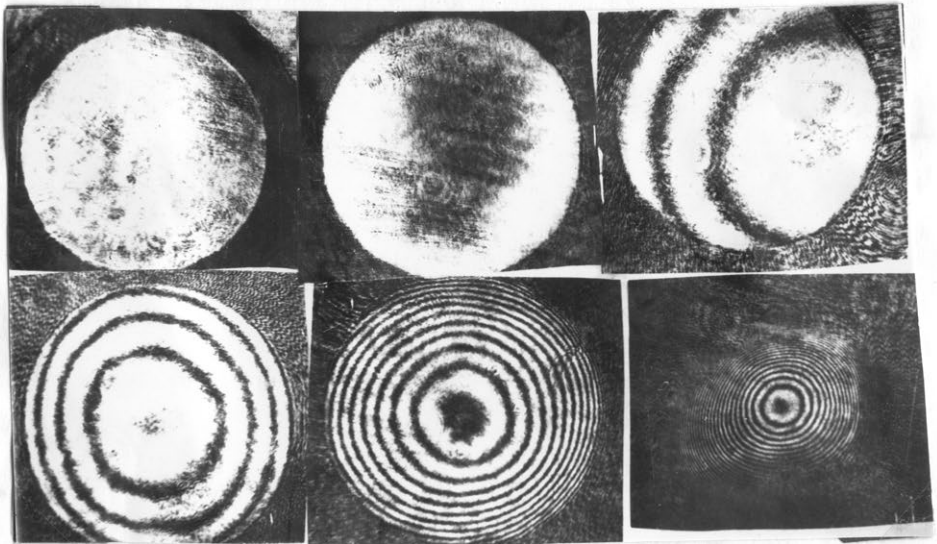
surface stress and elastic constant, provided the stress and strain are independent, the curvature  $R$  is proportional to  $t^2$  where  $t$  is the crystal thickness. On the other hand



1)

2)

3)



4)

5)

6)

Figure 4.F.4

PLOTTING LOG R VERSUS LOG  $t$  FOR TYPE 1, 2A AND 2C GERMANIUM CRYSTALS. THE LINES DRAWN HAVE A SLOPE OF 2. THE PHOTOGRAPHS ILLUSTRATE THE FRINGE PATTERN OBTAINED. IN 1 THE CRYSTAL IS IN THE MOUNT. THE OTHERS SHOW THE CURVATURE AS THE CRYSTAL IS PROGRESSIVELY THINNED BY ETCHING, 2 - 6. (MAGNIFICATION X 7).

equation E.1.6,  $U = Y t^3 / 24 R^2 (1 - \nu)$ , shows that a relationship of the form  $R \propto t^{3/2}$  would hold if the bulk energy were constant. Drum has measured this relationship on AlN crystals grown from the vapour phase.

The method used here in carrying out this experiment has already been outlined in section 3.4.3.4. The crystal thicknesses used, varied from 15 microns upwards to 150 microns. It would have been desirable to conduct these measurements over a much larger range of crystal thicknesses. However this was not easy to achieve, particularly at the lower thickness ranges. In this range, continuous handling resulted many times in crystal breakages. It also proved difficult to prevent the polished sides from being etched as no pressure at all could be applied to them when placing them on the wax. At thicknesses higher than 150 microns, the curvatures of the crystals were below detection level unless the crystals were extensively damaged. With these crystals it was then impossible to measure the low thickness ranges.

Plots of R versus t are shown in figure 4.F.4 for type 1, 2A and 2C crystals. The accompanying photographs are of a type 2A crystal. These have been drawn on a log-log scale. All the points shown can be fitted to a reasonable degree by an  $R \propto t^n$  curve where  $n = 2$ , although the curves of best fit for the various types of surfaces involved powers of t differing by up to 20%

from the number 2. Therefore, to within the accuracy of the method, the square law dependence of R on t predicted by E.1.3, is not contradicted by these measurements. A law of the form  $R \propto t^{1.5}$  such as would follow if the bulk strain energy per unit surface area were a constant for a given surface treatment E.1.6 would not fit the range of observed results.

It was necessary to establish that R did not change in any way because of handling. This includes placing the polished face in the wax, letting the wax dry, dissolving it in p-xylene, and then washing the crystal. It then has to be placed on a mount so that its curvature can be measured. That R does not change by this treatment was simple to establish. A crystal with a known radius of curvature was mounted as it would normally be prior to chemical thinning. Then without etching it at all it was removed from the wax and its curvature measured. This was repeated many times.

It was found that no changes occurred because of handling.

4.6

#### SILICON RESULTS.

The work carried out on silicon has been done only for type 1 and type 2A crystals, and only ones that had been polished on one side. The results obtained for ion bombardment, annealing and chemical thinning are

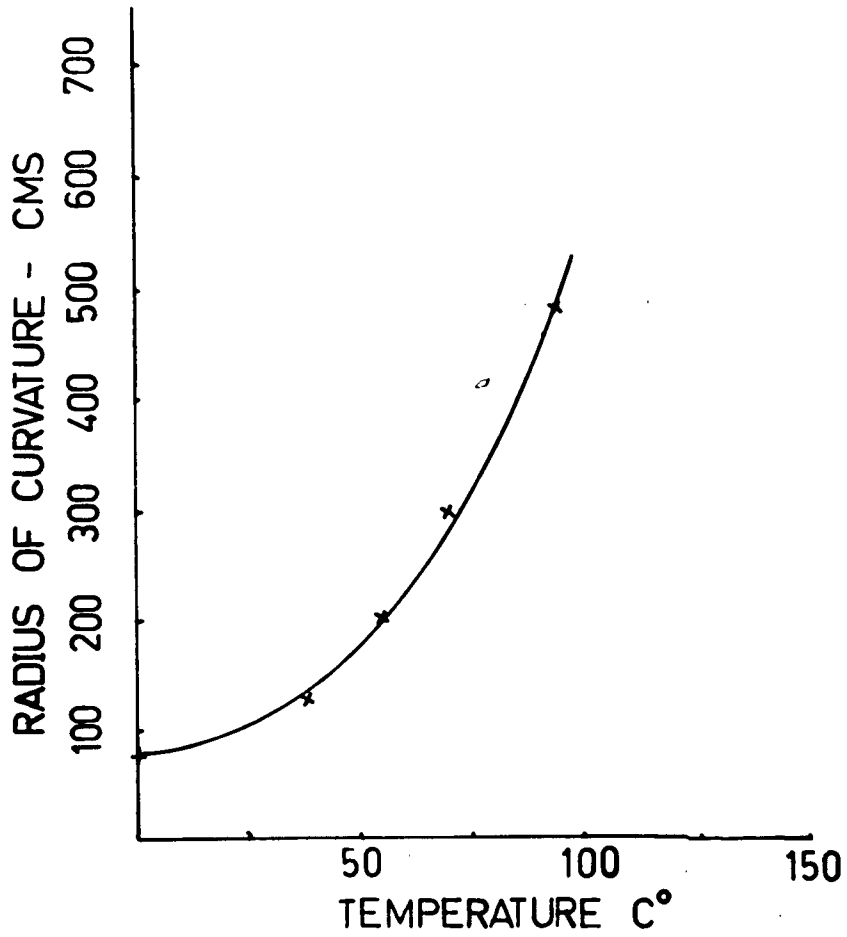


Figure 4.F.5

SHOWING THE EFFECT OF ANNEALING ON A TYPE 1 SILICON CRYSTAL. ANNEALING FOR 15 MINUTES AND READINGS TAKEN AT ROOM TEMPERATURE.

essentially the same as those for germanium.

The notable exception in the preparation of the specimen samples was that, because of its greater hardness than germanium, it proved much more difficult to prepare and polish the sample, sometimes taking a week or more to prepare one single crystal that was usable.

In all, six crystals were tested. In general the results were similar to those for germanium. It was found that with continued ion bombardment a convex crystal became flat. As estimated by the surface stripping, the depth to which the polishing damage extends into the surface has been found to be about  $\frac{1}{2}$  that found for germanium.

Annealing temperatures were found in all cases to increase the radius of curvature. A plot for a type 1 silicon crystal as a function of temperature is given in 4.F.5. This may be compared with a similar curve for germanium in 4.F.2. Overall, silicon appeared to be less sensitive to annealing than germanium.

Chemical thinning of the crystal, carried out in a manner identical to that described for germanium, resulted again in an  $R \propto t^2$  relationship being able to be fitted to experimental results indicating a surface rather than a bulk effect.

Because of the similarity with germanium

further details will not be given and the results for silicon are summarised below in the form of a table.

Depth of damage introduced by polishing with $\frac{1}{4}$ micron diamond paste.	$> \frac{1}{2}$ micron
Temperature of anneal at which observable damage begin.	$< 50^{\circ} \text{C}$
Functional Relationship	$R \propto t^2$

#### 4.7 INDIUM ANTIMONIDE RESULTS.

##### 4.7.1 INTRODUCTION.

The intended purpose here is to obtain clean surfaces of thin indium antimonide crystals with faces parallel to (111) planes. If such crystals, free from any other externally introduced stresses such as polishing, exhibit any curvature, it could be due to an intrinsic difference between the two opposite faces. We have already seen that a primary aim here is to look for such a difference for clean surfaces of indium antimonide and gallium antimonide.

The crystals used were generally about 20 microns thick, although sometimes thinner crystals than this were used, (8 - 20 microns), these proved difficult to obtain repeatedly.

Ideally, it would be preferable if both the surfaces could be produced clean by ion bombarding and

annealing both of them. This however proved difficult experimentally. The crystals would, in this case, have to be supported by the edges. Unless held, these thin, light and fragile crystals are highly unstable. Any form of support for them would result in appreciably non uniform ion bombardment. Alternatively, it could be arranged that one side and then the other be treated while inside the vacuum system. This however necessitates external manipulating devices which would have great difficulty in handling such fragile crystals without breaking them. The method finally adopted was the same as that used for germanium and silicon, the techniques in these cases having been well established. It was already found in these cases, that crystals chemically etched on one side and polished, then ion bombarded on the other, could have all surface damages removed to within the sensitivity available.

This means that the stresses obtained are not those between two clean surfaces but between clean and chemically etched surfaces. This however will not limit the significance of the results. Since for germanium and silicon the chemically etched faces did not give rise to measurable stresses, it is likely that similar low stresses will be present on etched  $111 - V$  faces.

The results obtained are in brief as follows.

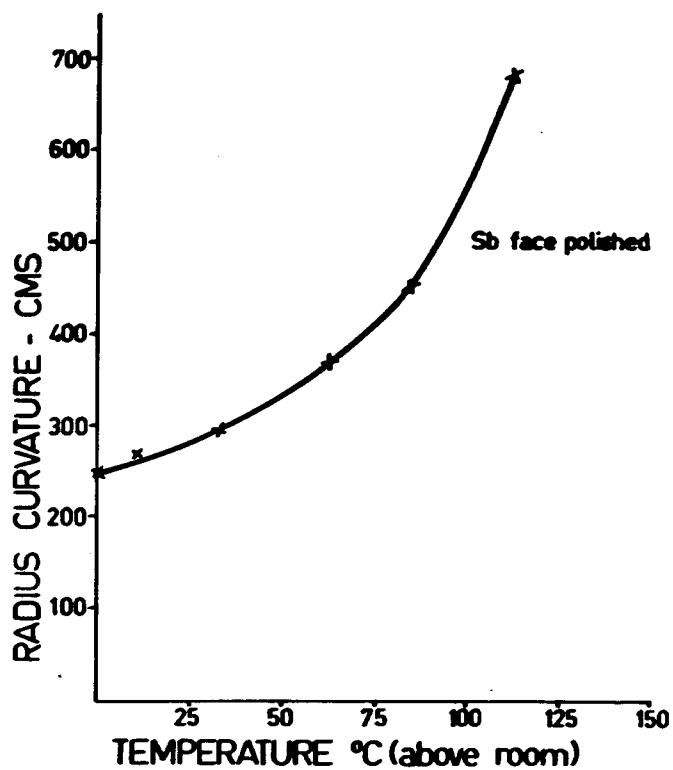


Figure 4.F.6.

SHOWING THE EFFECT OF 15 MINUTES ANNEALING TEMPERATURE ON AN InSb CRYSTAL WITH Sb FACE POLISHED AND In FACE CHEMICALLY ETCHED. MEASUREMENTS REFER TO ROOM TEMPERATURE AFTER ANNEALING.

For all crystals, the application of heat before or after ion bombardment resulted in the crystal becoming flatter. The ion bombardment results for the A and B surfaces are of fundamental importance. These showed that after prolonged surface stripping, sufficient to remove all surface damage, the radius of curvature becomes very large. This indicates that to the measurable limit there is no stress difference between these two surfaces, and the opposite etched surfaces.

The experimental environment for ion bombardment and annealing was an unbaked system with background pressure of  $5 \times 10^{-8}$  torr, conditions identical with those for germanium and silicon.

#### 4.7.2

#### ANNEALING AND ION BOMBARDMENT RESULTS:

Results for annealing and ion bombardment are given below. These were found to be independent of whether the indium face was polished and the antimony face chemically etched or vice versa. Not all the specimens were equally sensitive to heating. However in all cases, heating resulted in the crystal becoming flatter. This flattening appeared to take place to a greater extent for a given heat treatment, than in the case of germanium.

In figure 4.F.6 we see the effect of heat treatment on a crystal with damage corresponding to an intermediate range between type 1 and type 2A (1 - 2A).

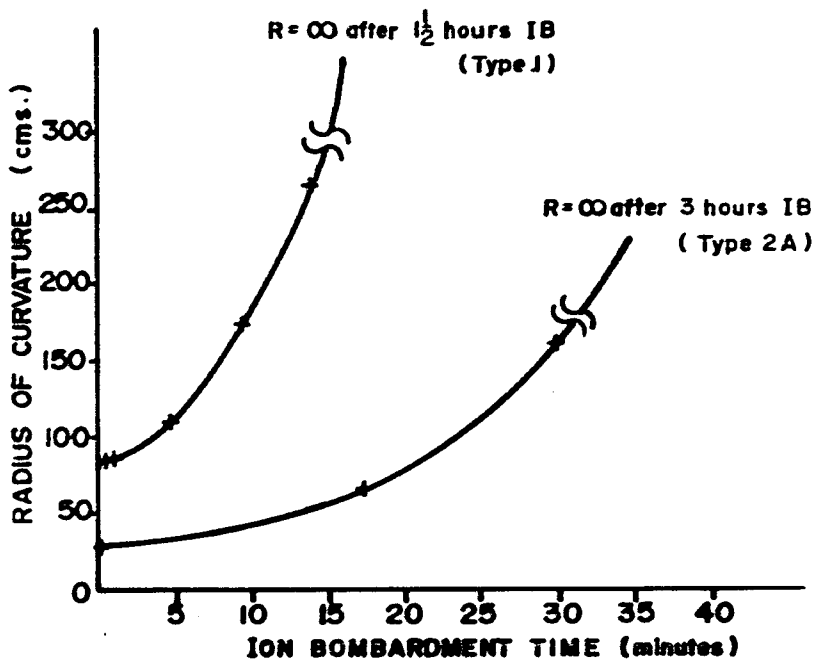


Figure 4.F.8

RADIUS OF CURVATURE VERSUS TIME OF ION BOMBARDMENT FOR InSb SAMPLE WITH THE Sb FACE BEING SPUTTERED IN BOTH CASES. TYPE 1 WAS HEATED TO 113 C BEFORE COMMENCING ION BOMBARDMENT WHILE TYPE 2A WAS ALWAYS KEPT AT ROOM TEMPERATURE. RATE OF SURFACE REMOVAL 2 MICRONS / HOUR. NOTE NO INITIAL RECOVERY.

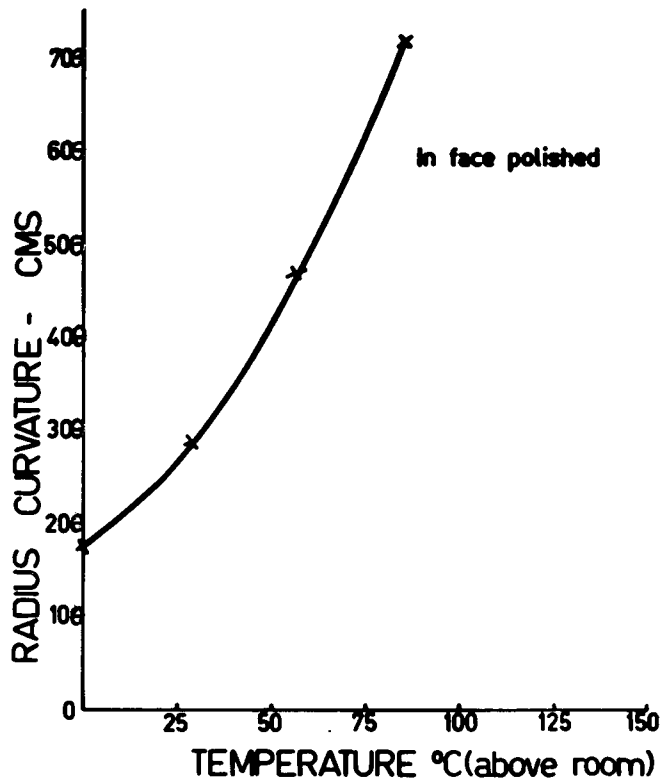


Figure 4.F.7.

SHOWING THE EFFECT OF 15 MINUTES ANNEALING TEMPERATURE ON AN InSb CRYSTAL WITH In FACE POLISHED AND Sb FACE CHEMICALLY ETCHED. MEASUREMENTS REFER TO ROOM TEMPERATURE AFTER ANNEALING.

In this the antimony face has been polished. Figure 4.F.7 shows the same for the indium face. We see that annealing occurs at surprisingly low temperatures.

Ion bombardment results are given in figure 4.F.8 for the case where the antimony side has been polished. Generally, the indium side behaves in the same manner.

A common feature of all the indium antimonide crystals treated in this way is that they showed little, if any, initial recovery at the onset of ion bombardment. This suggests that the temperatures reached were sufficient to cause permanent annealing with any surface films not playing a dominant role. Since indium antimonide shows a much lower ( $\frac{1}{1000}$ ) sticking coefficient for gases than germanium<sup>7)</sup> it is possible that weaker surface films form during the annealing.

It is of importance at this stage to note the following: after any particular crystal was ion bombarded for a time sufficiently long enough (as indicated by the flattening) for all the surface damage to be removed, it never, after this stage, ever became convex again due to heat treatment. Thus an intrinsic bending due to differing surface tension was never noted for the clean surfaces.

Crystals were next tried with damage corresponding to type 2A - 2B, that is, the surfaces were

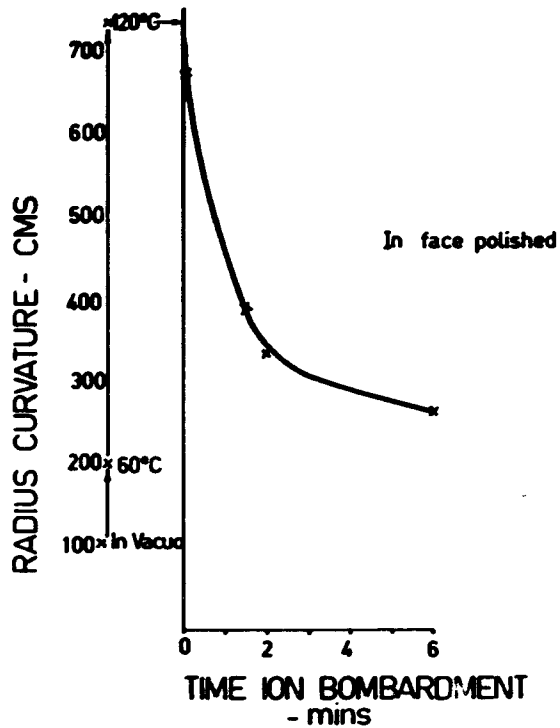


Figure 4.F.9.

THIS SHOWS THE COMBINED EFFECT OF ANNEALING AND INITIAL RECOVERY FOR A TYPE 2A - 2B (HEAVIER DAMAGE) InSb CRYSTAL WITH THE In FACE POLISHED. CONTINUED ION BOMBARDMENT RESULTS IN THE RADIUS OF CURVATURE INCREASING.

more heavily damaged. In this case, increase in annealing temperature again caused the crystal to flatten. However when ion bombardment was commenced, these crystals showed a recovery of curvature region before flattening out completely with continued ion bombardment. This result is independent of the face etched and polished. It strongly suggests that damage plays an important role in both the permanent and "reversible" annealing. A result for this is shown in figure 4.F.9.

Some additional results on the role of the damage were also obtained on indium antimonide specimens polished on both sides. The results for this are given in appendix 5.

Attempts were made to establish the effects of various gases on the crystals, at various stages. This applies to the four crystal types. These gases included argon, oxygen, water vapour and air. They were introduced into the vacuum system under the following circumstances.

- a) After the crystals were in vacuum, but unbaked with no heat treatment or ion bombardment.
- b) In vacuum, unbaked, and after varying amounts of ion bombardment.
- c) Repeats of a) and b) with both sides polished, and with one side polished, the other chemically etched.
- d) During heating and baking out periods.
- e) Various other combinations of a, b, c and d.

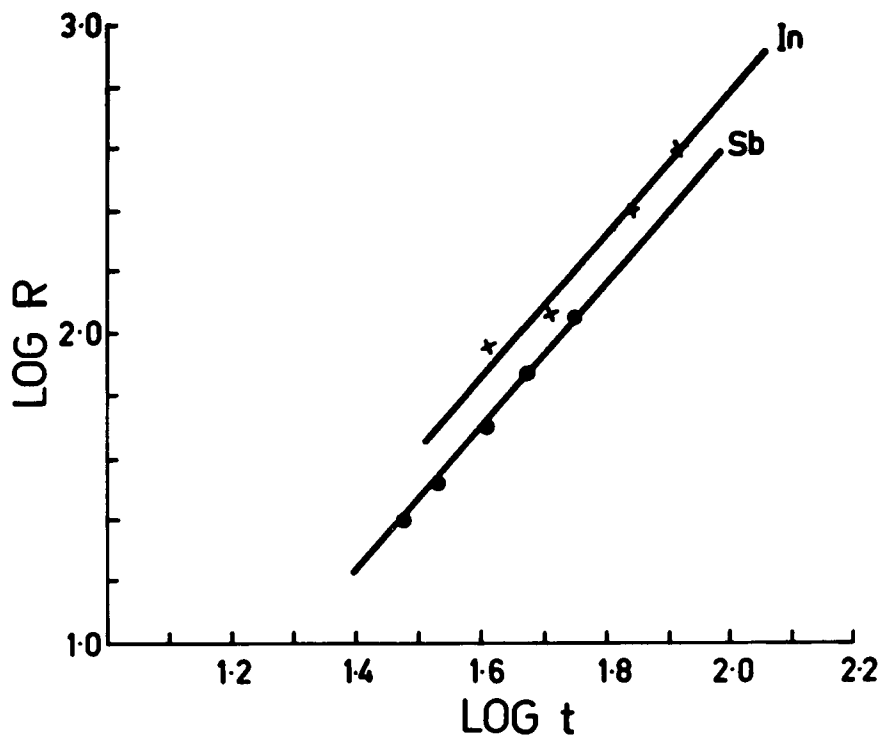


Figure 4.F.10.

PLOT OF LOG R VERSUS LOG  $t$  FOR InSb.  
THE LINES HAVE A SLOPE OF 2.

In no case was any effect on the curvature found, due to the admission of gases (to pressures) ranging from  $10^{-3}$  torr to atmospheric pressures.

#### 4.7.3 CURVATURE AS A FUNCTION OF THICKNESS FOR INDIUM ANTIMONIDE.

Radius of curvature versus thickness experiments were also carried out on indium antimonide, for both the A and B surfaces. The procedures were exactly as described above for Germanium, with the exception, that the particular surface being continuously etched, had to be identified.

A typical result is given in figure 4.F.10. This is for the case where the indium side was polished (In) and the antimony side chemically etched, and when the antimony side was polished (Sb) and the indium face etched. Two features of importance of these curves are the following. Firstly,  $R \propto t^2$ , as for germanium, secondly, the crystals though of type 1 - 2A, show similar behaviour, when compared with figure 4.F.4, as type 2B - 2C germanium. This shows that a similar polishing operation results in a greater extent of damage to indium antimonide than germanium. It may appear from 4.F.10 as if there is a difference in  $\Delta\sigma$  between the indium face polished and antimony etched and the antimony face polished and the indium face etched. This point was investigated and was found not to be the case. Any differences that were found between these two faces were

generally due to their not being treated "identically" during preparation.

#### 4.7.4 CONCLUSION AND DISCUSSION.

The above experiments were carried out to see if any stress difference between the A and B surfaces could be detected.

The results show that the surface stress difference between the cleaned antimony face and the etched indium face on the one hand, and between the cleaned indium face and etched antimony face on the other, were both found to be below the detection limit, which, from equation E.1.3 is  $400 \text{ dyne cm}^{-1}$ . Further, crystals with both sides chemically etched as here, always appear flat. Since therefore the etched indium and etched antimony faces had similar values of  $\sigma$ , we conclude that these surfaces have surface stresses which differ by less than  $800 \text{ dyne cm}^{-1}$ , as well as being individually less than  $400 \text{ dyne cm}^{-1}$ .

The depth of damage, as determined by ion bombardment, was found to be greater, for any particular polishing operation, than that for germanium. For type 1 crystals, this depth was found to be greater than 2 microns as compared with 1 micron for germanium. This is also suggested by the  $R \propto$  thickness measurements in section 4.7.3.

The behaviour of the crystals when subjected to heat treatment is of particular importance.

Since it seems that any temperature above that at which the polishing damage was introduced (room), is sufficient to cause permanent annealing, the nature of the damage seems to be an equilibrium situation in which the bulk forces tending to increase the radius of curvature of the crystals are balanced by other forces preventing this.

The fact that the gases had no apparent effect on the crystals was at first surprising. Clearly, the formation of surface films which are removable by ion bombardment indicate, in fact, that gases must be playing some role in respect to the damaged region during annealing. However the films which cause an observable effect on the stress are caused during heating. This would result in a thicker and more intimately bonded surface layers than those obtained by merely exposing to gases at room temperature. Finally we note again that, as in the case of germanium and silicon, any damage introduced by the actual argon ion bombardment is again below the detection limit of the apparatus.

4.8

#### GALLIUM ANTIMONIDE RESULTS

The ion bombardment, annealing, and chemical thinning results for gallium antimonide were found to be entirely similar to indium antimonide. Again no difference was detected between the opposite (111) surfaces.

In all five type 1 - 2A crystals were tested.

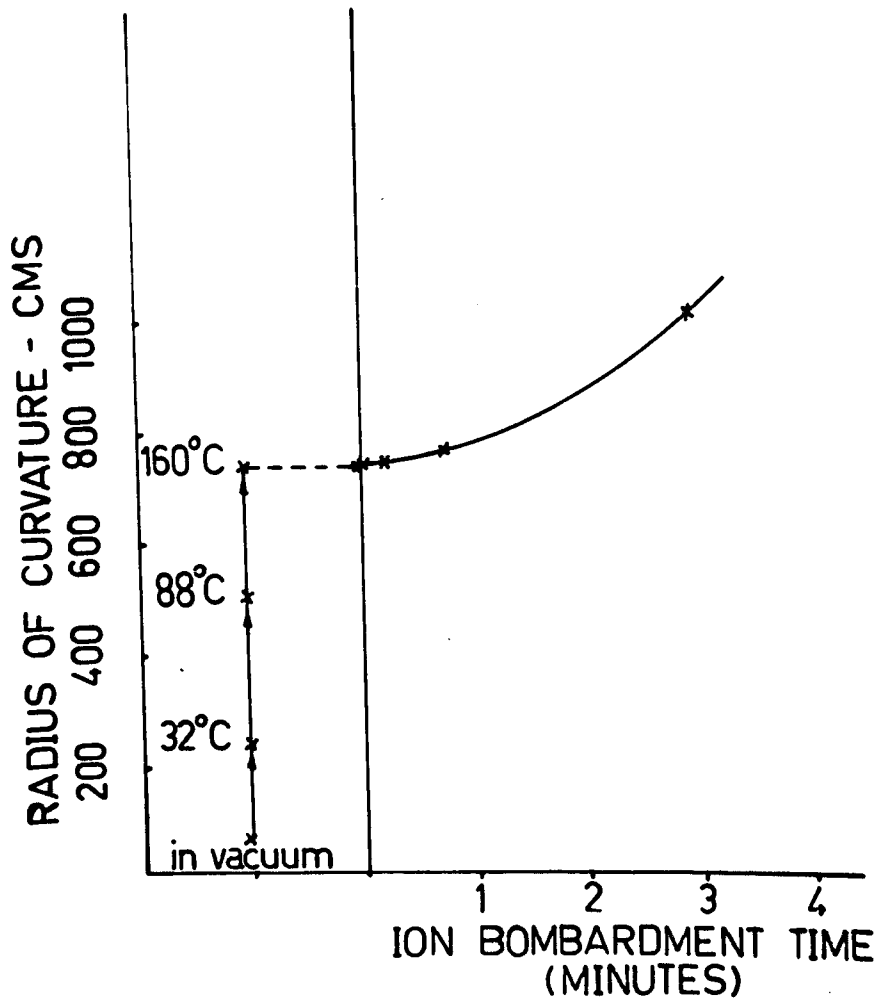


Figure 4.F.11

COMBINED ANNEALING / ION BOMBARDMENT  
EFFECT ON A GALLIUM ANTIMONIDE CRYSTAL.

Chemical thinning gave an  $R \propto t^2$  relationship similarly to indium antimonide with no difference being detected between these two substances.

Annealing was also found to occur at relatively low temperatures with gallium antimonide being slightly less sensitive than indium antimonide. Ion bombardment measurements showed that the polishing damage extends into the surface to the same extent as for indium antimonide. A combined annealing/ion bombardment result on a gallium antimonide crystal with the gallium face polished is given in figure 4.F.11. This shows the curvature of a crystal in vacuum and before any heat was applied. The curvature is then seen with the crystal annealed to  $32^\circ\text{C}$ ,  $88^\circ\text{C}$  and  $160^\circ\text{C}$ , the readings being taken at room temperature. Ion bombardment shows a continuous increase in the radius of curvature.

The results for gallium antimonide are summarised below in table 4.T.4 where they are compared with the results for germanium, silicon, and indium antimonide.

TABLE 4.T.4

	<u>Ge.</u>	<u>Si.</u>	<u>InSb.</u>	<u>GaSb.</u>
Depth of damage introduced by polishing with $\frac{1}{4}$ micron diamond paste	> 1 micron	> $\frac{1}{2}$ microns	> 2 microns	> 2 microns
Commencement of temperature of anneal at which observable changes begin.	< 50 °C	< 50 °C	< 50 °C	< 50 °C
Functional relationship	$R \propto t^2$	$R \propto t^2$	$R \propto t^2$	$R \propto t^2$
Sensitivity to annealing temperature	InSb more than GaSb more than Ge more than Si.			

---

## 4.9

GENERAL CONCLUSION.

It seems clear from the above that the four crystal types behave in a similar manner with regard to the surface damage and annealing properties, differing from one another only in degree.

This suggests that a mechanism which might explain in detail the damaged region for one of these could be extended to the four materials.

For example, it has been suggested that the resultant curvature in indium antimonide is due to an equilibrium balance of forces which is affected by an increase in temperature, causing the crystals to flatten.

Clearly this explanation may hold for the

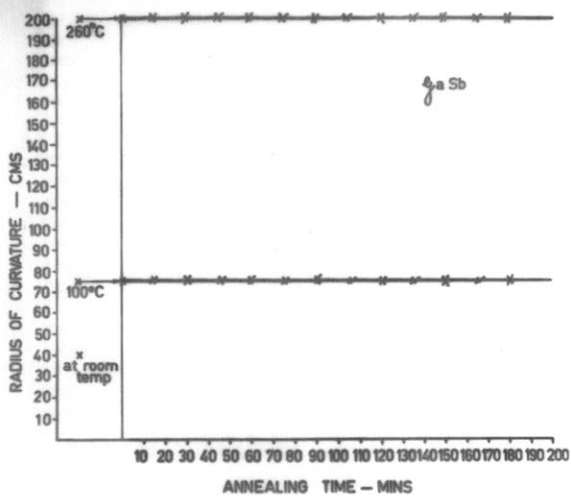
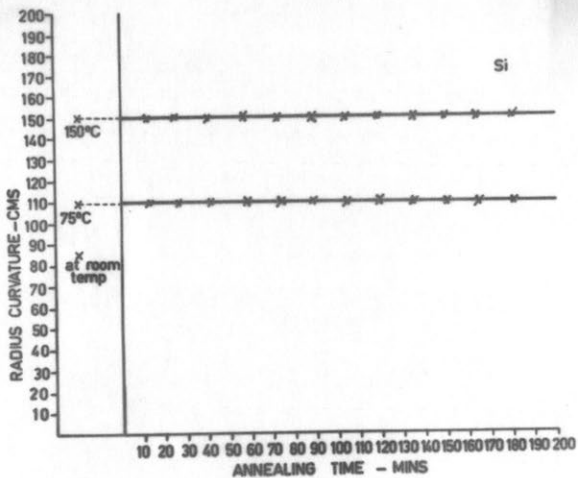
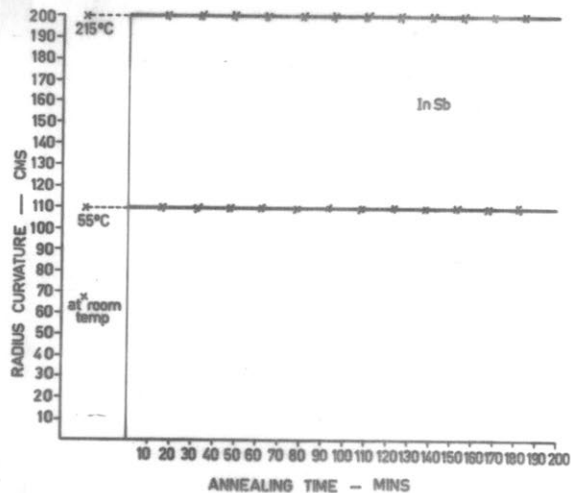
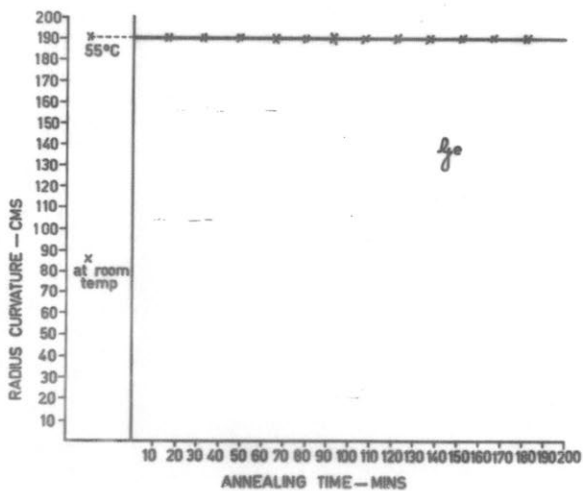


Figure 4.F.12.

ANNEALING RESULTS FOR THE FOUR CRYSTALS.

other crystal types as well.

To give a further insight into the mechanism causing annealing experiments were carried out to indicate whether the change in the radius of curvature was more sensitive to absolute temperature or to the time of application of any one particular temperature. Results for the four materials are given in figure 4.F.12. This figure may be explained by considering the indium antimonide results.

In this the radius of curvature at room temperature and before any annealing is 67 cms. The temperature of the crystal is then raised to 55<sup>o</sup> C and after reaching room temperature its curvature is now 110 cms. The temperature is then raised to 55<sup>o</sup> C again for 15 minutes and after cooling down its curvature measured. This is repeated at this temperature for 180 minutes, with all measurements being made at room temperature.

This is then repeated at a higher temperature, 215<sup>o</sup> C.

These results favour first of all an equilibrium model and secondly illustrate further the similarity of the four crystal types with regards to their annealing properties.

A proposed explanation in terms of a surface mismatch model will be given in more detail later after obtaining supplementary information from e.p.r. measurements in the next chapter.

## CHAPTER 5. ELECTRON PARAMAGNETIC RESONANCE.

### 5.1 INTRODUCTION.

All the previous stress measurements carried out on germanium, silicon, indium antimonide and gallium antimonide have shown, rather unexpectedly, annealing at relatively low (50 - 100 C) temperatures.

To obtain further insight into the mechanism responsible for the surface stress and consequent annealing, polished silicon crystals were subjected to e.p.r. studies.

These studies involve the effect of temperature on signal height, line shape and line width. The active gases, hydrogen and oxygen, were also introduced to see their effect on the signal. Attempts were made to investigate the other semiconductors in a similar fashion but their low resistivity and other factors made measurements difficult and less detailed work was done.

### 5.2 ELECTRON PARAMAGNETIC RESONANCE (e.p.r.) THEORY.

#### 5.2.1 INTRODUCTION.

We give a very brief outline of some e.p.r. principles. Excellent and more extensive reviews may be found elsewhere.<sup>1,2)</sup> Electron paramagnetic resonance makes use of the angular momentum, magnetic moment and charge of electrons.<sup>3,4)</sup> These quantities allow the detection of the electron by its interaction with the surroundings. This

means that e.p.r. may be used to study substances which have a resultant electronic magnetic moment. A resultant moment would be expected in two cases;

- 1) Breaking normal bonds leaving unpaired electrons.
- 2) Unfilled valency shell leaving unpaired electrons.

It follows from this therefore, that e.p.r. may be used to detect such centres as impurities, vacancies which trap electrons, unpaired electrons, damage sites with unpaired electrons and conduction electrons in semiconductors.

5.2.2

#### DETECTION OF e.p.r. SIGNALS.

The unpaired electrons are detected by measuring the energy absorbed when the electrons are induced by a high frequency field to jump from one energy level to another, or, classically, from one precession to another, when placed in an externally applied, strong static magnetic field  $H_0$ . Larmor showed classically that under such conditions the electrons will experience a torque making them precess with a frequency proportional to the magnetic field and the electronic magnetic moment. This frequency  $\omega$ , the Larmor precession frequency, is given by

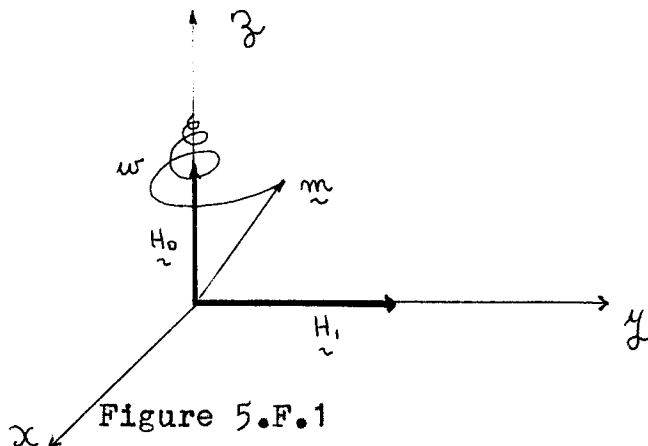
$$\omega = \gamma H_0 \quad \text{E.5.1}$$

where  $\gamma$  is the gyromagnetic ratio,  $\gamma = \frac{2\mu}{\hbar}$ ,  $\hbar$  being the reduced Planck's constant and  $\mu$  the electronic magnetic moment.

In a system containing many of these unpaired electrons the random phase of each of the electrons with its neighbouring ones, would make their Larmor precession physically unobservable.

If however, an oscillating magnetic field  $H_1$ , with frequency the same as the Larmor frequency is superimposed on the system, then, (See figure 5.F.1),

- 1) The electrons are supplied with a phase reference, by induction.
- 2) A torque is exerted on each electron tending to flip the magnetic moment relative to  $H_0$ . This will alter the energy of the electrons in the strong applied field. This energy is absorbed from the oscillating field  $H_1$ , making the Larmor precession observable.



SHOWING THE PRECESSION OF THE ELECTRONIC MOMENT.

Instruments for measuring this frequency are now available commercially. The present work was carried out on two models, a Japan Electron Optics and a Varian Spectrometer.

### 5.2.3 THE SPLITTING FACTOR "g", LINE SHAPE AND SIGNAL HEIGHT.

#### 5.2.3.1 THE "g" FACTOR.

According to the Zeeman effect, the energy levels of an electron may be split by interaction with an externally applied magnetic field. The resulting energy levels may be given by, figure 5.F.2,

$$E = E_0 + g \beta H M \quad E.5.2$$

where  $\beta = \frac{e \hbar}{2 mc}$  the Bohr magneton. (The moment of a single electron spin =  $0.927 \times 10^{-20}$  e.m.u.).

H = the applied magnetic field.

M = the magnetic quantum number.

g = the spectroscopic splitting factor.

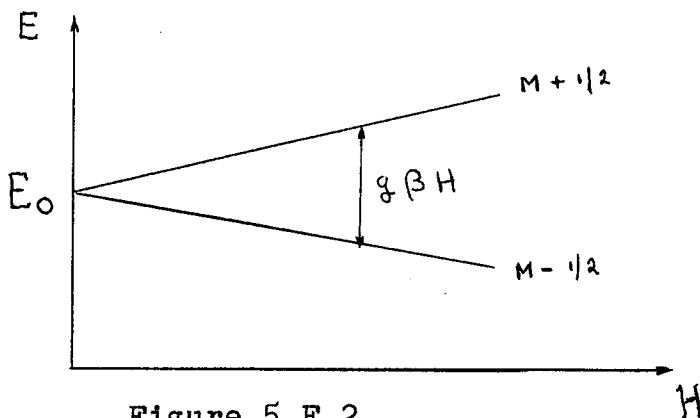


Figure 5.F.2.

MAGNETIC SPLITTING OF ENERGY LEVELS.

It is seen that the amount of splitting depends on the g factor. This factor is a measure of the degree of coupling that exists between the orbital and spin angular momentum of the electron, as well as including the nature of the electron itself. Equation E.5.3 which can be derived under certain assumptions,<sup>3,5)</sup> shows that g depends on L as well as S,

$$g = \frac{(J(J+1) + S(S+1) - L(L+1)) + 1}{2J(J+1)} \quad \text{E.5.3}$$

where  $J = L + S$ .

In this, S is the electron spin momentum vector, L the orbital angular momentum vector, and J the total angular momentum.

As such it is a measure of the effective magnetic moment, which we have seen (Section 5.2.2) to be the physically measurable quantity. A pure orbital magnetic moment ( $S = 0$ ) has a g factor of 1 while a pure spin magnetic moment ( $L = 0$ ) a g of 2, from the above formula. Measurements of<sup>6)</sup> g values of unpaired electrons in crystals have been found to be close to the free electron value of 2.0023. This is a result of the orbital momenta being heavily clamped by the electrostatic field arising from the crystal lattice, making the spin angular momenta the major contributor to the effective magnetic moment of the electron.

The interest here lies in trying to correlate any change in

$g$  values with temperatures with the corresponding change in surface stress. If the e.p.r. centres are located at the surface then any change in surface stress may change the interaction between the electron and its surroundings.

The simplest and best method of determining the  $g$  value of an unknown sample is to compare it with that of a standard sample whose  $g$  value is accurately known. The standard used in this case was a  $\text{Mn}^{++}$  salt having a six line resonance spectrum. The unknown  $g$  value is then obtained by measuring the difference in magnetic fields at which the known and unknown resonance occur as may be seen in figure 5.F.3.

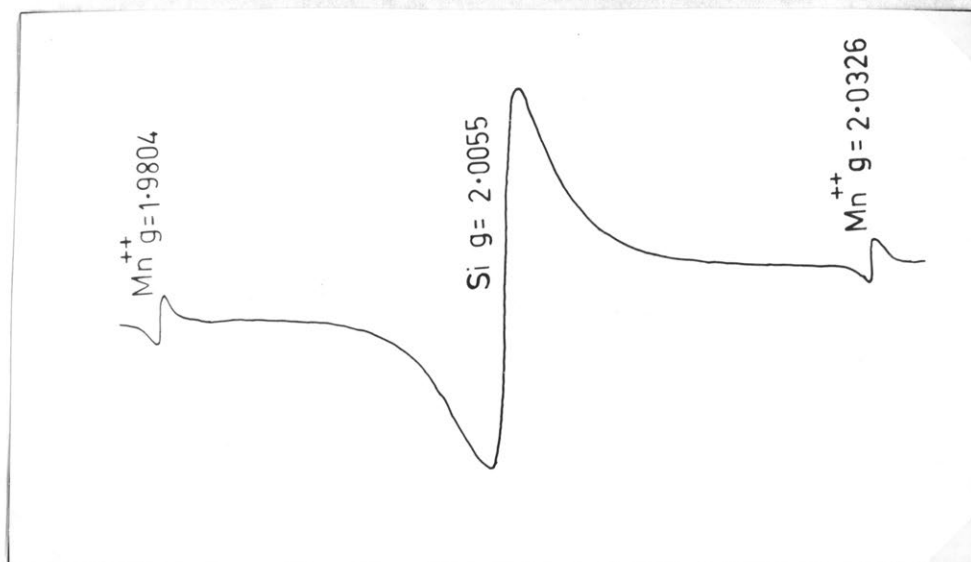


Figure 5.F.3.

THE STANDARD  $\text{Mn}^{++}$  MARKER WITH THE SIGNAL FROM POLISHED SILICON.

## 5.2.3.2

THE LINE WIDTH.

Further correlation between e.p.r. signals and surface stress may be obtained by a study of the absorption line - width as a function of temperature.

When a paramagnetic system is placed in a magnetic field its behaviour will essentially depend on the interaction of the electronic angular momenta with each other, and with the crystal lattice. These interactions will tend to establish thermodynamic equilibrium for the entire system.

When a resonant or near resonant oscillating magnetic field is superimposed on the system, absorption and spontaneous radiative emission will occur.<sup>7)</sup> The number of absorptions produced by this field will, however, be much greater than that radiated because of the resonant condition. This excess energy will be absorbed by the system until a steady state is achieved, i.e. the population densities of the various states remain constant.

It is seen therefore that the absorption line spectra obtained are related to the mechanisms governing dipole - dipole, and dipole - lattice relaxations.

These processes may be described in terms of two relaxation times  $T_1$  and  $T_2$ .  $T_1$ , which is temperature dependent, can be called the spin - lattice relaxation time

since it determines the rate at which energy is transferred from the paramagnetic dipoles to the crystal lattice.  $T_2$ , which is not very temperature dependent is called the spin - spin relaxation time and describes the rate at which energy of the dipole interactions are changing, i.e. the rate at which they get out of phase with each other. <sup>8,9)</sup>

The relation between  $T_1$  and  $T_2$  and the line-width, (measured as the peak to peak distance of the differentiated absorption spectra), as a function of temperature may be found elsewhere. <sup>5)</sup>

It is sufficient here to state that, in general, the temperature dependence of the relaxation time shows that if the line - width of the absorption is determined by spin - lattice interactions then the line - width will decrease rapidly with decrease of temperature. If however the spin - spin interactions are dominant the temperature dependence of the line - width will be slight.

### 5.2.3.3

#### THE LINE SHAPE.

The line shape of the absorption line, and any changes with temperature, can give further understanding to the predominant interactions in paramagnetic substances, and perhaps some correlations with surface stress.

A complete microscopic quantum theory is difficult to construct, mainly because of lack of understanding of the basic mechanisms governing relaxation times.

It is possible however to obtain approximate line shapes by making approximations regarding the interactions.

Using Bloch's phenomenological equations<sup>10)</sup> it is possible to obtain, E.5.4 a Lorentzian line shape for the case where the interaction is primarily due to spin-spin coupling and the spin-lattice coupling is small,

$$I(\omega) = \frac{T_2}{2} / \left( \pi \left( 1 + \frac{(\omega - \omega_0)^2}{T_2^2} \right) \right) \quad \text{E.5.4}$$

where  $\omega_0$  is the resonant frequency.

By making some reasonable assumptions<sup>11,12)</sup> Van Vleck obtains the line shape which would result if purely dipolar interactions were dominant, as a Gaussian function,

$$I(\omega) = \exp \left( - \frac{(\omega - \omega_0)^2}{2 \Delta^2} \right) / \Delta \sqrt{2\pi} \quad \text{E.5.5}$$

where  $\Delta$  is the half width expressed in units of the external magnetic field.

These equations are not stringent but give a degree of explanation for observed results. Experimentally one plots these functions and then fits the experimental points to them.

Use is made of the following table 5.T.1,<sup>13)</sup> which is taken from the Varian manual .

TABLE 5.T.1

SHOWING A PLOT OF THE DERIVATIVES OF E.5.4, E.5.5.

Height %	Position Lorentzian	Position Gaussian
100	a	a
80	1.65 a	1.5 a
60	2.10 a	1.8 a
40	2.75 a	2.1 a
20	3.80 a	2.5 a
10	5.00 a	2.8 a

In the table "a" is the half distance from peak to peak. The signal height at this corresponding point in the experimental absorption line is made equal to 100% and the experimental line shape drawn accordingly.

5.2.3.4

SIGNAL HEIGHT.

It is possible that the surface stress is due to such things as defects, vacancies and interstitials. If so, and if these are the source of the e.p.r. signal, a correlation regarding absorption line shape and height as a function of temperature, with surface stress as a function of temperature, may be possible.

Absolute measurements of the numbers of centres giving the signal are difficult.<sup>14)</sup>

Generally they are estimated by comparing the e.p.r. spectra of an unknown substance, with spectra which contain unpaired electrons capable of being measured by other means.

As an approximation it can be shown that the intensity is proportional to the first moment of the derivative resonance line and is given by

$$I(w) = K w^2 h \quad \text{E.5.6}$$

where  $w$  = peak to peak distance

$h$  = peak to peak height

$K$  is a constant determined by the line shape and is shown to be 1.81 for Lorentzian and 0.52 for Gaussian line shapes.

In the present work, empirical equations giving the number of spins in terms of a standard sample and other measurable parameters were not used. Since only relative height was important we found it sufficient to plot only peak to peak height as a function of temperature. To avoid errors introduced by handling, the heating experiments were carried out in situ and the same settings in the spectrometers were used. The signal height was further compared with that of the standard Mn <sup>++</sup> marker. In this way possible errors were less than 5%.

### 5.3 EXPERIMENTAL ARRANGEMENTS AND RESULTS.

#### 5.3.1 EXPERIMENTAL ARRANGEMENTS.

The crystals were placed in the experimental tube shown below, 5.F.4. Prior to attaching the

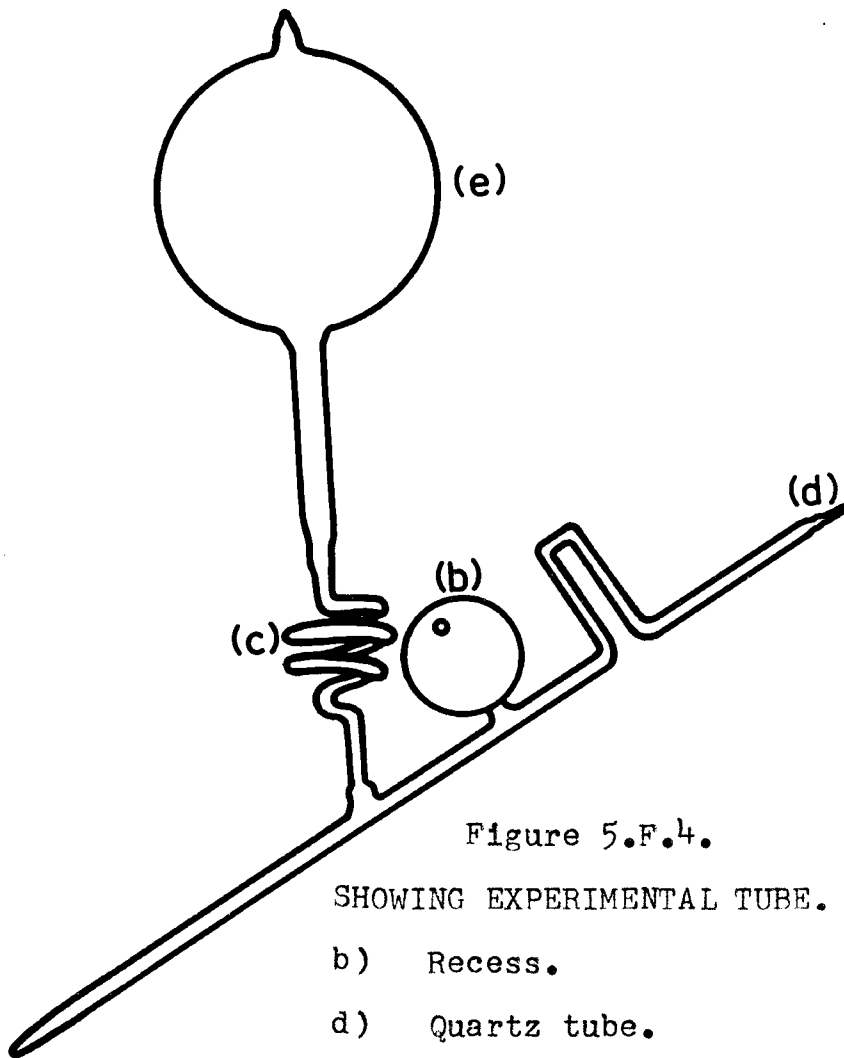


Figure 5.F.4.

SHOWING EXPERIMENTAL TUBE.

- b) Recess.
- d) Quartz tube.
- e) Spare volume to reduce the overall gas pressure when the tube is sealed off from main vacuum system.
- c) Glass coil.

tube to the vacuum system the crystals were gently tapped so that they rested in the recess in the side of the tube. This was necessary to allow the bottom of the quartz tube, the part that is finally placed in the resonant cavity, to be degassed by flaming without heating the crystals. Care had to be taken that the recess was deep enough otherwise the very light crystals were sucked out when the backing pump was turned on initially. The system was not baked and low pressures ( $5 \times 10^{-8}$  torr) were obtained by torch flaming all parts of the system except in the vicinity of the crystals. When necessary gases were leaked into the tube from containers attached to the vacuum line.

### 5.3.2

#### EXPERIMENTAL PROCEDURES.

The silicon samples used were prepared in exactly the same way as those used for stress measurements (Chapter 2). This means that the samples have at some time or another been treated with black wax, p-xylene, etc. It was first of all necessary therefore to make sure that the e.p.r. signal obtained did not occur because of any of these impurities.

#### 5.3.2.1

##### TESTING FOR IMPURITIES.

It was possible that a signal could be given by:

- a) Metadi fluid used in the polishing.
- b) Canada Balsam.
- c) Black Wax.

- d) Polishing diamond paste.
- e) p-xylene solvent.
- f) acetone.

All of these were tested separately and in various combinations. A signal was obtained only in the sample that contained the black wax and the diamond paste either singly or in combination with the others. It was finally concluded that black wax and diamond paste did in fact give a similar signal to that of silicon.

To ensure that the signal obtained was not due to either of these, two types of tests were conducted.

- 1) The  $g$  values of the black wax and diamond paste were measured. These proved to be different from the silicon  $g$  value.

i.e. Black Wax  $g = 2.0028$

Diamond Paste  $g = 2.0025$

Polished Silicon  $g = 2.0055$

- 2) The first test indicated that in fact there were no traces of either of these left in the silicon sample. To make sure, germanium samples which were treated identically were placed in the tube. Polished germanium gives no signal. By careful tuning it was possible to obtain a relatively high Mn marker signal. This meant that if the

Figure 5.F.5.

PLOT OF THE RELATIVE SIGNAL HEIGHT AS A FUNCTION OF TEMPERATURES. THE CIRCLES INDICATE SILICON CRUSHED IN AIR; THE CROSSES THE POLISHED SILICON. THE CRYSTALS WERE ALL ANNEALED FOR 30 MINUTES AT TEMPERATURES AS SHOWN. READINGS WERE ALL TAKEN AT ROOM TEMPERATURE.

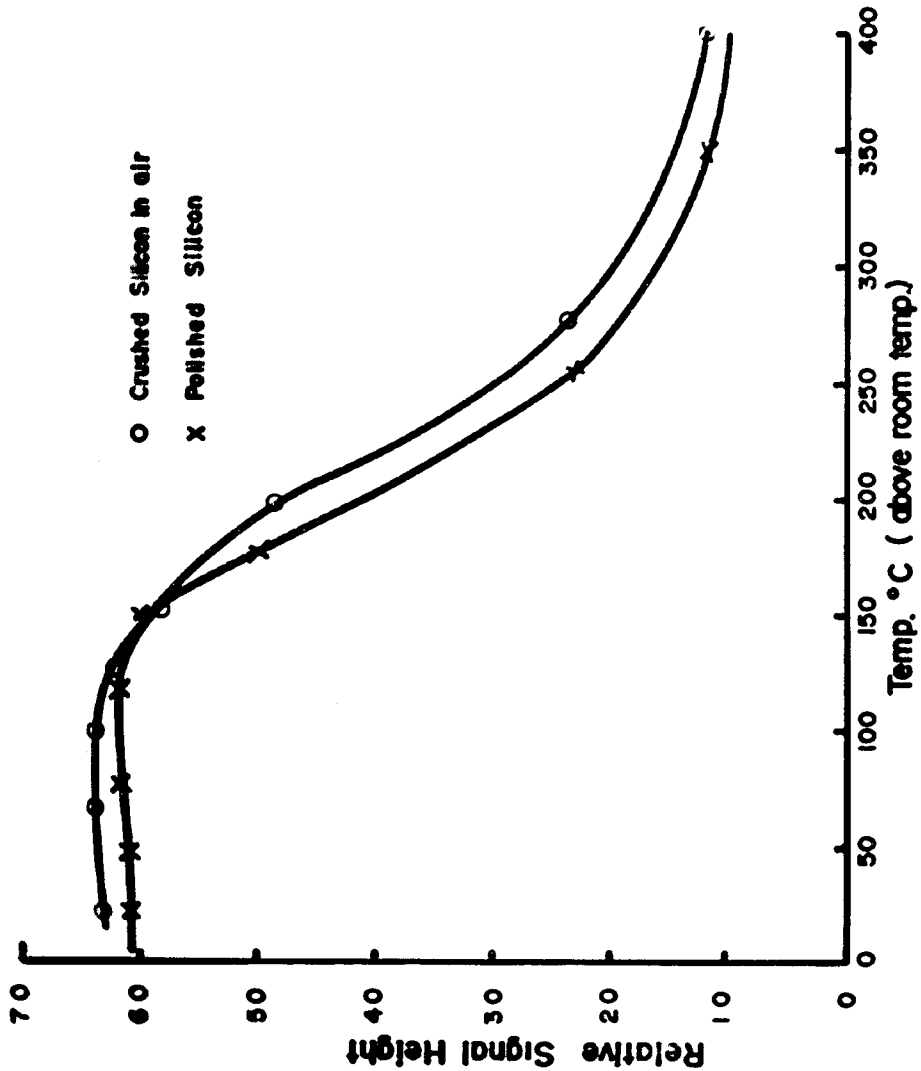


Figure 5.F.6.

PLOT OF THE RELATIVE SIGNAL HEIGHT AS A FUNCTION OF TEMPERATURE. IN THIS CASE HYDROGEN / OXYGEN HAS BEEN INTRODUCED INTO THE SYSTEM WHEN  $5 \times 10^{-8}$  TORR PRESSURE HAD BEEN ATTAINED. THE CRYSTALS WERE ALL ANNEALED FOR 30 MINUTES AT TEMPERATURES AS SHOWN.

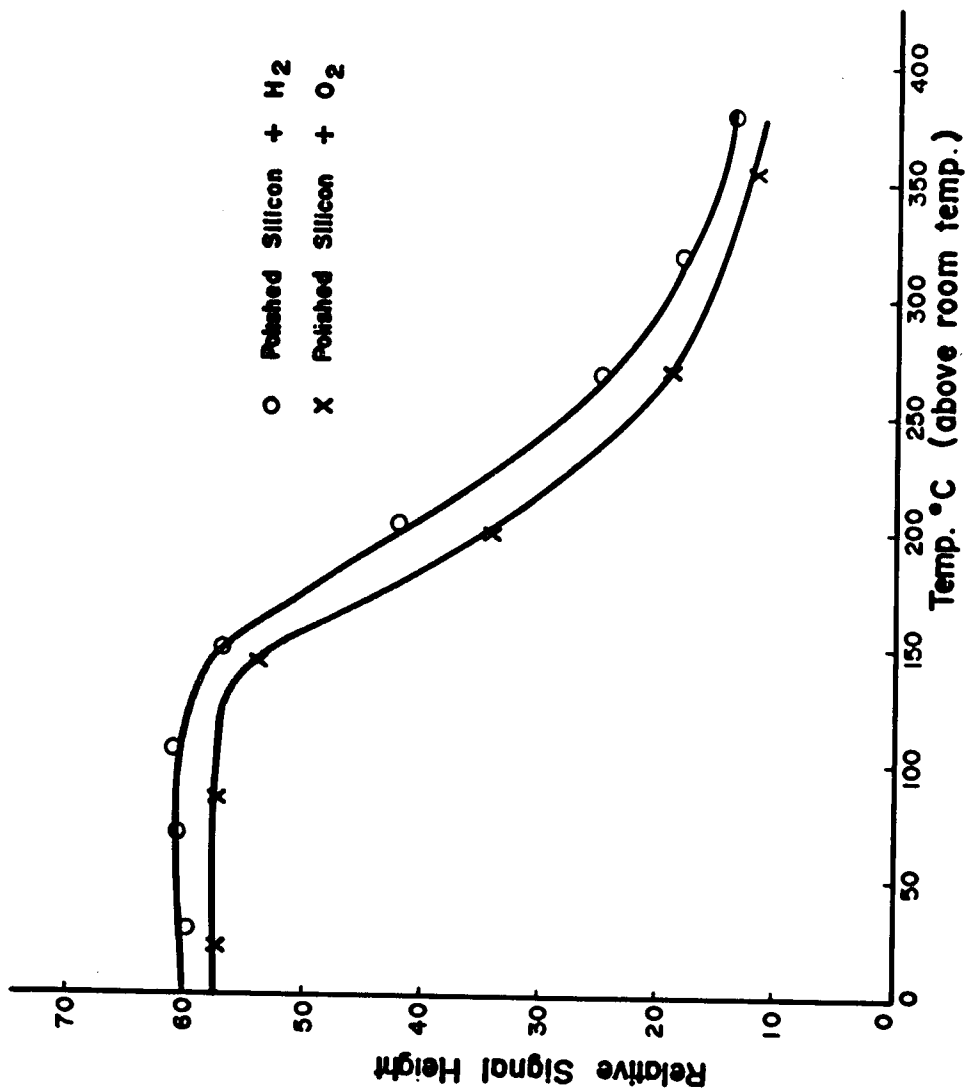


Figure 5.F.7.

LINE WIDTH VERSUS TEMPERATURE FOR  
POLISHED SILICON. ANNEALING FOR  
30 MINUTES. READINGS TAKEN AT  
ROOM TEMPERATURES.

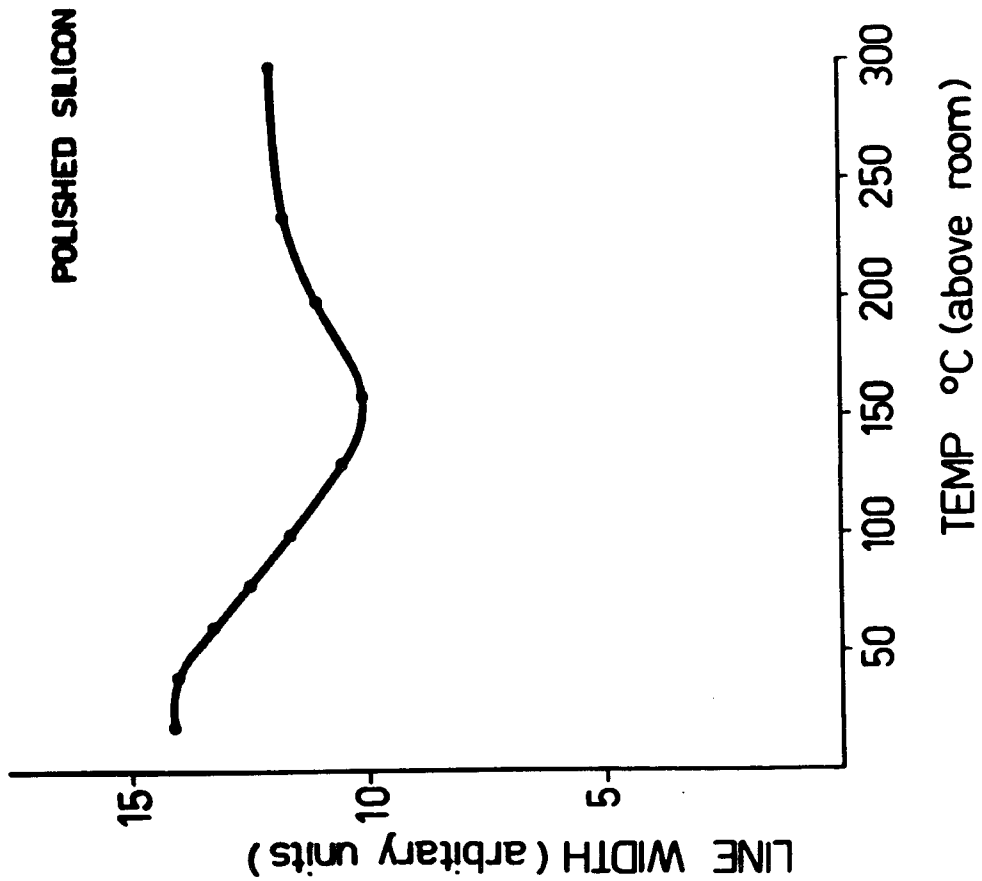
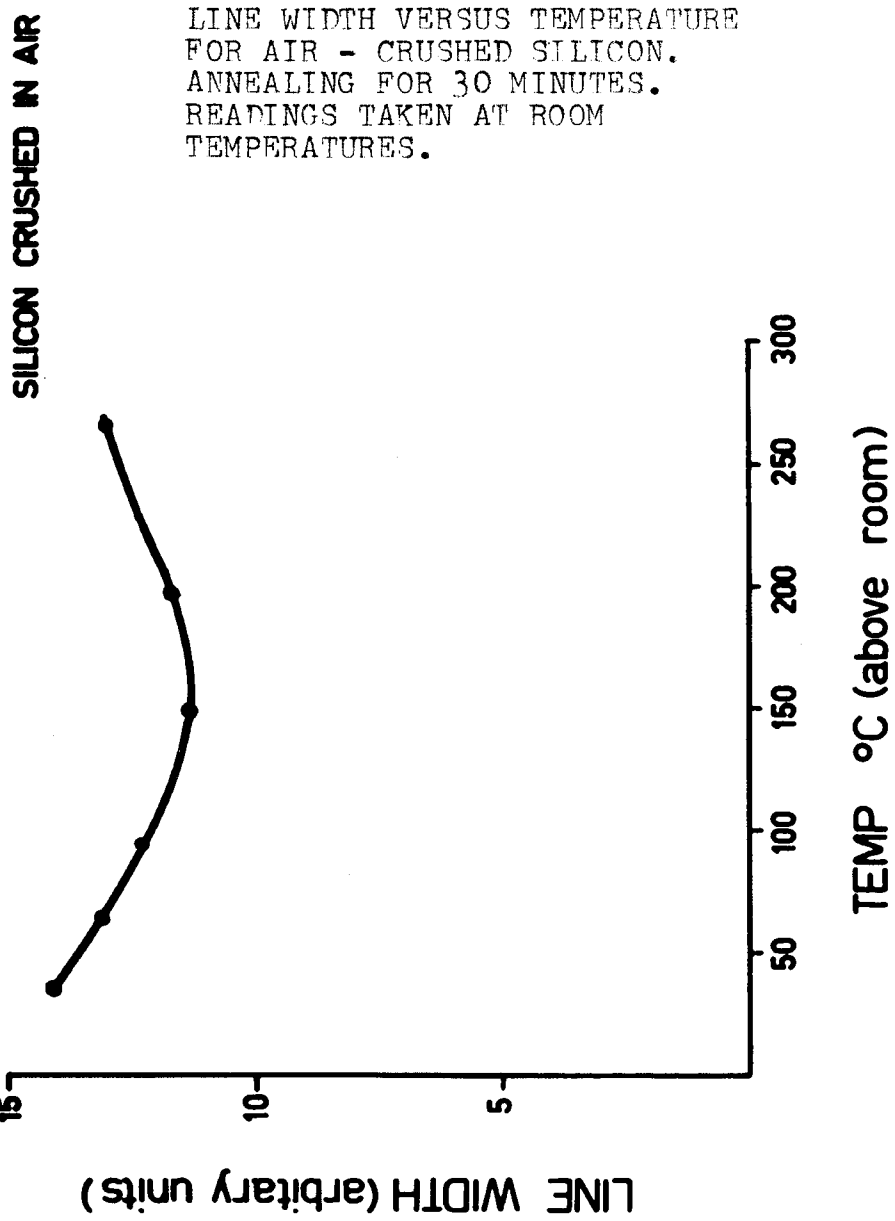


Figure 5.F.8.



SILICON CRUSHED IN AIR

□ In Vacuum ( $5 \times 10^{-8}$ ) no bakeout

△ 220°C above room temperature

Figure 5.F.9.

LINE SHAPE FOR AIR CRUSHED SILICON IN VACUUM AT ROOM TEMPERATURE, AND AT 220°C ABOVE ROOM TEMPERATURE. THESE ARE COMPARED WITH THE LORENTZIAN AND GAUSSIAN LINE SHAPES.

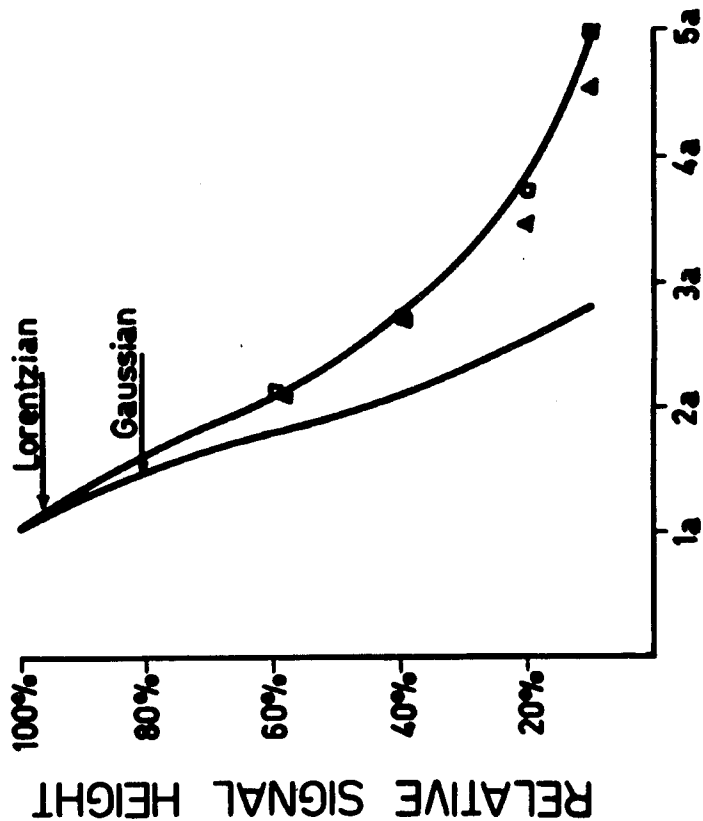
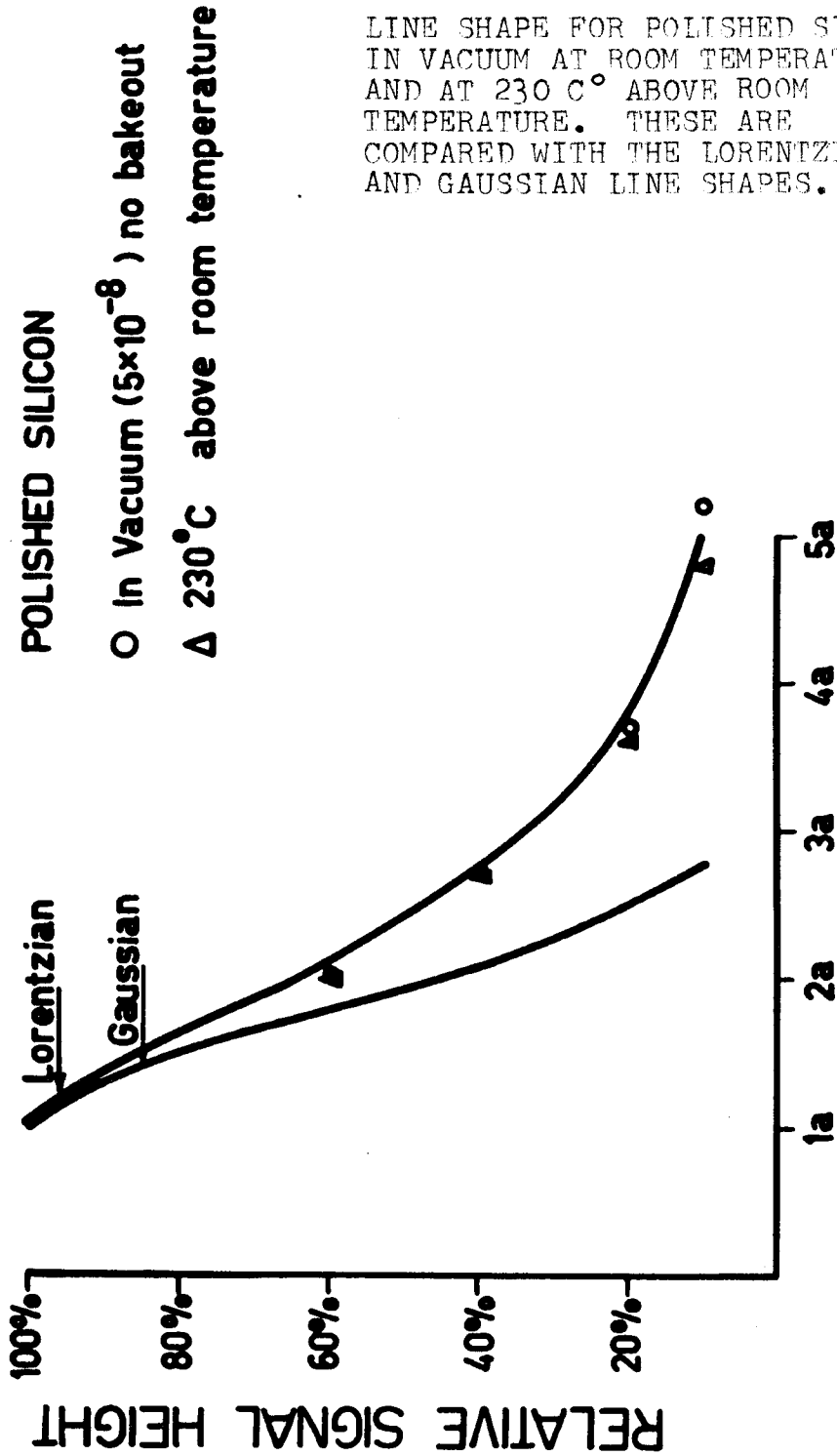


Figure 5.F.10.



germanium contained black wax - diamond paste impurities of amounts even as low as about  $10^{-8}$  cc, that they would be observable. In fact no signals were detected, showing that the polishing media, if present, were below detection limit.

Although it is well known that surface damage causes an e.p.r. signal, the present work confirms that even very fine polishing, with ( $\frac{1}{4}$  - 1) micron diamond paste, causes a signal to appear. Silicon crystals that had not been polished showed no signal. The signal arising out of the polished side was found not to be affected by chemical etching of the unpolished side. If however the polished face of the crystal was continually etched the signal height reduced and finally disappeared.

It was concluded therefore that the signal was due to effects of the polishing treatment on the silicon and not due to the polishing media themselves.

### 5.3.3

#### EXPERIMENTAL RESULTS.

The experimental results are given in the six figures opposite. The first figure, 5.F.5, is a plot showing the relative signal height versus temperature. In this, the tube was removed from the vacuum system under high vacuum ( $5 \times 10^{-8}$  torr), and the crystals gently tapped into the bottom of the quartz tube. This was then placed in the spectrometer cavity which had facilities for heating without having to remove the sample. The temperature quoted in all

the following results is the temperature to which the samples were heated. The actual readings were taken at room temperature.

The curves show the results for silicon crushed in air and for polished silicon. It is seen that the signal height (in both cases) stays the same until about 150 °C and then commences to drop, levelling off at about 400 °C.

A similar result is obtained for the case when the polished silicon is sealed in an oxygen / hydrogen atmosphere of 0.1 torr, the gas being let in after the high vacuum was obtained, figure 5.F.6. One may conclude from this that these gases have had little effect as far as the signal height is concerned.

The following two figures 5.F.7, 5.F.8, show the variation of line width with temperature. It is seen in this case, that for both the polished silicon and silicon crushed in air, the line width decreases until about 150 °C and then increases again.

The final figures show the effect on line shape of annealing. In 5.F.9 the experimental points for silicon crushed in vacuum, and after heating to 220 °C, are shown relative to the Lorentzian and Gaussian lines. This is repeated in 5.F.10 for polished silicon.

No change in  $g$  value with temperature was observed.

5.4

DISCUSSION AND CONCLUSION.

The occurrence of an e.p.r. signal from silicon samples which have been subjected to damage by sand-blasting, crushing or abrading has been known for some time.<sup>15,16,17)</sup> Recently a similar signal was reported for silicon crushed in vacuum.<sup>18)</sup>

In most of these cases however no details of the origin of the paramagnetic centres were given, although reference was made to such defects as vacancies, interstitials and dislocations.<sup>17)</sup> More explicitly Chung and Haneman<sup>18)</sup> have shown that the origin of the signal for vacuum crushed silicon appears to be unpaired surface electrons.

A conclusion as to the source of the e.p.r. centres in polished silicon specimens may be made in the light of the present work on surface stress and on effects of annealing on the stress, g value, line shape, line width and signal height. These results are summarised in table 5.T.2.

Principally it is required to determine whether the origin of the e.p.r. signal which is obtained for both the silicon crushed in air, and for polished silicon and which is centered at  $g = 2.0055$ , can be related to stress measurements and annealing results.

It has already been determined<sup>18)</sup> that

silicon crushed in ultra high vacuum has unpaired surface electrons which are created by the breaking of normal bonds during the formation of the surface. The e.p.r. signal in this case also had a  $g$  value of 2.0055 but was found to be affected by exposure to the active gases oxygen and hydrogen.

In the present case these gases had no effect, since the surfaces had been exposed to ambient.

Further it might be expected that the signal obtained by crushing silicon in air will also have dangling bonds which would however be modified by ambient.

TABLE 5.T.2

EFFECTS OF ANNEALING ON FINE POLISHED SILICON.

<u>Measured Quantity.</u>	<u>Effect of Annealing.</u>
	Decreases with annealing.
"g"	Not changed with annealing.
Line Width	Decreases with annealing.
Signal Height (Crushed & Polished)	Constant until 150 C then decreases with annealing.
Signal Height (Polished + $\frac{O}{2}$ / + $\frac{H}{2}$ )	Constant until 150 C then decreases with annealing.
Line Shape	Originally Lorentzian and remains so.

---

Therefore since silicon polished in air has the same  $g$  value and same annealing behaviour as the silicon crushed in air, we conclude that the e.p.r. centres in the polished silicon and in the air crushed silicon are the same, i.e. dangling bonds which have been modified by ambient.

This result leads us to suggest a model for the source of surface stresses and the associated e.p.r. signal in silicon.

We have already concluded above that the e.p.r. signal and surface stresses are both generated at or very near the surface.

Although the relation between stresses and e.p.r. signal is as yet not clear we believe that the two are related. It is proposed that during mechanical damage such as polishing, sandblasting or crushing, fresh clean surfaces are momentarily exposed, containing the active e.p.r. centres. These surfaces are quickly (nanoseconds) covered by surrounding ambients. Thus the signal from powders crushed in air or mechanically polished specimens is due to freshly created and immediately contaminated surfaces. This explains why the behaviour of the e.p.r. signal with annealing is the same both for air crushed powders and polished surfaces, since the centres are the same.

The regions surrounding the cracks and

fissures would be under a tensile stress and would result in the observed bending of the crystal.

However such microcracks or fissures would not in themselves be sufficient to give the observed stresses, as the surface would tend to close up again, since the bulk of the crystal is under compression. It follows therefore that associated with these openings there must be an effect which keeps the surface under tension.

This would occur from any of the following:

- a) Imbedded polishing, or chipped material.
- b) Vacancies.
- c) Interstitials.
- d) Dislocations.
- e) Surface mismatching.
- f) A combination of these.

If any of these are assumed they must also account for the observed low temperature annealing effects.

It seems that the first of these a) may be discounted. An imbedded particle, due either to polishing material or part of the broken crystal would be of a permanent nature and it is difficult to see how the stress generated by such a particle could be removed by low temperature annealing.

Definite identification of vacancies, interstitials and dislocations are difficult at the present

TABLE 5.T.3

$E_v$ ,  $E_d$ ,  $E_I$  ARE MIGRATION ENERGIES FOR VACANCIES,  
DISLOCATIONS AND INTERSTITIALS RESPECTIVELY.

Silicon	$E_v$	=	0.005 eV	Whan R.E. (1965). <sup>21)</sup>
	$E_d$		Not Calculated.	
	$E_I$	=	0.51 eV	Bennemann K.H. (1965). <sup>22)</sup>
	$E_I$	=	0.22 eV	Hasiguti R.R. (1966). <sup>23)</sup>
Germanium	$E_v$	=	0.005 eV	Whan R.E. (1965).
	$E_d$	=	0.55 eV	Friedel J. (1964). <sup>24)</sup>
	$E_I$	=	0.44 eV	Bennemann K.H. (1965).
	$E_I$	=	0.25 eV	Hasiguti R.R. (1966).

stage. This is partly due to the lack of understanding of their mechanisms and to insufficient experimental data.<sup>20)</sup>

It would seem that vacancies might have low enough migration energies to account for the low temperature annealing while those for interstitials and dislocations are too high.

In table 5.T.3 these energies are given for both silicon and germanium.

We see that if these values of energies for dislocations and interstitials are accepted as being of the right order of magnitude, it is improbable that they would explain the experimental results. However vacancies alone may be ruled out as they would result in a shrinking rather than expanding surface area.

Of course it cannot be excluded that combinations of b), c) and d) are responsible, although the independence of the annealing as a function of temperature for the four crystal types (Chapter 4) seems to mitigate against a diffusion mechanism which would result in such a combination.

However we propose here a different model.

Recent studies of controlled cracks in germanium have indicated that when fissures are formed the steps and irregularities on the surface have an average height of about  $\frac{1}{4}$  -  $\frac{1}{2}$  microns. In this case unless the crack is<sup>25)</sup>

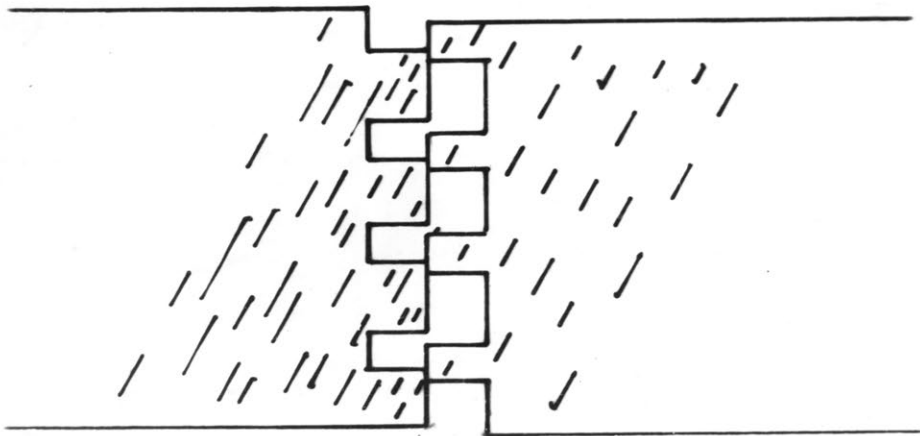


Figure 5.F.11.

PROPOSED SURFACE "MISMATCH" MODEL. TOP VIEW  
OF SURFACE CONTAINING CRACK SHOWING  
MISMATCHED IRREGULARITIES DUE TO  
DISPLACEMENT OF RIGHT HAND SIDE WITH  
RESPECT TO LEFT HAND SIDE.

longer than 0.1 m.m. the steps do not fully disengage. Therefore on relieving the stress the cracks can close completely.

However in the present case such control during the formation of the cracks and fissures is impossible. The rough treatment to which the surfaces are subjected would result in the forces creating the splits having various components. Any sideway component on the steps would prevent the cracks from closing.

Therefore we conclude that some cracks remain open due to the mismatching of surface irregularities. This is illustrated schematically in figure 5.F.11.

This mismatching would cause the lattice to stay wedged open at various places. This would then give rise to the measured stress.

It is of interest to see if this model agrees with, or at least is consistent with, experimental results.

In the previous chapter, when discussing the experimental results for InSb, we made the observation that it appeared as if an equilibrium situation existed. With this model we see that the bulk forces are in equilibrium with the forces of the mismatched surfaces. These surfaces, since not fully closed, would also give rise to the broken bonds detected by e.p.r.

We note first of all that the measured  $g$  value, 2.0055, is close to the free electron value of 2.0023. This indicates that the main contribution is coming from the electronic angular momentum, rather than orbital angular momentum. As such we would expect that the electrons belong to atoms whose atomic shells are more than half full. A broken surface bond in a silicon crystal certainly possesses this property.

The results for signal height and line width, while being consistent with the dangling bond model, also show some possible correlation with the stress measurements. Since the number of spins is proportional to  $h \times w^2$  (equation E.5.6) we see from the combination of 5.F.5 and 5.F.7 that the number of spins decreases even at relatively low temperatures. This would be expected in the above model since any heat energy supplied would unbalance the equilibrium causing some of the surface irregularities to close up with the resulting decrease in both e.p.r. intensity and stress.

We conclude therefore that for the case of silicon the e.p.r. signal is caused by unpaired surface electrons originating at surfaces created during the polishing operation. Atomic mismatching of surfaces of fissures is considered to be the source of the measured surface stress.

CHAPTER 6.            COMPUTER CALCULATIONS OF SEMICONDUCTOR  
SURFACE STRUCTURES.

6.1                    INTRODUCTION.

In the introductory chapter we gave as one of our aims the correlation of the present experimental results with L.E.E.D. measurements and perhaps, from this, to postulate models for the surface structure. In this chapter some possible structures are investigated by computational calculations.

Although it appears from L.E.E.D. measurements (chapter 1) that the clean surfaces of many semiconductors have atomic arrangements which differ from those of the corresponding planes in the bulk, it has not, to date, been possible to definitely establish the structure. There have been a number of experiments reported however, which provide indirect evidence. These involve measurements of L.E.E.D. <sup>1,2,3,4,5,6,7,8)</sup> surface state properties, <sup>9)</sup> spin resonance <sup>10)</sup> and surface mating characteristics. <sup>11)</sup>

It was considered useful at this stage to obtain further evidence about the structure from theoretical calculations of surface energy using the principle that the surface energy is a minimum for an equilibrium structure, and comparing the results with quantitative energy measurements.

In principle such a calculation requires that, starting from an ideal structure, one deduces a

structure which has minimum energy. To do this involves specifying, in the surface, parameters involving atomic position vectors and atomic force constants. The equilibrium structure is then calculated by allowing the atoms to vary their positions such as to minimise the energy.

Originally a self consistent method was attempted. Having described the energy as a function of atomic position vectors and different force constants, to account for different nearest neighbours, the surface atoms were made to move in a random manner, and, for each new atomic position, the energy minimised. This allowed the determination of the unknown parameters. These calculated parameters were then used to describe the new energy and the procedure repeated.

However, because of the very large number of degrees of freedom possible in choosing combinations of atomic movements, this calculation required excessive amounts of computation time. It was felt that, in view of the uncertainties in the knowledge of the inter-atomic potential function, such time consuming calculations were not warranted. Instead, the problem was kept finite by adopting a particular expression of the above approach. This was to adopt a particular model for the surface structure. The one chosen was that proposed by Haneman,

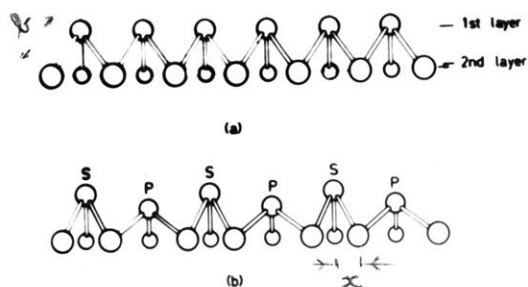


Figure 6.F.1.

- (a) SECTIONAL VIEW OF "IDEAL" (111) SURFACE. ARROWS DEPICT ATOM SHIFTS. ATOMS IN REGULAR GROUPS IN 2ND. LAYER EACH MOVE A DISTANCE  $\tau_0^+$  AS SHOWN, TOWARDS CENTROID OF EACH GROUP OF 3. BOND LENGTH  $b$  TO 1ST. LAYER ATOMS IS KEPT CONSTANT. THIS RESULTS IN BUCKLING OR RUMPLING OF SURFACE, AS SHOWN IN (b).
- (b) RESULTANT STRUCTURE, CORRESPONDING TO THAT PREDICTED THEORETICALLY BY HANEMAN USING DANGLING BOND DEHYBRIDISATION CONCEPTS. THE RAISED ATOMS HAVE S DANGLING BONDS, THE LOWERED ONES HAVE p DANGLING BONDS.

which was originally derived from dangling bond dehybridisation concepts, and discussed in detail in chapter 1, where it was shown to be consistent with current L.E.E.D. and other measurements. The essential feature of the model is a general rumpling of the surface with atoms being raised and lowered. This lends itself to simpler computation by varying only one parameter. Thus the positions of atoms in the second layer are varied such that the distance of a second layer atom from the projection of a surface atom onto the second layer is varied in line. Refer to figure 6.F.1 (a). We see from this that if the bond lengths to the surface atoms are kept constant the surface will automatically buckle. (6.F.1 (b)).

The above structure has been found to be consistent with recent L.E.E.D. <sup>8)</sup> and mating data <sup>11)</sup> for the (111) surfaces of germanium. It is therefore of interest to deduce quantitative parameters for it from surface energy minimisation.

6.2

### THE INTERATOMIC POTENTIAL FUNCTION.

One of the major unknown factors, and hence a great limitation, in any calculations dealing with surfaces, is the potential energy function. It was decided here to use as an inter-atomic function the Morse potential  $M(r)$ . This is defined by:

$$M(r) = D (\exp(-2a(r - r_0)) - 2 \exp(-a(r - r_0))) \quad \text{E.6.1}$$

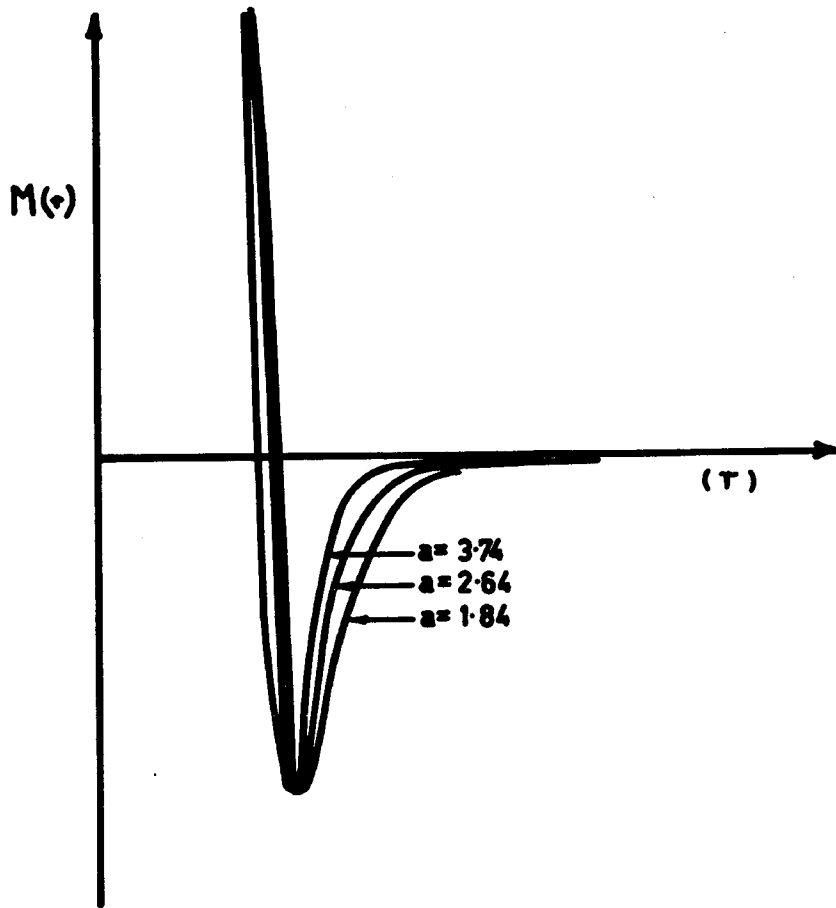


Figure 6.F.2.

PLOTTING  $M(r)$  AS A FUNCTION OF  $r$  FOR  
VARYING VALUES OF "a".

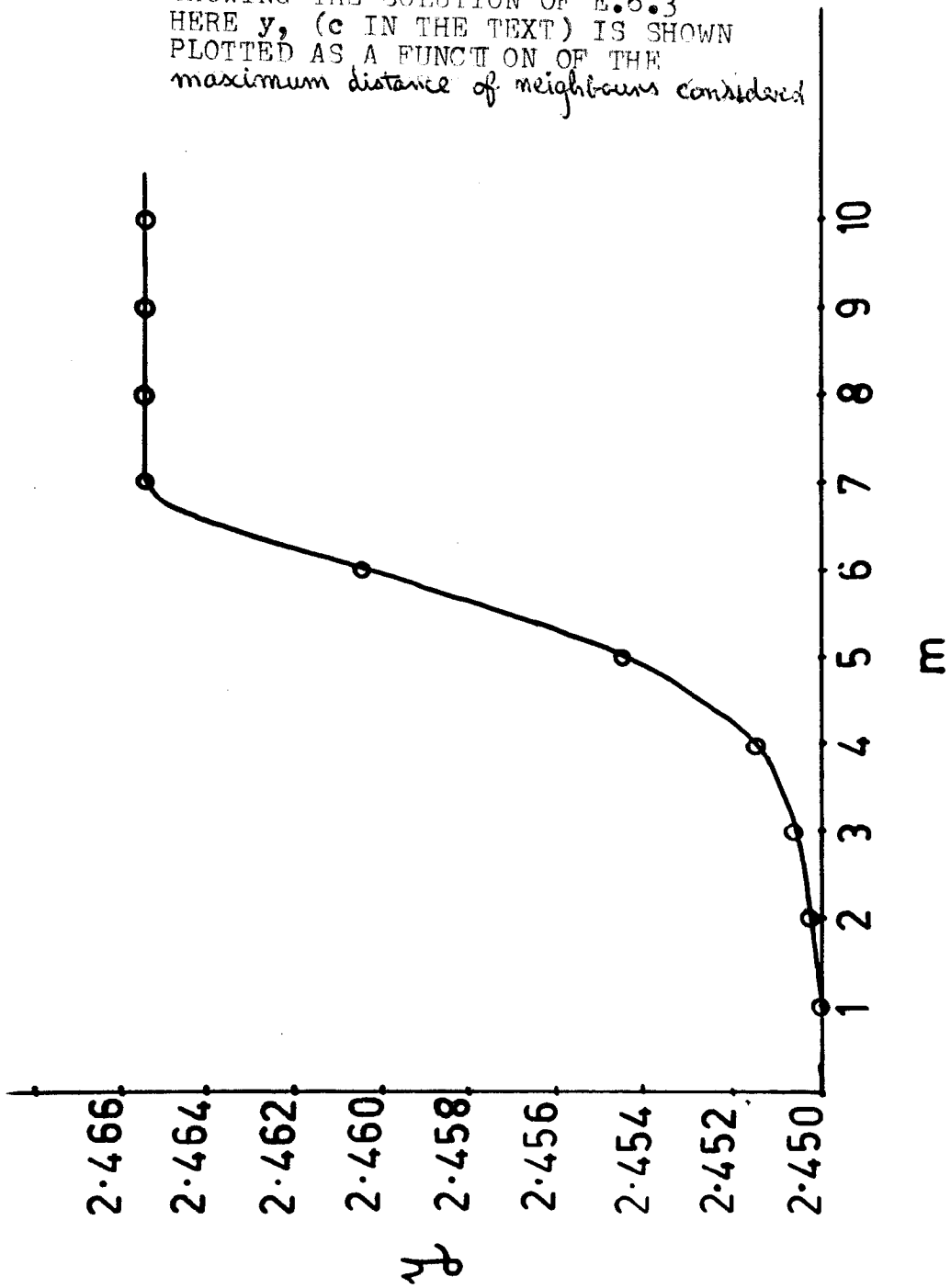
where  $D$  is the energy of dissociation of a bond and the parameter " $a$ " determines the steepness of the potential as shown in figure 6.F.2. The variable  $r$  is the distance between two atoms whose equilibrium spacing is  $r_0$ .

This function was chosen for several reasons. It is a standard potential and one that might be expected to approximate to a reasonable extent the actual potential, particularly when  $D$ , and especially " $a$ ", are regarded as adjustable parameters. Girifalco and Weizer<sup>12)</sup> have successfully calculated the elastic constants for both face centred and body centred cubic metals with this potential. Swalin<sup>13)</sup> used it in calculating enthalpies and entropies of diffusion of vacancies for silicon and germanium. More recently a similar type of potential (Born-Mayer)<sup>14)</sup> has been used by Hasiguti to determine migration energies of interstitials in germanium and silicon. The Morse potential has also been employed by Nicholas<sup>15)</sup> in calculating surface energies of metals.

A calculation was performed to see whether the Morse potential is consistent with the germanium, (and in general the F.C.C.) structure. This was done in case it proved that the germanium lattice could not be described by this potential. If this were the case, the calculated lattice would be unstable, and an equilibrium configuration

Figure 6.F.3.

SHOWING THE SOLUTION OF E.6.3  
HERE  $y$ , (c IN THE TEXT) IS SHOWN  
PLOTTED AS A FUNCTION OF THE  
*maximum distance of neighbours considered*



corresponding to the known lattice could not be obtained.

To do this the energy of the unknown lattice was first computed as

$$E_T = \sum_{i=0}^{N-1} n_i D(\exp(-2a(x_i - c)) - 2\exp(-a(x_i - c))) \quad E.6.2$$

Where  $E_T$  is the total energy of the lattice,  $x_i$  the inter-atomic distances in a lattice of known geometry.  $i = 0$  for first neighbours, 1 for second nearest neighbours etc., and  $n_i$  is the number of such neighbours, and where the summation is carried out over  $N$  nearest neighbours ( $n/n$ ). We note that all the  $x_i$  are expressed in terms of factors of  $x_0$ . The quantity  $c$  is to be determined and corresponds to the equilibrium distance between first  $n/n$  in the calculated lattice. This was found by minimising the energy expression so that

$$\left( \frac{\partial E_T}{\partial x_0} \right)_{x_0 = r_0} = 0 \quad E.6.3$$

where  $r_0 = 2.45 \text{ \AA}$  is the equilibrium distance of the known lattice, and  $a = 1.8 \text{ \AA}^{-1}$ . The result of this computation is shown in figure 6.F.3. Here the calculated value of  $c$  is plotted as a function of the closeness of neighbours considered. We see that the Morse potential predicts an equilibrium distance of  $2.4655 \text{ \AA}$  as compared with  $2.45 \text{ \AA}$  for the known lattice.

It is possible that adopting a similar procedure for the other adjustable parameters could result in a closer "fit". However the following calculations in this chapter were found not to be sensitive to this difference and in fact the value of  $2.45 \overset{\circ}{\text{A}}$  was used. Note too that there is little effect beyond the seventh nearest neighbours.

A further possible difficulty in choosing the Morse function is that it results in central forces only. Distorting a diamond type lattice however involves non central forces as well because of the directional character of the bonds. It was felt, however, that for a computation of the energy of a given configuration the potential would be reasonably accurate, particularly for strong covalent substances like silicon and germanium where the central forces are most important in determining the energy. <sup>16)</sup>

### 6.3 CALCULATION OF THE MINIMUM ENERGY OF A RUMPLED GERMANIUM (111) SURFACE.

#### 6.3.1 SCOPE OF INTERACTIONS.

The minimum energy of the rumped surface is calculated by considering the following interactions.

a) The first layer is made to interact with first and second nearest neighbours.

This means that the energy calculation extends to the third layer.

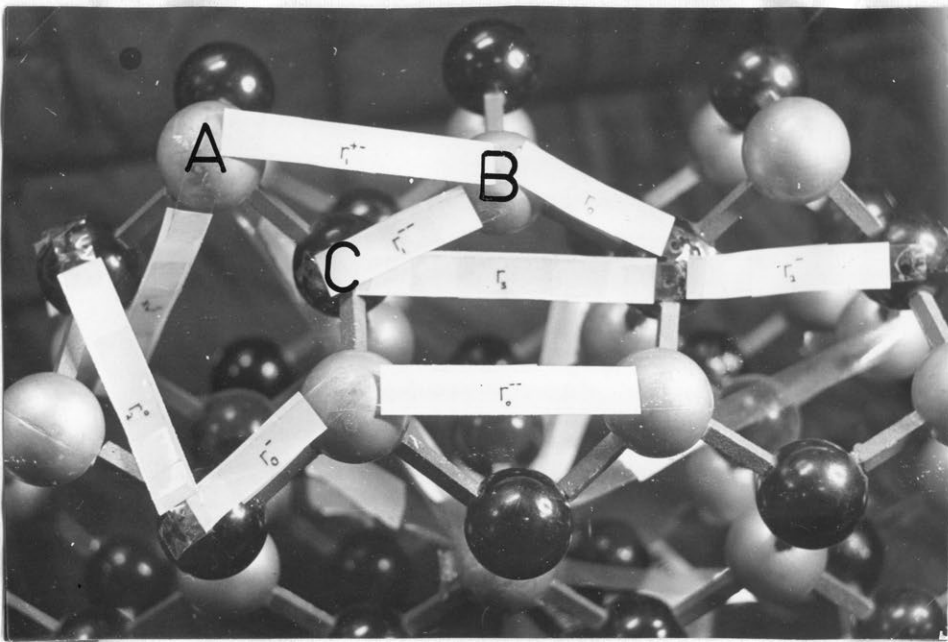
b) The second layer is made to interact in the following manner.

- 1) With its first nearest neighbour, i.e. the third layer.
- 2) With its second nearest neighbour contained only in the second layer.

The basic assumption is that there is a general displacement  $r^+$  (x in figure 6.F.1) by a second layer atom in this plane. All other distances are then given in terms of this one displacement. This results in atoms of the first layer being raised and lowered.

The following distances are used in the calculations, where the distances are between;

- 1)  $r^{\circ}$  The raised atoms with the second layer atoms which have moved inwards (also equals equilibrium nearest neighbour distance in normal state).
- 2)  $r_1^+$  The raised atoms with the second nearest neighbour atoms in the third layer.
- 3)  $r_1^{+-}$  The raised atoms with the second nearest neighbour atoms on the surface, that have been lowered.
- 4)  $r^{\circ-}$  The lowered atoms with those in the second layer that have not moved.
- 5)  $r_1^{--}$  The lowered atoms with those in the third layer, i.e. second nearest neighbour.
- 6)  $r^{\circ--}$  The <sup>un</sup>lowered atoms with <sup>un</sup>lowered atoms, both in first layer ( $\equiv r_1$ ).



The model is of a 3 - 5 structure, represented by the black and white balls. This model may represent the germanium lattice if the balls are considered as being identical. Some of the distances used in the computer calculation are shown in the model. Three of the "atoms" are marked indicating

- A - atom raised
- B - atom lowered
- C - atom moves towards raised atom

- 7)  $r_2^*$  Second layer atoms that moved, with the third layer atoms underneath.
- 8)  $r_2^-$  Second layer atoms that moved, with those that have also moved (shrunk triangle) both in second layer.
- 9)  $r_2^0$  Second layer atoms that moved, with those that did not move (both in second layer).
- 10)  $r_0$  The lowered atoms with those in second layer which moved.
- 11)  $r_3$  The second layer atoms that have expanded with those others that have also expanded (expanded triangle).
- 12)  $r_0$  Second layer not moved with third layer not moved.
- 13)  $r_1$  The distance between any two nearest neighbours in normal state.

(An illustration of some of these distances are shown on the model opposite).

### 6.3.2 FUNCTIONAL RELATIONSHIP BETWEEN DISTANCES.

Use is made of the following parameters:

$h^*$  is the vertical distance from a raised first layer atom to the second layer.

$h^-$  is the vertical distance from a lowered first layer atom to the second layer.

$\Theta$  is the angle subtended between any atom and two nearest second neighbours forming a triangle in the plane.

$\phi$  is the distance between the apex of this triangle and its centroid.

The symbols DD and  $\alpha$  are illustrated below in figure 6.F.4.

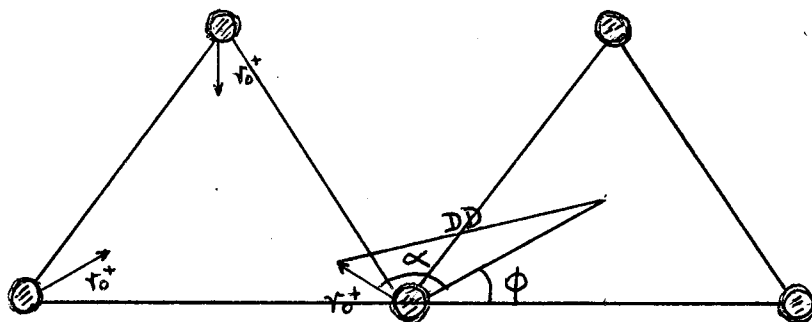


Figure 6.F.4

VIEW OF SECOND LAYER SHOWING ATOM SHIFTS AND ANGLES.

With these parameters the following relationships hold.

$$1) \quad \phi = r_1 \cos(\theta/2) / 2$$

$$2) \quad DD^2 = (r_0^+)^2 + \phi^2 - 2r_0^+ \phi \cos \alpha$$

$$3) \quad r_0^- = DD^2 + (h^-)^2$$

$$4) \quad h^+ = (r_0^2 - (\phi - r_0^+)^2)^{\frac{1}{2}}$$

$$5) \quad h^- = (r_0^2 - DD^2)^{\frac{1}{2}}$$

$$6) \quad r_1^{\pm} = \left( (h^+ - h^-)^2 + r_1^2 \right)^{\frac{1}{2}}$$

$$7) \quad r_1^{--} = \left( \phi^2 + (r_o + h)^{-2} \right)^{\frac{1}{2}}$$

$$8) \quad r_1^{+} = \left( \phi^2 + (r_o + h)^{+2} \right)^{\frac{1}{2}}$$

$$9) \quad r_2^{+} = \left( r_o^2 + (r_o)^{+2} \right)^{\frac{1}{2}}$$

$$10) \quad r_2^{-} = 2 \left( \phi - r_o^{+} \right) \times \cos (\theta/2)$$

$$11) \quad r_2^o = \left( (r_o)^{+2} + (r_1^2) \right)^{\frac{1}{2}}$$

$$12) \quad r_3 = 2 \left( \phi + r_o^{+} \right) \times \cos \theta/2$$

$$13) \quad r_o^{-} = \left( (h)^{-2} + \phi^2 \right)^{\frac{1}{2}}$$

## 6.3.3

PROCEDURE.

The total specific energy of the surface is given by

$$E = \sum_i n_i M(r_i) \quad E.6.4$$

where  $n_i$  are the number of bonds of length  $r_i$ ,  $r_i$  being a function of  $r_o^{+}$ . The energy is a function of three parameters,  $r_o^{+}$ , and the Morse parameters "a" and D, and is minimised by setting

$$\frac{\partial E}{\partial r_o^{+}} = 0 \quad E.6.5$$

Figure 6.F.6.

PLOTTING "a" VERSUS  $r^+$  FOR WHICH THE  
MINIMUM ENERGY OF THE GERMANIUM (111)  
SURFACE OCCURS.

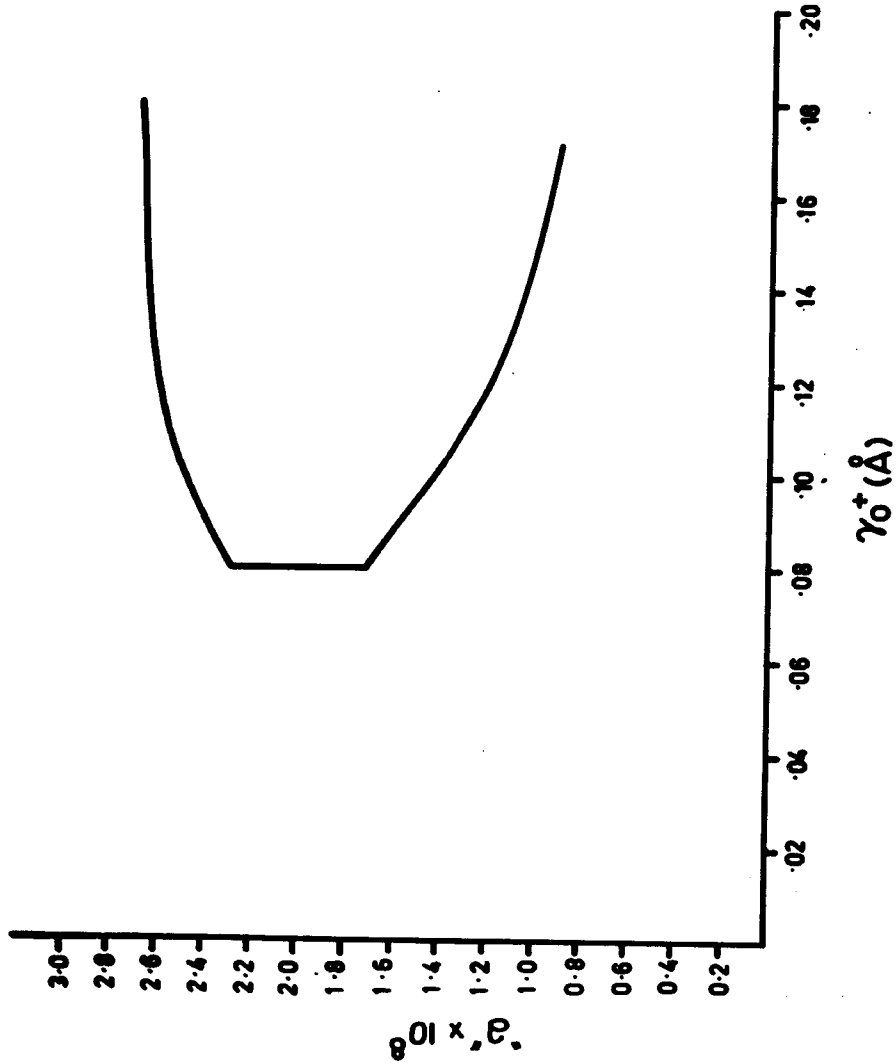
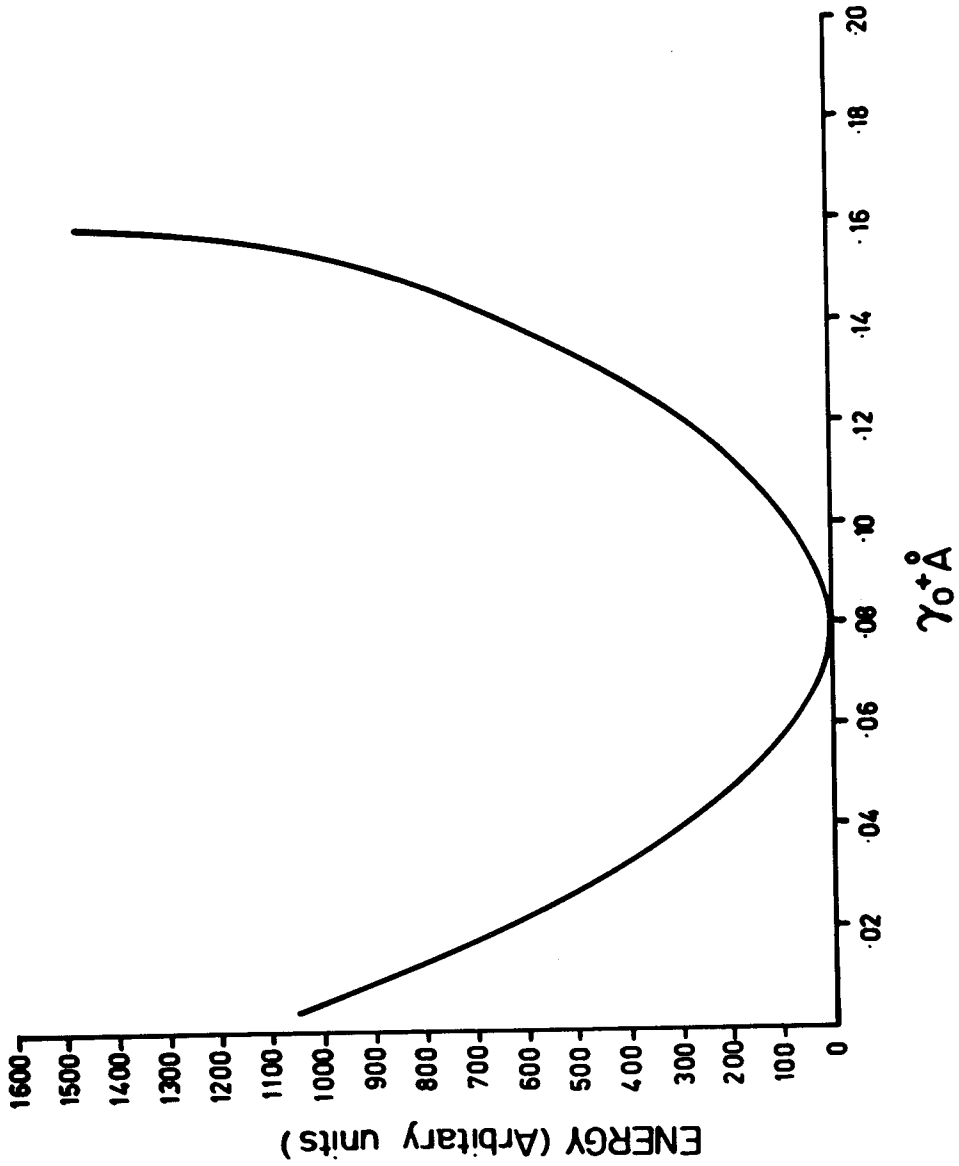


Figure 6.F.5.

MINIMUM ENERGY OF A RUMPLED (111) GERMANIUM SURFACE AS A FUNCTION OF  $r_0$ .



for particular values of  $D$  and " $a$ ". In practice, values of  $r^+$  and  $D$  were chosen and minimum energies for a range of values of " $a$ " determined. This was repeated for various  $r^+$  and  $D$  ("nesting 3 DO loops"), (appendix 1), on an I.B.M. 360/50 computer.

#### 6.3.4 RESULTS.

Figure 6.F.5 shows the variation of the energy of the ruffled surface as a function of the displacement  $r^+$ . This was calculated for a particular value of " $a$ " equal to 1.8. Similar curves are also obtained when " $a$ " lies in the range between 0.8 to 3.6. It is interesting to note that the energy is indeed lowered if the "ideal" structure changes to the H-model. The energy is seen to become a minimum if the atom in the second layer is shifted by 0.08 Å.

A curve was also drawn showing the variation of " $a$ " with the value of  $r^+$  at which the minimum energy occurs. This is shown in figure 6.F.6. We note here that the minimum shift in  $r^+$  is approximately 0.08 Å and that it occurs for a range of " $a$ " values, (approximately 1.7 to 2.3).

More definite information can be obtained if the parameters " $a$ " and  $D$  of the potential function can be specified. This may be done by regarding them as two unknown quantities which are to be "fitted" to known

experimental results. Therefore at least two different measurements are required to determine them. Suitable measured quantities used here are the surface energy, the sublimation energy and the elastic constants.

#### 6.4 CALCULATION OF THE SURFACE ENERGY of the (111) GERMANIUM SURFACE.

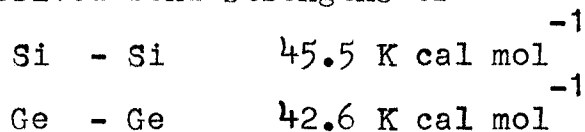
##### 6.4.1 INTRODUCTION.

We have already defined the surface free energy as the reversible work required to create unit area of surface by separation of the material, example cleavage. Since the (111) plane is a cleavage plane for germanium and silicon, the surface energy of this plane can be obtained by splitting crystals along the (111) cleavage planes. The absence of plasticity at room temperature and below, makes theoretical interpretation of the measurements less complex.

Measurements of the force required to just propagate a preexisting crack in a crystal were made by Gilman<sup>17)</sup> and Jaccodine,<sup>18)</sup> using Gilman's analysis to derive the surface energy.

This analysis is in error by an undetermined amount,<sup>19)</sup> but the derived values 1240 and 1230 ergs cm<sup>-2</sup> for silicon and 1060 ergs cm<sup>-2</sup> for germanium, are at least a guide and consistent within 20% with theoretical value of Zadumkin<sup>20)</sup> who, using a Debye approximation obtained 1430 and 1109 ergs cm<sup>-2</sup> for silicon and germanium

respectively. Knowing the density of bonds along the (111) plane Jaccodine derived bond strengths of



#### 6.4.2

##### PROCEDURE.

As can be seen from the definition, the surface free energy may be calculated as the reversible work required to break the bonds by separating the material along a (111) plane and determining the energy to "cut" these bonds. Only bonds up to seventh n/n were taken into account. Higher order neighbours were shown not to increase the accuracy significantly. This might have been expected in view of figure 6.F.3.

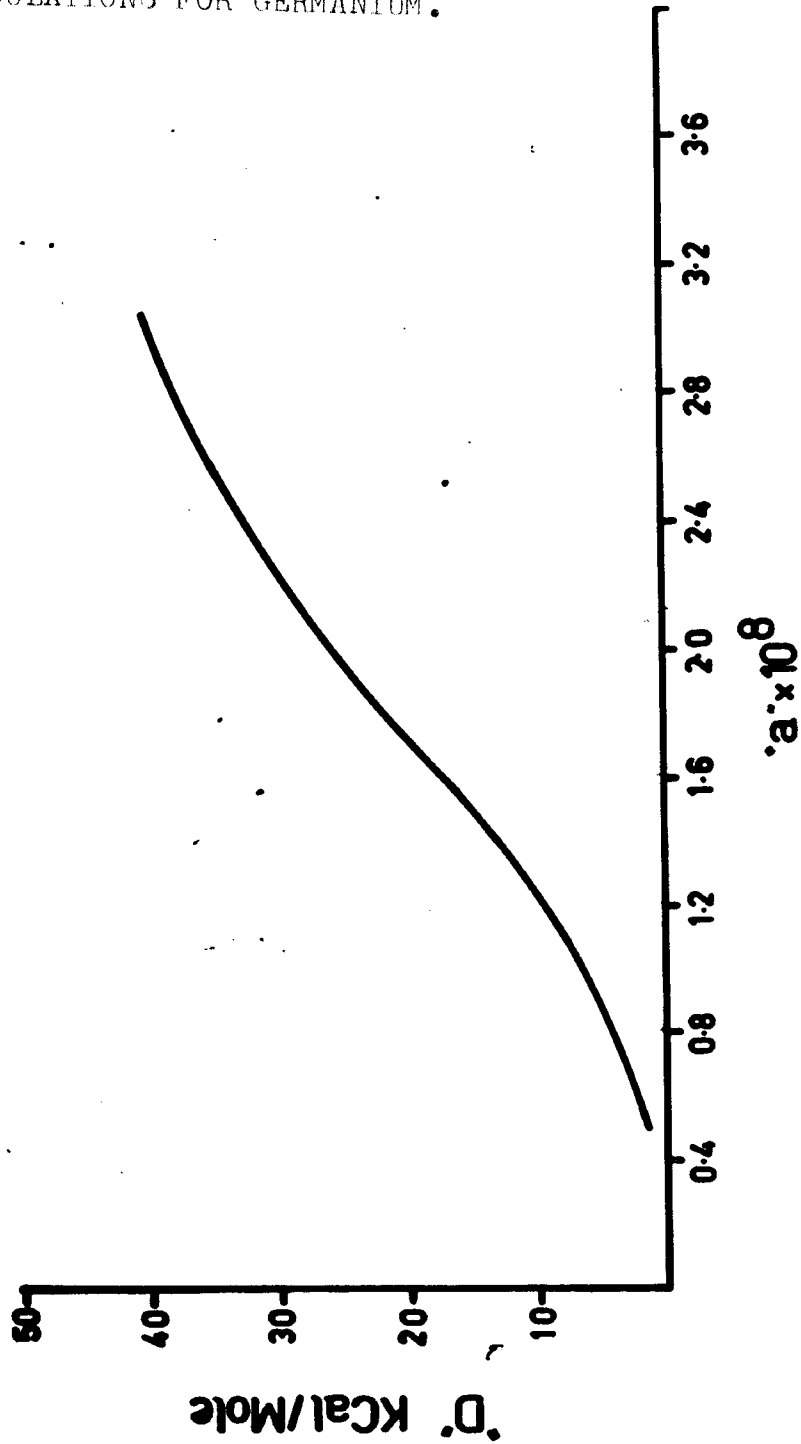
For the purpose of the calculation an imaginary (111) plane was drawn through the crystal. From any atom on one side of this plane, distances to the atoms on the other side of the plane were calculated. With the factor of 2 taken into account for the two surfaces the total surface energy is then given by:

$$E_S = \sum_i n_i M(r_i) \quad \text{E.6.7}$$

where  $n_i$  are the number of bonds and  $M(r_i)$  the relevant Morse function. We note that this expression is only in terms of the two Morse parameters "a" and D. Again incorporating two "nested DO loops" in the program (see

Figure 6.F.7.

SOLUTION OF (111) SURFACE ENERGY  
CALCULATIONS FOR GERMANIUM.



appendix 2) whole ranges of "a" and D were tried. The values of "a" and D chosen were those which gave an energy agreeing with the experimental results.

#### 6.4.3 RESULTS AND CONCLUSION.

In figure 6.F.7 the values of the possible "a" and D are shown. We note that this curve by itself does not give any conclusive results as solutions exist for "a" in the range 0.4 to 3.2 corresponding to a D range of 2 to 40, for germanium.

#### 6.5 CALCULATION OF THE SUBLIMATION ENERGY FOR GERMANIUM.

##### 6.5.1 INTRODUCTION.

Further information is clearly required to establish unique values of "a" and D. In an attempt to achieve this, the experimental sublimation energy was fitted to calculated values.

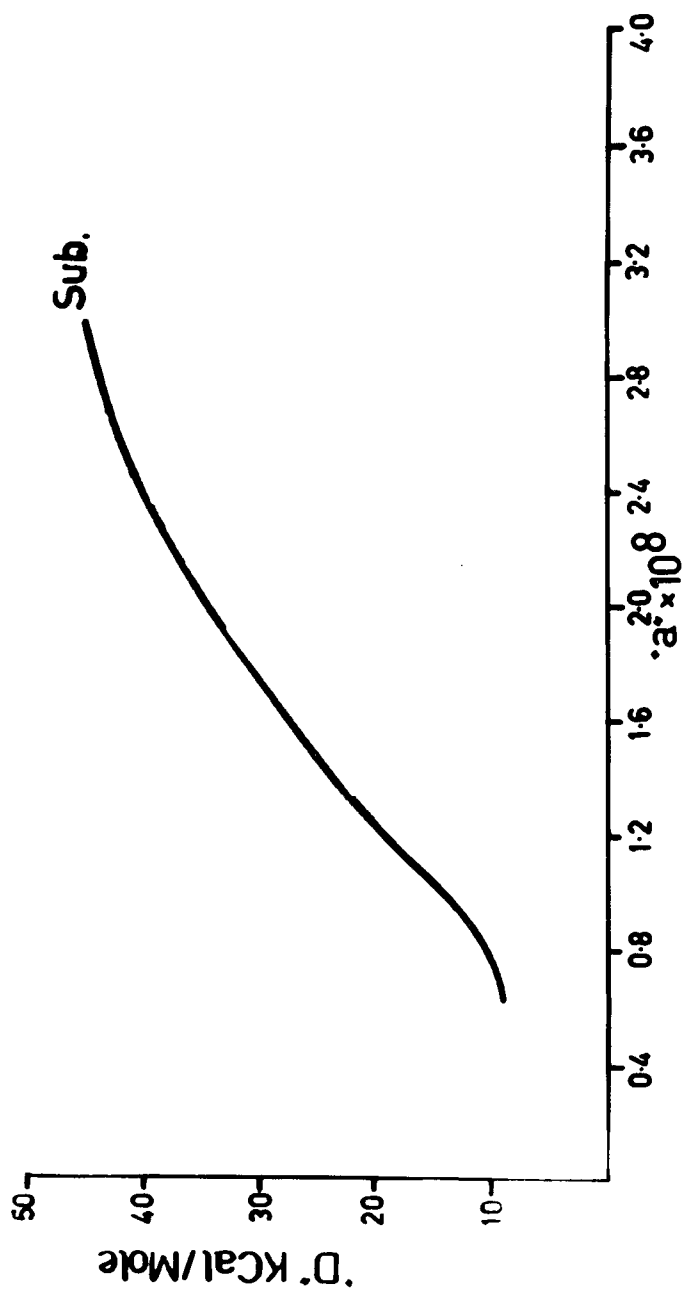
##### 6.5.2 PROCEDURE.

Sublimation energy is defined as the total energy required to remove an atom from the bulk of the crystal to infinity. In the calculation, an atom was taken inside the bulk, and its total interaction energy, with its neighbours, as described by the Morse potential, calculated. It was found sufficient to only include up to 7 n/n. Thus the expression for the sublimation energy may be written as,

$$E^S = \sum_i n_i \times M(r_i) \quad \text{E.6.8}$$

Figure 6.F.8.

SOLUTION OF SUBLIMATION ENERGY  
FOR GERMANIUM.



where  $E^S$  is the sublimation energy,  $n_i$  the number of bonds and  $M(r_i)$  the Morse function. Here again the expression is only in terms of the two adjustable parameters "a" and D. The procedure was as before. Two "DO loops", (see appendix 3), were nested and various combinations of "a" and D chosen.

### 6.5.3 RESULTS AND CONCLUSION.

The experimental value of sublimation energy for germanium is approximately  $89 \text{ K cal mol}^{-1}$ . Those values of "a" and D which gave this result are plotted, the rest being ignored. The result for this is shown in figure 6.F.8.

Here again we see that a whole range of "a" (0.6 to 3.0) and D (9 to 45) are possible and no unique values can be attributed. However it is noted that the results are consistent with those found by the surface free energy calculation. Clearly other experimental data has to be fitted.

### 6.6 CALCULATION OF THE ELASTIC CONSTANT C FOR GERMANIUM. 11

#### 6.6.1 INTRODUCTION.

The "a" and corresponding D values were finally restricted by fitting the experimental values of the elastic constant  $C_{11}$  for germanium. This constant has been reported as  $13.16 \times 10^{11} \text{ dyne cm}^{-2}$ . In the calculation of this constant it would be particularly desirable if we

could take into account the non central forces which are known to exist for germanium and silicon. Keating<sup>16)</sup> has discussed this problem and argues that there are no purely non central first neighbour interactions present in any nonmetallic crystals. By using only central first n/n forces and non central higher neighbours, he has deduced an expression for  $C_{11}$  which is in close agreement with the measured value. This has allowed a check on the computational calculations. In terms of the Morse potential the first neighbour force constant is given by a  $D$ . Equating this to the force constant deduced by Keating allows "a" to be plotted against  $D$  and thus may be used as a guide to the validity of the calculation.

## 6.6.2

PROCEDURE.

If the interaction between the atoms in a lattice can be expressed by a central force potential  $M(r)$  then it can be shown<sup>22)</sup> that

$$C_{11} = \frac{d^4}{2V} \sum_i M_{\lambda}^4 H_{\lambda}^2 (M(r_i)) \quad \text{E.6.9}$$

where "d" is the unit cell spacing and  $r_i$  is the atom position coordinate expressed in terms of cartesian coordinates as

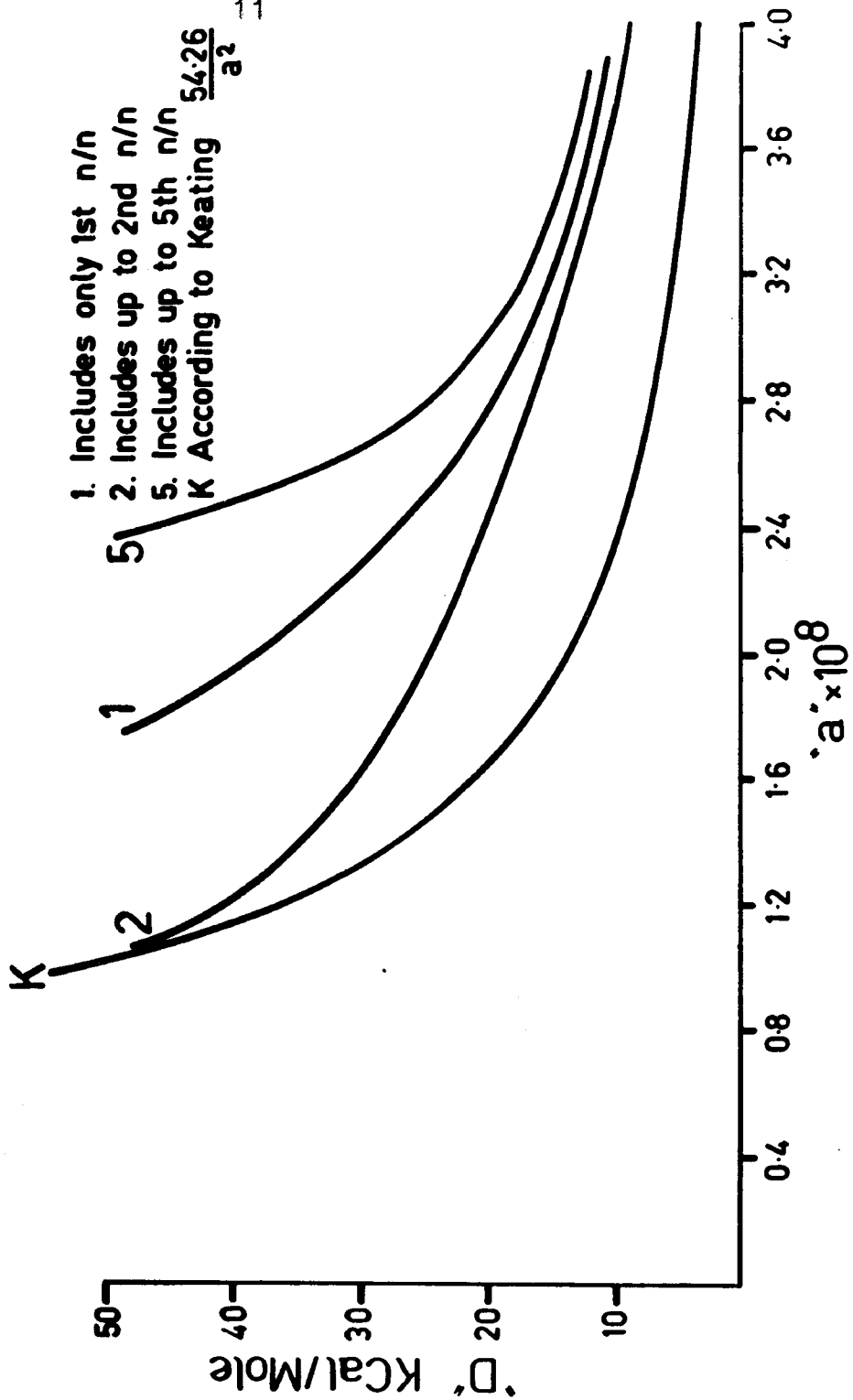
$r_i = (m_i, l_i, q_i)$ . The volume per unit atom is  $V$  and the

operator

$$H_i = \frac{1}{r_i} \left( \frac{d}{dr_i} \right) \quad \text{E.6.10}$$

Figure 6.F.9.

THE EXPRESSION DERIVED FROM KEATING IS DRAWN TOGETHER WITH THE SOLUTION OF THE GERMANIUM ELASTIC CONSTANT C<sub>11</sub>.



With the Morse potential used here, the expression for  $C_{11}$  involves only the parameters "a" and D. Two DO loops were (See appendix 4) incorporated in the computer program and values of "a" and D selected which resulted in values of  $C_{11}$  within 1% of the experimental value.

### 6.6.3 RESULTS AND CONCLUSION.

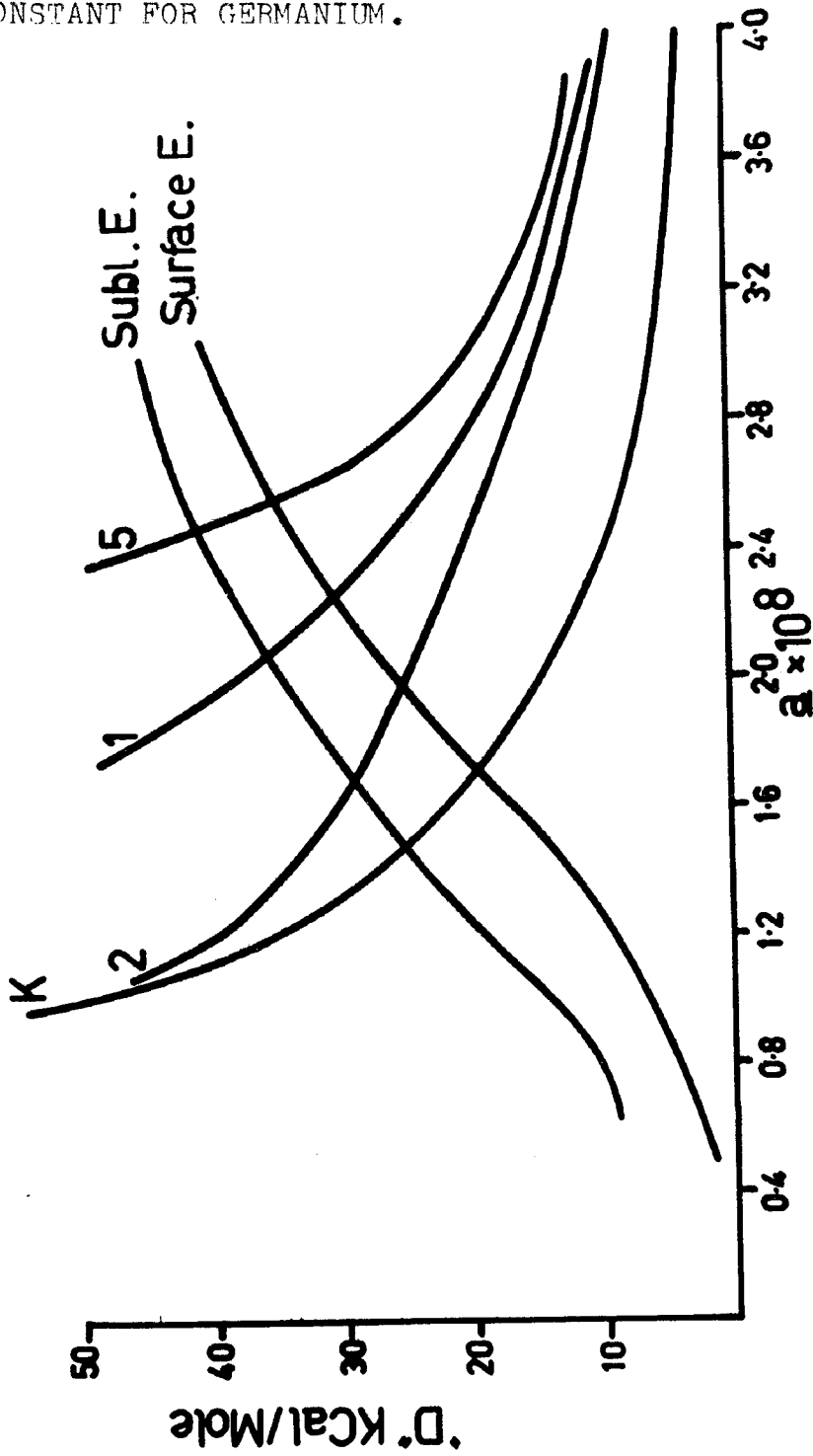
The results are shown in figure 6.F.9. To illustrate the effect of neighbours the calculation was performed taking into account 1) (see figure) first n/n only, 2) including up to second n/n and 3) including up to fifth n/n. The plot of "a" versus D according to Keating is also shown (K) in this figure.

### 6.7 GENERAL DISCUSSION AND CONCLUSION FOR GERMANIUM.

Combining the results for the surface energy, the sublimation energy and the elastic constant  $C_{11}$  should uniquely define, or at least, restrict, the values of "a" and D to be used. The curves are shown combined in figure 6.F.10. While it may be possible to adduce arguments in favour of using some of the elastic constant curves over the others, in view of the various uncertainties mentioned above, we will not engage in such discussion. Instead we draw attention to the broad fact that the range of "a" values covered by the intersections of the curves is approximately 1.6 to 2.6. Referring to figure 6.F.6 we see

Figure 6.F.10.

COMBINATION OF SURFACE FREE ENERGY,  
SUBLIMATION ENERGY AND THE ELASTIC  
CONSTANT FOR GERMANIUM.



that this corresponds to a second layer atom displacement of  $0.08 \overset{\circ}{\text{A}}$ . From this one may calculate the heights of the depressed ( $h^-$ ) and raised ( $h^+$ ) first layer atoms, and compare them with values deduced by Hansen and Haneman<sup>23)</sup> from L.E.E.D. data analysis, as in table 6.T.1.

TABLE 6.T.1

HEIGHTS OF SURFACE ATOM ABOVE SECOND LAYER.

	<u>Computed here.</u>	<u>Predicted from L.E.E.D. analysis.</u>
$h^+$	$1.02 \overset{\circ}{\text{A}}$	$0.98 \overset{\circ}{\text{A}}$
$h^-$	$0.69 \overset{\circ}{\text{A}}$	$0.68 \overset{\circ}{\text{A}}$
$h^{\circ}$ (ideal)	$0.817 \overset{\circ}{\text{A}}$	$0.817 \overset{\circ}{\text{A}}$

---

The agreement between the values is striking. However the L.E.E.D. intensity data used were those of Lader and Morrison,<sup>4)</sup> which differ from the more recent data of Palmberg and Peria.<sup>8)</sup> Also the degree of validity of the assumptions used by Hansen and Haneman is open to discussion at the present stage of uncertainty of L.E.E.D. analysis. Consequently the agreement in Table 6.T.1 may be fortuitously close.

6.8

SILICON RESULTS.

Identical calculations to those performed

Figure 6.F.11.

MINIMUM ENERGY OF A RUMPLED (111) +  
SILICON SURFACE AS A FUNCTION OF  $r_0$ .

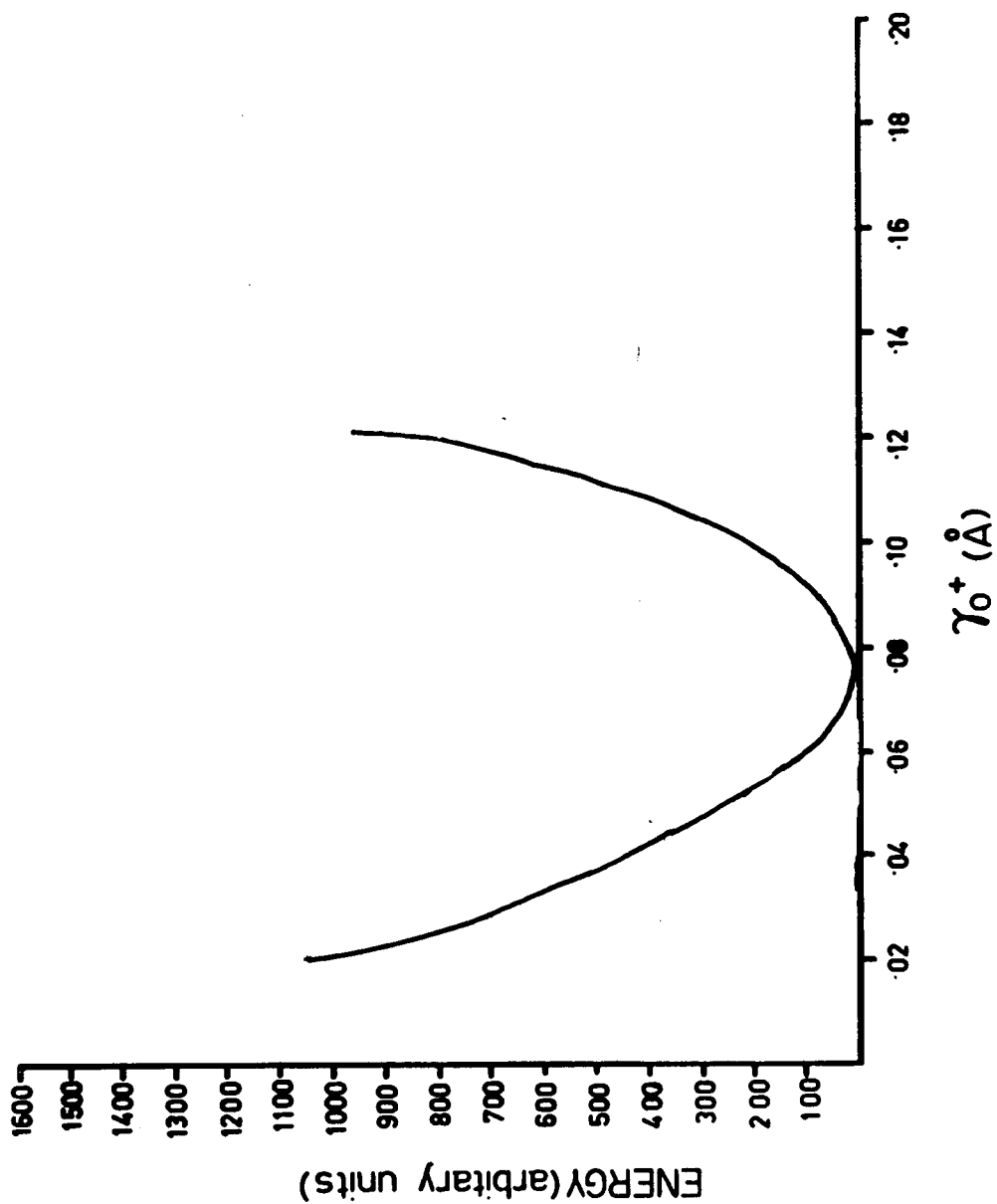


Figure 6.F.12.

PLOT OF "a" VERSUS  $r^+$  FOR WHICH THE  
MINIMUM ENERGY OF THE SILICON (111)  
SURFACE OCCURS.

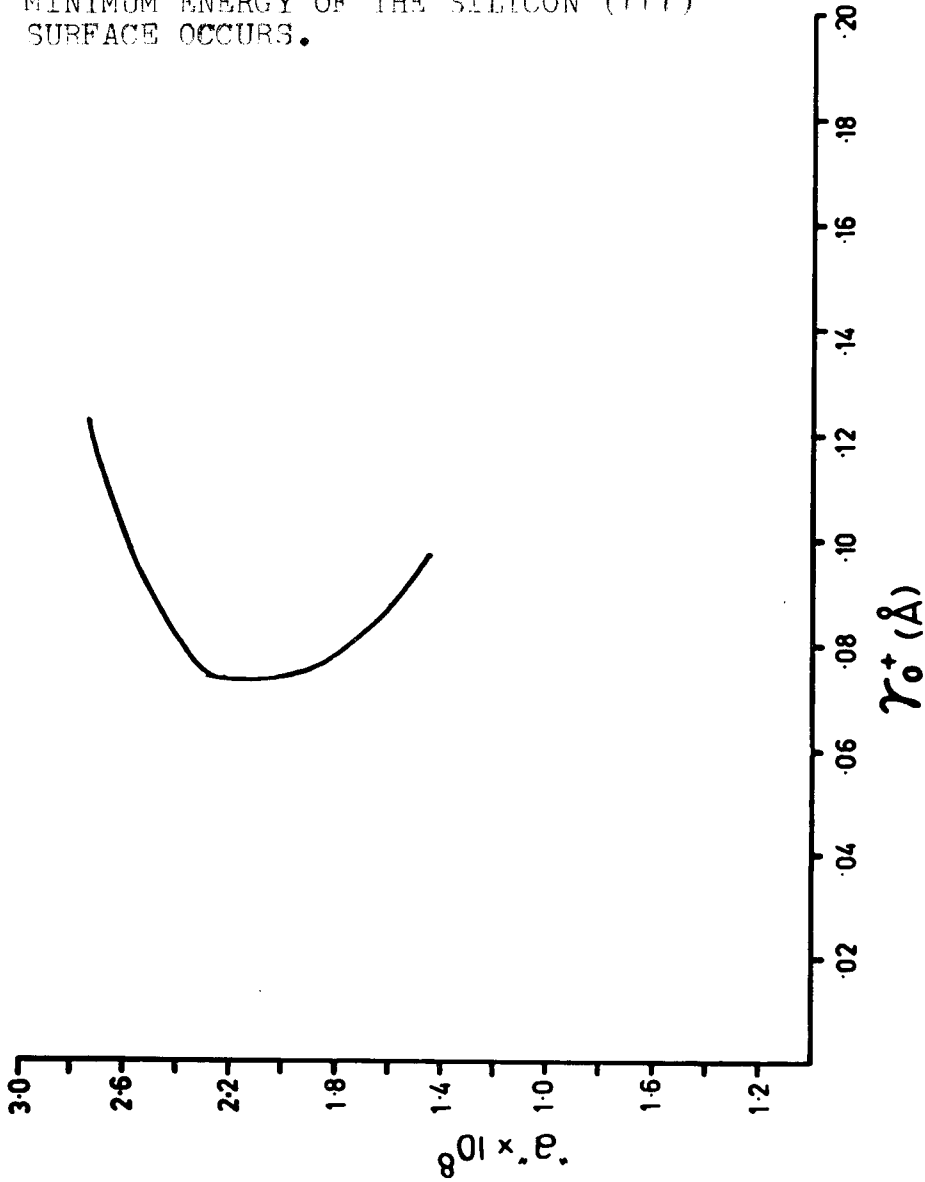


Figure 6.F.13.

SOLUTION OF SURFACE ENERGY  
CALCULATION FOR SILICON.

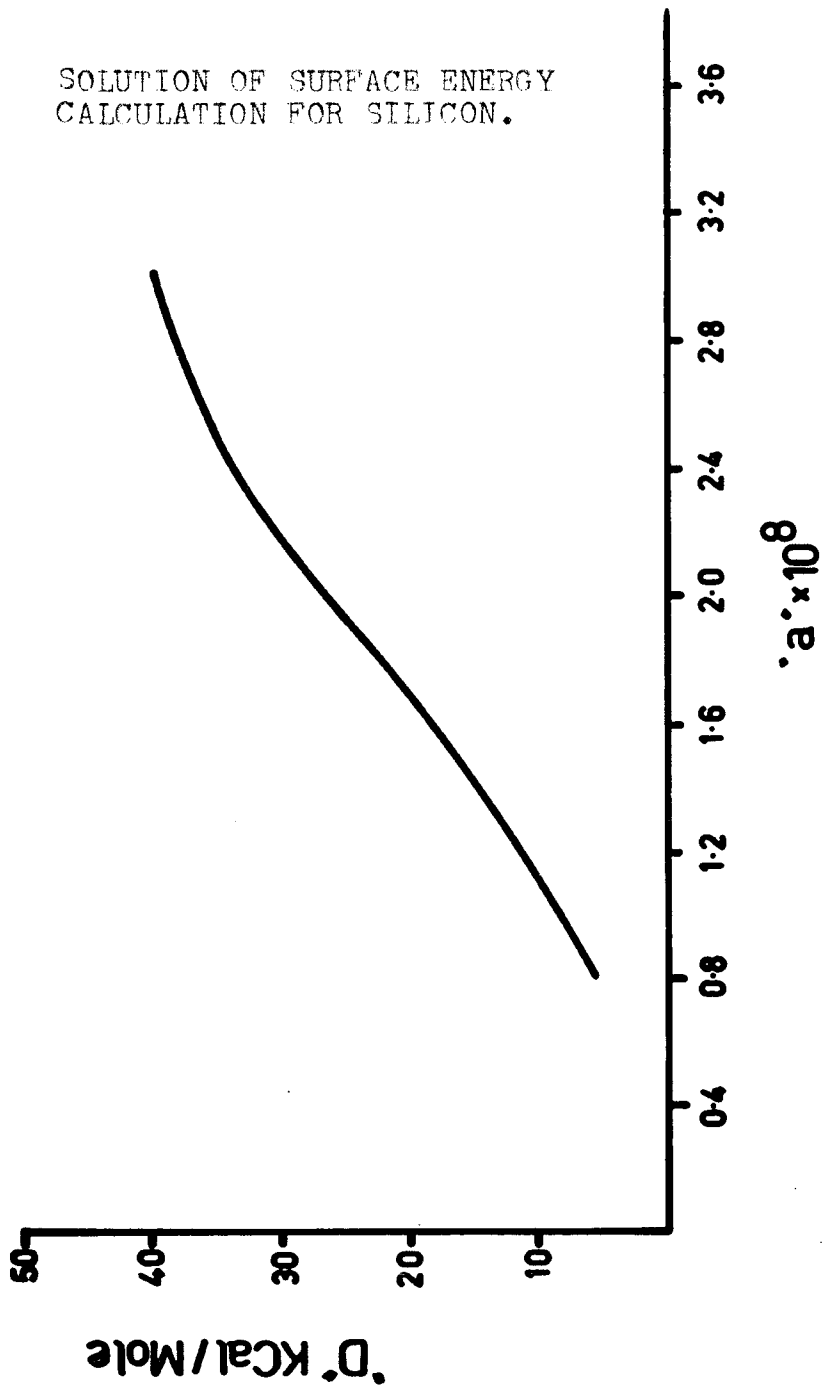


Figure 6.F.14.

SOLUTION OF SUBLIMATION ENERGY  
FOR SILICON.

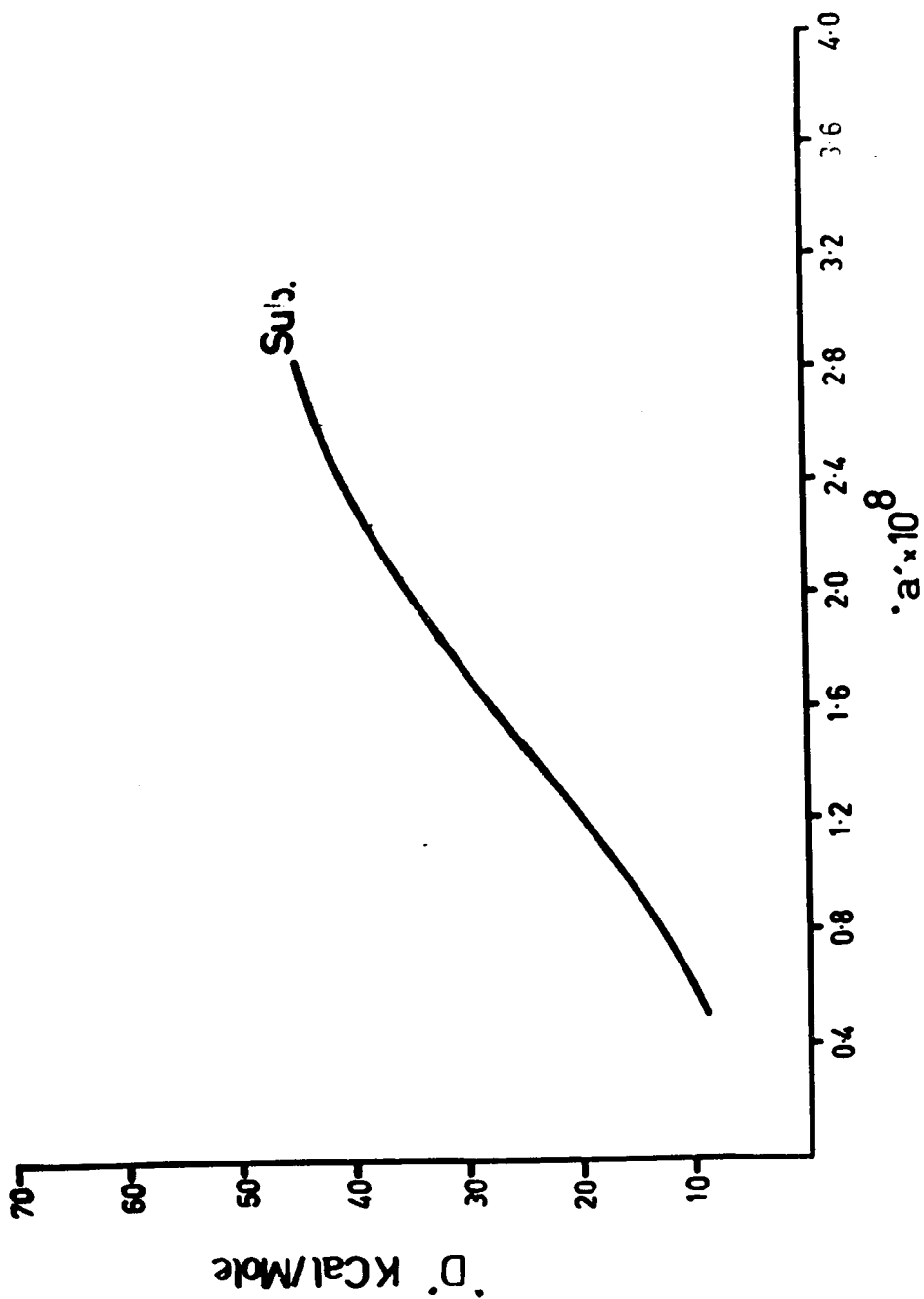


Figure 6.F.15.

THE EXPRESSION DERIVED FROM KEATING IS  
DRAWN TOGETHER WITH THE SOLUTION OF  
THE SILICON ELASTIC CONSTANT C

11

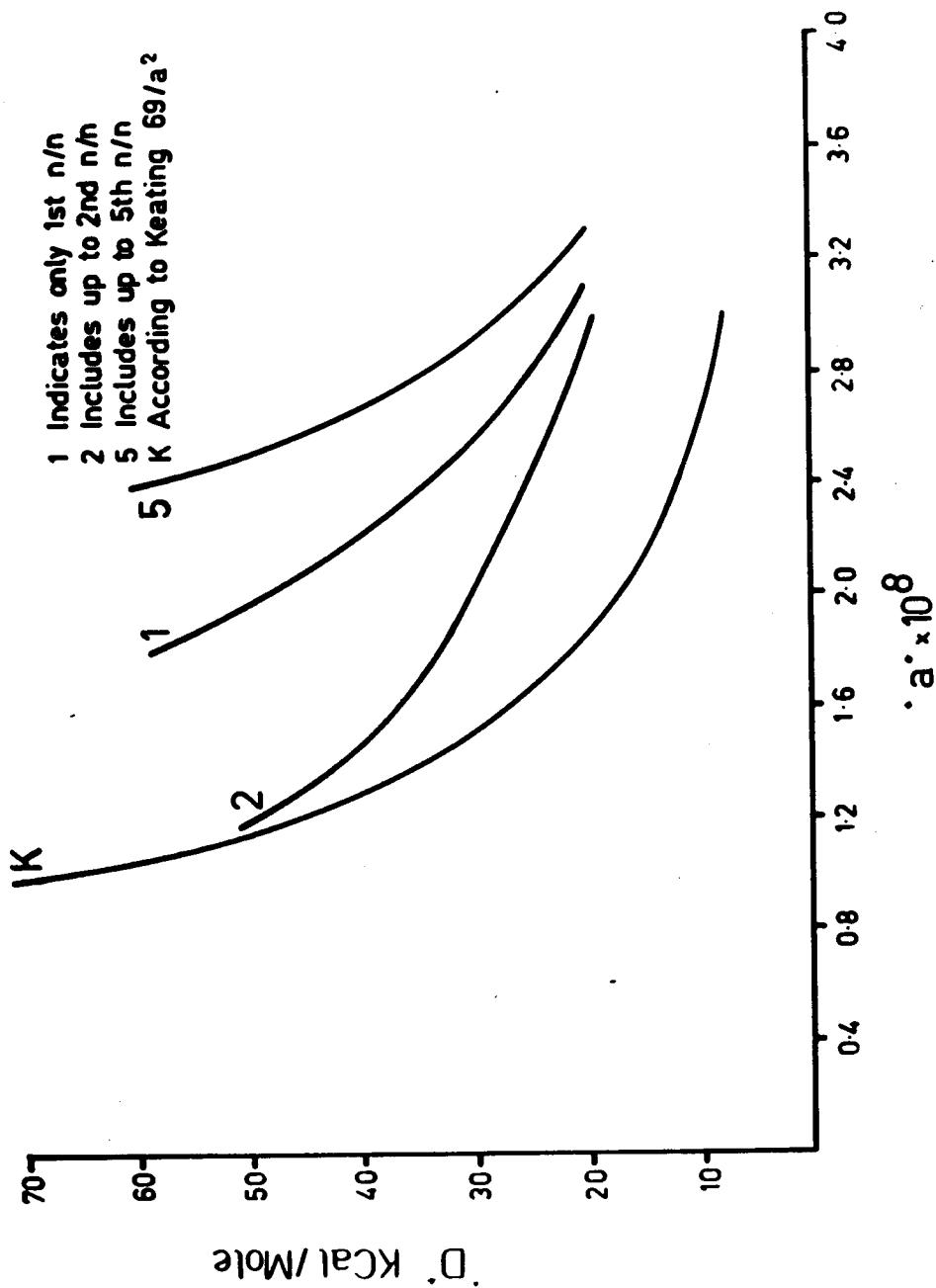
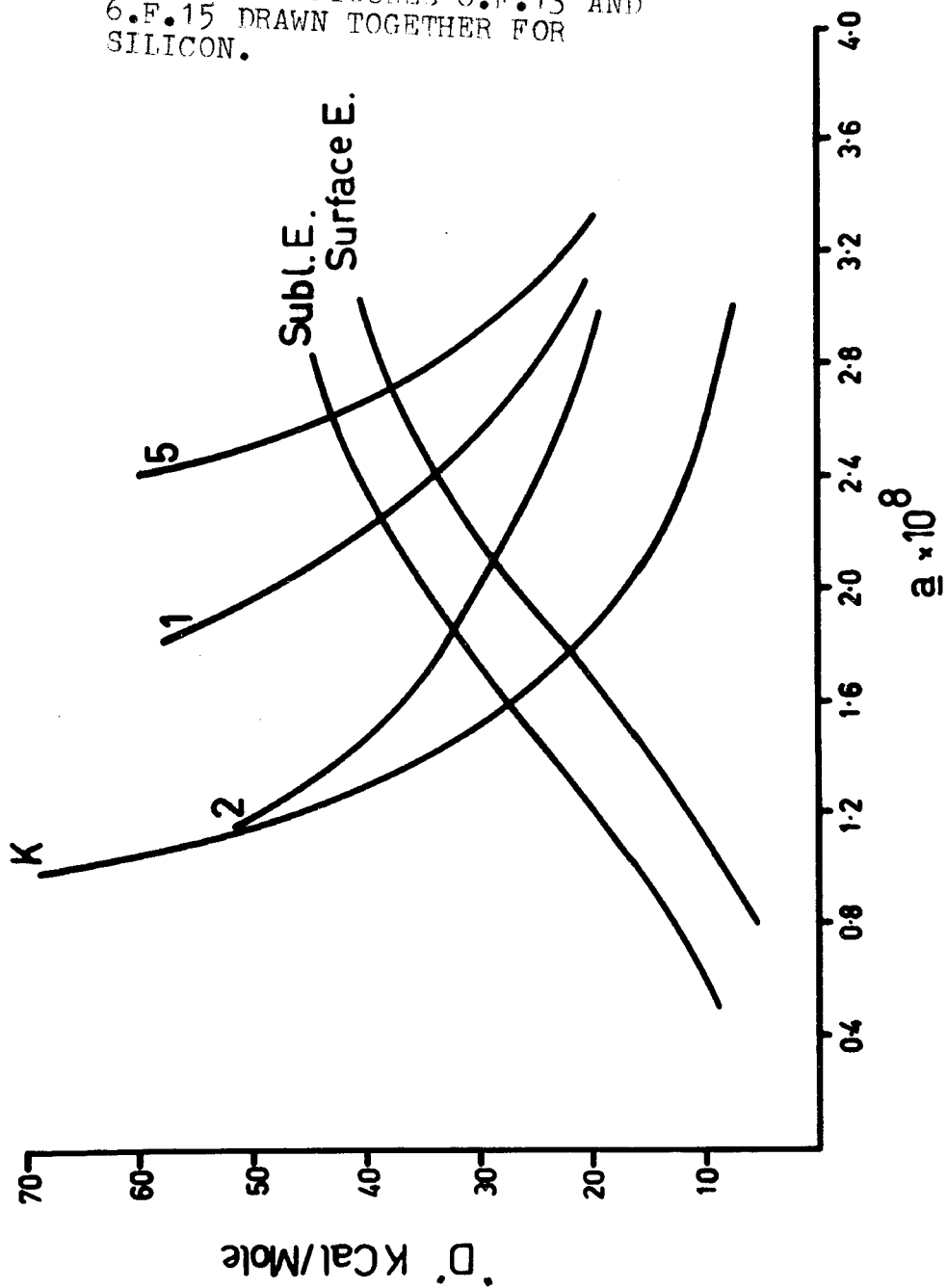


Figure 6.F.16.

THIS SHOWS FIGURES 6.F.13 AND 6.F.15 DRAWN TOGETHER FOR SILICON.



on the germanium surface were also carried out with silicon. Since the potential is a central one, the only difference between the two calculations was in the unit cell and bond length distances. The results for silicon are given in the figures 6.F.11 to 6.F.16.

According to these, the value of "a" lies in the range

$$1.6 < a^* < 2.7$$

which corresponds to a  $r^*$  value of 0.072 Å. The corresponding displacements of the first layer atoms from the second layer are then given as:

$$\begin{aligned} h^* &= 0.964 \text{ Å} \\ h^- &= 0.671 \text{ Å} \\ h^{\circ}(\text{ideal}) &= 0.784 \text{ Å} \end{aligned}$$

Since no theoretical predictions have been made for silicon, these figures cannot be compared with theory. We note however that the values are of reasonable magnitude and that  $r^*$  for silicon is less than that of germanium as might be expected in view of the silicon bond being stronger than germanium.

## 6.9 111 - V COMPOUNDS.

### 6.9.1 INTRODUCTION.

It would be informative if calculations similar to that on silicon and germanium could be carried out on the 111 - V compounds. However, in view of the

paucity of corroborative evidence, lack of surface energy data and extra complexity of the 111 - V problem, it was decided not to attempt to deduce structures for these compounds. Instead deductions were made concerning the differences between the A and B faces.

It is necessary, however, as in the case of silicon and germanium, to start the calculations with some type of interatomic potential as well as some guide to the possible structure.

A Morse potential was again chosen, with values of "a" and D being open both for the A and for the B faces of a given compound. As discussed before, by treating "a" and D as adjustable parameters, the potential can be made a reasonable approximation, and in this case differences between the A and B faces are considered rather than absolute properties; this imposes less severe conditions on the exact form of the potential.

No firm models of 111 - V surfaces have been proposed. Pending further information we take the simplest approach here and use the same type of surface rearrangement as for silicon and germanium, namely a second layer atom shift such that the surface buckles to produce a 2 X 2 unit cell. Such cells have been observed (Chapter 1) for InSb and GaSb, the A surfaces of GaSb and GaAs and also for both opposite surfaces of the related material CdS.

For germanium and silicon, surface energy and elastic constant measurements were used to tie down the Morse parameters. This is not possible here. Since 111 - V compounds cleave preferably along (110) planes due to the ionic component in their bonding, surface energy measurements for (111) cleavage surfaces are not available. Elastic constant measurements are not of direct help since we are allowing the Morse constants for the A and B faces to be different, whereas only one set for the bulk can be used, and the relation between the bulk and surface values is not well known. (For germanium and silicon whose opposite (111) surfaces are identical, the same Morse constants for bulk and surface were used, the possible errors in using the same value being encompassed within the broad range of resultant "a" values that were considered).

However two experimental results are available which may be used to assess the computed results. The first of these are the differences in the surface stress between the A and B surfaces which has been measured in the present study.<sup>24)</sup>

Secondly, further evidence is available from thermal decomposition measurements.

For InSb, GaSb and GaAs, it has been found that the onset of observable surface decomposition in high

vacuum occurs at temperatures which are different for the A and B faces.<sup>25)</sup> This was interpreted to be due to the surface bonding forces on the two faces being different. From the data, the ratio of the central (stretching) bonding force constants, ( $\alpha$ ) for the two opposite faces were deduced and are shown in Table 6.T.2, which also gives the surface stress differences, ( $\sigma_B - \sigma_A$ ) found in Chapter 4.

TABLE 6.T.2

PROPERTIES OF CLEAN (111) SURFACES OF III - V COMPOUNDS.

Material	Surface Stress Difference	Ratio of Stretching Force Constants
	$(\sigma_B - \sigma_A)$ dyne cm <sup>-1</sup>	$\alpha_A / \alpha_B = a_A^2 D_A / a_B^2 D_B$
InSb	<  800	1.04
GaSb	<  800	0.97
GaAs		1.01

As mentioned above, the central first neighbour force constant for a Morse potential is proportional to  $a^2 D$ . Therefore the numerical values in the third column of Table 6.T.2,  $\alpha_A / \alpha_B$ , can be set equal to  $a_A^2 D_A / a_B^2 D_B$ .

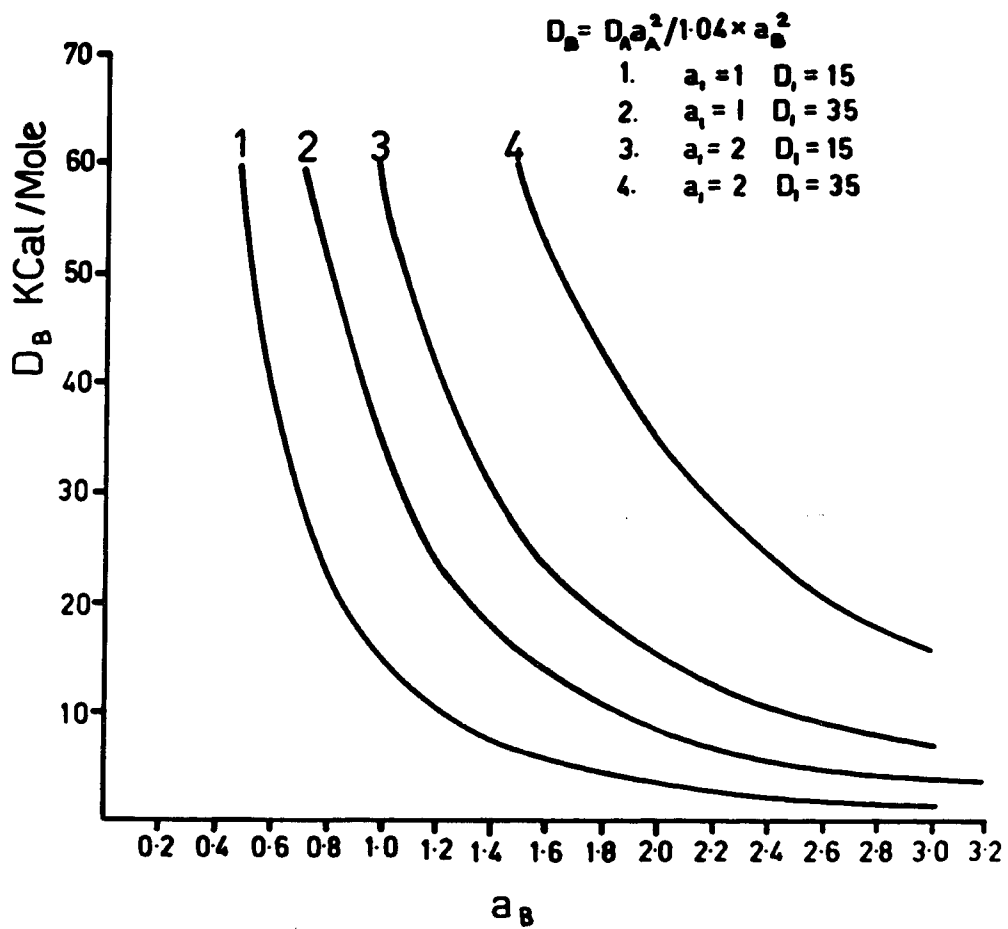


Figure 6.F.17.

A PLOT OF THE RATIO OF THE TWO FORCE  
CONSTANTS WITHIN THE HANEMAN - RUSSELL  
RESTRICTIONS.

6.9.2

PROCEDURE AND RESULTS FOR THE INDIUM  
ANTIMONIDE CALCULATION.

For indium antimonide the possible values of  $a_A$ ,  $D_A$ ,  $a_B$  and  $D_B$  can be restricted by putting

$$\frac{a_A^2 D_A^2}{a_B^2 D_B^2} = 1.04 \quad \text{E.6.12}$$

This function is shown plotted in figure 6.F.17 for varying values of  $a_A$  and  $D_A$ . We see that choosing a particular value of  $a_A$  and  $D_A$  imposes certain limits on  $a_B$  and  $D_B$ . A second condition can be obtained by computing the ratio of the surface work values,  $\sigma_B' / \sigma_A'$  from the expression:

$$\sigma_B' / \sigma_A' = \frac{E(D, a_B, r_0^+ = 0) - E(D, a_B, r_0^+)}{E(D, a_A, r_0^+ = 0) - E(D, a_A, r_0^+)} \quad \text{E.6.13}$$

The energy  $E(D, a, r_0^+)$  is obtained from Eq. E.6.1, using the Morse potential with parameters  $a$  and  $D$ , and atom displacement  $r_0^+$  from the equilibrium separation. In Eq. E.6.4 the surface work value  $\sigma'$  is the energy expended in passing from the "ideal" structure ( $r_0^+ = 0$ ) to the actual structure. (This term equals the surface stress under certain conditions, not necessarily satisfied here). It is assumed that  $D$  and  $r_0^+$  are the same for the opposite surfaces, only the  $a$ 's having different values. Further computations of  $\sigma_B' / \sigma_A'$  were made by assigning the same  $a$ 's to the

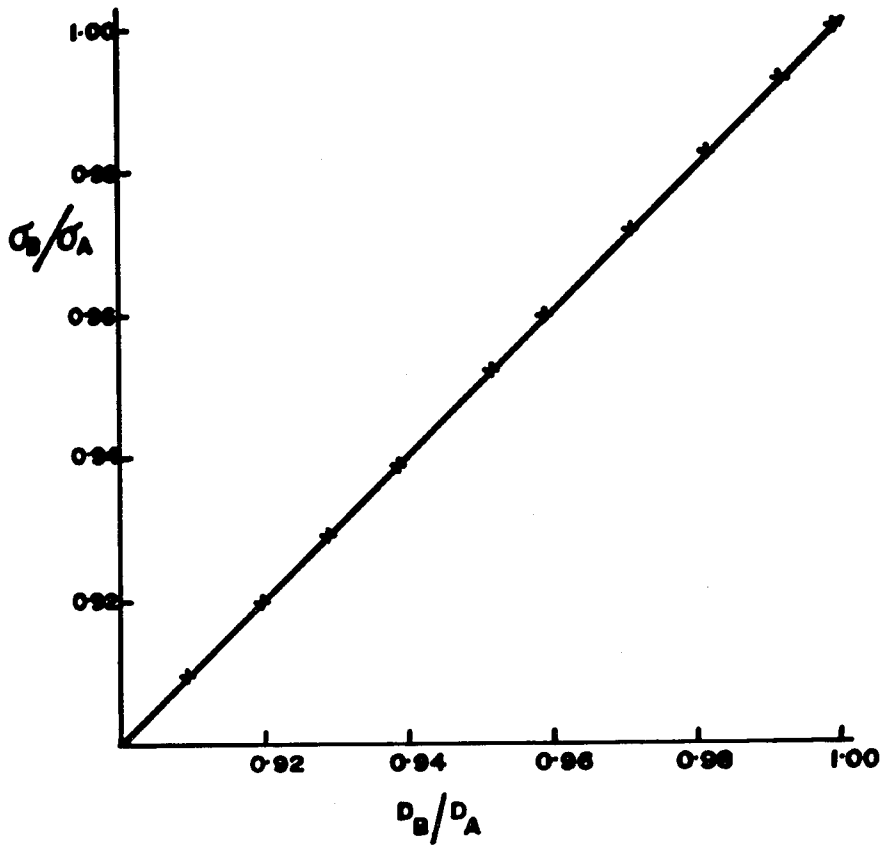


Figure 6.F.18.

$\sigma_B / \sigma_A$  VERSUS  $D_B / D_A$

opposite surfaces and considering a range of differing  $D$  values.

$$\sigma'_B / \sigma'_A = \frac{E(D_B, a, r_0^+ = 0) - E(D_B, a, r_0^+)}{E(D_A, a, r_0^+ = 0) - E(D_A, a, r_0^+)} \quad \text{E.6.14}$$

subject in both cases to the limitation on  $a^2 D_A / a^2 D_B$ .

The results are shown in Figures 6.F.18 and 6.F.19. The significance can be assessed from a knowledge of  $\sigma'_B / \sigma'_A$ . The measurements in Table 6.T.2 only refer to  $(\sigma'_B - \sigma'_A)$ , but the comparatively small numerical value found for this quantity would tend to suggest that the individual values of  $\sigma'_B$  and  $\sigma'_A$  are not greatly different and hence also  $\sigma'_B$  and  $\sigma'_A$  might be similar. A theoretical prediction of  $\sigma'_B / \sigma'_A$  by Cahn and R.E. Hanneman (26) quotes a magnitude of 0.5. From Figure 6.F.19, such a value would require very different values of  $a_B$  and  $a_A$ , and / or  $D_B$  and  $D_A$ .

### 6.9.3 CONCLUSION.

The calculation was only performed on indium antimonide, although similar results can clearly be obtained for gallium antimonide.

The results are presented as a numerical guide to the differences in surface forces that would have to be assumed, in the framework of the assumptions used, to

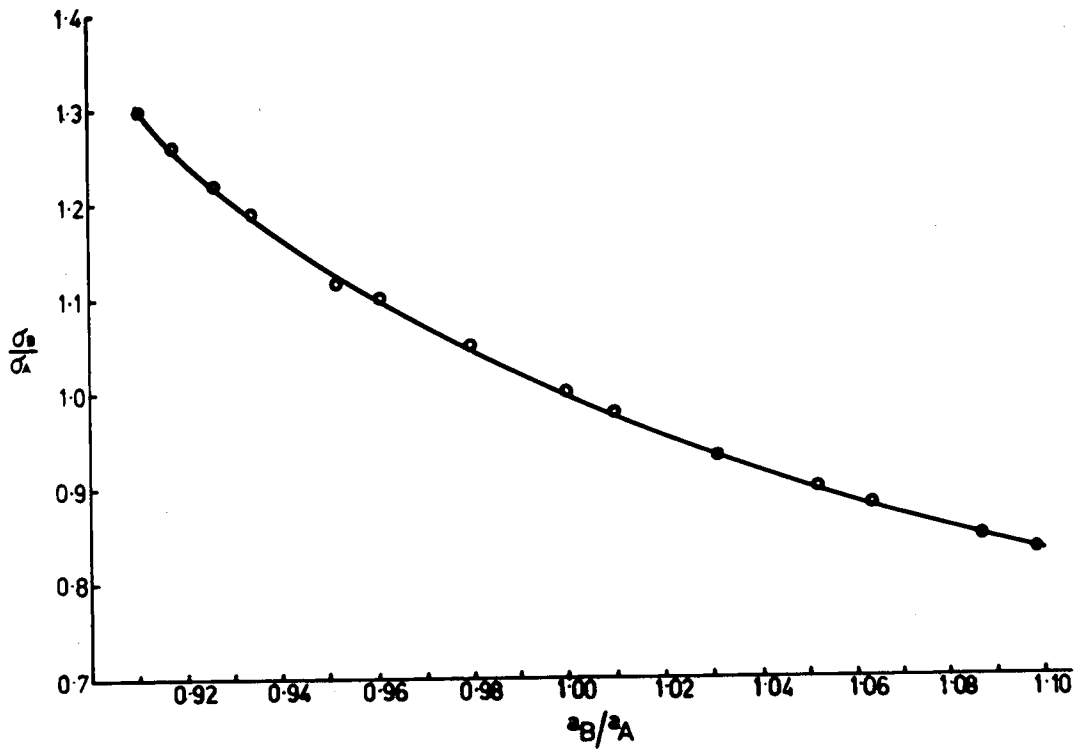


Figure 6.F.19.

$\frac{r_B}{r_A}$  /  $\frac{r_A}{r_B}$  VERSUS  $\frac{a_B}{a_A}$  /  $\frac{a_A}{a_B}$

interpret particular ratios of surface energies and stresses for opposite (111) surfaces of 111 - V compounds.

Finally we note that, if the similarity of  $\overset{i}{\sigma}_B$  and  $\overset{i}{\sigma}_A$  is accepted, the calculations are entirely consistent with the measured low value of  $(\overset{i}{\sigma}_B - \overset{i}{\sigma}_A)$ .

CHAPTER 7. DISCUSSION AND CONCLUSION.7.1 SURFACE STRESSES FOR CLEAN A AND B SURFACES OF 111 - V COMPOUNDS.

A main conclusion concerns the surface tension difference between the A and B surfaces of indium antimonide and gallium antimonide. The measured radius of curvature of these substances, arising between clean ion bombarded surface on one side and etched on the other, give a value greater than 1000 cms., which was the measuring limit of the apparatus used. From this we concluded that the clean 111 - V faces of these compounds have values of  $\sigma$  which differ by less than 800 dyne / cm as well as being individually less than 400 dyne / cm.

7.2 POLISHING DAMAGE.

Here we saw the effect of the surface damage introduced during the polishing operation on the four crystal types, germanium, silicon, indium antimonide and gallium antimonide. We verified that the bendings of the crystals were due in all cases, to a resultant damage introduced by the polishing operation.

For the particular case of the real surfaces of indium antimonide and gallium antimonide, the sign of the curvature was not found to depend on any intrinsic differences between these two surfaces.

7.3

ARGON ION BOMBARDMENT.

With the crystals inside the vacuum system, ion bombardment was utilised to remove polishing damage and obtain a clean surface. For crystals polished on one side only, continued ion bombardment always resulted in the crystals finally attaining a radius of curvature greater than 1000 cms., which was the measurable limit of the apparatus.

This result was used to establish certain important facts:

- a) By knowing the depth of surface stripped during the ion bombardment, the depth to which the damage extends into the crystal was determined for the four crystal types. The interferometric method adopted for measuring the curvature allowed us to measure this depth even when polishing with  $\frac{1}{4}$  micron particles. This had not been achieved previously. In general, the results indicate that the damaged region extends into the crystal to a depth of at least twice that of the diameter size of the polishing particles used. This value is about 100% greater than had previously been reported.
- b) Since continued ion bombardment always resulted in the crystals becoming flat, we concluded that argon ion bombardment does not damage the surface to the extent that is measurable here.

- c) With regard to clean surfaces of indium antimonide and gallium antimonide the results show that any difference in surface stress between the A and B surfaces, if it exists, is below the detection limit of  $800 \text{ dyne cm}^{-1}$ .
- d) Chemical thinning of crystals allowed a functional relationship to be found between the radius of curvature and crystal thickness. This relationship is of the form  $R \propto t^2$  indicating that we are dealing with an effect very close to the surface rather than in the bulk.

7.4

ANNEALING.

The annealing results were of particular interest. It was shown that permanent annealing, as determined by an increase in the radius of curvature, commenced at relatively low temperatures, ( $50^\circ \text{C}$ ). That this was a genuine annealing effect was confirmed by the lack of recovery of type 2C crystals when ion bombarded. It was further established that this annealing depended on the absolute temperature rather than the time for which a crystal was kept at a particular temperature. This suggested ruling out a diffusion mechanism as the cause of the annealing.

The four crystal types were thus seen to behave rather similarly in their annealing, ion bombardment,

and surface damage properties, differing from one another only in degree.

7.5

#### E.P.R. MEASUREMENTS.

Information about the damaged region was obtained by investigating the variation of the "g" value, line width, line shape, and signal height of the e.p.r. signal from polished and crushed silicon with temperature. By comparing the results of polished silicon to those of vacuum crushed and air crushed silicon we concluded that there were unpaired surface electrons associated with the damaged region.

A model was then postulated to explain the observed results.

We generalise this model to include the four crystal types.

7.6

#### POSTULATED MODEL.

It appears to us that the model suggested for silicon might well be generalised. This is considered plausible in view of the similarity of the results, particularly the low temperature annealing.

We thus consider that on the initial damaging of the surface during the polishing, many cracks and fissures are formed in the vicinity of the surface. While these would normally tend to close up again upon the removal of the stress, because of the rough treatment to

which these surfaces are subjected, sideways components are present which dislodge these cracks or steps sideways, preventing them from closing. It is the forces associated with the wedged open fissures that result in the crystals bending against bulk forces.

#### 7.7 MODEL TESTED WITH EXPERIMENTAL RESULTS.

This model may be seen below to be consistent with the observed results;

- a) Heavier Damage - Greater Bending: This would be expected from the above model since, for greater damage and deeper fissures and cracks, the mismatching would occur to a greater distance below the surface. This would be true for crystals polished on one or both sides.
- b) Ion Bombardment Removal of Damage: Continued ion bombardment would strip the surface layers and thus would simultaneously remove the mismatched surface region.
- c)  $R \propto t^2$ : The mismatching occurs very close to the surface and not inside the bulk. Hence an  $R \propto t^2$  relationship might be expected to hold rather than an  $R \propto t^{3/2}$ .
- d) Low Temperature Annealing: With this model even mild heating might be expected to result in small sideways displacements allowing some of the mismatched "steps" to match.

- e) The model has been shown to be consistent with e.p.r. results. This was seen by the combined results of the variation of signal height and line width, with temperature. We saw that the number of unpaired electrons decreases even at relatively low temperatures. According to the model this would be due to the matching up of the "steps" at these low temperatures.

7.8

#### COMPUTER CALCULATIONS.

Computer calculations were carried out on the surface structure of germanium and silicon as well as determining the ratio of the surface stresses for the A and B surfaces of indium antimonide. The results appear to give correct orders of magnitude for surface atom positions and may be used as a guide. Of particular interest is the rather surprising agreement with L.E.E.D. analysis predictions for the H model for germanium. For the case of indium antimonide the results are consistent with the low measured value of surface stress.

### ACKNOWLEDGEMENTS.

The author wishes to express his gratitude to the various members of the school of physics for their assistance in connection with this thesis.

In particular he would like to express his great appreciation to his supervisor, Professor D. Haneman, for the many discussions and fruitful advice given.

He is also grateful to Mr. S. Armstrong for helping to set up the glass vacuum system, to Mr. C. Tenukest for instructions on the polishing of the crystal surfaces, and to Mr. S. Budniak for help in building the electronic equipment.

Last but not least, to his wife, Carol and his children, Paul and Leanne, many thanks for their patience and understanding during the course of this thesis.

APPENDIX 1

COMPUTER LISTING OF THE SOLUTION OF THE GERMANIUM  
SURFACE STRUCTURE USING THE MORSE POTENTIAL.

1 ///READ ABCD

2 C SOLUTION OF THE GERMANIUM SURFACE STRUCTURE

3 C WITH THE MORSE POTENTIAL

4 C

5 C MAIN PROGRAM

6 C

7 C PARAMETERS FOLLOW

8 C

9 ASTORE # 1.E&30

10 BSTORE # 1.E&30

11 ZZ # 0.

12 RO # 2.45

13 R1 # 4.0

14 A1 # 3.

15 A2 # 3.

16 A3 # 6.

17 A4 # 1.

18 A5 # 3.

19 A6 # 4.

20 A7 # 1.

21 A8 # 2.

22 A9 # 2.

23 A10 # 3.

24 A11 # 2.

25 A12 # 1.

26 T # 42.6

27 FI # 2.3094688

28 BB # 1.1547344

29 B # - 0.5

30 DO 3 J # 1,10

31 AJ # J

32 D # 0.1\*AJ\*T

33 C VARIATION OF ABULK

34 DO 2 K # 1,35

35 AK # K

36 ABULK # 0.1\*AK

37 C VARIATION OF ROP

38 DO 1 I # 1,100

39 AI # I

40 ROP # 0.01\*AI

41

42

```

1 C VARIATION OF APLMS
2 APLMS # ABULK
3 C VARIATION OF APLUS
4 APLUS # ABULK
5 C VARIATION OF AMINUS
6 AMINUS # ABULK
7 C LIST OF DEFINED PARAMERTERS FOLLOW
8 C MAIN CALCULATIONS
9 EO#R1-RO
10 BA=RO*RO
11 BC=RCP*ROP
12 CC=FI*FI
13 EJ=ROP*FI
14 DD #SQRT%ABS%BC&CC-2.*EJ*B<<
15 AC=DD*DD
16 HM # SQRT%ABS%BA-AC<<
17 CB=HM*HM
18 FA=FI-ROP
19 HP # SQRT%ABS%BA-FA*FA<<
20 EN=RO & HP
21 R1P # SQRT%CC & EN**2<
22 EA=R1P-RO
23 EL=HP - HM
24 EK=R1*R1
25 R1PM # SQRT%ABS%EL**2 & EK<<
26 EB=R1PM-RO
27 ROM # SQRT%CB & CC<
28 EC=RCM-RO
29 EM=RO & HM
30 R1MM # SQRT%CC & EM**2<
31 ED=R1MM-RO
32 R2P # SQRT%BA & BC<
33 EF=R2P-RO
34 R2M # %2.*FA</BB
35 EG=R2M-RO
36 R2O # SQRT%BC & EK<
37 EH=R2O-RO
38 FU=FI & ROP
39 R3 # %2.*FU</BB
40 EI=R3-RO
41
42

```

```

1      ZZ # ZZ & 1
2      C LIST OF DEFINED PARAMERTERS FOLLOW
3      TL # -2.*ABULK*EO
4      TLX # - ABULK*EC
5      TO # -2.*APLUS*EA
6      TOX # - APLUS*EA
7      TA # -2.*APLMS*EB
8      TAX # - APLMS*EB
9      TB # -2.*AMINUS*EC
10     TBX # - AMINUS*EC
11     TC # -2.*AMINUS*ED
12     TCX # - AMINUS*ED
13     TD # -2.*ABULK*EF
14     TDX # - ABULK*EF
15     TE # -2.*ABULK*EG
16     TEX # - ABULK*EG
17     TF # -2.*ABULK*EH
18     TFX # - ABULK*EH
19     TG # -2.*ABULK*EI
20     TGX # - ABULK*EI
21     C MAIN MCRSE EQUATIONS
22     AMRO # -T
23     AMR1P # D*%EXP%TO< - 2.*EXP%TOX<<
24     AMR1PM # D*%EXP%TA< - 2.*EXP%TAX<<
25     AMROM # T*%EXP%TB< - 2.*EXP%TBX<<
26     AMR1MM # D*%EXP%TC< - 2.*EXP%TCX<<
27     AMR2P # T*%EXP%TD< - 2.*EXP%TDX<<
28     AMR2M # D*(EXP(TE) - 2.*EXP(TEX))
29     AMR2O # D*%EXP%TF< - 2.*EXP%TFX<<
30     AMR3 # D*%EXP%TG< - 2.*EXP%TGX<<
31     AMROMM # D*%EXP%TL<-2.*EXP%TLX<<
32     WRITE(3,11)AMR1P,AMR1PM,AMROM,AMR1MM,AMR2P,AMR2M,AMR2O,AMR3,
33     1AMROMM
34     11 FORMAT(1X,9(E11.4,1X))
35     C MAIN FORCE EQUATIONS FOLLOW --THESE WERE OBTAINED BY
36     C DIFFERENTIATION OF THE ENERGY EXPRESSION
37     C WITH RESPECT TO ROP
38     ZMR1PM # A3*%-2.*APLMS*D*%EL/R1PM<*%FA/HP&%2.*ROP-2.*FI*B
39     1/%2.*HM<<<<*%EXP%TA<-EXP%TAX<<<
40     ZMR1MM # A5*%2.*AMINUS*D*%EM*%ROP-FI*B</%R1MM*HM<<
41
42

```

```

1      1*(EXP(TC)-EXP(TCX)))
2      ZMR1P # A2*-2.*APLUS*D**%EN*FA</%R1P*HP<<*&EXP%
3      1TO<-EXP%TOX<<<
4      ZMR2P # A7*-2.*ABULK*D**%ROP/R2P<*&EXP%TD<-
5      1EXP%TDX<<<
6      ZMR2M # A8*%4.*ABULK*D**%1./BB<*&EXP%TE<-
7      1EXP%TEX<<<
8      ZMR2O # A9*%-2.*ABULK*D**%ROP/R2O<*&EXP%TF<-
9      1EXP%TFX<<<
10     ZMROM # A4*%2.*AMINUS*D**%ROP- FI*B</%ROM<<<*&EXP%TB<-
11     1EXP%TBX<<<
12     ZMR3 # A11*%-4.*ABULK*D**%1./BB<*&EXP%TG<-
13     1EXP%TGX<<<
14     ENERGY # A1*AMRO &A2*AMR1P & A3*AMR1PM & A4*AMROM & A5*AMR1MM &
15     1A6*AMRCMM & A7*AMR2P & A8*AMR2M &A9*AMR2O & A10*AMRO &
16     1A11*AMR3 & A12*AMRO
17     FORCE # ZMR1PM & ZMR1MM & ZMR1P & ZMR2P & ZMR2M &
18     1ZMR2O & ZMROM & ZMR3
19     AA # ABS%ENERGY<
20     IF%AA-ASTORE<98,99,99
21     98 WRITE%3,78<ROP,APLUS,AMINUS,APLMS,ABULK,ENERGY,HP,HM,FORCE,D
22     78 FORMAT('OROP',9X,'APLUS',9X,'AMINUS',9X,'APLMS',9X,
23     1'ABULK',9X,'ENERGI',9X,'HP',9X,'HM',/1X,
24     1E10.3,2X,E10.3,3X,E10.3,3X,E10.3,5X,E10.3,4X,E13.6,1X,E10.3,
25     12X,E10.3,1X,E13.6,1X,E9.2)
26     ASTORE # AA
27     99 CONTINUE
28     YY # ABS%FORCE<
29     IF%YY - BSTORE<33,34,34
30     33 WRITE%3,40<ROP, APLUS,AMINUS,APLMS,ABULK,ENERGY,HP,HM,FORCE
31     40 FORMAT%@OROP@,9X,@APLUS@,9X,@AMINUS@,9X,@APLMS@,9X,
32     1@ABULK@,9X,@ENERGY@,9X,@HP@,9X,@HM@,9X,@FORCE@,/1X,
33     1E10.3,2X,E10.3,3X,E10.3,3X,E10.3,5X,E10.3,4X,E13.6,1X,E10.3,
34     15X,E10.3,2X,E13.6<
35     BSTORE # YY
36     34 CONTINUE
37     C EVERY VALUE IS PRINTED
38     IF%ZZ-1 <55,56,56
39     56 WRITE%3,77<ROP,APLUS,AMINUS,APLMS,ABULK,ENERGY,HP,HM,FORCE
40     77 FORMAT('OROP',9X,'APLUS',9X,'AMINUS',9X,'APLMS',9X,

```

1 'ABULK', 9X, 'ENERGY', 9X, 'HP', 9X, 'HM', /1X,  
2 1E10.3, 2X, E10.3, 3X, E10.3, 3X, E10.3, 5X, E10.3, 4X, E13.6, 1X, E10.3,  
3 15X, E10.3, 2X, E13.6<

4 ZZ # 0

5 55 CONTINUE

6 5 CONTINUE

7 4 CONTINUE

8 1 CONTINUE

9 2 CONTINUE

10 3 CONTINUE

11 STOP

12 END

13 // #

APPENDIX 2

COMPUTER LISTING OF THE SOLUTION OF THE SURFACE  
ENERGY FOR GERMANIUM USING THE MORSE FUNCTION.

1 ///READ ABCD

2 C SOLUTION OF SURFACE ENERGY FOR GERMANIUM

3 C USING THE MORSE FUNTION

4 C THIS PROGRAM IS GENERAL USING FRACTIONAL VALUES FOR D OF

5 C HIGHER NEIGHBCURERS

6 C SOLUTION OF VARIABLE PARAMERTERS A AND D IN THE MORSE POTENTIAL

7 C FOLLOWING IS A LIST OF DISTANCES TAKEN AND NUMBERS OF BONDS

8 C BROKEN

9 C 1 BOND OF LENTH SQRT%6<

10 C 6 BOND OF LENTH SQRT%16<

11 C 9 BOND OF LENTH SQRT%22<

12 C 6 BOND OF LENTH SQRT%32<

13 C 9 BOND OF LENTH SQRT%38<

14 C 24BCND OF LENTH SQRT%48<

15 C 18 BCND OF LENTH SQRT%54<

16 C PARAMERTERS FOLLOW

17 A1 # 1.

18 A2 # 6.

19 C A3 # 9.

20 A4 # 6.

21 A5 # 9.

22 A6 # 24.

23 A7 # 18.

24 H # 0.817

25 FI # 2.3994688

26 RO # 2.45

27 R1 # 2.45

28 R2 # 4.

29 R3 # SQRT%22.<

30 R4 # SQRT%32.<

31 R5 # SQRT%38.<

32 R6 # SQRT%48.<

33 R7 # SQRT%54.<

34 WRITE%3,65<H,FI,RO,R1,R2,R3,R4,R5,R6,R7

35 65 FORMAT%01H # @,E13.6/@OFI # @,E13.6/@ORO # @,E13.6/

36 5@OR1 # @,E13.6/@OR2 # @,E13.6/@OR3 # @,E13.6/

37 5@OR4 # @,E13.6/@OR5 # @,E13.6/@OR6 # @,E13.6/

38 5@OR7 # @,E13.6<

39 DO 1 I # 1,50

40 AI # I

```

1      D # 1.0*AI
2      WRITE%3,98<
3      98 FORMAT%@1D KCAL/MOLE@,5X,@A@,15X,@ENERGY@,14X,@ENERGY DYNES/CMS@,
4      110X,@RATIO OF REST/REALEN@,2X,@REST@<
5      DO 3 J # 1,5
6      AJ # J
7      PD # 0.2*AJ*D
8      DO 2 K # 1,30
9      AK = K
10     A = 0.1 * AK
11     QD # 0.3333*D
12     RD # 0.25*D
13     SD # 0.2*D
14     TD # 0.16666*D
15     UD # 0.1428*D
16     AMORC # -C
17     AMOR2 # PD*%EXP%-2.*A*%R2-RO<<-2.*EXP%-A*%R2-RO<<<
18     AMOR3 # QD*%EXP%-2.*A*%R3-RO<<-2.*EXP%-A*%R3-RO<<<
19     AMOR4 # RD*%EXP%-2.*A*%R4-RO<<-2.*EXP%-A*%R4-RO<<<
20     AMOR5 # SD*%EXP%-2.*A*%R5-RO<<-2.*EXP%-A*%R5-RO<<<
21     AMOR6 # TD*%EXP%-2.*A*%R6-RO<<-2.*EXP%-A*%R6-RO<<<
22     AMOR7 # UD*%EXP%-2.*A*%R7-RO<<-2.*EXP%-A*%R7-RO<<<
23     ENERGY # A1*AMORO & A2*AMOR2 & A3*AMOR3 & A4*AMOR4 & A5*AMOR5
24     8 & A6*AMOR6 & A7*AMOR7
25     REALEN # 25.4*ENERGY
26     AREST # A2*AMOR2 & A3*AMOR3 & A4*AMOR4 & A5*AMOR5
27     9 & A6*AMOR6 & A7*AMOR7
28     REST # 25.4*AREST
29     SHEP # REST/REALEN
30     WRITE%3,99<D,A,ENERGY,REALEN,SHEP,REST,PD
31     99 FORMAT%1X,E11.4,5X,E12.5,6X,E12.5,5X, E15.8,9X,E12.5,6X, E12.5,
32     43X,E10.3<
33     2 CONTINUE
34     WRITE(3,66)AMORO,AMOR2,AMOR3,AMOR4,AMOR5,AMOR6,AMOR7
35     66 FORMAT%@OAMORO # @,E13.6/@OAMOR2 # @,E13.6/@OAMOR3 # @,E13.6/
36     6@OAMOR4 # @,E13.6/@OAMOR5 # @,E13.6/@OAMOR6 # @,E13.6/
37     6@OAMOR7 # @,E13.6<
38     3 CONTINUE
39     1 CONTINUE
40     STOP

```

1 END

2 // #

3  
4  
5  
6  
7  
8  
9  
10  
11  
12  
13  
14  
15  
16  
17  
18  
19  
20  
21  
22  
23  
24  
25  
26  
27  
28  
29  
30  
31  
32  
33  
34  
35  
36  
37  
38  
39  
40  
41  
42

APPENDIX 3

COMPUTER LISTING OF THE SUBLIMATION ENERGY FOR  
GERMANIUM USING THE MORSE POTENTIAL.

1 ///READ ABCD

2 C CALCULATION OF SUBLIMATION ENERGY FOR  
3 C GERMANIUM FOR VARYING A AND D  
4 C USING THE MORSE FUNTION  
5 C THIS PROGRAM IS GENERAL USING FRACTIONAL VALUES FOR D OF  
6 C HIGHER NEIGHBOURERS

7 RO # 2.45  
8 R1 # 4.0  
9 R2 # SQRT(22.)  
10 R3 # SQRT%32.<  
11 R4 # SQRT%38.<  
12 A1 # 4.0  
13 A2 # 12.0  
14 A3 # 12.0  
15 A4 # 6.  
16 A5 # 12.

17 WRITE(3,32)

18 32 FORMAT('1A',21X,'D',21X,'AMR1',19X,'AMR2',19X,'ENERGY',14X,@ZD@<

19 DO 1 I # 1,25

20 AI # I

21 A # 0.2\*AI

22 DO 2 K # 1,30

23 AK # K

24 D # 10. & AK

25 DO 3 J # 1,10

26 AJ # J

27 ZD # 0.1\*AJ\*D

28 YD # 0.3333\*D

29 WD # 0.25\*D

30 XD # 0.2\*D

31 AMRO # -D

32 AMR1 # ZD\*(EXP(-2.\*A\*(R1-RO))-2.\*EXP(-A\*(R1-RO)))

33 AMR2 # YD\*(EXP(-2.\*A\*(R2-RO))-2.\*EXP(-A\*(R2-RO)))

34 AMR3 # WD\*(EXP(-2.\*A\*(R3-RO))-2.\*EXP(-A\*(R3-RO)))

35 AMR4 # XD\*(EXP(-2.\*A\*(R4-RO))-2.\*EXP(-A\*(R4-RO)))

36 ENERGI # A1\*AMRO & A2\*AMR1 & A3\*AMR2 & A4\*AMR3 & A5\*AMR4

37 ENERGY # ENERGI/2.

38 WRITE(3,33)A,D,AMR1,AMR2,ENERGY,ZD

39 33 FORMAT(1X,6(E13.6, 5X))

40 3 CONTINUE

1 2 CONTINUE

2 1 CONTINUE

3 STOP

4 END

5 // #

APPENDIX 4

COMPUTER LISTING OF THE SOLUTION OF THE ELASTIC  
CONSTANT C FOR GERMANIUM.

11

///READ ABCD

C SOLUTION OF THE ELASTIC CONSTANT C11 FOR GERMANIUM  
C USING THE MORSE FUNCTION

A0 # 5.65735  
R1 # (SQRT(3.)\*A0)/(4.)  
R2 # AC/(SQRT(2.))  
R3 # (SQRT(11.)\*A0)/(4.)  
R4 # AC  
R5 # (SQRT(19.)\*A0)/(4.)  
R0 # R1

C THE VARIABLE PARAMETER IN THE MORSE POTENTIAL IS DENOTED ALPHA

DO 1 I # 1,50  
AI # I  
ALPHA # 0.1\*AI  
DO 2 J # 1,50  
AJ # J  
D # AJ

BETA # EXP(ALPHA\*R0)  
A1 # 2.\*D\*ALPHA\*ALPHA\*A0\*A0\*BETA\*BETA  
A2 # D\*ALPHA\*ALPHA\*AC\*A0\*BETA  
A3 # D\*ALPHA\*AC\*BETA\*BETA  
A4 # D\*ALPHA\*AC\*BETA

VC111 # 4.\*A1\*((1./4.)\*\*4.)\*EXP(-2.\*ALPHA\*R1)/((R1/A0)\*(R1/A0))  
1 -4.\*A2\*((1./4.)\*\*4.)\*EXP(- ALPHA\*R1)/((R1/A0)\*(R1/A0))  
1 &4.\*A3\*((1./4.)\*\*4.)\*EXP(-2.\*ALPHA\*R1)/((R1/A0)\*(R1/A0)\*  
1(R1/AC))  
1 -4.\*A4\*((1./4.)\*\*4.)\*EXP(- ALPHA\*R1)/((R1/A0)\*(R1/A0)\*  
1%R1/AC<<

VC112 # 8.\*A1\*((1./2.)\*\*4.)\*EXP(-2.\*ALPHA\*R2)/((R2/A0)\*(R2/A0))  
2 -8.\*A2\*((1./2.)\*\*4.)\*EXP(- ALPHA\*R2)/((R2/A0)\*(R2/A0))  
2 &8.\*A3\*((1./2.)\*\*4.)\*EXP(-2.\*ALPHA\*R2)/((R2/A0)\*(R2/A0)\*  
2(R2/A0))  
2 -8.\*A4\*((1./2.)\*\*4.)\*EXP(- ALPHA\*R2)/((R2/A0)\*(R2/A0)\*  
2(R2/AC))

VC113 # 4.\*A1\*((3./4.)\*\*4.)\*EXP(-2.\*ALPHA\*R3)/((R3/A0)\*(R3/A0))  
3 -4.\*A2\*((3./4.)\*\*4.)\*EXP(- ALPHA\*R3)/((R3/A0)\*(R3/A0))  
3 &4.\*A3\*((3./4.)\*\*4.)\*EXP(-2.\*ALPHA\*R3)/((R3/A0)\*(R3/A0)\*  
3(R3/AC))  
3 -4.\*A4\*((3./4.)\*\*4.)\*EXP(- ALPHA\*R3)/((R3/A0)\*(R3/A0)\*  
3(R3/AC))

```

3      &8.*A1*((1./4.)**4.)*EXP(-2.*ALPHA*R3)/((R3/A0)*(R3/A0))
3      -8.*A2*((1./4.)**4.)*EXP(-  ALPHA*R3)/((R3/A0)*(R3/A0))
3      &8.*A3*((1./4.)**4.)*EXP(-2.*ALPHA*R3)/((R3/A0)*(R3/A0)*
3(R3/AC))
3      -8.*A4*((1./4.)**4.)*EXP(-  ALPHA*R3)/((R3/A0)*(R3/A0)*
3(R3/AC))
VC114 # 2.*A1*((1./1.)**4.)*EXP(-2.*ALPHA*R4)/((R4/A0)*(R4/A0))
4      -2.*A2*((1./1.)**4.)*EXP(-  ALPHA*R4)/((R4/A0)*(R4/A0))
4      &2.*A3*((1./1.)**4.)*EXP(-2.*ALPHA*R4)/((R4/A0)*(R4/A0)*
4(R4/AC))
4      -2.*A4*((1./1.)**4.)*EXP(-  ALPHA*R4)/((R4/A0)*(R4/A0)*
4(R4/AC))
VC115 # 8.*A1*((3./4.)**4.)*EXP(-2.*ALPHA*R5)/((R5/A0)*(R5/A0))
5      -8.*A2*((3./4.)**4.)*EXP(-  ALPHA*R5)/((R5/A0)*(R5/A0))
5      &8.*A3*((3./4.)**4.)*EXP(-2.*ALPHA*R5)/((R5/A0)*(R5/A0)*
5(R5/A0))
5      -8.*A4*((3./4.)**4.)*EXP(-  ALPHA*R5)/((R5/A0)*(R5/A0)*
5(R5/A0))
5      &2.*A1*((1./4.)**4.)*EXP(-2.*ALPHA*R5)/((R5/A0)*(R5/A0))
5      -2.*A2*((1./4.)**4.)*EXP(-  ALPHA*R5)/((R5/A0)*(R5/A0))
5      &2.*A3*((1./4.)**4.)*EXP(-2.*ALPHA*R5)/((R5/A0)*(R5/A0)*
5(R5/AC))
5      -2.*A4*((1./4.)**4.)*EXP(-  ALPHA*R5)/((R5/A0)*(R5/A0)*
5(R5/AC))
VC11 # VC111&VC112&VC113&VC114&VC115
WRITE(3,33)VC111,VC112,VC113,VC114,VC115,VC11,D,ALPHA
33 FORMAT(1X,8(E13.6,2X))
2 CONTINUE
1 CONTINUE
STOP
END

```

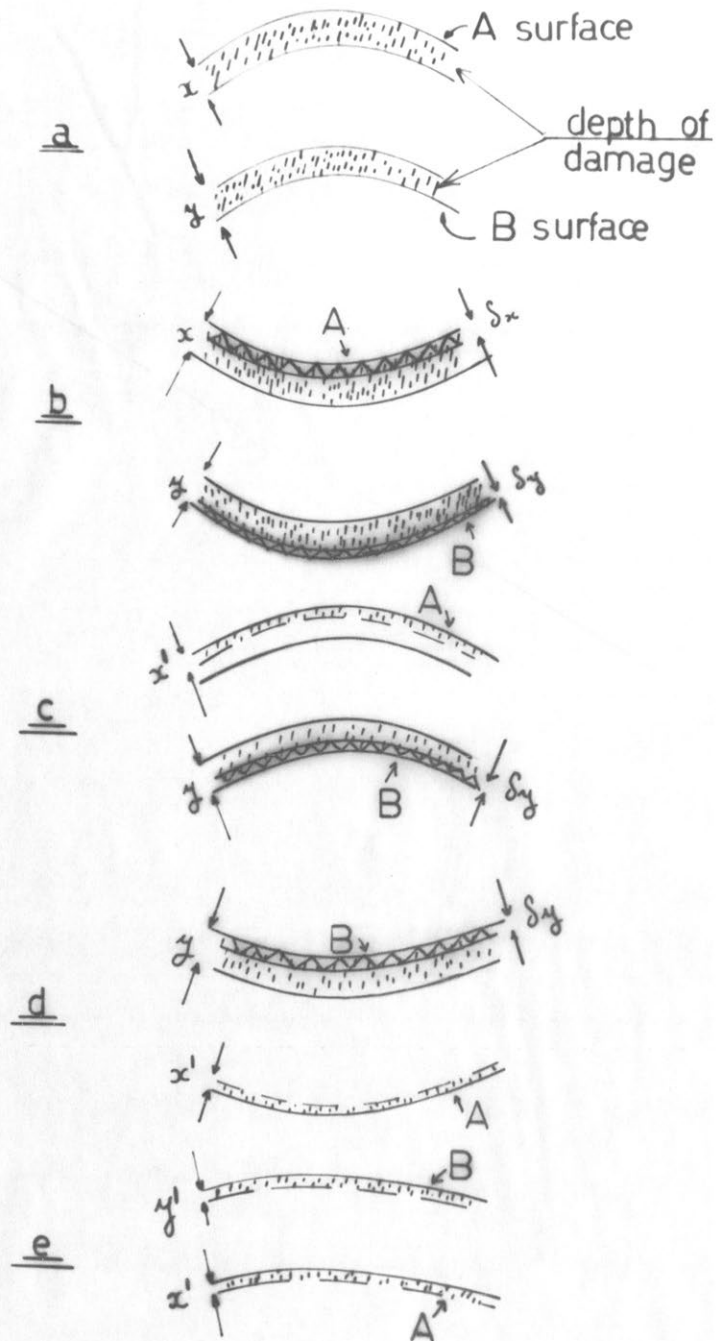
// #

APPENDIX 5

"Some Results on InSb Specimens Polished on Both Sides".

Some sequences of results were obtained for specimens polished on both sides with either the A or B side initially concave. The behaviour on heating and ion bombardment treatment of one side, followed by replacements of the specimen upside down and further treatment, was interesting. Details are given for a particular sequence and a possible explanation of the behaviour is presented. This is done for a crystal having the A surface convex and B side concave. The result is the same if the B surface had been convex and the A surface concave. This is indicated below and may be obtained by replacing A by B and B by A in the text.

- (a) Both sides polished, A (or B) surface convex and B (or A) concave.
- (b) Heat treatment (up to 200<sup>o</sup> C) results in the A surface becoming concave.
- (c) Initial and continued ion bombardment results in the A surface becoming convex, the amount of curvature depending on the time of ion bombardment.
- (d) If the crystal is now taken out of the vacuum system, turned upside down, replaced in position, and the same pressure as previously obtained without bakeout, then the A surface is concave.
- (e) Initial and continued ion bombardment of this,



1) THE SCHEMATIC DIAGRAM ILLUSTRATES THE EFFECT OF ION BOMBARDMENT / ANNEALING ON INDIUM ANTIMONIDE CRYSTALS POLISHED ON BOTH SIDES.

results in the A surface becoming first convex and then to flatten out.

These phenomena can be explained as in the figure with the aid of schematic diagrams.

- (a) The A surface is more damaged than the B surface, as indicated in the diagram by  $x > y$ , and hence is convex.

+ heat

- (b) The surface film is greater for the more damaged surface i.e.  $\delta x > \delta y$  and since this film relieves strain, the crystal becomes concave.

+ ion bombardment

- (c) On removal of the stress-relieving film, the A surface becomes convex once again. Now  $x > x'$  and  $y > x'$  and the overall curvature is an equilibrium situation between the damaged / annealed / ion bombarded A surface and the damaged / annealed surface film B surface.

Turned upside down  
(Handling no effect).

- (d) B surface now concave.

+ ion bombardment

- (e) In this  $y' \approx x'$  and the crystal is almost flat.

These diagrams illustrate the roles of the permanent and non permanent parts of the annealing / ion bombardment cycle.

Clearly the annealing of the damage plays an important part in the relief of stress. However this is not all of a permanent nature as the crystal shows some recovery when the surface film is removed.

We also note that, for all crystals, elevated temperatures ( $400^{\circ}\text{C}$ ) caused a permanent change in the crystal ( $R = \infty$ ) which was not recoverable by any subsequent annealing or ion bombardment.

REFERENCES - CHAPTER 1.

- 1) Tamm I.E. Z.Phys. 76 1932 (849).
- 2) Shockley W. Phys.Rev. 56 1939 (317).
- 3) Microminiaturizations. Proceedings of the Agord. Conference, Oslo 1961. Pergamon Press 1962.
- 4) Special Issue on Integrated Electronics. Proceedings of the I.E.E.E. 52 12, 1964.
- 5) Bardeen J. Phys.Rev. 74 (1948) 230.  
Brattain W.H. 75 (1948) 203.
- 6) Many A. Semiconductor Surfaces. North Holland Publishing Co. Amsterdam. 1965.  
Goldstein Y.  
Grover N.B.
- 7) Gibbs J.W. Collected Works, Volume 1. Yale University Press 1948.
- 8) Gillis P.P. J.Appl.Phys. 36, 4, 1965.
- 9) Gilman J.J. J.Appl.Phys. 31, 12, 1960.
- 10) Jaccodine R.J. J.Elect.Soc. 110, 6, 1963.
- 11) Berry J.P. J.Appl.Phys. 34, 1, 1963.
- 12) Geguzin Ya.E. Soviet Physics Uspekhi. 5, 1, 1962.  
Ovcharenko N.N.
- 13) Honig R. R.C.A. Rev. 18, 2, 1957.
- 14) Zadumkin S.N. Soviet Physics - Solid State. 2, 5, 1960.
- 15) Ormont B.F. Doklady Akd.Nauk. U.S.S.R. 106, 1956.
- 16) Zadumkin S.N. Soviet Physics - Solid State. 1, 4, 1959.
- 17) Herring C. "Structure & Properties of Solid Surfaces". ed. Gomer & Smith (Univ. of Chicago Press), (1953) 13.
- 18) Nicolson M.M. Proc.Roy.Soc. A228, 1955.

- 19) Shuttleworth R. Proc.Phys.Soc. A62, 1949.
- 20) Shuttleworth R. Proc.Phys.Soc. A63, 1950.
- 21) Hanneman R.E. J.Phys.Chem.Solids 23, 1962.  
Finn M.C.  
Gatos H.C.
- 22) Finn M.C. Surface Science 1, 1964.  
Gatos H.C.
- 23) Gatos H.C. J.Electr.Soc. 107, 5, 1960.  
Lavine M.C.
- 24) Cahn J.W. Surface Science 1, 1964.  
Hanneman R.E.
- 25) Timoshenko S. Strength of Materials. Von  
Nostrand. New York. 1953.
- 26) Huntington H.B. Solid State Physics. 7, 1958.
- 27) Haneman D. Brit.J.Appl.Phys. 16, 1965.
- 28) Gatos H.C. Proc.International Conference  
Lavine M.C. Semiconducting Phys. Prague.1960.  
Warekois E.P.
- 29) Gatos H.C. J.Appl.Phys. 31, 1960.  
Lavine M.C.  
Warekois E.P.
- 30) Pugh E.N. J.Appl.Phys. 35, 1964.  
Samuels L.E.
- 31) Landau L.D. Pergamon Press. New York.1959.  
Lifshitz E.M.
- 32) Lander J.J. Progress in Solid State  
Chemistry. Vol 2, (Pergamon  
Press). 1964.
- 33) May J.W. Industrial & Engineering  
Chemistry. July 1965.
- 34) Lander J.J. Surface Science 1, 2, 1964.
- 35) Calbick C.J. Physics Teacher (May) 1963.
- 36) Palmberg P.W. Surface Science 6, 1, 1967.  
Peria W.T.

- 37) Haneman D. Report of the Inter.Conf. The Physics of Semiconductors. (Exeter) 1962.
- 38) Haneman D. Phys.Rev. 121, 4, 1961.
- 39) Hansen N.R. Surface Science 2, 1964.  
Haneman D.
- 40) Lander J.J. J.Appl.Phys. 34 1963 (1403).  
Morrison J.
- 41) Seiwatz R. Surface Science 2 1964 (473).  
Bull.Am.Phys.Soc. 8 1963 541.
- 42) MacRae A.U. Surface Science 4 1966 247.
- 43) Lander J.J. J.Appl.Phys. 34 1963 (2298).  
Gobeli G.W.  
Morrison J.
- 44) Miller D. Miller - B Sc.Honours Thesis 1965.  
University of N.S.W.  
School of Physics.
- 45) MacRae A.U. J.Appl.Phys. 35 1964 (1629).  
Gobeli G.W.
- 46) Chung M.F. J.Appl.Phys. 37 1966 (1879).  
Haneman D.
- 47) Watkins G.D. Phys.Rev. 134 5A 1964 (1359).  
Corbett J.W. Phys.Rev. 138 2A 1965 (543).
- 48) Bemski G. J.Appl.Phys. 30 1959 1195.

REFERENCES - CHAPTER 2.

- 1) Warekois E.P.  
Metzger P.H. J.Appl.Phys. 30, (960) 1959.
- 2) White J.G.  
Roth W.C. J.Appl.Phys. 30, (946) 1959.
- 3) Faust (Jr) J.W.  
Sagar A.J. J.Appl.Phys. 31, (331) 1960.
- 4) Gatos H.C.  
Lavine M.C. J.Phys.Chem.Solids 14 (169)1960.
- 5) Gatos H.C.  
Lavine M.C. J.Electr.Soc. 107 (427) 1960.
- 6) Venables J.D.  
Broudy R.M. J.Appl.Phys. 29 (1025) 1958.
- 7) Faust (Jr) J.W. Compound Semiconductors Vol.1.  
Preparation of III - V  
compounds. Reinhold  
Publishing Corp. 1962.

REFERENCES - CHAPTER 3.

- 1) Dushman S.                    Scientific Foundations of Vacuum  
Technique.  
John Wiley & Sons Inc. 1962.
- 2) Farnsworth H.E.            J.Appl.Phys.    26            1955,    252.  
Schlier R.E.                J.Appl.Phys.    29            1958,    1150.  
George T.H.  
Burger R.M.
- 3) Haneman D.                J.Phys.Chem.Solids    11 (1959) 205.
- 4) Roberts R.W.              Brit.J.Appl.Phys.    14 (1963) 537.
- 5) Farnsworth H.E.            Surface Chemistry of Metals & Semi-  
conductors. Ed. H.C.Gatos.  
New York. John Wiley.
- 6) Many A.                    Semiconductor Surfaces.  
Goldstein Y.                North - Holland Co. 1965.  
Grover N.B.
- 7) Zdanuk E.J.                J.Appl.Phys.    36            1965.  
Wolsky S.P.
- 8) Werner G.K.                "Sputtering Data in 100 - 600 eV  
Range".  
General Mills report 2309, 1962.
- 9) Haneman D.                J.Phys.Chem.Solids    14, 162 (1960)
- 10) Haneman D.                Brit.J.Appl.Phys.    16, 1965.
- 11) Hanneman R.E.            J.Phys.Chem.Solids    23, 1962.  
Finn M.C.  
Gatos H.C.
- 12) Instruction Manual for Reichert microscopes "MIKRO  
523/111" page 29.
- 13) Tolansky S.                High Resolution Spectroscopy  
Pitman, New York 1947.  
Multiple Beam Interferometry.  
Oxford University Press 1948.  
Surface Microtopography.  
Longmans, Green & Co. Ltd. 1960.  
Proc.Royal Society A184, 51, 1965.

- 14) Heavens O.S.            Optical Properties of Solid Films.  
London. Butterworth's Scientific  
Publication.
- 15) Brossel J.            Multiple Beam Localized Fringes.  
Proc. Phys. Soc. 59 224, 1947.
- 16) Holden J.            Proc. Phys. Soc. 62 1949 405.
- 17) Jenkins F.A.        Fundamentals of Optics.  
White H.E.            McGraw Hill 1957.
- 18) Born M.            Principles of Optics.  
Wolf E.            Pergamon Press 1965.
- 19) Herkart P.G.        R.C.A. Review Sept. 1953.  
Kurshan J.

REFERENCES - CHAPTER 4.

- 1) Buck T.M. "The surface chemistry of metals and semiconductors", edited by H.C.Gatos. (John Wiley, New York) 1960, 107.
- 2) Pugh E.N. J.Electr.Soc. 109 1962 409  
Samuels L.E. 108 1961 1043.
- 3) Warekois E.P. J.Appl.Phys. 31 1960 1302  
Lavine M.C.  
Gatos H.C.
- 4) Pugh E.N. J.Appl.Phys. 35, 6 (1964) 1966.  
Samuels L.E.
- 5) Rosenberg D. J.Appl.Phys. 33 (1962) 1842  
Wehner G.K.
- 6) Drum C.M. Phil. Mag. 13 (1966) 1239
- 7) GREEN M. SURFACE SCIENCE 3, 1965, 419



- 16) Feher G. Phys.Rev.114 1219 (1959).
- 17) Walters G.K.  
Estle T.L. J.Appl.Phys. 32 1854 (1961).
- 18) Chung M.F.  
Haneman D. J.Appl.Phys. 37 1879 (1966).
- 19) Wilson D.K.  
Feher G. Phys.Rev. 124 1068 (1961).
- 20) Hasiguti R.R.  
Ishino S. Proc.Symp. on Radiation damage  
in semiconductors.(7th.  
international conference  
Paris 1964).
- 21) Whan R.E. Appl.Phys.Letters 6, 221,(1965).
- 22) Benneman K.H. Phys.Rev. 137 (1965) A1497.
- 23) Hasiguti R.R. J.Phys.Soc.Japan. 21 10,  
1927, 1966.
- 24) Friedel J. "Dislocations".Pergamon Press.  
1964.
- 25) Haneman D.  
Roots W.D.  
Grant J.T.P. J.Appl.Phys. 38, 2203 1967.

REFERENCES - CHAPTER 6.

- 1) Schlier R.E.  
Farnsworth H.E. J.Chem.Phys. 30 (1959) 917.
- 2) Haneman D. J.Phys.Chem.Solids 14 (1960)162.
- 3) Haneman D. Phys.Rev. 121 (1961) 1093.
- 4) Lander J.J.  
Morrison J. J.Chem.Phys. 37 (1962) 729.  
J.Appl.Phys. 34 (1963) 1403.  
J.Appl.Phys. 34 (1963) 3517.  
Surface Science 4 (1966) 241.
- 5) Lander J.J.  
Gobeli G.W.  
Morrison J. J.Appl.Phys. 34 (1963) 8.
- 6) MacRae A.U.  
Gobeli G.W. J.Appl.Phys. 34 (1963) 2298.
- 7) MacRae A.U. Surface Science 4 (1966) 247.
- 8) Palmberg P.W.  
Peria W.T. Surface Science 6, (1967) 57.
- 9) Aspnes D.E.  
Handler P. Surface Science 4, (1966) 353.  
- and references therein -
- 10) Chung M.F.  
Haneman D. J.Appl.Phys. 37 (1966) 1879.
- 11) Haneman D.  
Roots W.D.  
Grant J.T.P. J.Appl.Phys. 38 (1967) 2203.
- 12) Girifalco L.A.  
Weizer V.G. Phys.Rev. 114, 3, (1959).
- 13) Swalin R.A. J.Phys.Chem.Solids 18, 4, (1961).
- 14) Hasiguti R.R. J.Phys.Soc.of Japan 21, 10(1966).
- 15) Nicholas Private Communication.
- 16) Keating P.N. Phys.Rev. 145, 2, (1966) 637.
- 17) Gilman J.J. J.Appl.Phys. 31, 2208, (1960).

- 
- 18) Jaccodine R.J. J.Elect.Soc.110, 6, (1963).  
19) Berry J.P. J.Appl.Phys. 34 62, (1963).  
20) Zadumkin S.N. Fizika Tverdogo Tela, 2, 5, May 1960.  
21) Huntington H.B. Solid State Physics 7, 1958.  
22) Born M. Pro.Cambridge Phil.Soc. 36, (1940) 160.  
23) Hansen N.R. Surface Science 2, (1964) 566.  
Haneman D.  
24) Taloni A. Surface Science in press (1967).  
Haneman D.  
25) Russell G.J. J.Appl.Phys. 37, (1966) 3328.  
Ip H.K.  
Haneman D.  
26) Cahn J.W. Surface Science 1 (1964) 387.  
Haneman R.E.

PUBLICATIONS.

- a) SURFACE STRESS IN POLISHED AND CLEAN (111)  
SURFACES OF Ge, InSb AND GaSb.  
A. TALONI and D. HANEMAN  
SURFACE SCIENCE (IN PRESS 1967).
- b) SUBMITTED FOR PUBLICATION.  
COMPUTER CALCULATIONS OF SEMICONDUCTOR  
SURFACE STRUCTURES.  
A. TALONI and D. HANEMAN.  
SURFACE SCIENCE 1967.
- c) E.P.R. MEASUREMENTS OF EFFECTS OF HEAT  
TREATMENT ON SILICON SURFACES.  
D. HANEMAN. M.F. CHUNG. A. TALONI.  
SURFACE SCIENCE 1967.

## SURFACE STRESS IN POLISHED AND CLEAN (111) SURFACES OF Ge, InSb AND GaSb

A. TALONI and D. HANEMAN\*

*School of Physics, University of New South Wales, Australia*

Received 19 December 1966

Surface stresses have been obtained by measuring the bending of thin specimens in high vacuum using a laser interferometer. The surface stresses for surfaces cleaned by ion bombardment and annealing were in all cases below the detection limit of  $400 \text{ dyne cm}^{-1}$ , for Ge, and A and B surfaces of InSb and GaSb. These values are considerably less than those for fine polished surfaces, but not inconsistent with theoretical estimates. The depths of damage in Ge due to polishing were obtained by measuring the surface stress while stripping the damaged layer by ion bombardment. These depths were considerably larger than observed by other methods being  $1 \mu\text{m}$  for  $\frac{1}{2} \mu\text{m}$  polishing material and  $40 \mu\text{m}$  for  $25 \mu\text{m}$  polishing material. The stresses were relieved by annealing, which had an effect at temperatures as low as  $40^\circ\text{C}$ . InSb and GaSb recovered more readily than Ge and fine polished surfaces faster than coarser polished ones. Mechanisms for the low temperature annealing effects are discussed.

### 1. Introduction

The structures of atomically clean surfaces of various semiconductors are known to be different from those expected from normal terminations of a bulk lattice<sup>1-4</sup>). In the case of III-V compounds, differences between opposite (111) faces are expected and have been observed by LEED<sup>3,4</sup>). Presumably the surface atoms rearrange to minimize surface energy, the structure at the surface being different because the bonding at the surface is different from the bulk. It is of interest to determine the stresses in such surfaces, as a guide to the magnitude of forces and strains which are present in clean surface structures. Previous measurements of surface stresses in polished or etched III-V compounds have been discussed in terms of clean ideal surface concepts<sup>5-7</sup>). However, such interpretations are doubtful<sup>8</sup>) and it is necessary to make measurements on clean surfaces in ultra high vacuum. Such measurements are reported here.

### 2. Surface energy, surface tension and surface stress

The above terms have been given various definitions in the literature. If  $\gamma$

\* Visiting Professor, Brown University, Providence, R. I., U.S.A.

is the reversible work required to create (unit) area of surface by separation of planes (e.g. cleavage), then  $\gamma$  has been called both "surface free energy"<sup>7, 8)</sup> and "surface tension"<sup>10, 11)</sup>. If  $\sigma$  is the work required to alter the surface area by elastic deformation, then  $\sigma$  has been called "surface tension"<sup>7)</sup> and "surface stress"<sup>10, 11)</sup>. Further some authors<sup>7)</sup> formulate the surface tension as the components of inherent surface stresses parallel to the surface.

To avoid confusion we define the quantities used in this paper, using the names which we think are best suited to the meanings. The "(specific) surface free energy"  $\gamma$  is the reversible work required to create (unit) area of surface by separation of planes (e.g. cleavage). The "(specific) surface tension"  $\sigma$  has dimensions of a force per unit length in the surface, having a magnitude equal to the work required to create (unit) area by deforming the original surface in the direction of the force. The "surface stress" is the force per unit length in the plane of the surface.

In general surface tension and surface stress as defined above are tensors, since both the orientation of the force and of the surface area must be defined with respect to chosen axes.

Briefly, surface energy refers to surfaces created by cleavage, subtracting any irreversible work such as plastic deformation and kinetic energy; whereas surface tension refers to surfaces created (or annihilated) by elastically deforming a given surface. The concepts differ in a solid because the density of atoms in the surface is altered during surface deformation (unlike an ideal liquid); whereas surfaces created by separation of planes would, prior to possible reconstructions involving irreversible processes, have the normal surface density of atoms\*.

### 3. Method of measurement

The surface stress difference between opposite surfaces of a crystal wafer can be deduced from the net curvature of the wafer if the curvature is due principally to surface region rather than internal forces. In the case of a rectangular or circular specimen it may be shown from standard elasticity that<sup>7)</sup>

$$\sigma_B - \sigma_A = Yt^2/6R(1 - \nu),$$

where A and B subscripts refer to the opposite faces,  $\sigma$  is the surface stress,  $R$  net radius of curvature,  $t$  the thickness,  $Y$  is the Young's modulus provided

\* In the case of a surface reconstruction involving "buckling"<sup>9)</sup> which is reversible, some surface atoms are higher than others, in principle creating two surface layers out of the original one. These two layers are counted as one, as far as surface atom density is concerned.

$R \gg t$ , corresponding to elastic conditions, and  $\nu$  the Poisson's ratio. Previous measurements have been made on rectangular or hexagonal specimens<sup>5,6,8,9</sup>), but circular specimens, having an isotropic shape, are closer to the theoretically ideal situation and were used in this work. Another parameter of interest is the bulk strain energy  $U$  (due to the strain in the curved specimen) per unit area of surface

$$U = Yt^3/24R^2(1 - \nu).$$

We shall return to the significance of these expressions later.

Although direct microscopic observation of the curvature has been frequently employed<sup>5,6,8</sup>), measurements of the curvature by interference methods are a more sensitive indication of the overall curvature of the entire surface. In the standard Newton's rings method the curvature of the sample surface is compared with that of a reference surface by forming interference fringes between them, using a monochromatic source for high precision. In our experiments the crystal surfaces were placed in an ultra high vacuum system subjected to bakeout, gas exposure and other experimental perturbations of the environment, which necessitated that the reference surface be outside the vacuum system to preserve its constancy. The relatively large spacing ( $\sim 10$  cm) required in consequence between the specimen and reference surface made interference fringe production possible only with a highly coherent light source. Using a He-Ne gas discharge laser (wavelength 6328 Å) and the optical and vacuum system shown in fig. 1, interference fringes from the specimen surface could be readily observed in situ during ion bombardment, heating and gas exposures. Typical fringes from a highly curved ( $R=50$  cm) and relatively flat ( $R=450$  cm) surface of Ge are shown in fig. 2.

The crystals were laid on a stable (outgassed) block of molybdenum below the viewing window. A gun with filament shielded from the crystals was mounted in a side tube at as near normal incidence as possible for electron bombardment purposes. A shielded thermocouple made contact with the block, beneath which was placed a small filament for electron bombardment and radiation heating. The arrangement is shown in fig. 3.

For ion bombardment, spectroscopically pure argon was admitted through a bakeable metal valve to about  $10^{-3}$  Torr and ionized by the hot filament gun. Any glass parts which could gather sputter deposits which might be charged negatively by the filament and thus resputter onto the crystal, were also shielded. The crystal was flanked by two dummies of the same size separately connected through holes in the molybdenum supporting block. Thus the current to the dummies indicated the ion current reaching those areas of the block during bombardment, and hence its distribution (uniform),

from which the current to the crystal was obtained without attempting to provide it with a separate connection. It was found important during bombardment to have the thin ( $20\ \mu\text{m}$ ), light and fragile crystal resting on a solid base without any retaining projections or other irregularities which distorted the ion paths, resulting in irregular bombardment of the crystal surface. In the final arrangement, the evenness of bombardment was further checked by applying it long enough to develop microscopic pits and hillocks. The

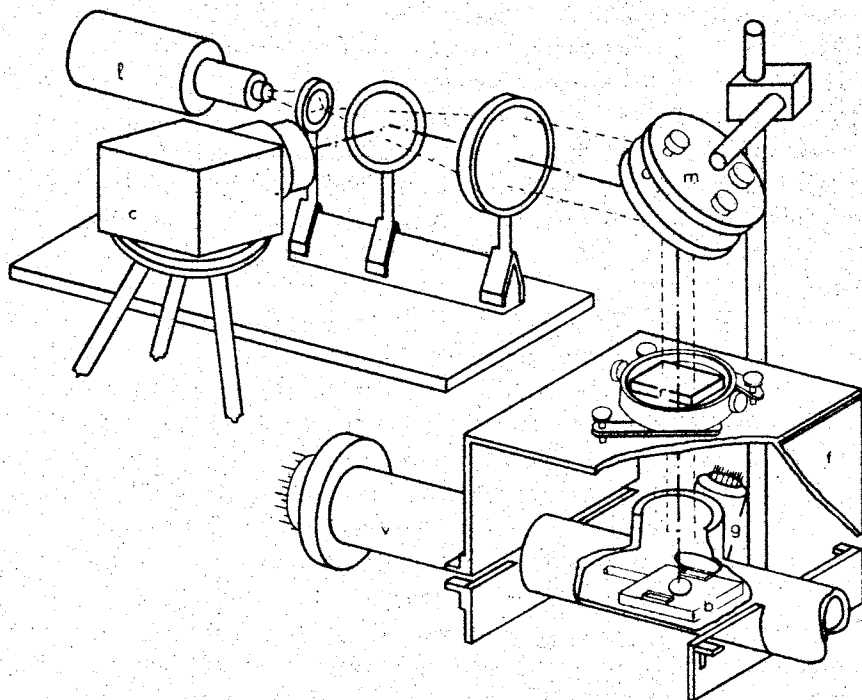


Fig. 1. Laser interferometer. (l) He-Ne laser, (m) adjustable mirror, (r) adjustable reference surface, (b) molybdenum block with circular crystal and rectangular dummies, (f) supporting frame, (g) ion gun, (v) vacuum tube, (c) camera.

distribution of damage on the surface could then be examined by high power microscopy. The bombardment in the final arrangement was uniform over the surface, using  $400\text{--}500\ \text{eV}$ ,  $50\text{--}100\ \mu\text{A cm}^{-2}$  bombardment.

#### 4. Crystal preparation

To minimize edge effects and to facilitate fitting of results to theory, specimens were prepared as 5 mm diameter circular discs, produced from a



Fig. 2. Interference fringes. (a)  $R=450$  cm, (b)  $R=50$  cm.

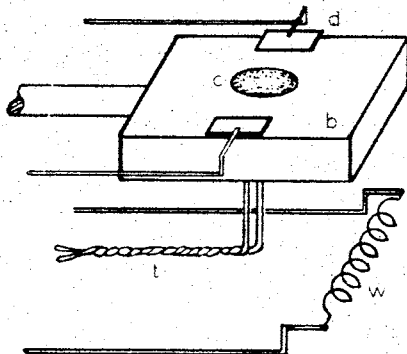


Fig. 3. Crystal holder. (b) molybdenum block, (c) circular crystal, (d) rectangular dummy, (t) thermocouple, (w) heating filament.

lapped plate. This was masked by black wax in which circular rings were exposed by a tubular tool. The rings were etched through with acid and the resulting discs freed of wax.

The lower side of the crystal, to be in contact with the molybdenum support block, was chemically etched so as to remove a layer many times the thickness conceivably damaged by previous mechanical treatment (e.g. 0.5 mm removed by acid after grinding and polishing).

Since the crystals were to be thinned by polishing to 10–20  $\mu\text{m}$ , the etched face had to be very flat to avoid appreciable undulations. A satisfactory and simple technique of obtaining sufficiently uniform etching was to join the crystal surface to a polythene pad with an acid drop supported by surface tension, and to describe polishing motions with the pad suspended above the crystal surface.

### 5. Depth and nature of polishing damage in germanium

Since mechanical polishing was frequently involved in the preparation of the crystals it was desirable to determine the depth of damage. This is of interest as in some experiments, chemical etching of the damaged layer is employed and it is desirable to ensure complete removal of the damaged layer. (E.g., we have found a correlation between the number of ion bombardment anneal cycles required to produce good LEED patterns and the extent of preparatory polishing and etching treatments.) Measurements by optical inspection of taper sections and by checking chemical and electrical properties<sup>12, 13</sup> have established that the damage depth for Ge is roughly of the same order as the size of polishing particles used. Results have also been reported for GaAs and InSb<sup>14, 15</sup>).

The extent of damage is a parameter whose value depends upon which aspect of it is of concern. These aspects range from obvious topological disturbances (seen in section), generated dislocations and other defects (revealed in part by etching and by noting changes in electrical and chemical properties), to long range strain, the latter in principle extending throughout the crystal though to a degree diminishing with distance from the surface.

In the present measurements the strain introduced by polishing, which is the longest range effect, was monitored by measuring the curvature of thin crystals with one side polished and the other heavily chemically etched. The etched side has a surface stress below detection limit ( $400 \text{ dyne cm}^{-1}$ ). The polished side was progressively stripped by argon ion bombardment, the curvature being continuously monitored by observing the interference pattern during the process. The damage depth due to the ion bombardment itself was negligible, ( $20 \text{ \AA}^{16}$ ). By knowing the rate of removal of the material by sputtering, using a previous calibration<sup>16</sup>), curves of surface stress versus thickness of surface removed could be obtained, as in fig. 4.

To avoid annealing effects (described later) the vacuum system was not baked. Background pressures were of order  $10^{-8}$  Torr. The curvatures were

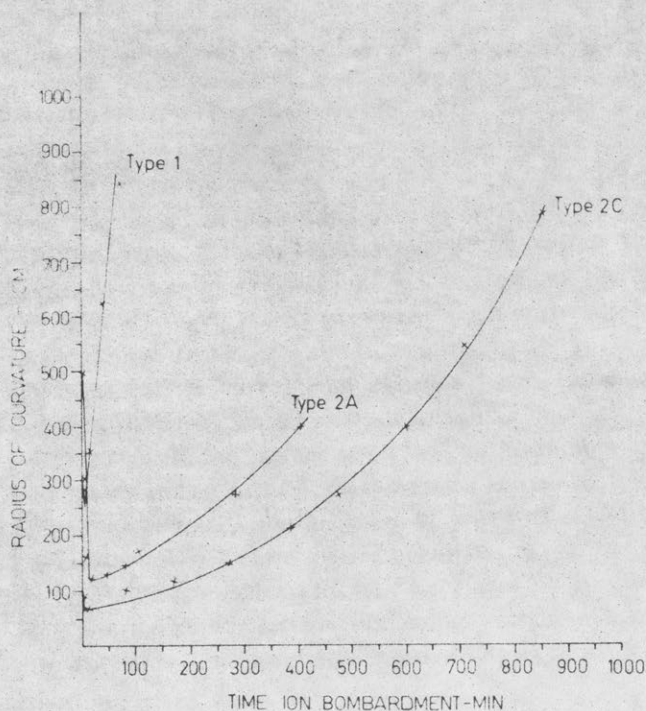


Fig. 4. Radius of curvature versus time of ion bombardment. Rate of surface removal equals  $1 \mu\text{m}$  per 60 min.

TABLE I  
Mechanical polishing treatment of germanium

Type	1st treatment after diamond saw	2nd treatment	3rd treatment
1	CP4 (heavy)	$\frac{1}{4}$ $\mu\text{m}$ diamond	
2A	25 $\mu\text{m}$ B <sub>2</sub> O <sub>3</sub>	12 $\frac{1}{2}$ $\mu\text{m}$ particles to remove 5–15 $\mu\text{m}$	$\frac{1}{4}$ $\mu\text{m}$ particles to remove 15–25 $\mu\text{m}$
2B	25 $\mu\text{m}$ B <sub>2</sub> O <sub>3</sub>	12 $\frac{1}{2}$ $\mu\text{m}$ particles to remove 5–15 $\mu\text{m}$	$\frac{1}{4}$ $\mu\text{m}$ particles to remove 5–15 $\mu\text{m}$
2C	25 $\mu\text{m}$ B <sub>2</sub> O <sub>3</sub>	12 $\frac{1}{2}$ $\mu\text{m}$ particles to remove 5–15 $\mu\text{m}$	$\frac{1}{4}$ $\mu\text{m}$ particles to remove 5 $\mu\text{m}$

not affected either by argon gas or allowing the background to increase slightly by torching glass parts of the system.

The type of polishing treatment was classified as type 1 (light) and type 2 (heavier). In type 1 the surface, after production by a diamond saw, was heavily etched with CP4 and then polished with  $\frac{1}{4}$   $\mu\text{m}$  diamond paste on a Buehler No. 40-7058 felt pad. In type 2 a less safe but more typical treatment was used. The 0.25 mm slab was thinned to 100–110  $\mu\text{m}$  using 25  $\mu\text{m}$  size grinding particles (B<sub>2</sub>O<sub>3</sub>) on a Buehler pad. From 5–15  $\mu\text{m}$  were then removed with 12 $\frac{1}{2}$   $\mu\text{m}$  particles on a 40-7008 pad. The final treatments determine the following subclassification as in table 1. The amount removed in type 2C was just enough to be able to observe interference fringes on the polished surface. Clearly remanent damage from prior treatments would be absent in type 1 surfaces, and present in type 2 surfaces, least in 2A and most in 2C.

As seen in fig. 4, the initial curvature of the crystals (polished side convex) decreased (radius of curvature  $R$  increased) as the damaged layer was removed. Values of  $R$  greater than 1000 cm corresponded to about 1 interference fringe on a crystal and this represents about the detection threshold, the sagitta of the curve being less than  $\frac{1}{4}$   $\mu\text{m}$ . This corresponds to a high degree of flatness. Since the crystals became flat after abraded layers were sputtered away, the surface stress of an ion bombarded face is similar to that of an etched face, both being small, less than 400 dyne  $\text{cm}^{-1}$  using eq. (1). As expected, the thickness of crystal that had to be removed from the polished face, before the remanent strains were as small as those from the etched face, were least for type 1 surfaces and most for type 2C surfaces. Note too the slower recover (flattening) of type 2C than type 2A surfaces (fig. 4). Table 2 shows the "depths of damage" as detected by the above criterion.

One observes that the depth of damage due to polishing with  $\frac{1}{4}$   $\mu\text{m}$  diamond paste is at least 1  $\mu\text{m}$ , as determined by strain, and the depth

TABLE 2  
 Depths of polishing damage in Ge detected by strain

Surface	Max. abrasive particle size used ( $\mu\text{m}$ )	Average depth removed with $12\frac{1}{2}\ \mu\text{m}$ particles ( $\mu\text{m}$ )	Average depth removed with $\frac{1}{2}\ \mu\text{m}$ particles ( $\mu\text{m}$ )	Remanent damage depth from fig. 4 ( $\mu\text{m}$ )	Deduced original damage depth due to particles in column 2 (add columns 3 and 4 to column 5) ( $\mu\text{m}$ )	Max. original damage depth from taper section techniques ( $\mu\text{m}$ )
Type 1	$\frac{1}{2}$	0	not relevant	1	1	-
Type 2A	25	10	20	> 7	> 37	12
Type 2C	25	10	5	> 15	> 30	12

due to 25  $\mu\text{m}$  particles is about 40  $\mu\text{m}$ . This may be compared with the maximum value of about 20  $\mu\text{m}$  deduced by taper section, electrical and chemical techniques<sup>12,13</sup>) for the maximum depth of the cracked layer due to 25  $\mu\text{m}$  particle size polishing. As pointed out<sup>12,13</sup>), factors such as type of slurry, pressure and polishing motions affect the results. The present methods of preparation involved the types of lap, cloth and slurries mentioned above, which are not harsh, and normal light polishing actions. The appreciably greater extent of the damage revealed by strain than by sectioning shows, as expected, that the lattice distortions introduced by abrasion and polishing extend below the bottoms of the deepest fissures.

Clearly the results of abrasion are such as to cause the surface to expand. Removal of segments of surface by the chipping action of abrasion on brittle semiconductors cannot by itself cause expansive effects. These must be the result of wedging something into the surface, either microscopic particles of polishing materials or of the semiconductor itself, into fissures, or of the fissures staying open due to mismatch of cleavage steps; alternatively also, forcing extra atoms into the lattice structure, such as whole planes (edge dislocations) or small units (interstitials). The effective strain region around a dislocation is generally taken as only about 0.01  $\mu\text{m}$ <sup>17</sup>), so to account for the present results the dislocations and interstitials must extend to about the depths of damage measured, i.e. well below the observed fissures. This conclusion is of significance.

## 6. Effects of annealing and ion bombardment on surface stress

Further information regarding the nature and origins of stress in mechanically abraded germanium surfaces was obtained by noting the effects on the specimen curvature of heat treatment. In the first instance it was found that the curvature of crystals was invariably reduced by the bakeout (200 °C) of the pyrex glass vacuum system, typically by a factor of about 2. However, a few seconds subsequent ion bombardment sufficed to restore the curvature to close to its original value in the case of type 2 (but not type 1) crystals. This suggested that adsorbed contamination from the relatively high ( $10^{-4}$  Torr) local pressures of water vapour and other gases during the 5–12 hour bakeout affected the surface tension, but the contaminants were quickly removed by light sputtering. To help distinguish the annealing effects of heating from those of enhanced contamination, it was necessary to eliminate the bakeout process. Pumping for sufficient time with oil diffusion pumps (with liquid nitrogen trap) and getter ion pumps to base pressures of  $5 \times 10^{-8}$  Torr without bakeout, was used in subsequent work.

Heat was applied to the crystal from a 200 W focussed projection lamp operated at fractional power. The only parts to become warm were the molybdenum support block and a small part of the vacuum glass envelope (pre-outgassed), but no pressure rise from these was detected at low ( $\sim 70^\circ\text{C}$ ) temperatures. As the crystals became warm, the interference fringes moved, making dynamic measurements difficult. Hence all measurements were made by heating to the required temperature for 15 min and then measuring the fringes after return to room temperature. (An equilibrium curvature was in fact reached after heating for only 5 min, after which little further change took place.)

Effects of heat on the curvature are shown in fig. 5, where it is seen that

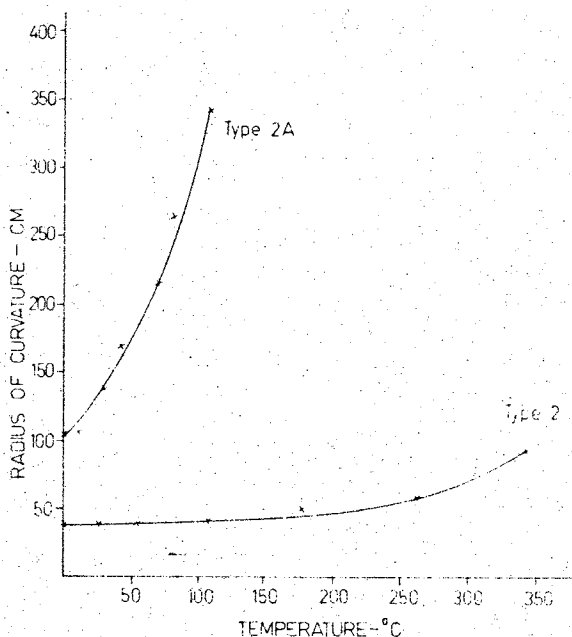


Fig. 5. Radius of curvature versus temperature of anneal for type 2A and 2C crystals.

the crystals tended to flatten. It is obvious that specimens with heavy surface damage were far less sensitive to heat treatment than those with light remanent damage. The latter, type 2A, were affected by heat treatment for a few minutes to temperatures even as low as  $20^\circ\text{C}$  above surroundings.

The sensitivity to low heating temperatures was surprising. To confirm that the crystals were actually at the temperatures indicated by the thermocouple embedded in the supporting block, an experiment was carried out using a dummy Ge crystal provided with electrical leads. The resistance of this (round) crystal was monitored as a function of temperature in a separate

uniform oven. Using this calibration, the temperature of this crystal in the experimental tube could be obtained from its resistance, thus providing a calibration of the true crystal temperature as a function of the thermocouple reading. (The true temperature exceeded the thermocouple reading by 2 °C at 20 °C increasing to 15 °C at 140 °C. The results in fig. 5 refer to true temperatures.)

Although the background pressure did not alter appreciably during low (70 °C) temperature heating, the possibility of a change at these temperatures in surface films occurring and affecting the surface tension could not be excluded. A clue to a method of distinguishing contamination from true annealing effects was afforded by the aforementioned fast recovery of crystals subjected to a few seconds ion bombardment after bakeout. Since the rate of surface stripping (ion current density approx.  $100 \mu\text{A cm}^{-2}$  at 500 eV) was approximately  $1 \mu\text{m}$  per 60 min, corresponding to about  $170 \text{ \AA}$  per min, a few seconds of ion bombardment should remove a surface film. Changes in fringes were indeed observed within a few seconds of the nominal beginning of ion bombardment of type 2 crystals after bakeout. However, in the case of type 1 crystals, there was usually very little or no recovery and further ion bombardment simply caused more flattening.

From this behaviour it is concluded that heating caused two kinds of effect, one, a genuine annealing of the damage induced by polishing, and two, some change in surface films. The annealing effect is much weaker on more damaged surfaces, as seen from fig. 5, and hence the effects of surface film changes are mainly present after heating in poorer vacuum. This is quickly removed by ion bombardment. However, type 1 crystals are appreciably affected by annealing and removal of a surface film by ion bombardment has little influence on the curvature.

Prolonged ion bombardment in all cases caused the crystals to become flat, indicating that cleaned surfaces had surface stresses below detection threshold ( $400 \text{ dyne cm}^{-1}$ ). Annealing of these surfaces up to 500 °C caused no bending. Such bombarded and annealed surfaces correspond to those from which good LEED patterns are obtained, which thus have surface stresses less than  $400 \text{ dyne cm}^{-1}$ .

An interesting sequence of heating and ion bombardment on a type 2A crystal is shown in fig. 6. The effects of bakeout (200 °C at  $10^{-4}$  Torr) are mostly removed by a few seconds ion bombardment. With further stripping of the surface the crystal starts to flatten again, a process accentuated by periods of mild heating (42 min at 53 °C, 150 min at 53 °C, and 42 min at 76 °C). The effects of this heating are partially removed ( $R$  reduced from 650 to 350 cm) by a few seconds i.b. after which 3 min (500 Å stripped) bombardment are required to nearly restore the pre-heating curvature. Annealing

at  $76^\circ\text{C}$  for 42 min again causes flattening ( $R=500$  cm), some of which is removed by a few seconds i.b. after which a slower recovery of the curvature occurs. About 12 min bombardment ( $0.2\ \mu\text{m}$  stripped) takes place.

These types of results show that the curvature before or after ion bombardment is reduced by heating. For type 2 crystals, subsequent i.b. causes a fast (few seconds i.b.,  $10\ \text{\AA}$  stripped) recovery of the curvature, corresponding to the removal of an annealed layer. Further ion bombardment then

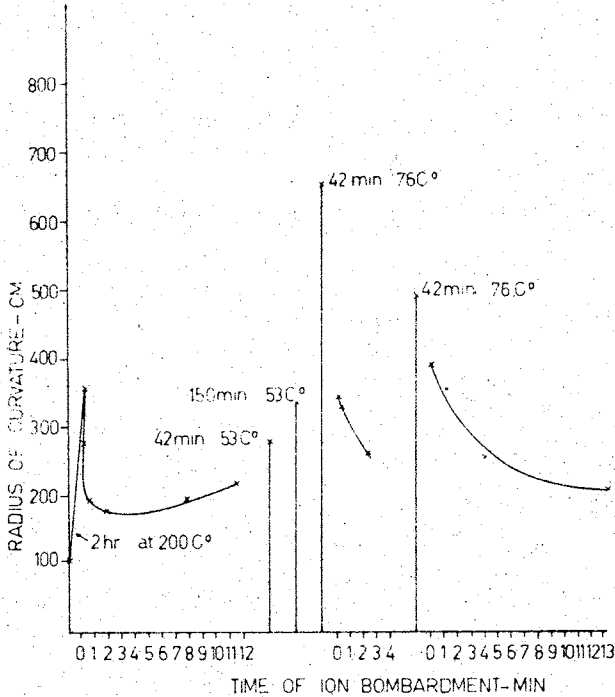


Fig. 1. Radius of curvature versus time of ion bombardment showing various heating cycles. Rate of removal  $1\ \mu\text{m}$  per 60 min.

causes the crystal to flatten again, corresponding to the damaged layer which originally caused the curvature being removed.

The precise nature of the annealing processes are of interest. It is of particular note that they occur at such low ( $50^\circ\text{C}$ ) temperatures, where dislocations are believed to be immobile. At present we believe that microcracks remain open due to cleavage steps not matching their original opposite recesses. With slight heating, small lateral motions of the crack sides are possible, allowing the cleavage steps to move opposite to their original recesses, enabling some microcracks to close. A detailed study of such matching has been performed<sup>18</sup>).

### 7. Curvature as function of thickness

According to eq. (1), for given surface stress difference and fixed elastic constants, the radius of curvature  $R$  is proportional to  $t^2$ , where  $t$  is the thickness. Since the curvature increases for thinner crystals, the surface becomes more stretched and hence the equation only holds provided the surface stress is independent of strain. For maximum surface strains in the

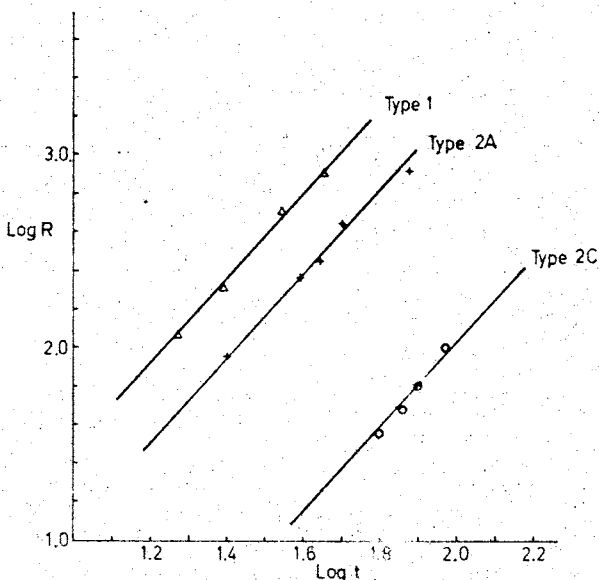


Fig. 7. Plot of  $\log R$  versus  $\log t$  for type 1, 2A and 2C germanium crystals. The lines drawn have a slope of 2.

experimental range measured previously<sup>5-9</sup>) this appears to be a valid approximation.

A test of the variation of curvature as a function of thickness has been made by Drum for AlN crystals<sup>9</sup>). These were produced by growth from the vapour phase. The radius of curvature  $R$  was measured for different crystals varying in thickness from 380 Å to 3500 Å ( $R$  varied from about  $3 \times 10^{-3}$  cm to about 0.1 cm) and was found indeed to obey  $R \propto t^2$ . The thickness and radii of curvature were orders of magnitude less than in our cases. Furthermore it had to be assumed that the surface tensions were the same for different crystals of different thicknesses, and although this appeared to be reasonable, a variation between crystals could not be ruled out.

It was therefore considered desirable to test the dependence of  $R$  on  $t$  for

Ge crystals by thinning a given crystal with a given surface finish. The procedure was as follows.

After removal from the mechanical polishing mount, the crystal thickness  $t$  was measured by optical microscopy, and the radius of curvature  $R$  determined from the ring fringe system observed with the laser interferometer (fig. 1). Further thinning was carried out by mounting the crystal with polished face down in a thin cold solution of black wax dissolved in p-xylene, which dried at room temperature. The back was chemically etched uniformly by the technique described earlier and measurements of  $t$  and  $R$  repeated after removal from the mount by dissolution of the wax. A set of these measurements was carried out for crystals whose first surfaces were of type 1 or 2 mechanical polishing finish. Plots of  $\log R$  versus  $\log t$  are shown in fig. 7. The range of thicknesses is not, unfortunately, large enough to establish the form of the dependence of  $R$  on  $t$  to close limits, but a wider range of thicknesses on a given sample is difficult to achieve. All the points can be fitted to a reasonable degree by an  $R \propto t^n$  curve, where  $n=2$ , although the curves of best fit for the various types of surface involved powers of  $t$  differing by up to 20% from 2, as can be seen from inspection of fig. 7. However, to within the accuracy of the method, the square law dependence of  $R$  on  $t$  predicted by eq. (1) is not contradicted by these measurements. A law of form  $R \propto t^{1.5}$ , such as would follow if  $U$ , the bulk strain energy per unit surface area, were a constant for a given surface treatment, eq. (2), would not fit the range of observed results.

### 8. Surface stresses of clean (111) surfaces of InSb and GaSb

The surface stresses of clean (111) surfaces of InSb and GaSb were the principal object of this study. The absolute values of the stresses were of interest for comparison with predictions of theoretical models and to help in formulating the structure. Since the wafers had opposite (111) faces, which are ideally composed of group III atoms for one face and group V atoms for the other, a possible difference in surface stress would result in a net curvature of a wafer having opposite clean sides. However the simultaneous production of opposite clean surfaces by ion bombardment and annealing was difficult. Wafers supported on their edges were not uniformly bombarded. This coupled with other unsatisfactory experimental features resulted in the same techniques being used as for germanium, these techniques having been well tested.

Wafers were prepared with a type 1 surface, produced by polishing with  $\frac{1}{4}$  (or 1)  $\mu\text{m}$  diamond abrasive after heavy ( $\frac{1}{2}$  mm removed) chemical etching of the original flat ground wire sawn surface. The opposite face was

chemically etched. Thickness of the wafers was generally close to  $20\ \mu\text{m}$ . All exhibited curvature upon removal from the polishing mount, always with the polished side convex.

### (a) InSb

In all 10 wafers were studied, six with the (A or group III or) indium side polished, four with the (B or group V or) antimony side polished. The opposite sides were chemically etched and the wafer laid etched side down on the molybdenum block in the vacuum system, being therefore convex side up.

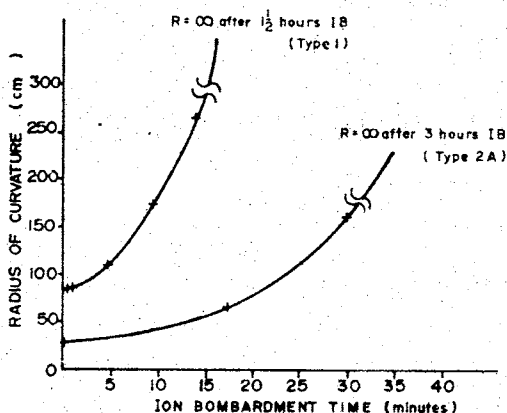


Fig. 8. Radius of curvature versus time of ion bombardment for InSb sample with Sb face being sputtered in both cases. Type 1 was heated to  $113^\circ\text{C}$  before commencing ion bombardment, while type 2A was always kept at room temperature. Rate of surface removal  $2\ \mu\text{m}$  per hour.

For all crystals the application of heat either before or after ion bombardment, resulted in the crystals becoming flatter. The environment was an unbaked vacuum system, background pressure  $5 \times 10^{-8}$  Torr, conditions identical with those for germanium described above. Not all specimens were equally sensitive to heating. However, flattening in general appeared to take place to a greater extent for a given heat treatment, than in the case of germanium. Subsequent ion bombardment continued to cause the wafer curvature to decrease until eventually it became zero. Thereafter annealing to temperatures up to those required to produce clean surfaces after ion bombardment,  $350^\circ\text{C}$ , caused no change from the flat condition. A fairly typical sequence is shown in fig. 8. As the damaged layer in the (top) antimony face is sputtered away the crystal becomes flat. The depth of damage determined in this way from the strain appeared to be  $2\text{--}3\ \mu\text{m}$ , considerably

greater than the visible damage in taper sections, as was to be expected. Significant differences in depth between the A and B faces were not established. Warekois et al.<sup>14</sup>) have reported such differences in taper sections, but Pugh and Samuels did not observe significant differences<sup>15</sup>).

The methods of ion bombardment and annealing (i.b.a.) used to clean surfaces in these experiments were the same as those found successful in obtaining good LEED patterns characteristic of clean surfaces<sup>3,4</sup>). Active gases have very low sticking coefficients (e.g.  $10^{-5}$  for oxygen) on such surface<sup>3,4</sup>). The top surfaces of the wafers were therefore atomically clean to a high degree. Since the net curvature of treated wafers were below detection limit one concludes that the surface stress difference between the cleaned Sb face and the etched In face on the one hand, and between the cleaned In face and the etched Sb face on the other, were both below  $400 \text{ dyne cm}^{-1}$ . Crystals with both sides chemically etched as here always appear flat. (Curvatures in etched crystals reported elsewhere<sup>6</sup>) were possibly due to differences in etches used). Since therefore the etched In and etched Sb faces had similar values of  $\sigma$ , the clean Sb and In faces had surface stress differences of less than  $800 \text{ dyne cm}^{-1}$ , as well as being individually less than  $|400| \text{ dyne cm}^{-1}$ .

#### (b) GaSb

Three wafers were studied and showed behaviour generally similar to InSb. The wafers became flat either by heating and/or ion bombardment. It is similarly concluded that the clean (annealed to  $450^\circ\text{C}$ ) Sb and Ga faces of GaSb have surface stress differences less than  $800 \text{ dyne cm}^{-1}$ .

### 9. Discussion

The findings of only small surface stresses on opposite (111) faces of InSb and GaSb cleaned by ion bombardment and annealing may be compared with theoretical estimates. Cahn and Hanneman<sup>7</sup>) computed the surface stresses of A and B surfaces by assuming the surface atom arrangements were those expected from normal terminations of a bulk lattice, except that the group III surface atoms on the A surface were pulled in towards the surface and the group V surface atoms on the B surface were further out. They obtained a formula for what they called the surface tension  $\sigma$  (actually surface stress as defined here) in terms of bulk elastic constants such that it was directly proportional to a quantity  $\Delta\xi$  introduced as the difference in radians between the normal angle for bonding of a surface atom when trivalently bonded in a separate molecule, and the tetrahedral angle. The theoretical predictions<sup>7</sup>) and present results are shown in table 3.

TABLE 3  
Calculated and experimental surface stresses

Material	$\Delta\xi_A$	$\Delta\xi_B$	Calculated (dyne $\text{cm}^{-1}$ ) <sup>2</sup>			Experimental (dyne $\text{cm}^{-1}$ )
			$\sigma_A$	$\sigma_B$	$\sigma_A - \sigma_B$	$\sigma_A - \sigma_B$
InSb	0.183	$-\frac{1}{2}\Delta\xi_A$	-600	300	900	$<  800 $
GaSb			-800	400	1200	$<  800 $

Considering the uncertainties in choosing values of  $\Delta\xi_A$  and  $\Delta\xi_B$ , the theoretical predictions are not inconsistent with the experimental results. At this stage, however, any theory that predicts values of  $\sigma$  of about 500 dyne  $\text{cm}^{-1}$  or less could match the measurements. Cahn and Hanneman compared their prediction with measurements on surfaces produced by polishing or etching in air, and found agreement for InSb measured by Hanneman, Finn and Gatos<sup>5</sup>), but not for GaAs, InAs, or GaSb (measured by Finn and Gatos<sup>6</sup>)). As pointed out by one of us earlier<sup>8</sup>), such surfaces are quite different from clean surfaces and there is little significance in whether or not clean surface theory matches surface stresses for such surfaces. The opposite (0001) surfaces of AlN platelets measured by Drum had surface stress differences of  $\sigma_B - \sigma_A = 3.6 \times 10^3$  dyne  $\text{cm}^{-1}$ . Due to lack of knowledge of elastic constants a theoretical prediction of  $\sigma_B - \sigma_A$  was not made. These as-grown surfaces however had been exposed to ambient before study of curvature in an electron microscope, and the degree of applicability of clean surface theory to the experimental results is uncertain. For example adsorbed films can affect the surface stresses and tensions markedly<sup>6</sup>).

A proper theoretical treatment of the surface stresses requires precise knowledge of the surface structure. Measurements by LEED on III-V compounds indicated larger than normal unit cells and hence rearrangement of the surface atoms on (111) surfaces<sup>3,4</sup>). For some conditions of surface preparation the unit cells on the A and B faces were of different size<sup>4</sup>). Since the structure was not solved, one can conclude little more than that theory based on a model of the surface with only a normal unit cell cannot be completely correct.

It would be desirable to obtain still lower limits to the surface stress for comparison with theories based on various surface structures. This could be achieved by using still thinner crystals. Although an occasional specimen of thickness down to 8  $\mu\text{m}$  has been produced, improvements on this by a significant factor would seem to demand different techniques. The stress upper limits found here, however, provide some limits to proposed theoretical structure differences between A and B faces.

### Acknowledgement

The authors thank Mr. C. Tenukest for advice and assistance with the electro polishing operations.

### References

- 1) R. E. Schlier and H. E. Farnsworth, *J. Chem. Phys.* **30** (1959) 917.
- 2) J. J. Lander and J. Morrison, *J. Appl. Phys.* **34** (1963) 1403.
- 3) D. Haneman, *Phys. Rev.* **121** (1961) 1093;  
D. Haneman, *J. Phys. Chem. Solids* **14** (1960) 162.
- 4) A. U. Mac Rae, *Surface Sci.* **4** (1966) 247.
- 5) R. E. Hanneman, M. C. Finn and H. C. Gatos, *J. Phys. Chem. Solids* **23** (1962) 1553.
- 6) M. C. Finn and H. C. Gatos, *Surface Sci.* **1** (1964) 361.
- 7) J. W. Cahn and R. E. Hanneman, *Surface Sci.* **1** (1964) 387.
- 8) D. Haneman, *Brit. J. Appl. Phys.* **16** (1965) 411.
- 9) C. M. Drum, *Phil. Mag.* **13** (1966) 1239.
- 10) C. Herring, in: *Structure and Properties of Solid Surfaces*, Eds. Gomer and Smith (University of Chicago Press, 1953) p. 13.
- 11) W. W. Mullins, *Metal Surfaces* (Am. Soc. for Metals, 1963) p. 17.
- 12) T. M. Buck, in: *The Surface Chemistry of Metals and Semiconductors*, Ed. H. C. Gatos, (John Wiley, New York, 1960) p. 107.
- 13) E. N. Pugh and L. E. Samuels, *J. Electrochem. Soc.* **109** (1962) 409; **108** (1961) 1043.
- 14) E. P. Warekois, M. C. Lavine and H. C. Gatos, *J. Appl. Phys.* **31** (1960) 1302.
- 15) E. N. Pugh and L. E. Samuels, *J. Appl. Phys.* **35** (1964) 1966.
- 16) R. J. MacDonald and D. Haneman, *J. Appl. Phys.* **37** (1966) 1609, 3048.
- 17) H. F. Matare, *J. Appl. Phys.* **30** (1959) 581.
- 18) D. Haneman, W. D. Roots and J. T. P. Grant, *J. Appl. Phys.* **38** (1967) 2203.